TARGETING PROTEIN ARGININE METHYLTRANSFERASE 5 AS A NOVEL THERAPEUTIC APPROACH IN PANCREATIC & COLORECTAL CANCER

Lakshmi Milind Prabhu

Submitted to the faculty of the University Graduate School

in partial fulfillment of the requirements

for the degree

Doctor of Philosophy

in the Department of Pharmacology and Toxicology,

Indiana University

December 2018

Accepted by the Graduate Faculty of Indiana University, in partial fulfillment of the requirements for the degree of Doctor of Philosophy.

Doctoral Committee

_____
Tao Lu, Ph.D., Chair

_____
Ahmad Safa, Ph.D.

May 7, 2018

_____
Karen Pollok, Ph.D.

_____
Todd Skaar, Ph.D.

_____
Jian-Ting Zhang, Ph.D.

DEDICATION

This dissertation is dedicated to my Aai (mom) and Baba (dad). It is only because of their unconditional support, love and encouragement that this journey has been made possible. Forever grateful.

ACKNOWLEDGMENTS

My mentor, Dr. Tao Lu has shown tremendous support and patience over the years as I matured as a graduate student while conducting the work in this thesis. Her knowledge, discipline, love and dedication for science is an inspiration and has helped me grow as a person, both in my professional and personal life. Her role in my success is indispensable.

I would also like to acknowledge my committee members, Dr. Ahmad Safa, Dr. Karen Pollok, Dr. Todd Skaar and Dr. Jian-Ting Zhang for their timely and astute suggestions to propel my project forward and challenge me as a graduate student to do even better. I would also like to take the opportunity to thank the faculty in the Department of Pharmacology and Toxicology and at Indiana University School of Medicine (IUSM), who helped me to become a better scientist, either through their classroom teaching, scientific discussion or collaboration.

My present and former labmates, Matthew Martin, Antja-Voy Hartley, Jiamin Jin, Dr. Han Wei and Rasika Mundade have provided scientific support and stimulating suggestions. I am thankful for their enjoyable companionship throughout graduate school.

A special thank-you to all the collaborators whose hard work has contributed to critical experiments in this project as well as have been co-authors in the published work that has been included in this thesis: Dr. Han Wei for some colorectal cancer related experiments in Chapters 3 and 4, Drs. Zhong-Yin Zhang, Lan Chen, Thomas Hurley, Lifan Zeng for guidance with high-throughput

screen development and compound synthesis in Chapters 4 and 5; Drs. Rommie Amaro and Ozlem Demir for their help with structural docking analysis in Chapters 4 and 5; Drs. Olaf Weist and Haining Liu for their help with computer-based screening of predicted derivatives in Chapter 4; Dr. Melissa Fishel for her help with the 3D culture experiment in Chapter 4; Dr. Jing-Yuan Liu for her guidance with the isothermal calorimetry experiment in Chapter 4; Drs. Jingwu Xie and Dongsheng Gu for permission and assistance to use the fluorescence microscope in their lab; Dr. George Sandusky, Dr. Constance Temm and Kyle McElyea for their assistance with Immunohistochemistry (IHC) analysis in Chapter 3; Dr. Keith Condon for his help with H&E staining; Dr. Murray Korc for providing the pancreatic cancer cell lines used in this project; Dr. Karen Pollok, Anthony Sinn and Courtney Hemenway for their critical support with mouse experiments in Chapter 4; Dr. David Jones and Andi Masters for their support with pharmacokinetic studies and Dr. Paul Territo and Brian McCarthy for their help with bioluminescent imaging and analysis in Chapter 4.

A special mention to the great support staff at IUSM for their continued help throughout graduate school. Tara Hobson-Prater and Brandy Wood from Graduate Division have played invaluable roles in my student success here. I am also thankful to Amy Lawson, Britney Heiser and Joanna Plew who have endured through hours of questions and paperwork that I had for them. A big thank you to Lisa King for her professional support and proof reading of my publications and to Andy Boyll who provided critical help in preparing my predoctoral grant applications. I would also like to thank Rob Lawson for his help

navigating through technical and software issues. Thank you to the travel grants from Department of Pharmacology and Toxicology, IUSM Graduate Division, IUPUI Graduate Office and IUPUI Graduate and Professional Student Government (GPSG) that aided the opportunity to present my research at national and international scientific meetings.

I would also like to thank mentors and teachers throughout my childhood and adult life that have been critical in my growth as a student and as a person. A special thank you to Dr. Sandy Bernstein, my MS thesis mentor. In his lab, I gained the confidence and skills that helped me to be successful in my PhD career.

Last but certainly not the least, my friends and family have been my greatest champions and words are not enough for how grateful I am for their support. A big thank you to the friends I made for life in graduate school: Dr. Sudha Savant, Trupti Shetty, Sreeparna Majumdar, Jenny Beebe, Emma Mills and Dr. Lisa Darby, without whom this journey would not have been as fun as it turned out to be. A huge shoutout to my roommate and friend, Eshaani Mitra for enduring my company all these years! I would like to give my thanks to friends and colleagues from the Toastmasters Club at IUSM. I am also grateful for the life-long friendship of my buddies from junior high (Ninad Manerikar, Dipti Joshi, Roshni Karnik, Tanvi Raykar, Mansi Shende, Sumeel Parab, and Ankit Bhalwankar) and our conversations that have provided a safe space to vent my frustrations during challenging times over the years. A special mention to Vrushali Kapileshwari who is the greatest friend and travel buddy anybody could

ask for. A note of thanks to my friend from college, Aditi Singh who has been a patient listener whenever I have needed one. To my grandparents (Smita and Balkrishna Bagwe), thank you for never letting my spirit fall even during the hardest of times. Finally, to my parents (Shubha and Milind Prabhu), all I can say is thank you. Thank you for instilling me the values of kindness, dedication, perseverance and hard work ever since I was a little girl. Thank you for always providing a shoulder to lean on and tough love when required. I will love you forever!

Lakshmi Milind Prabhu

TARGETING PROTEIN ARGININE METHYLTRANSFERASE 5 AS A NOVEL THERAPEUTIC APPROACH IN PANCREATIC & COLORECTAL CANCER

Pancreatic ductal adenocarcinoma (PDAC) and colorectal cancer (CRC) are among the most commonly diagnosed forms of cancer in the United States. Due to their widespread prevalence and high mortality rate, it is vital to develop effective therapeutic drugs to combat these deadly diseases. In both PDAC and CRC, the multifunctional factor nuclear factor kappa B (NF-κB), a central coordinator of cellular immune responses, is activated abnormally, leading to tumorigenesis and cancer progression. Therefore, controlling NF-κB activity is critical in the treatment of these cancers. In a previous study, we identified a new mechanism by which NF-κB activity is regulated by an epigenetic enzyme known as protein arginine methyltransferase 5 (PRMT5). We showed that overexpression of PRMT5 not only activated NF-κB, but also significantly promoted several characteristics associated with cancer, including increased cell proliferation, migration, and anchorage-independent growth in both PDAC and CRC cells. Moreover, in order to examine the therapeutic potential of PRMT5 in these cancers, we adapted the state-of-the-art AlphaLISA technique into a high throughput screen (HTS) platform to screen for PRMT5 inhibitors. As a result, we successfully identified the small molecule PR5-LL-CM01 as our lead hit. Further validation experiments confirmed that PR5-LL-CM01 is a potent and specific PRMT5 inhibitor that exhibits significant anti-tumor efficacy in both *in vitro* and *in vivo* models of PDAC and CRC. Additionally, in a second screen, we discovered

two natural compounds, P1608K04 and P1618J22, that can also function as the PRMT5 inhibitors. These findings further highlight the robustness of the PRMT5-specific AlphaLISA HTS technique. To conclude, we describe here for the first time a novel role of PRMT5 as a tumor-promoting factor in PDAC and CRC through NF-κB activation. By successfully developing and applying an innovative AlphaLISA HTS technique, we discovered PR5-LL-CM01, P1608K04, and P1618J22 as novel PRMT5 inhibitors, with PR5-LL-CM01 showing the strongest potency in both PDAC and CRC models. Therefore, we demonstrated that PRMT5 is a promising therapeutic target in PDAC and CRC, and the novel PRMT5 inhibitor PR5-LL-CM01 could serve as a promising basis for new drug development in PDAC and CRC.

Tao Lu, Ph.D., Chair

TABLE OF CONTENTS

LIST OF TABLES

LIST OF FIGURES

LIST OF ABBREVIATIONS

aDMA	asymmetric x-NG, NG-dimethylarginine
AlphaLISA	amplified luminescent proximity homogeneous assay-linked immunosorbent assay
AP-1	activator protein 1
APC	adenomatous polypoabsent small homeotic discs 2-like
ATCC	American Tissue Culture Collection
$AUC_{0-\infty}$	area under the plasma concentration-time curve from 0-infinity
Avg	average
β-barrel	beta-barrel
Bcl-2	B-cell lymphoma-2
Biotin-H4R3me2	histone H4 pre-methylated at arginine 3
bp	base pairs
BSA	bovine serum albumin
C	carbon
Caenorhabditis elegans	*C. elegans*
CDK2	cyclin dependent kinase 2
cDNA	complementary deoxyribonucleic acid
CETSA	cellular thermal shift assay
CF I(m)	mammalian cleavage factor I
CHX	cycloheximide

Cl/F	clearance/availability
C_{max}	maximum concentration
CNBr	cyanogen bromide
CRC	colorectal cancer
C-terminus	carboxy terminus
D	aspartic acid
Da	daltons
DMEM	Dulbecco's Modified Eagle medium
DMSO	dimethyl sulfoxide
DNA	deoxyribonucleic acid
DTT	dithiothreitol
E	glutamine
EBNA-2	Epstein-Barr virus nuclear antigen 2
ECL	enhanced chemiluminescence
EDTA	ethylenediaminetetraacetic acid
EGFR	epidermal growth factor receptor
F	phenylalanine
FBS	fetal bovine serum
FDA	Food and Drug Administration
FEN1	flap endonuclease 1
5-FU	5-fluorouracil
FOLFIRINOX	combination of 5-fluorouracil, leucovorin, oxaliplatin, and irinotecan

FOLFOX	combination of 5-fluorouracil, leucovorin and oxaliplatin
G	glycine
GAPDH	glyceraldhyde 3-phosphate dehydrogenase
GAR	glycine- and arginine-rich
GI	gastrointestinal
h	hour
H2AR3	third arginine on histone H2A
H3R2	second arginine on histone H3
H3R8	eighth arginine on histone H3
H4R3	third arginine on histone H4
HDAC	histone deacetylase
HEPES	4-(2-hydroxyethyl)-1-piperazineethanesulfonic acid
HIF1α	hypoxia inducible factor 1-alpha
HOXA9	homeobox A9
HPLC	high performance liquid chromatography
HRP	horseradish peroxidase
HTS	high throughput screen
IACUC	Institutional Animal Care and Use Committee
IC_{50}	half maximal inhibitory concentration
IκB	inhibitor of kappa B
IκBα	inhibitor of kappa B alpha
IL1a	interleukin 1 alpha

IL8	interleukin 8
IP	immunoprecipitation
i.p.	intraperitoneal
IRES	internal ribosome entry site
IS	internal standard
ITC	isothermal calorimetry
IUSM	Indiana University School of Medicine
kg	kilogram
Kras	ki-ras2 Kirsten rat sarcoma viral oncogene homolog
L	liters
LC-MS	liquid chromatography-mass spectrometry
18q LOH	long arm of chromosome 18
LSm	Sm-like
MEP50	methylosome protein 50
mg	milligram
min	minutes
MMA	x-NG-monomethylarginine
MMP2/9	matrix metalloproteinase 2/9
mRNA	messenger ribonucleic acid
miRNA	micro RNA
MS	mass spectrometry
MTT	[(3-(4, 5-dimethylthiazolyl-2)-2, 5-diphenyltetrazolium bromide)]

m/z	mass divided by charge number
N	nitrogen
Na_V	voltage-gated sodium channel
NF-κB	nuclear factor kappa b
NK cells	natural killer cells
NM23	nonmetastatic 23
NSG	NOD.Cg-*Prkdc*^{scid} Il2rg^{tm1Wjl}/SzJ
N-terminus	amino terminus
O	oxygen
O_2	oxygen
p53	tumor protein p53
Panin	pancreatic intra-epithelial neoplasia
PBS	phosphate buffered saline
PDAC	pancreatic ductal adenocarcinoma
PD	pharmacodynamics
PDCD4	programmed cell death 4
PGM	proline-, glycine- and methionine-rich
PH	pleckstrin homology
PI3K	phosphoinositide 3-kinase
PK	pharmacokinetics
PMSF	phenylmethylsulfonyl fluoride
PRMT	protein arginine methyltransferase
PTM	posttranslational modification

PVDF	polyvinylidene fluoride
QPCR	quantitative polymerase chain reaction
R	arginine
Rb	retinoblastoma
RGF	reduced growth factor
RNA	ribonucleic acid
RNAP II	RNA polymerase II
rpm	revolutions per minute
RPMI	Roswell Park Memorial Institute medium
RPS10	ribosomal protein s10
R.T.	room temperature
S	sulphur
SAH	s-(5'-adenosyl)-l-homocysteine
SAM	s-adenosylmethionine
S/B	signal versus background ratio
SD	standard deviation
sDMA	symmetric x-NG, N0G-dimethylarginine
SDS-PAGE	sodium dodecyl sulfate polyacrylamide gel electrophoresis
sdme-R	anti-symmetric dimethyl arginine
sec	seconds
SEM	standard error of mean
SH3	SRC homology 3 domain

SID	single injection daily
Smad4	C. elegans gene *Sma* (S) and the Drosophila gene 'mothers against decapentaplegic' (Mad)
snRPD1	small nuclear ribonucleoproteins SmD1
snRPD3	small nuclear ribonucleoproteins SmD3
ST7	suppressor of tumorigenicity 7
STR	short tandem repeat
$t_{1/2}$	half-life
3D	three dimensional
TIM	triosephosphate isomerase
t_{max}	time of maximum concentration
TNFα	tumor necrosis factor alpha
TR-FRET	time-resolved fluorescence energy transfer
unmeH4R3	unmethylated third arginine on histone H4
US	United States
VCAM1	vascular cell adhesion molecule 1
Vd_{ss}/F	apparent volume of distribution
VEGF	vascular endothelial growth factor
v/v	volume by volume
WB	western blot
WT	wild-type
w/v	weight by volume
XIAP	X-linked inhibitor of apoptosis protein

X. laevis	*Xenopus laevis*

CHAPTER 1. INTRODUCTION

1.1 Pancreatic and Colorectal Cancer

1.1.1 Risk factors, Genetic Causes and Stages

Gastrointestinal cancer refers to malignant conditions of the gastrointestinal tract (GI tract) and accessory organs of digestion. Among them, pancreatic ductal adenocarcinoma (PDAC) and colorectal cancer (CRC) are two of the most challenging cancer types (Siegel *et al.*, 2013). For instance, PDAC has a very poor prognosis with a median survival between 6-8 months and ~8% of 5-year survival rate (Hidalgo 2010). Equally devastating, CRC is the second leading cause of death in men and women combined in the United States and the lifetime risk of developing this disease for both the sexes is 6% (Hawk and Levin 2005; Ferlay *et al.*, 2015). Despite important advances in recent years, more than 40% of CRC patients will experience disease recurrence following primary therapy. Additionally, PDAC and CRC have different risk factors and genetic causes. The following sections elaborate on these topics in more detail:

1.1.1A *Pancreatic Cancer*

Several factors have been linked to an increased risk of developing pancreatic cancer. Some of these factors are lifestyle related, including obesity, tobacco use, and exposure to certain chemicals. However, other factors like age (most patients are older than 45 years), race (African-Americans have a higher incidence rates than Caucasians), family history of pancreatic cancer and personal history of chronic pancreatitis can also increase the risk of this cancer.

There are two broad categories of pancreatic cancer based on the cell type that the tumor originates from: exocrine and endocrine. Exocrine tumors are the most common type and arise mostly from the pancreatic ducts and are termed as PDAC. On the other hand, endocrine tumors account for only about 1% of the pancreatic cancer cases and originate in the islet cells of the pancreas. According to the American Cancer Society, PDACs represent the majority of the pancreatic cancer cases. PDAC progression is characterized by the generation of precancerous lesions termed as low-grade pancreatic intra-epithelial neoplasia (PanIN) (**Figure 1**). It is now widely accepted that mutation in an oncogene termed *Kras* is the initiating genetic modification that occurs in pancreatic cancer and is seen in almost all PDAC specimens (Kern S, 2000, Hingorani *et al.*, 2003, Hezel *et al.*, 2006). *Kras* mediates a variety of functions like cell proliferation, survival and differentiation in normal cells. Point mutation in *Kras* ($Kras^{G12D}$) causes constitutive activation of the gene and leads to development of PanINs in mice, which eventually progresses to PDAC formation. This particular mutated *Kras* form has been difficult to target via drugs, as directly targeting it has been an issue. This is because *Kras* lacks binding pockets for drugs to bind except for the site that binds to GDP/GTP. Since GDP/GTP show exceptionally tight binding to *Kras*, employing competitive nucleotide analogs with therapeutic effects has not been successful (Ye and Zhou, 2016). Apart from *Kras*, mutations in other genes have also been shown to accelerate PDAC formation. These include

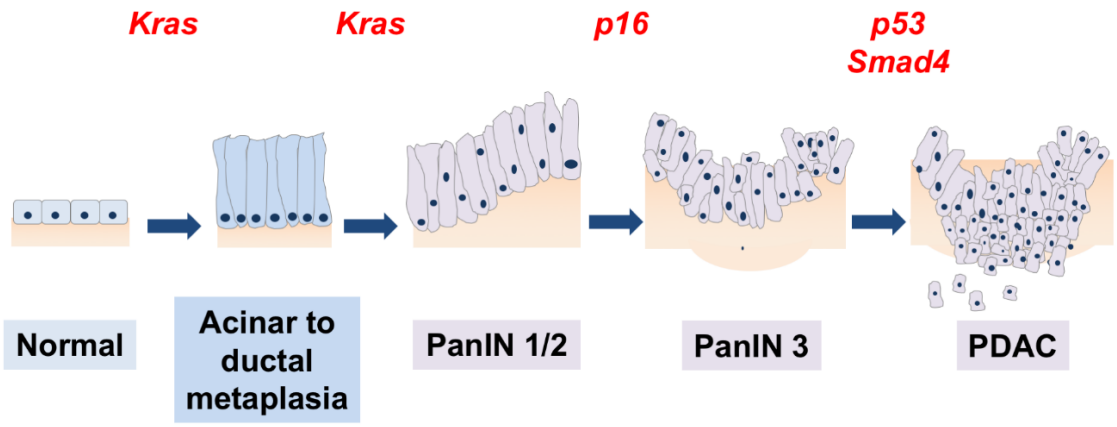

Figure 1. Stages in Pancreatic Ductal Adenocarcinoma (PDAC) Development
Accumulation of oncogenic mutations leads to conversion of normal acinar cells of the pancreas into a more ductal-like phenotype called acinar-to-ductal metaplasia (ADM). ADM lesions can progress into pancreatic intraepithelial neoplasia -1 and 2 (PanIN-1/2). In this stage, the cells change their morphology to a more cuboidal form. The nuclei remain in their basal position as seen in normal cells. PanIN-3 stage is characterized by loss of cell polarity and atypical nuclei with initiation of invasion of the basement membrane. PanIN-3 progressively leads to PDAC. This stage is characterized by with uncontrolled cell growth and metastasis. Cellular mutations that play a critical role for progression in each stage are highlighted in red and described in more detail in the text. Adapted from Hezel *et al.*, 2006.

mutation in the gene *p16* that accelerates the PanIN 1/2 stages to the PanIN-3 stage, which is designated as a carcinoma *in situ*. p16 regulates cell cycle progression from G1->S phase, and a loss-of-function can therefore lead to unchecked cell growth. Additional loss-of-function mutations in critical tumor suppressor genes like *p53* and *C. elegans* gene Sma (S) and the Drosophila gene 'mothers against decapentaplegic' (Mad) (*Smad4* (Horii et al, 1992) eventually lead G1->S- progression and evasion of apoptosis thereby completing the progression to PDAC. Clearly, pancreatic cancer formation is a result of a variety of mutations that can affect several downstream signaling pathways, resulting in a complex disease etiology.

1.1.1B *CRC*

CRC has become one of the more prominent cancers in developed countries spurred by a combination of factors including rising older population, unfavorable diet, smoking, low physical activity and obesity, that lead to an accumulation of somatic mutations (Slattery 2000). The risk of colorectal cancer is also increased in patients suffering from ulcerative colitis (Lakatos and Lakatos 2008).

CRC is comprised of a series of genetic and epigenetic changes in colon epithelial cells, with successive mutations that accumulate over time (Daniluk *et al.*, 2012). This cancer originates in the colon and/or rectum at the inner lining in the form of an abnormal growth of tissue called a “polyp”. Polyps are benign in

nature and have not spread to surrounding tissue in the early stages and over time can undergo malignant transformation to give rise to metastatic forms of CRC. In later stages such as the late adenoma and metastatic stages, the cancer cells begin to invade the walls of the colon and rectum. The late adenoma stage thus leads to metastasis marked by with uncontrolled cell growth and spreading to neighboring and distant tissue and lymph nodes (**Figure 2**). There are several pathways that lead to chromosomal instabilities in CRC. These mutations result in activation of oncogenes such as *Kras* and inactivation of tumor suppressor genes such as the loss of *APC*, *p53*, and heterozygosity for the long arm of chromosome 18 (18q LOH) (Mundade *et al.*, 2014) and lead to uncontrolled cell growth, escape from pro-apoptotic signals and eventually ability to metastasize as the cancer progresses from the early to the more advanced stages of CRC.

1.1.2 Current Treatment Options and Limitations

The available options for treatment are hardly adequate in improving the quality of life of PDAC and CRC patients. For PDAC, current therapy mainly consists of surgery, if diagnosed in the early stages. In more advanced stages, combined local treatment of radiation therapy and drugs is prescribed. The first-line treatment for PDAC used to be gemcitabine, a nucleoside analog that gets incorporated into DNA and inhibits DNA synthesis. However, gemcitabine resistance is common (de Sousa Cavalcante and Monteiro, 2014). Combination studies of gemcitabine with the common chemotherapeutic drug nab-paclitaxel have shown limited promise in recent studies (De Vita *et al.*, 2016, Corrie *et al.*,

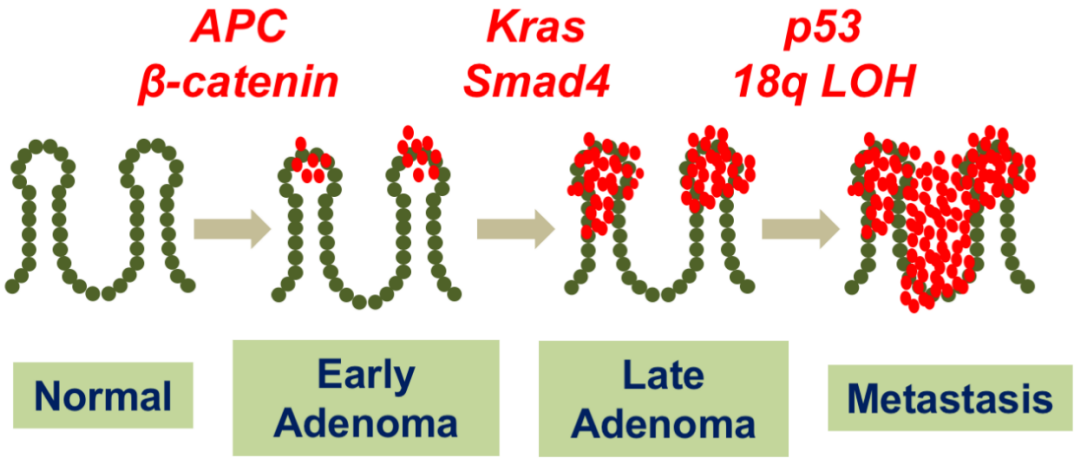

Figure 2. Stages in Colorectal Cancer (CRC) Development
Early cancer stages in CRC are marked by accumulation of cancerous lesions called polyps (denoted in red) in normal colon cells. In this stage, the cancer is benign and has not spread to surrounding tissue. As the cancer progresses to the late adenoma stage, it starts to invade the walls through neighboring structures. The late adenoma stage then leads to metastasis characterized by with uncontrolled cell growth and spreading to the surrounding and distant tissue and lymph nodes. Cellular mutations that play a critical role for progression in each stage are highlighted in red and described in more detail in the text. Adapted from Martin *et al.*, 2018.

2017). Combination of a group of 4 drugs, termed FOLFIRINOX consists of leucovorin, 5-fluorouracil (5-FU), irinotecan and oxaliplatin showed longer overall median survival (11.1 months) compared to patients treated with gemcitabine alone (6.8 months) with no change in the quality of life (Conroy *et al.*, 2011). In the FOLFIRINOX combination regimen, leucovorin is used to reduce the toxic effects of 5-FU (Rustum 1990). Another component of the FOLFIRINOX regimen, 5-FU is a pyrimidine analog that primarily inhibits the enzyme thymidylate synthase activity by blocking thymidine synthesis and subsequent production of DNA. Irinotecan, a third component of the FOLFIRINOX regimen, inhibits the activity of topoisomerase I, an enzyme that prevents supercoiling of DNA and leads to double-strand DNA breakage and cell death (Chabot 1997). Lastly, oxaliplatin is platinum-based agent and forms platinum-DNA adducts (Raymond *et al.*, 1998). Since 2011, FOLFIRINOX has been used as a first-line treatment for advanced metastatic PDAC, with gemcitabine prescribed as a second-line therapy in some cases.

On the other hand, for CRC, in early stages, the available options for treatment includes removal of some or all parts of the colon (colectomy) with adjuvant chemotherapy. A part of the FOLFIRINOX regimen, namely FOLFOX (combination treatment of 3 drugs with 5-FU, leucovorin, and oxaliplatin) has shown efficacy for CRC treatment. For more aggressive tumors, targeted therapies such as bevacizumab [monoclonal antibody that prevents vascular endothelial growth factor (VEGF) activity] as well as cetuximab and panitumumab

[monoclonal antibody that prevents epidermal growth factor receptor (EGFR) activity] have been approved by the Food and Drug Administration (FDA) (Mundade *et al.*, 2014). VEGF and EGFR lead to increased angiogenesis and cell growth respectively in CRC, and thus can serve as targets for these therapies.

However, in addition to having a number of side effects, all the options listed above barely extend the life span of the patient (~3-4 months) and provide little chance for a cure for both these cancers. An ideal treatment strategy requires a combination of drugs that can simultaneously target upstream/downstream regulators in multiple signaling pathways and work in conjunction with each other to block disease progression. An important way to regulate signaling pathways are posttranslational modifications (PTMs) of critical histone and non-histone proteins in the process. One such example is the transcription factor nuclear factor κB (NF-κB) that is important in inflammation and cancer progression in cells. Our lab recently made a significant discovery by identifying a novel PTM on NF-κB in the form of arginine (R) methylation, which led to its downstream activation (Wei *et al.*, 2013). The enzyme implicated for this PTM was a member of the epigenetic enzyme family of protein arginine methyltransferases (PRMTs), namely PRMT5. This was an exciting finding as NF-κB is a well-known tumor promoting factor and is constitutively activated in both PDAC and CRC. Furthermore, PRMT5-mediated NF-κB methylation could serve as a novel mechanism underlying NF-κB activation observed in these

cancers. Thus, targeting PRMT5 could decrease this activation, leading to potential therapeutic effects. In the next sections, the critical role of NF-κB signaling in cancer as well as an insight into the PRMT family and PRMT5 is discussed further.

1.2 NF-κB Signaling and Its Role in PDAC and CRC

In mammals, the NF-κB family consists of five members: RelA (p65), RelB, Rel (cRel), NF-κB1 (p50 and its precursor p105) and NF-κB2 (p52 and its precursor p100) (Ghosh *et al.*, 1998). All the members share a Rel homology domain in the N-terminus, which is essential for dimerization and binding to cognate DNA sequences.

1.2.1 NF-κB Signaling Pathway

The NF-κB signaling can be classified into either the canonical or the non-canonical pathway. The canonical pathway mainly regulates the transcription of genes involved in inflammation, innate immunity and cell survival. On the other hand, the non-canonical pathway is involved in the transcription of genes regulating B-cell maturation, humoral immunity and lymphoid organ development. Though there are two pathways, the canonical pathway has been documented to primarily play a role in PDAC and CRC, in which an inhibitor complex named IκBα (inhibitor of κB alpha) sequesters p65-p50 heterodimer in an inactive state in the cytoplasm (**Figure 3**). When a cell receives extracellular signals like stress, cytokine binding, etc., the IκB kinase phosphorylates IκBα, leading to its release

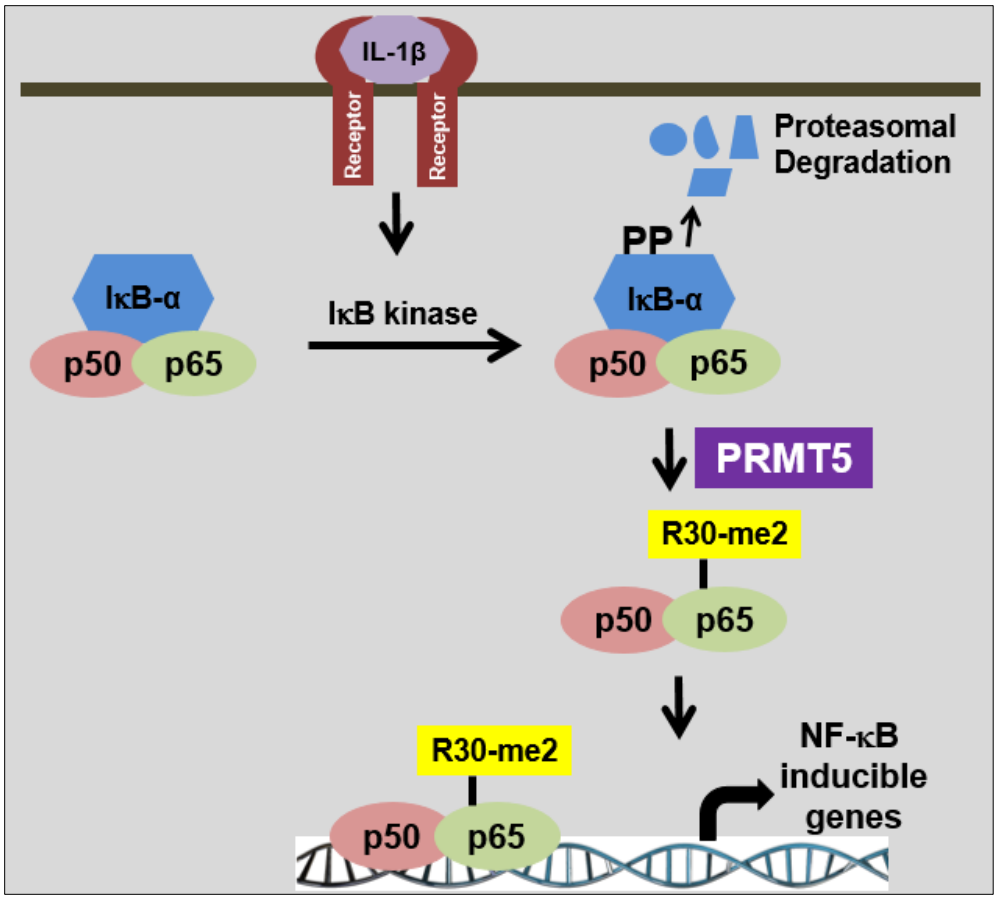

Figure 3. Canonical NF-κB signaling pathway
External stimuli like IL-1β binding to its receptor causes the activation of the complex. IκB kinase phosphorylates specific serine residues on IκBα, which is bound to the p65-p50 heterodimer. Phosphorylation of IκBα causes its degradation via the proteasomal pathway. The p65-p50 dimer then translocates to the nucleus and activates the transcription of its target genes. In disease conditions, these target genes can contribute towards the hallmarks of cancer, leading to disease progression.

and degradation, thus freeing the p65-p50 complex, and enables it to migrate into the nucleus and bind the κB consensus sequences in the promoters, resulting in the activation of specific genes. Abnormal upregulation of NF-κB target genes contribute to the pathology of a number of cancers, including PDAC and CRC. Some examples of target genes of the canonical NF-κB signaling pathway that contribute to six hallmarks of cancer are: **(i)** inflammation: *TNF* (tumor necrosis factor), *IL-1* (interleukin-1); **(ii)** cell survival: *Bcl-2* (B-cell lymphoma-2), *XIAP* (X-linked inhibitor of apoptosis protein); **(iii)** angiogenesis: *VEGF* (vascular endothelial growth factor), *HIF1α* (hypoxia inducible factor 1-alpha) **(iv)** cell death and anti-proliferative effects: *Fas*, *p53* **(v)** tumor promotion and metastasis: *MMP2/9* (matrix metalloproteinase 2/9), *VCAM1* (vascular cell adhesion molecule 1); and **(vi)** proliferation: *cyclin D*, *CDK2* (cyclin dependent kinase). Overall, constitutive activation of the canonical signaling pathway plays a crucial role in disease progression.

1.2.2 NF-κB Signaling in PDAC and CRC

Instances of canonical NF-κB pathway interacting with concurrent signaling pathways have been well documented in PDAC and CRC etiology. (Prabhu *et al.*, 2014). In terms of PDAC, $Kras^{G12D}$ mutation is observed in almost all PDAC cases and serves as the main driver of constitutive NF-κB expression in PanINs and PDACs through activation of AP-1. AP-1 is a transcription factor that is upregulated in *Kras* mutated cells and causes proteasomal degradation of the IκB complex. Degradation of IκB leads to nuclear translocation of NF-κB and

activation of its target genes (Ling *et al.*, 2012). In this context, previous research has shown that NF-κB pathway could upregulate the inflammatory response in PDAC cells via crosstalk with the Notch signaling pathway (Maniati *et al.*, 2011). Even in CRC, NF-κB is constitutively activated in 60-80% cases and promotes cell growth, metastasis and chemotherapeutic resistance (Hai *et al.*, 2016, Hassanzadeh 2011). A significant finding from our lab demonstrated that PRMT5 activated NF-κB by symmetrically dimethylating the R residue on the p65 subunit of NF-κB. Additionally, we showed that PRMT5 was significantly upregulated in a variety of cancer tissues accessed through the GeneNote database, including in PDAC and CRC. To build upon this important experimental foundation, my thesis focuses on the potential oncogenic role of PRMT5 through methylation of NF-κB in the context of PDAC and CRC, as well as the effort to discover small molecule inhibitors to inhibit PRMT5 in these two types of deadly GI cancers. In the next section, I elaborate on past efforts to develop compounds that target NF-κB and PRMT5 respectively and justify why targeting PRMT5 could prove to be a more viable therapeutic option than directly targeting NF-κB.

1.2.3 Current Status of NF-κB Inhibitors and Their Limitations

NF-κB pathway is an important player in PDAC and CRC and is a known contributor to disease initiation and progression. Intracellular signaling gets even more complicated since NF-κB interacts with other pathways that are also deregulated in PDAC and CRC. Thus, direct targeting of NF-κB can be

complicated as inhibition of NF-κB activity can result in affecting multiple downstream signaling pathways that could be critical for normal cell function.

To date, over a hundred inhibitors of the NF-κB pathway have already been documented, including small molecules, peptides, small DNA/RNA, viral proteins, and natural compounds (Prabhu *et al.*, 2014). However, there is no direct NF-κB inhibitor that has been approved in humans. Various steroids and anti-inflammatory drugs (aspirin) were found to block NF-κB, but they showed pleiotropic effects. To this date, none of them have been proven to have clinical applications specifically in cancers. There are various factors such as poor bioavailability, fast metabolism and slow absorption that impede the use of these compounds in the clinic. Moreover, selectivity can a problem, as other signaling pathways that interact with NF-κB could also be affected. This can result in unwanted secondary effects. In the future, targeting non-redundant cytosolic activators of NF-κB instead of NF-κB itself could represent a better approach to inhibit key processes in PDAC and CRC. In this regard, discovery of PRMT5 as a novel activator of NF-κB widens options for therapeutic targeting in PDAC and CRC treatment.

1.3 PRMT5, a Prominent Member of PRMTs Superfamily & Its Role in PDAC and CRC

As a recently identified novel activator of NF-κB, PRMT5 represents a potential new therapeutic target in PDAC and CRC. PRMT5 is a prominent member of the PRMTs superfamily, which we will elaborate on below:

1.3.1 PRMTs Superfamily Members & Overview of Their Structures

Over the years, several enzyme families have been discovered to be directly involved in a host of PTMs that affect biological function, right from early germline to adult human tissue. PTMs include methylation, acetylation, phosphorylation, ubiquitination, sumolyation amongst the major subtypes and are responsible for regulation of many cellular processes. However, the main focus of the work presented in this thesis is a member of the PRMT enzyme family that regulate R residue methylation PTM of proteins.

A recent chemogenetic analysis predicted the possibility of up to 44 PRMTs may be present in the human proteome (Richon *et al.*, 2011). However, only nine mammalian PRMTs have been definitively characterized so far. All nine PRMTs are ubiquitously expressed in different types of human tissue and disruption in activity of these enzymes has been shown to perturb critical signaling pathways that are important in various diseases, including cancer (Wei *et al.*, 2013).

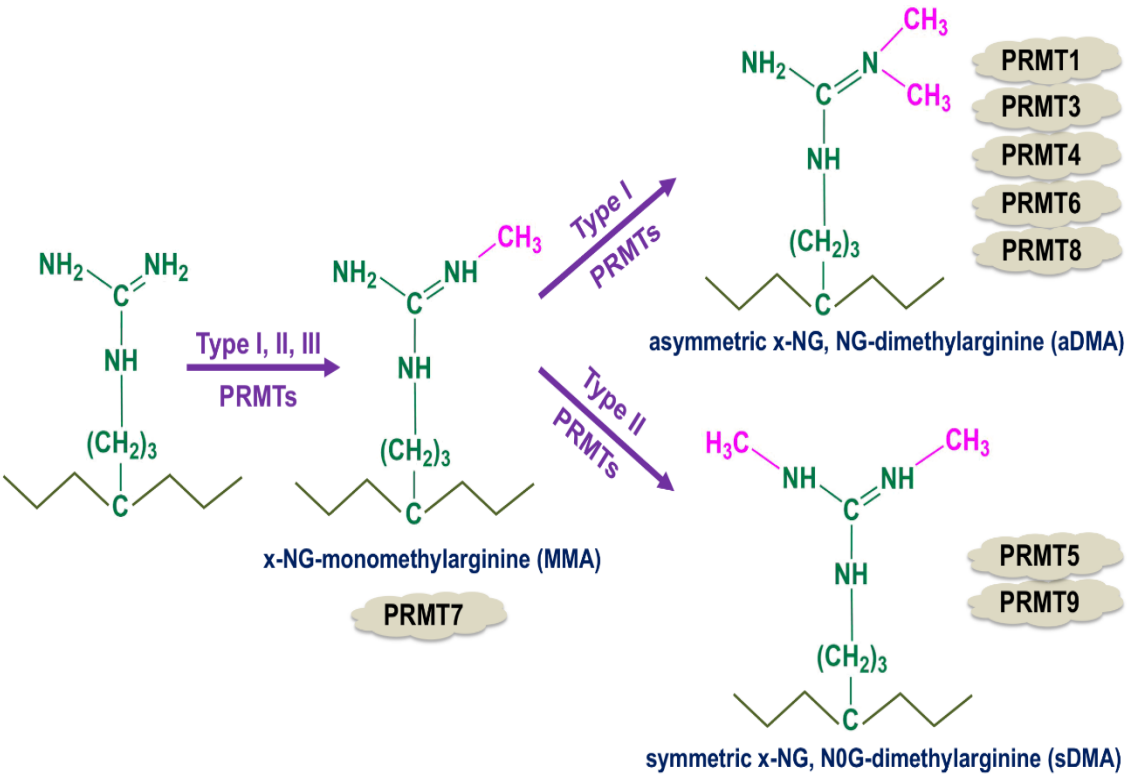

Figure 4. Methylation pattern of PRMT family members
Three types of methylated arginine patterns are observed in mammalian cells. The first is monomethylarginine (MMA), which is catalyzed by all PRMTs and involves addition of one methyl group on the terminal nitrogen atom of the arginine. Type III PRMT7 can only catalyze MMA. The second group of enzymes known as type I PRMTs (i.e. PRMT1,2,3,4,6,8) catalyze asymmetric dimethylarginine (aDMA), which involves addition of two methyl groups placed on the same terminal nitrogen atom of the arginine. The third and final methylation pattern is the symmetric dimethylarginine (sDMA), in which two methyl groups are placed on each of the terminal nitrogens of the arginine in a symmetric pattern. This is catalyzed by type II PRMTs, i.e. PRMT5 and PRMT9.

The 9 PRMTs are divided into three groups based on their symmetric or asymmetric R residue methylation pattern: **type I PRMTs** catalyze the formation of x-NG-monomethylarginine (MMA) and asymmetric x-NG, NG-dimethylarginine (aDMA); **type II PRMTs** catalyze the formation of MMA and symmetric x-NG, N0G-dimethylarginine (sDMA), and **type III PRMTs** bring about only monomethylation. Type I PRMTs include PRMT1, 2, 3, 4, 6, and 8, while PRMT5 and 9 are Type II PRMTs. PRMT7 is classified as a type III PRMT (**Figure 4**). Ratios of the three types of methylation in different cell types is estimated to be approximately 1500:3:2:1 for Unmethylated:ADMA:MMA:SDMA (Dhar *et al.*, 2013). There is a tenth form of PRMT characterized in yeast that catalyzes the monomethylation of an internal guanidinium nitrogen atom. However higher eukaryotes lack a homologue for this subtype (Zobel *et al.*, 1998). Majority of the PRMTs methylate glycine (G)- and R-rich (GAR) motifs in their substrates (Boffa *et al.*, 1977), with PRMT4 being the only exception in that it methylates R residues sequestered in proline (P)-, G- and methionine (M)-rich (PGM) regions (Lee *et al.*, 2002, Cheng *et al.*, 2007). PRMT5 can dimethylate R residues in both GAR and in PGM motifs (Branscombe *et al.*, 2001; Cheng *et al.*, 2007). These PRMTs, by adding mono- or dimethyl groups to R residue alter the availability of hydrogen donor sites on the substrate proteins as addition of methyl groups occupy these respective sites. Moreover, methylation leads to a change in the size of the protein, with either ~14 Da (MMA) or ~28 Da (aDMA or sDMA) added to its overall mass. Both of these alterations in protein structure can affect the potential interactions with its binding partners.

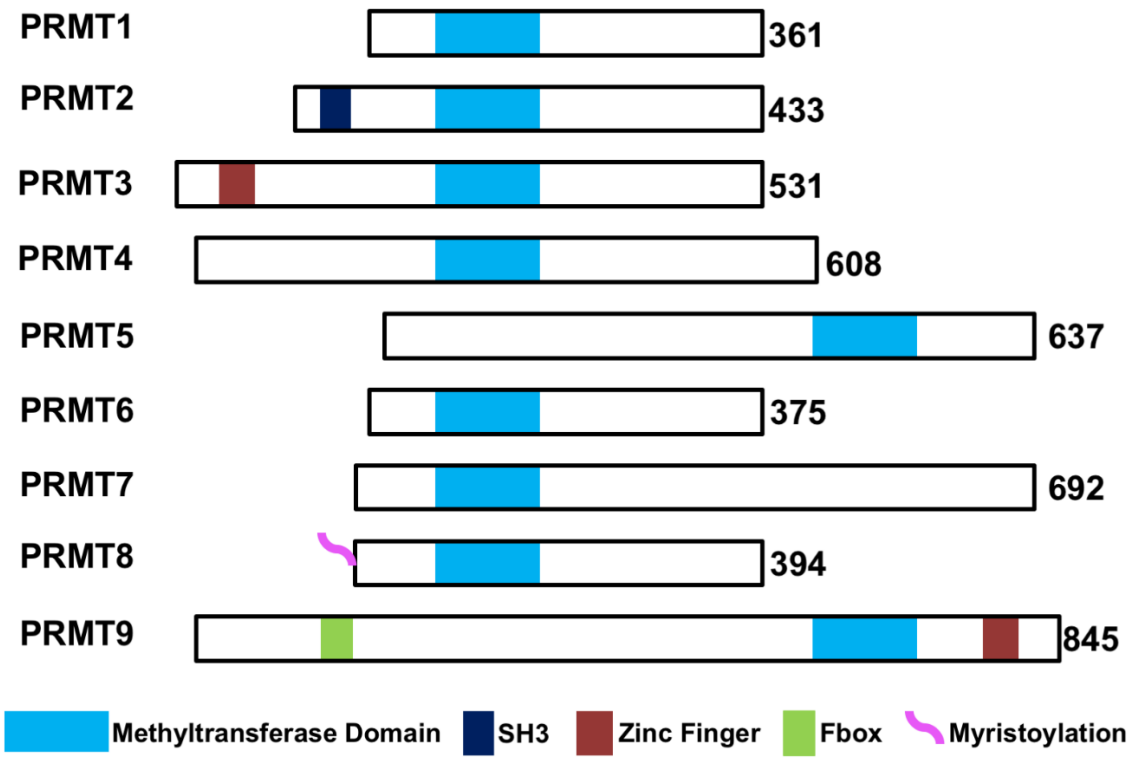

Figure 5. Structures of PRMT superfamily
All members of the PRMT have a common methyltransferase domain, denoted in light blue. Besides this, some members may have some distinct structures, such as a SRC homology 3 (SH3) domain (denoted in dark blue) in PRMT2, zinc finger in PRMT3 and 9 (denoted in red), F-box domain in PRMT9 (denoted in green) and a N-terminal myristoylation tag (denoted in pink). Adapted from Wei *et al.*, 2013.

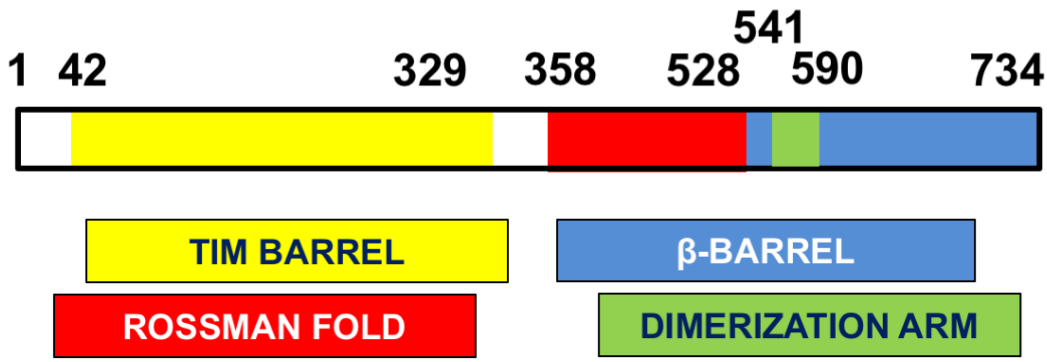

Figure 6. Human PRMT5 structure
PRMT5 consists of 3 major domains: TIM barrel at the N-terminus that mediates interactions with its cofactor methylosome protein 50 (MEP50) and promoting oligomerization by interacting with the catalytic domain. Rossman fold and β-barrel mediates interactions with the methyl donor SAM and substrates respectively. Dimerization domain aids in formation of possible multimeric complexes.

In terms of structure, all PRMT family members share a highly conserved methyltransferase domain in their structure (**Figure 5**). The Rossman fold contributes to co-factor binding whereas the β-barrel mediates substrate binding (Cheng *et al.*, 2005) **(Figure 6)**. Apart from these conserved core sequences, variation is seen at the N- terminus with respect to the structural domains present in different PRMTs. For instance, interactions with other proteins are mediated by an SRC homology 3 domain (SH3) domain in PRMT2, a zinc finger in PRMT3, a pleckstrin homology (PH) domain in PRMT4 and a triosephosphate isomerase (TIM) barrel in PRMT5 (Schapira *et al.*, 2014) (**Figure 5**). This contributes to the differences in the substrates and cellular functions within the members of the PRMT family.

Amongst these, PRMT5 has emerged as one of the most promising therapeutic targets in cancer mainly on the basis of findings specifically from our lab among others (Gulla *et al.*, 2018, Prabhu *et al.*, 2017, Chan-Penebre *et al.*, 2016). Overall, the focus of my dissertation has been to understand the potential of PRMT5 as a novel therapeutic target for PDAC and CRC. In the following sections, I provide an overview about PRMT5 and its critical substrate, NF-κB as well as elaborate on the rationale for developing inhibitors to reduce PRMT5 methyltransferase activity, therefore leading to the inhibition of cancer progression in PDAC and CRC.

1.3.2 PRMT5

As a type II methyltransferase, PRMT5 is responsible for majority of symmetric dimethylation occurring in human tissues. Though both PRMT5 and 9 belong to type II PRMTs, Yang *et al.* (2015) clearly demonstrated that PRMT5 was responsible for majority of the symmetric dimethylation observed in cells. And PRMT5 and PRMT9 did not show redundancy with respect to their substrates.

1.3.2A *More Aspects Regarding PRMT5 Structure*

A recent review describing the known structural information regarding PRMT5 indicated distinct homology between species (Schapira *et al.*, 2014). For instance, *Caenorhabditis elegans (C. elegans)*, *Xenopus laevis (X. laevis)* and human PRMT5 isoforms all comprise the Rossman fold sandwiched between the TIM barrel at the N-terminus and a β-barrel with a dimerization domain at the C-terminus (**Figure 6**).

Additionally, researchers found that a glutamine residue (E444) is critical for its methyltransferase activity and is located in the catalytic cleft of human PRMT5. A phenylalanine residue (F327) has been shown to be critical for specifically contributing the symmetric dimethylation activity (Sun *et al.*, 2011). Furthermore, mutation of F327 to M residue led PRMT5 to have both symmetric and asymmetric dimethylation activity, indicating that the steric interactions that occur at the F327 site play a crucial role in determining the specific symmetric dimethylation pattern of PRMT5.

1.3.2B *PRMT5, Global Biological Functions, and Its Role in Cancer*

PRMT5 is widely expressed in mammals and is universally found in embryonic as well as adult tissues (**Figure 7**). It has a wide-ranging role in terms of its substrates and the downstream functions that are affected. A complete list of known PRMT5 substrates is illustrated in **Table 1**. In fact, PRMT5 is very critical in early development, as previous work has shown that PRMT5 null mutants were embryonic lethal in mice due to an elimination of pluripotent stem cells in the blastocyst (Tee *et al.,* 2010). Moreover, PRMT5 is also required for cell proliferation of human embryonic stem cells (Gkountela et al., 2014). These cellular functions of PRMT5 are regulated via methylation of its substrates. Specific PRMT5 substrates include several histone proteins. For instance, the aforementioned biological functions, PRMT5 has recently been shown to methylate transcription factors, including NF-κB (Wei *et al.,* 2013), which we described in Section 1.2, and other examples, which we will further elaborate on histones H2A and H4 are methylated on R3 during germ cell development. Histone H3 is methylated on the R8 which may repress transcription and symmetric dimethylation of H3R2 supports euchromatin maintenance (Migliori *et al.,* 2012). In addition to histone proteins, other PRMT5 substrates include small nuclear ribonucleoproteins SmD1 (SNRPD1) and SmD3 (SNRPD3) and B/B', all of which are required for spliceosomal assembly and biogenesis (Brahms *et al.,* 2001; Meister *et al.,* 2001). PRMT5 can also methylate a domain in C-terminus of RNA polymerase II (RNAP II) to facilitate the resolving of RNA-DNA hybrids, a step that is critical for termination of transcription (Zhao *et al.*, 2016).

Interestingly, PRMT5 has also been shown to play a critical part in adult hematopoiesis as PRMT5 deletion led to a complete loss of both hematopoietic stem cells as well as progenitor cells in the bone marrow (Liu *et al.*, 2015). This suggests a possible role of PRMT5 in development of blood cell lineage, a crucial cellular function. Related to the role of PRMT5 within the bone marrow, another study highlighted that PRMT5 could activate osteoclast differentiation and inhibition of PRMT5 partially suppressed this process (Dong *et al.*, 2017). Osteoclast differentiation often occurs in conjunction with activation of inflammation-related pathways and thus provides evidence of a critical link between PRMT5 and inflammation in cells. Clearly, PRMT5 can play an important role in regulating the function of a wide variety of histone and non-histone proteins and in turn have direct and indirect downstream effects on critical signaling pathways and hence has an emerged as a protein of interest with potential implications in a diverse set of diseases, including cancer.

1.3.2C *PRMT5 in Cancer*

Recent research has highlighted the contribution of PRMT5 in various types of cancer. Symmetric dimethylation of H2AR3, H3R2, H3R8 and H4R3 can affect cellular proliferation and differentiation in leukemia and lymphoma cells. Methylation at these sites is associated with decreased transcription of several genes such as RB, ST7, and NM23 (Pal *et al.*, 2004, Wang *et al.*, 2008). Furthermore, in chronic myelogenous leukemia, silencing PRMT5 eliminated leukemia stem cells that have been shown to promote resistance to current

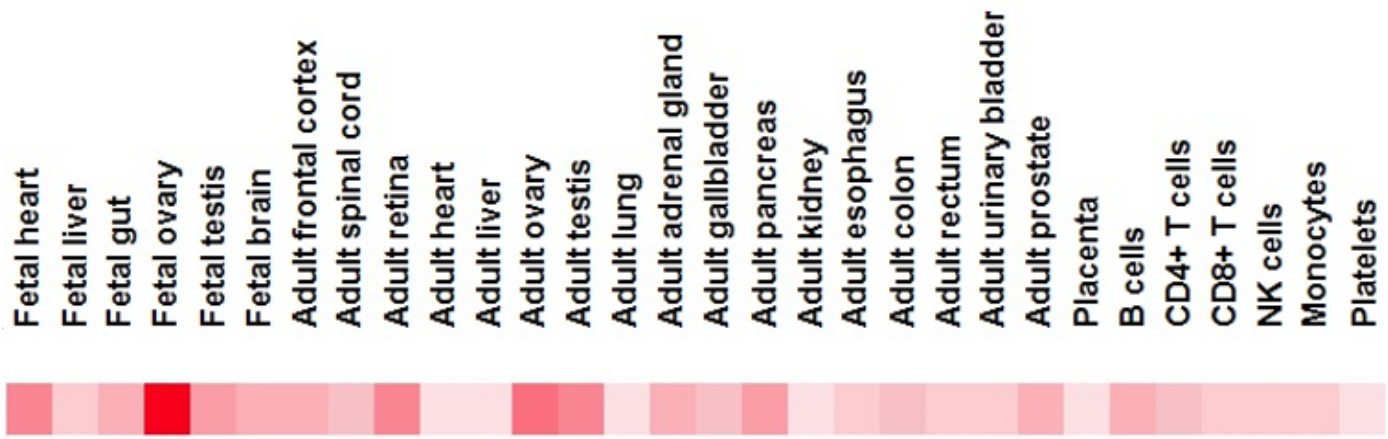

Figure 7. PRMT5 distribution in embryonic and adult human tissue
Using the human proteome map database (www.humanproteomemap.org), proteome-wide mass spectrometry analysis showed that PRMT5 is universally expressed in both embryonic and adult tissue (Kim *et al.*,2014).

Table 1. Known PRMT5 substrates and methylation sites

PRMT SUBSTRATE	KNOWN SITE	CITATION
ASH2L	R296	Butler *et al.*, 2011
CBP-1	R234	Yang *et al*., 2009
CF I(m)68	GAR Motif	Martin *et al.*, 2010
EBNA	GAR Motif	Shire *et al.*, 2006; Liu *et al.*, 2013
EGFR	R1175	Hsu *et al.*, 2011
FEN1	R192	Guo *et al.*, 2010
H2A	R3	Tee *et al.*, 2010
H3	R2	Yuan *et al.*, 2012; Tsai et al., 2013
H3	R8	Pal *et al.*, 2004 & 2007
H4	R3	Yue *et al.*, 2013; Girardot *et al.*, 2014
HOXA9	R140	Bandyopadhyay *et al.*, 2012
LSm4	--	Brahms *et al.*, 2001
$Na_V1.5$	--	Beltran-Alvarez *et al.*, 2013
NF-κB	R30, R35, R174	Wei *et al.*, 2013; Harris et al., 2014 & 2016
Nucleolin	--	Guderian *et al.*, 2011
Nucleoplasmin	GAR Motif	Wilczek et al., 2011
p53	R333, 335, 337	Jansson et al., 2008
PDCD4	R110	Powers et al., 2011
RNAPII	R1810	Zhao et al., 2016
RPS10	R158, 160	Ren et al., 2010
RUVBL1	R205	Clarke et al., 2017
SKI	R8	Tamiya et al., 2018
SmD1	GAR Motif	Brahms et al., 2001
SmD3	GAR Motif	Brahms et al., 2001
SPT5	R698	Kwak et al., 2003

therapies (Jin *et al*., 2016). Additionally, PRMT5 mutations are found in a wide range of cancers according to The Cancer Genome Atlas project database (Gao *et al.*, 2013). PRMT5 has also been dubbed as a “potential oncoprotein” as it upregulates factors involved in cell cycle regulation like G1 cyclins and cyclin dependent kinases as well as the phosphoinositide 3-kinase (PI3K)/AKT signaling pathway (Wei *et al.,* 2012). Gu *et al.* demonstrated that PRMT5 is essential for the growth of solid tumors like lung cancer cells by showing that PRMT5 knockdown in lung adenocarcinoma A549 cells partially downregulated the fibroblast growth factor receptor signaling pathway, which not only reduced cell growth and tumor (Gu *et al.,* 2012) but also promoted metastasis (Jing *et al.*, 2018), the latter phenotype reportedly through PRMT5-mediated regulation of miR-99. This showed that PRMT5 was capable of mediating tumor growth and metastasis through epigenetic regulation of micro RNAs. PRMT5 expression was also significantly upregulated in hepatocellular carcinoma tissue and correlated with higher cell proliferation, possibly via the Wnt/β-catenin signaling pathway. Silencing PRMT5 downregulated β-catenin expression and its downstream effector cyclin D1, thereby suggesting a link between PRMT5-mediated β-catenin-driven cell proliferation in these cells (Zhang *et al.*, 2015). Furthermore, in hepatocellular carcinoma cells, the ERK signaling pathway was also shown to be regulated by PRMT5, and subsequently had a profound effect on cell proliferation in these cells (Jiang *et al.*, 2018). Thus overall, PRMT5 plays a critical role in promoting the cancer phenotype through varied signaling pathways in hepatocellular carcinoma. Another critical signaling pathway, TGF-β has also

been shown to be regulated by PRMT5 via coupled arginine methylation of histones H3 and H4, leading to subsequent transcriptional activation and repression of key regulatory genes involved in cancer respectively (Chen *et al.*, 2017).

The well-known tumor suppressor gene p53 has also been shown to be a substrate of PRMT5 in osteosarcoma cells. For instance, ectopic expression of PRMT5 in osteosarcoma cells enhanced p53-mediated DNA damage repair (Jansson *et al.*, 2008). This is especially harmful in cancers as most chemotherapeutic drugs work on the principle of inducing DNA damage in cancer cells to cause cell death. Induction of DNA repair response reduces the efficacy of the chemotherapeutic drug, possible contributing to drug resistance. Furthermore, gene expression data also showed that PRMT5 is upregulated in a number of cancers including breast, cervix, liver, prostate, lung, ovary and bladder, and particularly in PDAC and CRC, which are the disease focus of my work (Wei *et al.*, 2013). Additionally, ulcerative colitis (a risk factor for CRC) was associated with increased local PRMT5 expression by regulating the activity of regulatory T cells (Zheng *et al*., 2017), indicative of its link to immune function in colon cells. Finally, as mentioned in the previous section, a complete list of known substrates with methylation mark introduced by PRMT5 is illustrated in **Table 1**. Several of the substrates have already been described in this chapter as important players in cancer such as EGFR, histones and p53 amongst others. Based on this compilation of its substrates, it is clear that PRMT5 can play an

important role in regulating the function of a wide variety of histone and non-histone proteins with critical implications in cancer.

In this thesis, we have focused on the PRMT5 substrate: NF-κB, based on our discovery that PRMT5 activates NF-κB through R30 methylation of the p65 subunit (Wei *et al.*, 2013). This finding has opened up additional possibilities of targeting PRMT5 as a novel approach to inhibit NF-κB, apart from the ones listed above. Since NF-κB is a well-known tumor promoting factor and is constitutively activated in both PDAC and CRC, as described in **Section 1.2**, inhibiting PRMT5-mediated NF-κB activation could offer the hope of new approaches to combat PDAC and CRC as well as other cancers. In the future, it will be interesting to explore the crosstalk between signaling pathways and specific substrates regulated by PRMT5 and possible implications in cancer as well as how they could be therapeutically targeted to design an effective solution for patients suffering from this deadly disease.

1.3.2D *Promise of Developing PRMT5 Inhibitors*

Epigenetic enzymes capable of catalyzing PTMs have emerged as an attractive target in recent times, with histone deacetylase (HDAC) enzyme family inhibitors such as Vorinostat and Romidepsin already approved by FDA for use in lymphoma patients. Inhibitors of other HDAC family members and sirtuins (protein deacetylases) have shown early clinical promise (Eckschlager *et al.*, 2017). Unfortunately, the clinical success seen in blood cancers has not been

replicated in clinical trials of HDAC inhibitors in solid tumors (Slingerland *et al.*, 2014; Qiu *et al.*, 2013). The exact reasons have not been established for this dichotomy, but differential drug accessibility and tumor microenvironments potentially could play a role in many drugs to work better in liquid tumors as compared to solid tumors. Other epigenetic enzyme families with previously unexplored potential as targets are now being considered in drug discovery for solid tumors.

With regards to PRMT5, there are no known inhibitors in clinical trials. In that regard, my thesis focuses on the role of PRMT5 as a therapeutic target, at least via reducing the constitutive activation of NF-κB observed in PDAC and CRC. While we were developing inhibitors of PRMT5, a PRMT5 inhibitor, EPZ015666 was identified by Epizyme Inc. and showed high efficacy in inhibiting PRMT5 in mantle cell lymphoma disease models (Chan-Penebre *et al.*, 2016). Since we were currently developing our own unique inhibitor at the time and EPZ015666 was commercially available for purchase, we used it in our own studies to compare its activity against our inhibitor in PDAC and CRC models, and these results have been included in **Chapters 4 and 5**.

1.4 Summary and Hypotheses

Previous studies have shown that PTMs of the p65 subunit like acetylation and phosphorylation can modulate NF-κB activity. However, methylation was not shown to affect its functional role until now. Our lab was the first to show that NF-κB activity can be modified by PRMT5. Symmetric dimethylation by PRMT5

leads to NF-κB activation and increased transcription of the NF-κB target genes. This suggests a mechanism by which PRMT5-mediated methylation of p65 could promote inflammation and anti-apoptotic responses in PDAC and CRC via upregulation of NF-κB target genes. This is also supported by the fact that expression of PRMT5 is greatly overexpressed in PDAC and CRC. Thus, PRMT5 can act as a tumor promoting factor, at least with respect to NF-κB activation in PDAC and CRC cells and therefore has great potential to be used as a novel drug target to treat these diseases.

Furthermore, we have adapted the AlphaLISA™ (Amplified Luminescent Proximity Homogeneous Assay-Linked immunoSorbent Assay) technique to sensitively quantify the levels of PRMT5 methylation that can be used to screen for small molecule inhibitors of PRMT5 activity. AlphaLISA assay is a bead-based chemiluminescent screen which recognizes the dimethyl tag specific to PRMT5 and the amount of detected signal is proportional to the amount of methylation of a substrate peptide by PRMT5. Hence this assay allowed us to quantify the enzymatic activity of PRMT5.

Overall, this research proposes a novel hypothesis that PRMT5 can contribute to PDAC and CRC pathogenesis, at least partly via NF-κB activation and can be used a novel drug target for their treatment. In this regard, we used the AlphaLISA technique to screen for drugs that can possibly benefit for PDAC and CRC patients.

CHAPTER 2. METHODS

2.1 *In Vitro* Experiments

2.1.1 Cell Lines & Materials

Pancreatic control (HPNE) and cancer cell lines (PANC1, MiaPaCa2 and AsPC1) were a kind gift from Dr. Murray Korc from Indiana University School of Medicine (IUSM). The normal colon cell line (FHC) and CRC (HT29, HCT116, DLD1) cell lines were purchased from the American Type Culture Collection (ATCC). All pancreas-derived cell lines were grown in Dulbecco's Modified Eagle Medium (DMEM) (GE Healthcare), supplemented with 1% of penicillin/streptomycin and 5% fetal bovine serum (FBS). CRC cells were maintained in Roswell Park Memorial Institute Medium (RPMI 1640) (GE Healthcare), containing 1% penicillin/streptomycin and 5% FBS, while FHC cells were cultured under the same conditions with further addition of 25mM HEPES (4-(2-hydroxyethyl)-1-piperazineethanesulfonic acid), 10ng/ml cholera toxin, 0.005 mg/ml insulin, 0.005 mg/ml transferrin and 100 ng/ml hydrocortisone. All cell lines were cultured at 37°C under 5% CO_2 and used between passages 2 to 5. Cell lines were authenticated using 9 Marker STR Profile by IDEXX Bioresearch.

For AlphaLISA, the methyl group donor SAM (S-adenosyl methionine) was purchased from New England Biolabs. Unmethylated biotinylated histone H4 peptide substrate at arginine (R) 3 (unmeH4R3) was obtained from AnaSpec. The 23-amino acid sequence of H4R3 peptide was as follows:

SGRGKGGKGLGKGGAKRHRKVLRGG-K(biotin)-NH2, with the third arginine site available for demethylation as per the assay protocol. For screening, dimethyl sulfoxide (DMSO) stock of library compounds comprising of approximately 10,000 small molecule inhibitors purchased from ChemDiv and another 10,000 group of compounds with pure natural products, semi-synthetic natural products and reported bioactives collectively purchased from Analyticon Discovery, MilliporeSigma and Microsource Discovery Systems Inc. The compound libraries were stored at -80°C. Anti-methyl-H4R3 AlphaLISA beads, Streptavidin-tagged Donor beads, 1X Epigenetics buffer, TopSeal™-A film, OptiPlate™-384 white opaque plates, and EnVision® Multilabel Reader were obtained from PerkinElmer.

2.1.2 Generation of Stable PRMT5 Overexpressing and Knockdown Cell Lines

Flag-tagged WT-PRMT5 or shPRMT5 cDNA was generated by from total mRNA derived from 293 cells. After confirming the insertion by sequencing, the cDNA constructs were cloned into pLVX-IRES-puro vector (Lu *et al.*, 2010). A pool of 5 shRNAs against PRMT5 (Sigma-Aldrich) were used to ensure efficient knockdown of this target. The respective lentiviral plasmids containing empty vector, WT-PRMT5 or shRNAs were transected into a 293T packaging cell line with high efficiency to produce viral preps that were used to infect PANC1 or HT29 cells. Upon 48h of infection, cells were exposed with 1µg/mL of puromycin, allowing further selection, as the lentiviral vector contains a puromycin resistance

gene. Western Blotting using PRMT5 Ab was used to confirm the overexpression and knockdown in these cells.

2.1.3 Western Blotting

Cultured cells were pelleted by scraping them in 1X phosphate buffered saline (PBS), followed by centrifugation at 5,500 rpm for 5 min. The supernatant was aspirated, and pellets were frozen overnight at -80°C. Next day, RIPA buffer [10mM Tris-Cl pH 8.0, 1mM EDTA, 1% Triton X, 0.1% sodium deoxycholate, 0.1% SDS (sodium dodecyl sulfate; electrophoresis grade), 14mM NaCl, 1mM PMSF] was added to the pellets, combined with intermittent vortexing and incubation on ice to promote lysis. The cells were pelleted at 5,500 rpm for 5 min. The supernatant for each sample was then tested for its protein concentration using the Protein Assay Reagent (Biorad) and absorbance values measured using a Genesys 10S Vis spectrophotometer (Thermo Fisher Scientific), to ensure equal loading of the samples on the gel. Prior to running the samples on the gel, equal protein concentrations are mixed with 2X SDS sample loading buffer [100mM Tris-Cl, pH 6.8, 4% (w/v) SDS, 0.2% (w/v) bromophenol blue, 20% (v/v) glycerol, 200mM β-mercaptoethanol]. Each sample mixture was then heated at 100°C for 5 min and gently spun down to gather all the sample at the bottom of the tube. These protein samples were then run on a 10% SDS-PAGE (sodium dodecyl sulfate polyacrylamide gel electrophoresis) gel and then transferred overnight to a polyvinylidene fluoride (PVDF) membrane (Fisher Scientific) at 4°C. Primary antibodies for anti-PRMT5 (Abcam), anti-Flag

(Sigma-Aldrich), anti-dimethyl arginine motif (sdme-RG) (Cell Signaling Technology), symmetric dimethylation at R30 subunit of p65 (detected by generating a customized polyclonal primary antibody in collaboration with GenScript Inc), β-actin (Sigma-Aldrich) and their corresponding secondary antibodies were used. The enhanced chemiluminescence (ECL) detection method (PerkinElmer) was conducted to detect the protein signal.

2.1.4 Immunohistochemistry Assay

Pancreatic and colon cancer tissue microarrays with matched normal adjacent controls were acquired from US Biomax Inc. The tissue microarrays were blocked using protein-blocking solution (Dako Corp.) for 30 min. All subsequent staining steps were performed using the Dako FLEX SYSTEM and an automated Immunostainer. Incubations were carried out at room temperature (R.T.) and Tris buffered saline containing 0.05% Tween 20, pH 7.4 (Dako Corp.) was used for all the washes and diluents. Anti-PRMT5 primary antibody (Abcam) was used to detect PRMT5 localization. Horseradish peroxidase-conjugated secondary antibody was then used, followed by addition of the chromogen, which formed a brown precipitate at the binding site of secondary antibody. Imaging was done using Aperio whole slide digital imaging system. The system imaged all slides at 20X magnification.

2.1.5 Cell Proliferation Assay

Stable PANC1 and HT29 cells with WT-PRMT5, shPRMT5 and empty vector control overexpression respectively were seeded in triplicates in 6-well

plates at $2X10^4$ cells/well. Cells were trypsinized at day 3, 5, 7, 9 and counted using a hemocytometer chamber.

2.1.6 Anchorage-Independent Growth Assay

2.5% and 1.25% agar were used to prepare the bottom and top layers of the soft agar, respectively. The bottom agar was added to each well of a 6-well plate. $2X10^5$ cells for each cell line were then mixed into top agar solution and layered on top of the bottom layer. The plates were incubated for 10-20 days at 37°C and 5% CO_2. Images were captured using a Canon EOS Rebel T3i Digital SLR camera and quantification of colony size and number was performed using ImageJ.

2.1.7 Migration Assay

Migration assay was conducted using Boyden chambers. 8μm pore size cell culture inserts (Corning) were placed in a 24-well plate. Each chamber was coated with gelatin on the side facing the lower chamber. $2X10^5$ cells were suspended in serum-starved media in the upper chamber of the well. Corresponding serum rich media was added to the lower chamber. Migrated cells were fixed using 4% formaldehyde followed by crystal violet staining and counting using a microscope at 20X magnification. The images were captured using a Canon EOS Rebel T3i Digital SLR camera.

2.1.8 NF-κB luciferase Assay

The NF-κB luciferase construct p5XIP10 (containing five tandem copies of the NF-κB site from the IP10 gene) was transfected transiently in the cell lines using Lipofectamine™ LTX Reagent and PLUS Reagents (Thermo Fisher Scientific). Luciferase activity was assayed 48h later (with or without PRMT5 small molecule inhibitor treatment, if applicable) by using the Luciferase Assay System with Reporter Lysis Buffer kit (Promega) as per the manufacturer's instructions. The activity was measured using a Synergy H1 Multi-Mode Reader (BioTek Instruments Inc).

2.1.9 Quantitative PCR

Cells were cultured to 90% confluence (followed by treatment with compound, if applicable) and total RNA was isolated using Trizol as described previously (Wei *et al.*, 2013). cDNA was prepared from total RNA by reverse-transcriptase PCR using the SuperScript III First-Strand Synthesis System (Invitrogen). qPCR was carried out using FastStart Universal SYBR Green Master ROX kit (Roche). Primers were designed by Primer Express 3.0 software and are listed in **Appendix A**.

2.1.10 PRMT5 Enzyme Purification

Flag-tagged PRMT5 enzyme was purified from 293 cells overexpressing Flag-PRMT5 by co-immunoprecipitating with Flag beads (MilliporeSigma). 293-Flag-PRMT5 cells were cultured in 15cm plates at ~90% confluency per plate.

After washing the cells with 1X PBS, the cells were spun down at 1,200 rpm for 10 min at 4°C. The pellets were lysed by adding lysis buffer (50mM Tris-HCl, pH 7.4, 150mM NaCl, 1mM EDTA, 100nM phenylmethanesulfonyl fluoride (PMSF), 0.5M Na_3NO_4, 1% Triton X-100 and protease inhibitor tablets) and vortexing 4-5 times over a period of 20 min. The lysed cells were spun at 3,400 rpm for 30 min, and the supernatant was transferred to the prewashed Flag beads suspended in 1X cold PBS. The lysed cells/beads mixture was rotated at 4°C. After overnight incubation, the beads were spun down and washed 4 times using 1X wash buffer (50mM Tris-HCl, pH 7.4, 150mM NaCl, 1mM EDTA, 0.5% Triton X-100). After the washing steps, the beads were mixed with Flag peptide and rotated for 1 h at 4°C, then spun down. Supernatant (the PRMT5 enzyme product) was added with storage buffer (40mM Tris, 110mM NaCl, 2.2mM KCl, 3mM dithiothreitol (DTT), 20% glycerol), and used immediately for the AlphaLISA assay or aliquoted at -80°C until further use.

2.1.11 AlphaLISA-based H4R3me2 Detection Assay

The AlphaLISA reaction was run in 384-well white opaque plates with a total reaction volume of 30µl. All the parameters of the assay were determined using standardized conditions by testing 10-100nM of unmeH4R3 and of 0.2-4000µM SAM. In the pilot experiments as well as the Z' test, the following protocol was used: the biotinylated unmeH4R3 substrate stock as well as the SAM stock was diluted using milliQ water with final concentrations of 30nM and 100nM respectively in the reaction well. The PRMT5 enzyme prep was diluted at

1:10 ratio in Assay buffer (30mM Tris, pH 8.0, 1mM DTT, 0.01% Bovine serum albumin, 0.01% Tween-20) before being used. 10µl of unmeH4R3:SAM mixture and 10µl of diluted enzyme stock were mixed in each well and incubated at R.T. for 1 h. Following this step, the Acceptor bead stock (with an antibody tag specific for H4R3me2) was diluted 1:50 using 1X Epigenetics buffer to a final concentration of 20µg/ml. 5µl of the diluted bead stock was dispensed in each of the reaction wells. After incubation with the Acceptor beads for 1 h at R.T., the streptavidin-coated Donor bead stock (specific for the biotinylated substrate) was diluted at 1:50 using 1X Epigenetics buffer to a final concentration of 20µg/ml, and 5µl was dispensed in each of the reaction wells (**Table 1**). Following incubation with Donor beads for 30 min in the dark, the plates were immediately read using the “Alphascreen” filter in the EnVision® Reader. To assess background of the reaction in the negative control wells, all the conditions were the same except 10µl of 1X assay buffer was added instead of enzyme stock.

2.1.12 High-throughput Screening

For the HTS, we used the optimized protocol as described in **Table 1**. Briefly, 10µL of the substrate 2X mix (60nM unmethylated peptide, 200µM SAM in MilliQ water) was dispensed using Multidrop into each well of the assay plates. The final reaction concentration was 30nM unmeH4R3 peptide and 100µM SAM. Next, 250nL of 1mM DMSO stock of the library compounds was transferred to columns 1-20, with a final compound concentration of 12.5µM and final DMSO of 1.25% in each well. 5% DMSO/water (1% DMSO final) was added to column 21-

24 to keep the DMSO concentration consistent with the wells in which the compounds were added. Next, 10μL of enzyme (ten-fold dilution of the enzyme prep in assay buffer) was dispensed to columns 1-22 using MultiFlo in each plate. At the same time, 10μL of the 1X assay buffer was added to columns 23-24 in each plate. Thus, columns 21-22 serve as positive “maximum signal” controls (no inhibitor, with PRMT5 enzyme added) and columns 23-24 act as “background signal” controls (no inhibitor, no enzyme added). Columns 1-20 in each plate had the different inhibitors added, with 1 replicate for each compound in the library. The plates were incubated at R.T. for 1 h. 5μL of anti-H4R3me2 Acceptor beads (1:50 dilution of the 5mg/mL stock in 1X Epigenetics Buffer) were then dispensed using MultiFlo into each well of the assay plates. The plates were incubated at R.T. for 1 h. 5μL of Donor beads (1:50 dilution of the 5mg/mL stock in 1X Epigenetics Buffer) were dispensed using MultiFlo into each well of the assay plates. The plates were incubated at R.T. for 30 min followed by Alpha signal reading on EnVision® reader.

We conducted two rounds of HTS as described: the first round included a set of 10,000 chemical inhibitor library from ChemDiv. For the second round, we used the following libraries: (1) LOPAC 1280 (2) Spectrum 2400 (3) AnalytiCon MEGx 1000 (4) AnalytiCon NATx 5000. LOPAC and Spectrum compound libraries comprise of known drugs, natural products and reported bioactives. AnalytiCon MEGx and NATx contain pure natural products and semi-synthetic natural products, respectively.

Table 2. Protocol for high throughput screening for PRMT5 AlphaLISA assay

Step	Parameter	Value	Description
1	Dispense substrate & cofactor	10µl	2X mix of SAM/peptide
2	Dispense compounds	250nL	80X compound (1.25% (v/v) DMSO)
3	Dispense enzyme	10µl	2X PRMT5 enzyme
4	Incubation time	1h	RT, sealed
5	AlphaLISA Acceptor beads	5µl	1:42 dilution of Acceptor beads mix
6	Incubation time	1h	RT, sealed
7	AlphaLISA Donor beads	5µl	1:42 dilution of Donor beads mix
8	Incubation time	0.5h	R.T., sealed
9	Assay readout	615nm	EnVision plate reader; Alphascreen mode

Step Notes:
1. Final concentrations are 30nM Biotin-unmeH4R3, 100µM SAM prepared in MilliQ water.
2. Final compound concentration: 12.5µM; columns 21-24 do not have compound and have only DMSO/water with a final DMSO concentration at 1.25%.
3. Columns 23 and 24 only has no enzyme, prepared in enzyme reaction buffer.
4. Plates sealed with adhesive film and covered with aluminum foil.
5. Final concentration is 20µg/ml for Acceptor beads mix, prepared in the dark using 1X Epigenetics buffer.
6. Plates sealed with adhesive film, covered with aluminum foil and kept in dark.
7. Final concentration is 20µg/ml for Donor beads mix, prepared in the dark using 1X Epigenetics buffer.
8. Plates sealed with adhesive film, covered with aluminum foil and kept in dark.
9. Alphascreen (615nm) emission filter

2.1.13 Quenching Experiment

In this assay, the incubation and assay conditions were relatively similar to the HTS assay described above. The major differences were: (1) histone H4 pre-methylated at arginine 3 (Biotin-H4R3me2) (AnaSpec) was used as a substrate at a final concentration of 15nM; (2) No PRMT5 enzyme or unmethylated substrate was included in the experiment, and (3) The plate design differed as follows: the first two columns did not have any compound (positive control). Columns 1-22 had pre-methylated Biotin-H4R3me2 substrate. The last two columns did not have this pre-methylated substrate (negative control; background). Diluted AlphaLISA beads (Acceptor and Donor) were added to each well.

2.1.14 MTT [(3-(4, 5-dimethylthiazolyl-2)-2, 5-diphenyltetrazolium bromide)] Assay

Cells were seeded at 60% confluence in Corning® Costar® clear flat-bottom 96-well plates and titrated with different dosages of respective compounds. After incubation for 4 days, 10µl of MTT dye (Sigma-Aldrich) was added directly to each well. The dye was incubated with the cells for 2 h at 37°C. The media was then aspirated and 10µl of DMSO was then added to each well. The colorimetric dye was quantified using Synergy H1 Multi-Mode Reader from BioTek Instruments Inc.

2.1.15 3D colony Formation Assay

500 cells per well were seeded in media containing 3% Reduced Growth Factor (RGF)-Matrigel (BD Biosciences) in a Corning® Costar® ultra-low attachment multiwell plate and allowed to form colonies. PR5-LL-CM01 stocks made in 100% DMSO were diluted using 3% RGF-Matrigel media and added to the respective wells, in a 2-fold serial dilution concentration range from 0.75 to 25μM on days 3 and 7 after seeding. On day 7 post first drug treatment, the cells were stained using Alamar blue dye (Fisher) and quantified using a Synergy H4 Multi-Mode Reader (BioTek Instruments Inc).

2.1.16 Co-immunoprecipitation Experiment

293 cells with stable overexpression of Flag-p65 protein, were treated with 20μM of PR5-LL-CM01 for 24 h. After the cells were lysed using the lysis buffer (50mM Tris-HCl, pH7.4, 150mM NaCl, 1mM EDTA, 1% Triton X-100, 100nM PMSF, 0.5M Na_3NO_4) and vortexing, p65 was then pulled down with anti-Flag-M2 beads. The samples were then run on a 10% protein gel and probed with anti-symmetric dimethyl arginine motif (sdme-R) antibody (Cell Signaling Technology), to check for dimethylation levels of p65.

2.1.17 Structural Analysis and Docking Experiments

This experiment was done in collaboration with Dr. Ozlem Demir at the University of California, San Diego under the guidance of Dr. Rommie Amaro. For docking, chain A of PRMT5 protein in 4X61.pdb from the Protein

Databank was used. All docking experiments were performed by Glide program (version 6.8) of the Schrodinger suite 2015-3 in standard precision mode (Halgren *et al.*,2004; Freisner *et al.*, 2004). The protein was prepared for docking by the Protein Preparation Wizard of Schrodinger suite 2015-3 (Sastry *et al.*, 2013). Control docking experiment was performed by deleting the ligand PR5-LL-CM01 or EPZ015666 from the crystal structure while keeping the ligand SAM. The control docking experiment was able to reproduce the binding pose of EPZ015666 seen in the crystal structure. An additional docking experiment was done by docking EPZ015666 into the PRMT5 active site after deleting the SAM ligand as well as EPZ015666 from the active site. PR5-LL-CM01 was docked into the PRMT5 active site in two separate docking experiments. In one experiment, the compound was docked into the PRMT5 active site in which EPZ015666 is deleted while SAM is kept. In the other experiment, PR5-LL-CM01 was docked into the completely empty active site in which both SAM and EPZ015666 were deleted. All the figures for this experiment were prepared with Maestro version 10.3.

2.1.18 Methyltransferase Assay for PRMT5 Family Members

The specificity of inhibition by PR5-LL-CM01 against the enzymatic activity of protein arginine methyltransferase family members was analyzed using the HotSpot radioisotope-based platform (Reaction Biology Corp) as described previously (Horiuchi *et al.*, 2013). PRMT family members 1,3,4,5,6,8 were included in the study based on the availability with Reaction Biology Corp offering the

methyltransferase screening service. Briefly, PR5-LL-CM01 was incubated with a protein arginine methyltransferase, substrate, and tritium-labeled SAM. The PR5-LL-CM01 stock solution was prepared in DMSO at 10mM. PR5-LL-CM01 was tested at 1, 10, 25, 50 and 100μM. The methyltransferase inhibitor SAH (S-(5'-Adenosyl)-L-homocysteine) was used as a positive control. All reactions were carried out with 1μM tritium-labeled SAM and 5μM of peptide substrate. The assays were performed using Reaction buffer (50mM Tris-HCl, pH 8.5, 5mM $MgCl_2$, 50mM NaCl, 0.01% Brij35, 1mM DTT). Reactions were performed for 1 h at 30°C. Radiolabeled methylated product was detected using a filter-binding method. Curve fits and IC_{50} determination were executed as described previously (Horiuchi *et al.*, 2013).

2.1.19 Sepharose Bead-Based Binding Study

CNBr-activated Sepharose 4B beads (GE Healthcare) were used to conjugate PR5-LL-CM01 in order to measure the binding interaction of PR5-LL-CM01 with PRMT5. The first step involved activating beads by dissolving in 1mM HCl followed by washing with 1mM HCl in a 0.22μM filter. 10μmol of PR5-LL-CM01 or cycloheximide (CHX) were dissolved in coupling buffer respectively (0.1M $NaHCO_3$, pH 8.3; 0.5M NaCl). CHX was used as a non-specific protein that would not bind to the beads. The compound and bead solutions were then mixed together in a stoppered vessel in a round bottom tube and rotated the tubes overnight at 4°C. Only coupling buffer was added to the Beads only control tube. Next day, the beads were washed with coupling buffer and any remaining

active groups were blocked with 0.1M Tris HCl, pH 8.0 overnight at 4°C. Next day, the beads were washed with at least three cycles of alternating pH of 0.1M sodium acetate/acetic acid, pH 4.0 containing 0.5M NaCl and 0.1M Tris HCl, pH 8.0 containing 0.5M NaCl. Same day, 293-PRMT5-Flag cell lysates were prepared by washing and scraping the cells into cold 1XPBS per plate. The cells were pelleted by spinning at 1,200 rpm for 10 min at 4°C. Lysis buffer (50mM Tris HCl, pH7.4; 150mM NaCl; 1mM EDTA; 1% Triton X; with protease inhibitors) ~2-fold volume of the pellet size) was added to each tube for cell lysis. Cell lysate was collected after spinning at 5,500 rpm for 10min. Before adding the cell lysate to the beads, the beads were blocked with non-fat milk in lysis buffer (no inhibitors) for 1 h at R.T. We tested several blocking conditions as highlighted in **Figure 36A**. After spinning down the beads, they were incubated with cell lysate by rotating at 4°C overnight. The next day, beads were spun down at 13,000 rpm for 40 sec and unbound proteins were removed by washing beads 4 times with washing buffer (50mM Tris-HCl, pH 7.4, 150mM NaCl, 1mM EDTA, 0.5% Triton X-100) at 4°C. Finally, after last wash, the beads were spun down at 13,000 rpm, 40 sec and all the residual liquid on top of the beads was removed carefully to avoid accidental aspiration of the beads. These samples were run on an SDS-PAGE gel and Western blotting was carried out as previously described in **Section 2.1.3** by probing with anti-PRM5 antibody and corresponding secondary antibodies to check for PRMT5 pulldown with PR5-LL-CM01 conjugated beads.

2.1.20 Isothermal Calorimetry (ITC)

The reaction system for ITC consists of a sample well and an injection syringe. 350µl of 100-200µM of PRMT5 was added to the sample well. 10 X 15 cm plates with 293-PRMT5-Flag cells were used for enzyme purification as described in **Section 2.1.10**. 100µl of 5mM of PR5-LL-CM01 (dissolved in DMSO) was placed in the injection syringe. Both the components were dissolved in 1X ITC buffer (1XPBS, 110mM NaCl, 2.2 mM KCl, 3mM DTT) such that the final concentrations of the buffer in both the well and syringe were equalized to avoid buffer mistmatch. The reaction system was set at 25°C. The inhibitor was then automated to set up 50 serial injections every 5 minutes of 2µl each from the injection loop into the sample well. A curve with heat changes in the system with every successive injection over time was obtained at the end of the experiment.

2.1.21 Cellular Thermal Shift Assay

PANC1 or HT29 cells were cultured to 95% cell density in 4 X 10 cm plates per cell line. 2 plates were treated with DMSO vehicle and 2 plates were treated with either 20µM PR5-LL-CM01 for PANC1 or 40µM PR5-LL-CM01 for 2 h at 37°C. Cells were then trypsinized and resuspended in R.T. 1X PBS per plate. Equal number of cells were counted for each condition and centrifuged at 1,200 rpm for 10 min at R.T. to pellet the cells. After removal of PBS, 1 ml of R.T. 1X PBS was added to gently resuspend the cells. 100µl of cell suspension was added in each PCR tube (Two groups total: compound treated and DMSO

treated. Each group had 10 tubes). Each tube was marked with a designated temperature. The tubes are kept at R.T. before the heat treatment step. 10 PCR tubes (2 samples per temperature: +/- PR5-LL-CM01) were heated with temperatures of 40, 43, 46, 49, 52, 55, 58, 61, 64, 67°C for 3 min in the 96-well thermal cycler. Immediately after heating, the tubes were incubated at R.T. for 3 min, followed by immediately snap-freezing in liquid nitrogen. Cells were then lysed using alternate freeze thawing. The tubes were vortexed briefly after each thawing. The resulting cell lysates were then centrifuged at 10,000 rpm for 10 min at 4°C to pellet cell debris together with precipitated and aggregated proteins. The respective supernatants with the soluble protein fraction were then run on a protein gel and were probed with anti-PRMT5 antibody using Western blotting technique described earlier. This helped to quantify PRMT5 expression in the cell lysates at different temperatures which was then plotted to obtain a melting curve.

2.1.22 Generation of PR5-LL-CM01 Derivatives

In collaboration with Dr. Lifan Zeng at IU Chemical Genomics Core, we generated a total of 20 derivatives of the parental compound PR5-LL-CM01. A detailed account of the synthesis process is included in **Appendix B**.

2.2 *In Vivo* Experiments

2.2.1 Mice

Male NOD.Cg-Prkdc^{scid} Il2rg^{tm1Wjl}/SzJ (NSG) mice were obtained from the *In Vivo* Therapeutics Core (IVT) at Indiana University Melvin and Bren Simon Cancer Center. These mice are extremely immunodeficient strain and they lack mature T cells, B cells, and natural killer (NK) cells. Ideally, a mixture of male and female mice should be used and moving forward this will be our plan. Animals were housed in a pathogen-free environment and maintained on Teklad Lab Animal Diet (Harlan Laboratories). Access to sterile water and food was provided ad libitum under a 12 h light-dark cycle. The room temperature was maintained at 22-24°C. All studies described here were performed in accordance with the guidelines and standards of the Institutional Animal Care and Use Committee (IACUC) and under the approved animal protocol #11066 by Indiana University.

2.2.2 *In Vivo* Toxicity of PR5-LL-CM01

This experiment was done in collaboration with the *In Vivo* Therapeutics Core at IUSM. After acclimation for 7 days, male NSG mice were injected with 20mg/kg and 50mg/kg of PR5-LL-CM01 intraperitoneally (i.p.) 3X a week for week one and single injection daily for week two. Body weights were measured every 3 days and physical observations in gait and posture. were consistently monitored to identify any signs of toxicity. Additionally, paraffin-embedded samples of tumor, liver and, lung tissue from both the vehicle and PR5-LL-CM01-

treated mice were stained with hematoxylin and eosin (H&E) to determine signs of tissue toxicity with the service of IUSM Histology Core.

2.2.3 Subcutaneous Xenograft Model of PDAC and CRC

Male NSG mice were obtained from the *In Vivo* Therapeutics Core at IUSM. After acclimation for 7 days, NSG mice (6-8 weeks old) were xenografted with Mycoplasma-free PANC1 or HT29 cells subcutaneously (s.c.) ($1X10^7$ PANC1 or $3X10^6$ HT29 cells used per mouse) in 0.2 ml of a 1:1 mix of PBS and Matrigel (BD Biosciences). 5 mice were randomized in each group when tumor volumes reached ~100mm^3. Mice were treated with either vehicle control or 20mg/kg of PR5-LL-CM01 (compound stock dissolved in 1:1 Cremophor:ethanol solution) i.p. 3 times per week. Tumor volumes and body weights were measured twice a week using calipers and weighing scale respectively.

2.2.4 Orthotopic Xenograft Model of PDAC

NSG mice were injected with PANC-1 cells transduced with the lentiviral vector pCL6LucEGwo containing luciferase and green fluorescent protein cDNAs respectively as described previously (Shannon *et al.*, 2015). The implant was done in collaboration with the *In Vivo* Therapeutics Core, with the cells injected directly in the pancreas. One week after implant, tumor growth was measured in collaboration with the Imaging core by injecting 150µg d-luciferin/mouse (Caliper Life Sciences) and visualized using the IVIS Imaging System. After the first

imaging session, mice were randomized based on the measured signal before by beginning the drug treatment every single day (SID) i.p. Imaging was then carried out every 7-14 days until the end of the study.

2.2.5 Pharmacokinetic Study of PR5-LL-CM01

This experiment was done in collaboration with the Clinical Pharmacology Analytical Core (CPAC) at IUSM. The method to quantify PR5-LL-CM01 in plasma was developed using liquid-liquid extraction (acetonitrile: 0.1% formic acid) and HPLC-MS/MS (ABSciex 5500 Q-TRAP). Acetaminophen was used as the internal standard. The mass spectrometer utilized an electrospray ionization probe run in positive mode. The multiple reaction monitoring Q1/Q3 (m/z) transitions for PR5-LL-CM01 and acetaminophen are 402.1/357.3 and 152.0/109.9, respectively. The lower limit of quantification was 0.1 ng/mL using 20µL of plasma. Variability was minimized in the method by using plastic tubes instead of glass tubes, and methyl tert-butyl ether instead of ethyl acetate, dichloroethane, or hexane:ethyl acetate. The mobile phase used formic acid instead of ammonium acetate. More details provided in **Appendix C**.

2.3 Statistical analysis

Statistical analysis for experiments mentioned in the entire Methods section was performed using Prism 6 software (GraphPad). The Z' factor was calculated using the formula described in Zhang *et al.*.: [Z' = 1- {3 X SD positive control + 3 X SD negative control} / (mean positive control – mean negative

control}]. Percent inhibition for the compound library was calculated as follows: [({Avg. maximum reading – Inhibitor reading}/ Avg. maximum reading) X 100]. Results have been presented as mean ± SD or mean ± SEM, as specified. A two-tailed Student's t test was used while comparing two means to test for significant differences for all other experiments. All statistics were calculated on triplicate experiments and p value < 0.05 was considered statistically significant.

CHAPTER 3. ASSESSING THE TUMOR PROMOTING ROLE OF PRMT5-MEDIATED NF-κB IN PDAC AND CRC

3.1 Background and Rationale

PDAC and CRC are the leading causes of deaths in men and women combined in the United States. Besides having high mortality rates, the treatment options for both these cancers remain limited. Identification of new mechanisms underlying tumor promotion could open up new avenues for developing novel treatments that could not only increase survival but also improve the quality of life of these patients.

An important common feature of both PDAC (Ling *et al.*, 2012; Fujioka *et al.*, 2003; Wang *et al.*, 1999) and CRC (Mundade *et al.*, 2014, Sakamoto *et al.*, 2009) is hyperactive NF-κB activity. NF-κB is a critical eukaryotic transcription factor whose family consists of five members: RelA (p65), RelB, cRel, NF-κB1 (p50 and precursor p105), and NF-κB2 (p52 and precursor p100) (Ghosh *et al.*, 1988). The canonical pathway has been well established as a key contributor to development of both PDAC (Prabhu *et al.*, 2014; Liou *et al.*, 2013) and CRC (Agarwal *et al*., 2005; Yu *et al*., 2004). In this pathway, upon receiving extracellular signals such as pro-inflammatory cytokines. IκB kinase phosphorylates the inhibitor of κB (IκBα), leading to its degradation. This process results in the release of the p65:p50 complex, and the activation of NF-κB target genes (Gilmore 2006; **Figure 3**). A number of these downstream NF-κB target genes have been implicated in cancer. Increased NF-κB activation is not only

associated with poor disease prognosis, but also with developing resistance against chemotherapy in PDAC and CRC (Arora *et al.*, 2013; Lind *et al.*, 2001). Thus, controlling NF-κB activity is critical to the treatment of PDAC and CRC.

Recently, our lab became the first to discover that protein arginine methyltransferase 5 (PRMT5) serves as a potent activator of NF-κB via dimethylating arginine 30 of its p65 subunit (Wei *et al.*, 2013). Previous studies have implicated PRMT5's role to promote cancer progression (Wei *et al.*, 2013; Gu *et al.*, 2012; Jansson *et al.*, 2008), however its role via NF-κB-mediated activation in cancer has never been studied.

The results depicted in this chapter provide the evidence that overexpression of PRMT5 correlated with promotion of several hallmarks of cancer including cell growth, anchorage-independent growth, and cell migration, at least partly via increased activation of NF-κB and activation of its downstream target genes, in both PDAC and CRC. Discovery of pathway-specific novel activators of NF-κB like PRMT5 can prove to be significant for drug target identification in PDAC and CRC treatment.

3.2 Results

3.2.1 PRMT5 is Overexpressed in PDAC and CRC Tissues

Before examining the potential role of PRMT5 in PDAC and CRC, endogenous PRMT5 levels were checked in tumor tissue to see whether they

were elevated in these specimens versus normal tissue. Human tissue microarrays (TMAs) for PDAC and CRC were used, each containing an assembly of normal tissue and tissue from various stages of the respective cancers. TMAs were used as they allowed for a high throughput approach to analyze multiple specimens in a rapid, inexpensive and efficient manner. The TMA slides were first stained with hematoxylin and eosin, followed by probing with anti-PRMT5 antibody, in collaboration with Dr. George Sandusky at IUSM. Brown pigmentation was indicative of PRMT5 expression in the tissue. As shown in **Figure 8,** PRMT5 was significantly higher in various stages of PDAC, and particularly in metastatic stage, as compared to the normal PDAC adjacent tissue. Similarly, for CRC TMA, PRMT5 had much higher expression in samples ranging from inflammation, polyp, to the metastatic stage of CRC as compared to adjacent normal tissue. A particularly high PRMT5 expression seems to occur in Stage II CRC, which could be suggestive of this event being an early contributor to advance into higher stages of CRC. These data clearly demonstrated that PRMT5 is substantially overexpressed in both PDAC and CRC.

3.2.2 PRMT5 is Overexpressed in PDAC and CRC Cells

In order to determine whether PRMT5 has tumor promoting function in PDAC and CRC, we further examined PRMT5 expression in cell lines for both cancers by Western blotting. We chose AsPC1, MiaPaCa2 and PANC1 for PDAC and HT29, HCT116 and DLD1 for CRC as representative cell lines respectively.

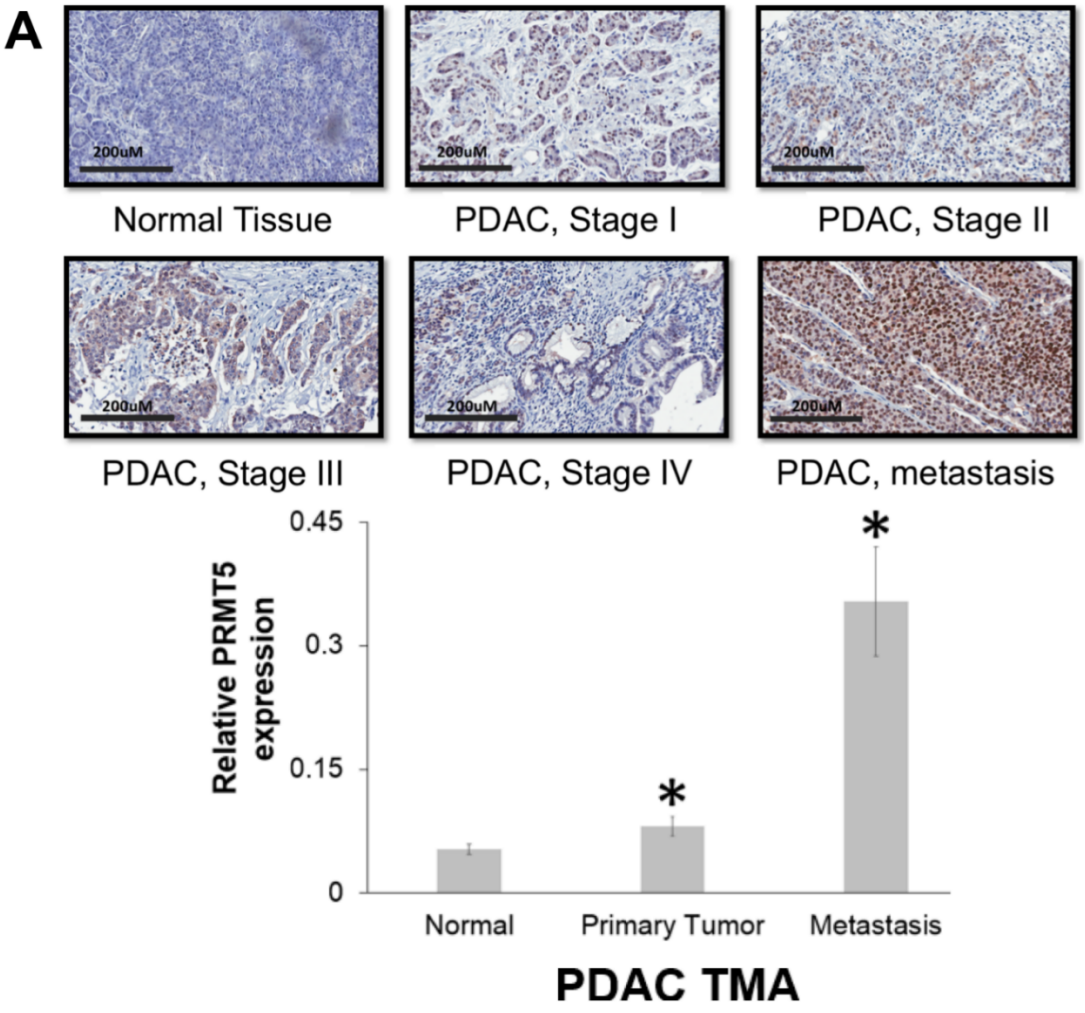
A
200uM
Normal Tissue
PDAC, Stage I
PDAC, Stage II
PDAC, Stage III
PDAC, Stage IV
PDAC, metastasis
Relative PRMT5 expression
0.45
0.3
0.15
0
*
*
Normal
Primary Tumor
Metastasis
PDAC TMA

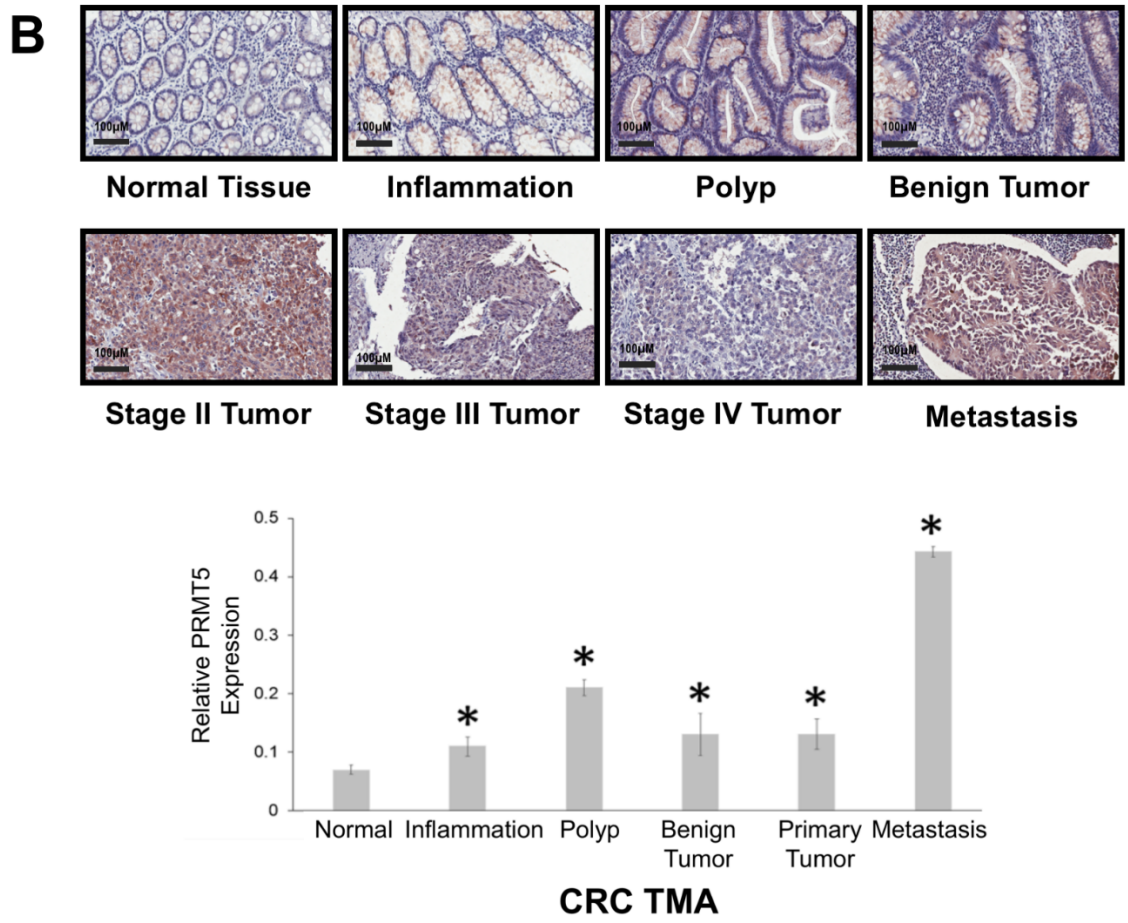

Figure 8. PRMT5 is overexpressed in pancreatic and colorectal cancer tissue

IHC staining, **A (upper panel).** showing that PRMT5 expression was higher in PDAC tumor tissues as compared to the normal tissue. **B (upper panel).** PRMT5 protein expression was higher in the inflammation, polyp, advanced stages of CRC and the metastatic stage as compared to the normal colon tissue. Quantification for IHC analysis of the PDAC and CRC tumor microarray (TMA). **A (lower panel).** Bar graph showing a significant increase in relative PRMT5 expression to normal tissue in primary stage tumor (n=19) and metastatic tumor patient tissue (n=6) vs. normal tissue (n=24) for the PDAC TMA. *p< 0.05, different samples vs. normal control. **B (lower panel).** IHC quantification of CRC TMA show a similar increase in relative PRMT5 expression compared to normal cancer adjacent tissue for the representative disease stages in the TMA, including inflammation (n=9), polyp (n=5), benign tumors (n=5), primary tumors (n=14) and metastatic tissue (n=20) vs. normal patient tissue (n=9). *P< 0.05, different samples vs. normal control.

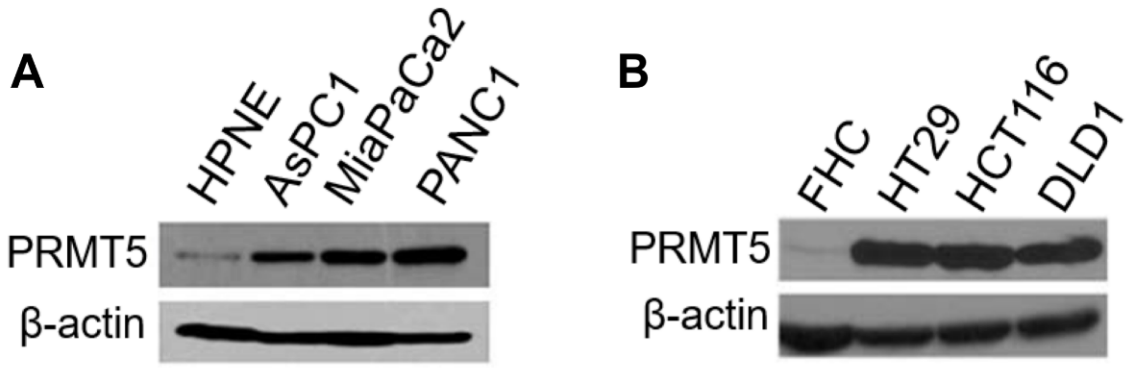

Figure 9. PRMT5 is overexpressed in PDAC and CRC cells
Western blots, **A**. showing that PRMT5 expression is higher in PDAC cells (AsPC1, MiaPaCa2 and PANC1) as compared to control pancreatic cells HPNE. **B.** PRMT5 expression is higher in CRC cells (HT29, HCT116 and DLD1) as compared to control colon cells FHC. β-actin was used as a loading control.

Both these sets of cell lines are well-established models in literature for the respective cancers (Ahmed *et al.*, 2013; Deer *et al.*, 2010). As shown in **Figure 9A,** PRMT5 was highly expressed in PDAC cells (AsPC1, MiaPaCa2 and PANC1) as compared to human normal pancreas HPNE cells. Similar experiments were carried out in a series of CRC cells (HT29, HCT116 and DLD1), with normal colon FHC cells as the control. Again, we observed that PRMT5 is highly expressed in CRC cells (**Figure 9B**). These data clearly demonstrated that PRMT5 is overexpressed in both PDAC and CRC cells. For further experiments, PANC1 and HT29 cells were chosen to generate the stable cell lines for PDAC and CRC respectively, since these are well-established cell line models, as described previously.

3.2.3 Generation of Stable PRMT5 Overexpression and shRNA Knockdown Cell Lines

Stable cells with either PRMT5 overexpression or shRNA knockdown were established in PANC1 (PDAC) and HT29 (CRC) cells by cloning Flag-tagged WT-PRMT5 or shPRMT5 cDNA into pLVX-IRES-puro vector (Lu *et al.*, 2010). Here, we overexpressed PRMT5 further in cancer cells which already have high PRTM5 expression to show the significance of modulating a single factor such as PRMT5 and checking if it plays a critical role in that particular property just by its own overexpression. However, in the future, it would be more prudent to first knockdown endogenous PRMT5 and then overexpress the same.

After transfecting the respective lentiviral plasmids containing empty vector, WT-PRMT5 or shRNAs into a 293T packaging cell line, viral preps were generated to infect PANC1 or HT29 cells. 1μg/mL of puromycin was used for further selection, as the pLVX vector contains a puromycin resistance gene. For all the experiments described further in this section, the experiment was done using three biological replicates and pool of early passage infected stable cells that were frozen down at -80°C. Finally, Western blotting was conducted to confirm the expected PRMT5 expression. As shown in **Figure 10**, significant overexpression was observed in WT-PRMT5-PANC1 and WT-PRMT5-HT29 respectively, as compared to the empty vector control. Conversely, shPRMT5-PANC1 and shPRMT5-HT29 showed knockdown of PRMT5 in these cells, compared to the control. β-actin was used as a loading control. Upon confirmation of PRMT5 expression, we used these cell lines to pursue further assays that checked for various aspects of cancer phenotype in these cells.

3.2.4 Overexpression of PRMT5 Promotes PANC1 and HT29 Cell Growth

Cancer cells have a characteristic to proliferate much more rapidly than their normal counterparts (Hanahan and Weinberg 2011). In order to test if elevated levels of PRMT5 correlated with promoting the cell proliferating ability of PDAC and CRC cells, cells were seeded in 6-well plates and checked for growth over a period of 9 days, by staining with crystal violet. These stained cells were then counted using a hemocytometer chamber.

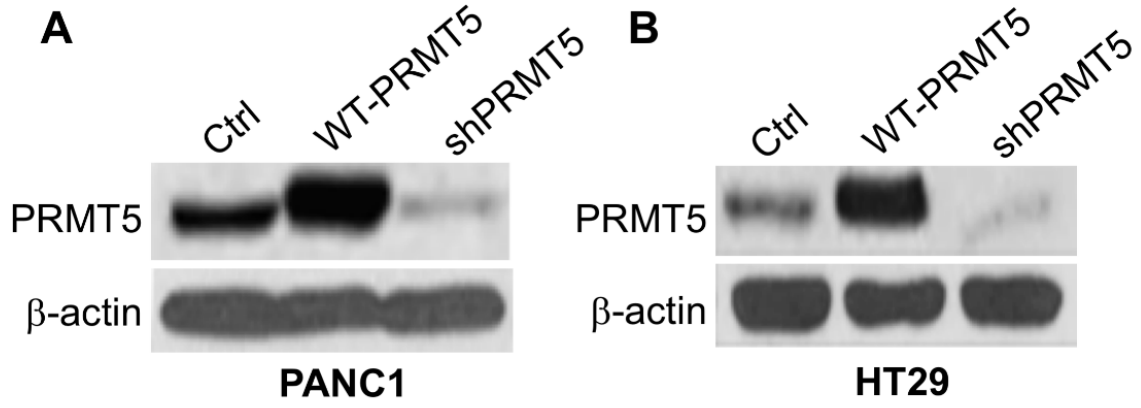

Figure 10. Generation of stable PRMT5 overexpression and shRNA knockdown cell lines
Western blot, confirming stable PRMT5 overexpression and shPRMT5 knockdown in **A**. PANC1 and **B**. HT29 cells. β-actin was used as a loading control.

We show that overexpression of PRMT5 promoted cell growth, while shRNA knockdown reduced this effect in both PDAC and CRC cells starting at day 5 (**Figure 11**) as compared to the control cells. This data confirmed that PRMT5 played an important role in promoting cell proliferation in these cells.

3.2.5 Overexpression of PRMT5 Promotes Migration of PANC1 and HT29 Cells

Another well-known property of cancer cells is their ability to migrate, which is critical for invasion and metastases by these tumors (Shaw 2005). Different methods have been used to quantify cell migration levels, including scratch-wound assays, cell-exclusion zone assays and Boyden Chamber assays. The Boyden Chamber assay is a widely accepted technique for studying cell migration and contains a plastic chamber with a porous membrane at its bottom. Inside this chamber are cells that are suspended in media with low serum, creating nutrient-starved conditions. Outside the chamber is medium containing high serum, replicating nutrient-rich conditions. Cells placed inside the chamber tend to migrate through the pores, from the area of low nutrient to high nutrients. The migrated cells are finally stained with crystal violet and counted using the hemocytometer chamber.

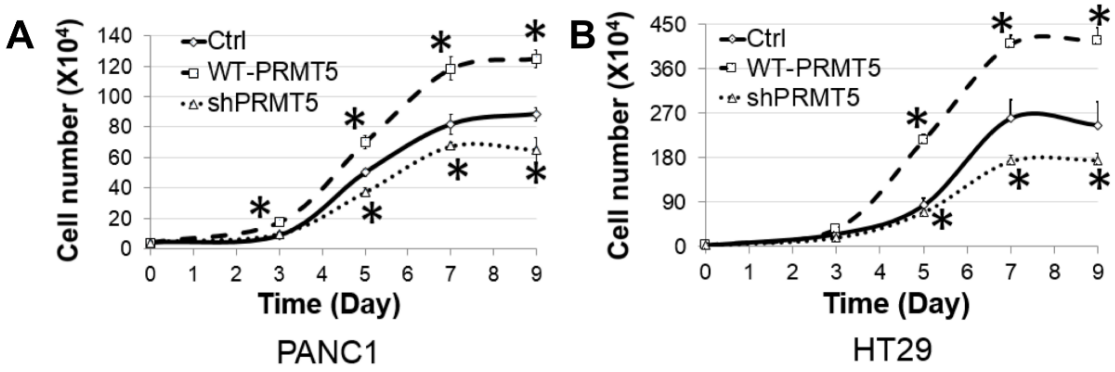

Figure 11. Overexpression of PRMT5 promotes PANC1 and HT29 cell growth

Cell proliferation assay, showing that cell proliferation was significantly higher in the WT-PRMT5 cell lines, while shPRMT5 cells exhibited quite opposite effect compared to empty vector Ctrl in both **A**. PANC1 and **B**. HT29 cells. *P < 0.05 *vs.* Ctrl.

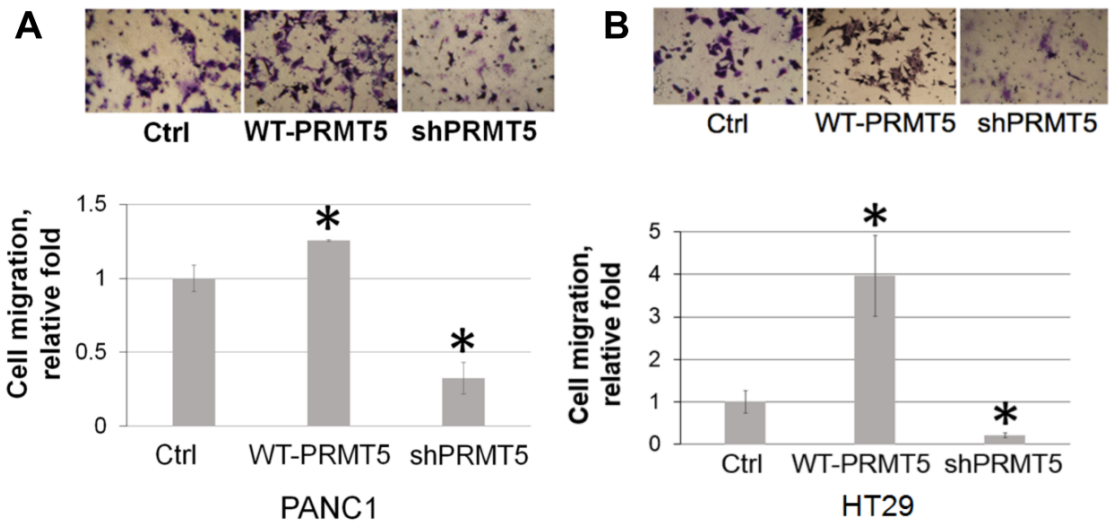

Figure 12. Overexpression of PRMT5 promotes migration of PANC1 and HT29 cells.

Cell migration assay, showing that cell migration was significantly higher in the WT-PRMT5 overexpression cells, while significantly reduced in the shPRMT5 cells. Upper panels, representative pictures in 20X magnification. Lower panel, quantification for the change in migration. *P < 0.05 *vs.* Ctrl.

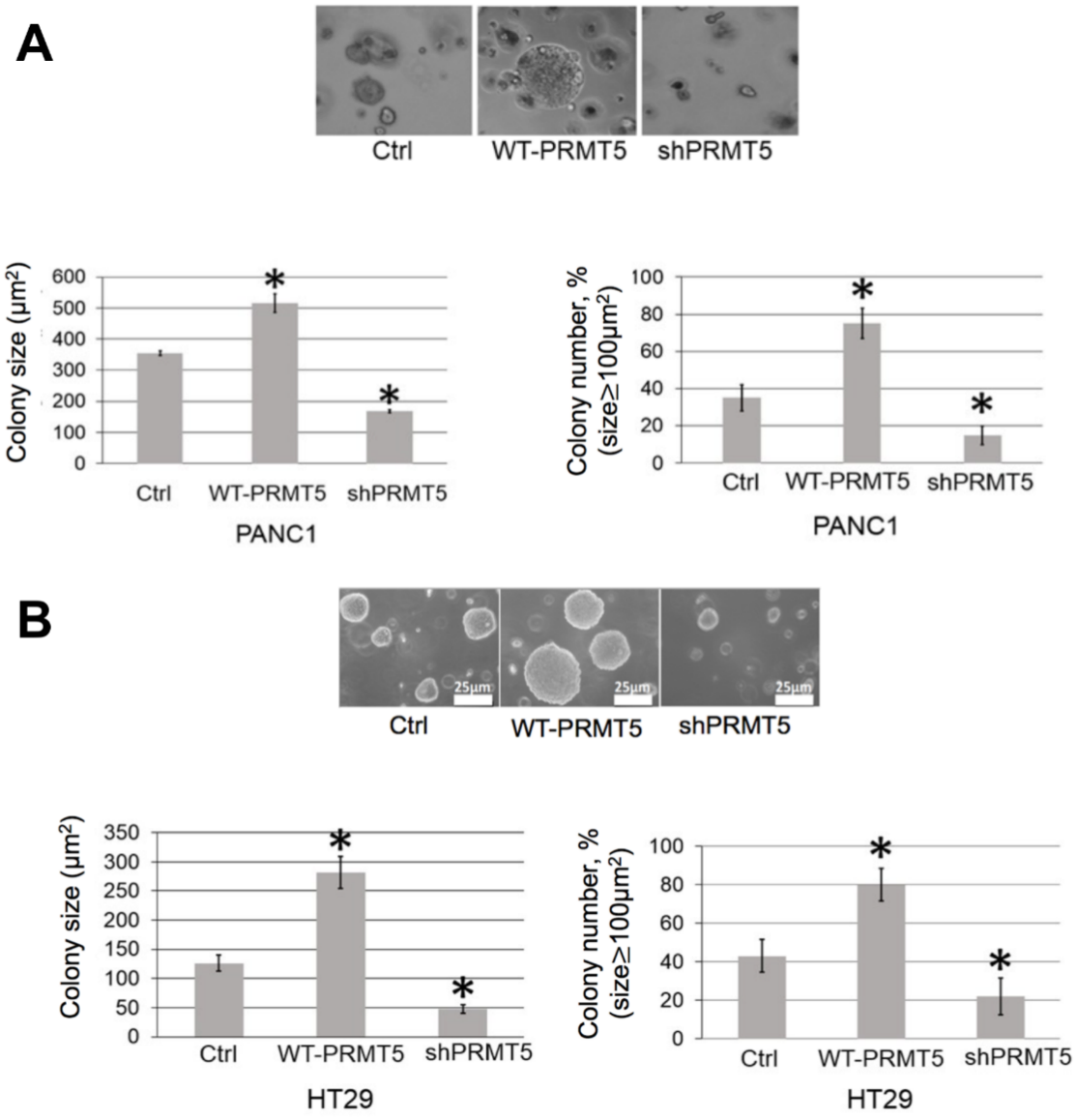

Figure 13. Overexpression of PRMT5 promotes colony independent growth of PANC1 and HT29 cells

Anchorage-independent growth was significantly higher in the WT-PRMT5 cell lines, while dramatically reduced in the shPRMT5 cells in **A**. PANC1 and **B**. HT29 cells. Both colony size and number are quantified at the bottom of the corresponding panels. *P < 0.05 *vs.* Ctrl group.

As observed in **Figure 12**, overexpression of PRMT5 increased the number of migrated cells (in purple), whereas shPRMT5 knockdown showed quite opposite effect. Representative pictures for each condition were taken in 20X magnification. Overall, these results indicate that PRMT5 enhanced the migratory ability of both PDAC and CRC cells.

3.2.6 Overexpression of PRMT5 Promotes Anchorage-Independent Growth of PANC1 and HT29 Cells

The ability to grow independently of a solid surface is a hallmark of cancer cells. In order to test if PRMT5 can affect this property, we conducted an anchorage-independent growth assay in soft agar (Borowicz *et al.*, 2014). Data suggested that PRMT5 overexpression led to a dramatic increase in both the colony size and number in PANC1 and HT29 cells (**Figure 13**), while shPRMT5 knockdown significantly reduced this ability, confirming the critical role that PRMT5 plays in promoting anchorage-independent cell growth in PDAC and CRC.

Overall, PRMT5 promoted several characteristics associated with cancer cells, including increased proliferation, migration and anchorage-independent growth. Next, we wanted to check how PRMT5 overexpression correlated with activation of its substrate NF-κB.

3.2.7 Overexpression of PRMT5 Activates NF-κB in PDAC and CRC Cells

Previously, we discovered that PRMT5 activates NF-κB through methylation of its p65 subunit in HEK293 cells (Wei *et al.*, 2013). This is a significant finding, as NF-κB has been shown to be constitutively activated in multiple cancers and is a well-established tumor promoting factor. However, it is also important for normal functioning of cells. Thus, direct targeting may not always be feasible. Discovery of factors like PRMT5 is significant, as it could allow for indirect targeting of NF-κB and thereby providing a viable therapeutic option.

In this regard, it was worth determining the impact of PRMT5 on NF-κB activation. NF-κB activity was measured using transient transfection of the construct p5XIP10 (containing five tandem copies of the NF-κB site from the IP10 gene upstream of the luciferase reporter gene) and addition of luciferase substrate 48 h after transfection. If PRMT5 affected NF-κB activation, then we would see increased binding of the active p65 subunit of NF-κB to its consensus site of the IP10 gene, leading to increased transcription and translation of the downstream luciferase reporter gene. Upon addition of luciferase substrate, a fluorescent product is formed by the luciferase enzyme which is directly proportional to the level of NF-κB activity in the cells, thus allowing to assay its activity.

As illustrated in **Figure 14**, overexpression of PRMT5 significantly enhanced NF-κB activity, while shPRMT5 knockdown exhibited a quite opposite

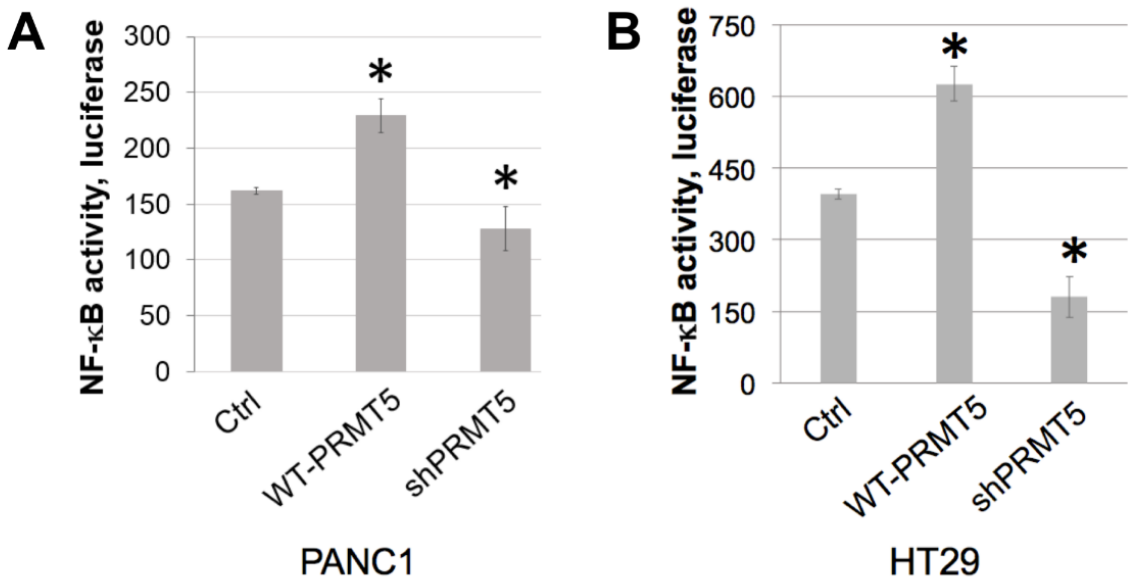

Figure 14. Overexpression of PRMT5 activates NF-κB in PDAC and CRC cells

NF-κB luciferase assay, showing that overexpression of WT-PRMT5 led to NF-κB activation, while shPRMT5 resulted in quite opposite effect in **A**. PANC1 and **B**. HT29 cells. *P < 0.05 *vs.* Ctrl.

effect, as compared to the control cells, indicating that PRMT5 indeed significantly activated NF-κB in both PDAC and CRC cells.

3.2.8 Overexpression of PRMT5 Induces the Expression of NF-κB Target Genes in PDAC and CRC Cells

Our lab previously showed that PRMT5-mediated NF-κB activation led to the induction of typical NF-κB target genes, such TNFα and IL8 in 293 cells (Wei *et al.*, 2013). Thus, in order to understand the effect of PRMT5 overexpression on the upregulation of these genes in PDAC and CRC cells, we performed quantitative PCR showed that upon stimulation with IL-1β, there was a substantial increase in the expression of TNFα and IL8 in PRMT5 overexpressing cells, while a dramatic reduction was observed upon shPRMT5 knockdown, in both PANC1 and CRC cells, indicating that activation of NF-κB by PRMT5 led to a further activation of known NF-κB-dependent downstream target genes TNFα and IL8 (**Figure 15**). Both these genes are highly expressed and critical players in the tumor microenvironment and disease progression (Mager et al, 2016; Błogowski *et al.*, 2014). More importantly, TNFα and IL8 were shown to be amongst the most highly upregulated genes in terms of their mRNA expression in a tissue microarray that compared PRMT5 overexpressed cells to vector control cells in a 293 background (Wei *et al.*, 2013). Other downstream NF-κB target genes may be affected that play a critical role in promoting different hallmarks of cancer and it would be interesting to check if PRMT5 can look into

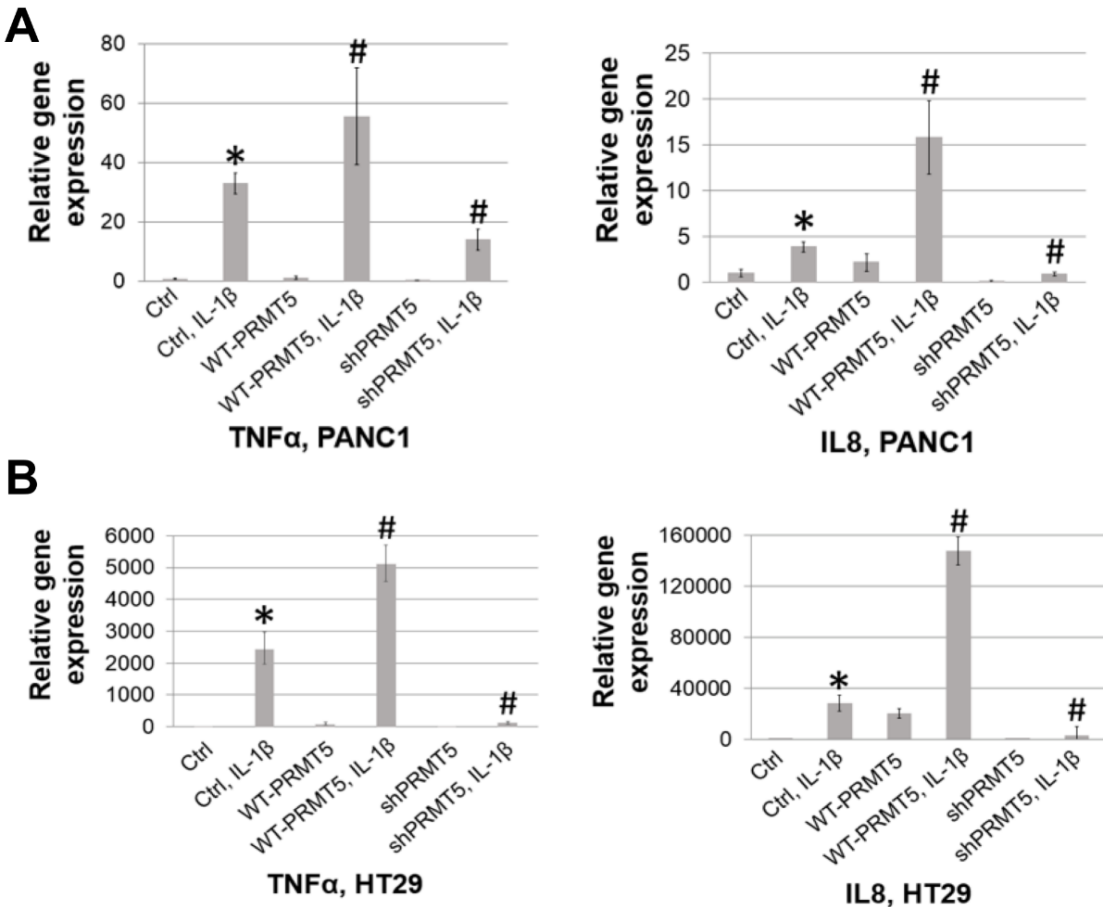

Figure 15. Overexpression of PRMT5 induces the expression of NF-κB target genes in PDAC and CRC cells

qPCR analysis, showing that overexpression of PRMT5 significantly enhanced IL-1β-triggered NF-κB target genes (TNFα and IL8) expression, while shPRMT5 exhibited quite opposite effect, in both **A**. PANC1 and **B**. HT29 cells. *P < 0.05 *vs.* Ctrl; #P < 0.05 *vs.* Ctrl+IL-1β-treated group.

those in the future. Thus, PRMT5 could have tumor-promoting function by upregulating NF-κB-directed activation of downstream target genes that are critical in the advancement of the disease phenotype.

3.3 Concluding Remarks

Here, we provide the first link for a PRMT5-mediated NF-κB signaling pathway in PDAC and CRC. Our findings show that PRMT5 promotes cell proliferation, migration and anchorage-independent growth, which are critical hallmarks of cancer. More importantly, overexpression of PRMT5 was capable of promoting NF-κB activation itself as well as activation of downstream target genes. This underlies the significance of a novel signaling mechanism responsible for NF-κB activation in PDAC and CRC. These findings also opened up the exciting possibility of PRMT5 having therapeutic relevance. Inhibiting PRMT5 activity could serve as a means to indirectly control constitutive NF-κB activation observed in PDAC and CRC, thereby leading to a possible alleviation of the cancer phenotype. In the next two chapters, we explore the therapeutic relevance of developing specific PRMT5 inhibitors in PDAC and CRC.

CHAPTER 4. DISCOVERY OF PR5-LL-CM01 AS A NOVEL PRMT5 SMALL-MOLECULE INHIBITOR FROM HIGH THROUGHPUT SCREEN #1

4.1 Background and Rationale

PRMT5, a member of PRMT superfamily, can contribute to cancer promotion, making it a potential target for cancer therapy. In **Chapter 3**, we highlighted the potential role of PRMT5 as a tumor promoting factor, at least partly via NF-κB activation. In this regard, *we hypothesized that inhibition of PRMT5 with small-molecule inhibitors could have potential therapeutic implications in PDAC and CRC.*

In this study, we developed a highly sensitive (Z' score = 0.6) robotic high throughput screen (HTS) platform by adapting the AlphaLISA™ technology to discover small molecule inhibitors of PRMT5. This assay could precisely quantify PRMT5 methylation of its substrate in a 384-well HTS platform. Compared to the conventional methods such as time resolved fluorescence energy transfer (TR-FRET) assay, the AlphaLISA technology is proved to be more sensitive, reliable, and adaptable for performing large-scale reactions. Thus, it proves to be a more robust assay to be used for screening as compared to other methods used in the past (Simard *et al.*, 2013, Quinn *et al.*, 2010). Additionally, PerkinElmer had highly specific reagents for our purpose, such as beads with antibodies highly specific for the dimethyl tag introduced by PRMT5 on its substrate. To date, AlphaLISA has never been used for screening of PRMT5 inhibitors in the HTS format. In collaboration with the IU Chemical Genomics

Core, we successfully modified this technique from bench scale to a condition that can provide robust results in a robotic system. Briefly, PRMT5 transferred the methyl groups from its methyl donor SAM to biotin-histone H4 peptide (a well-known PRMT5 substrate), leading to its symmetric dimethylation, which was recognized by the Acceptor beads conjugated with the anti-H4R3me2 antibody and the streptavidin tagged Donor beads. Upon excitation with light, emitted signal was detected by an EnVision® Reader, which was proportional to the amount of dimethylated H4R3 (**Figure 16**). Therefore, for any small-molecule inhibitor used to inhibit the activity of PRMT5, a reduced signal emission would be detected. Using this powerful approach, we identified a selective PRMT5 inhibitor PR5-LL-CM01, and further validated their efficacy and selectivity for inhibiting PRMT5. Importantly, it exhibited much more efficacy than the commercial PRMT5 inhibitor EPZ015666 in both PDAC and CRC cells. Overall, our work highlights a novel, powerful, and sensitive approach to identify specific PRMT5 inhibitors.

This chapter provides a detailed account of the development and optimization of the AlphaLISA protocol for an HTS to screen for small-molecule inhibitors of PRMT5, identification of PR5-LL-CM01 as a novel PRMT5 inhibitor, and the subsequent validation of its specificity and efficacy in both *in vitro* and *in vivo* models of PDAC and CRC.

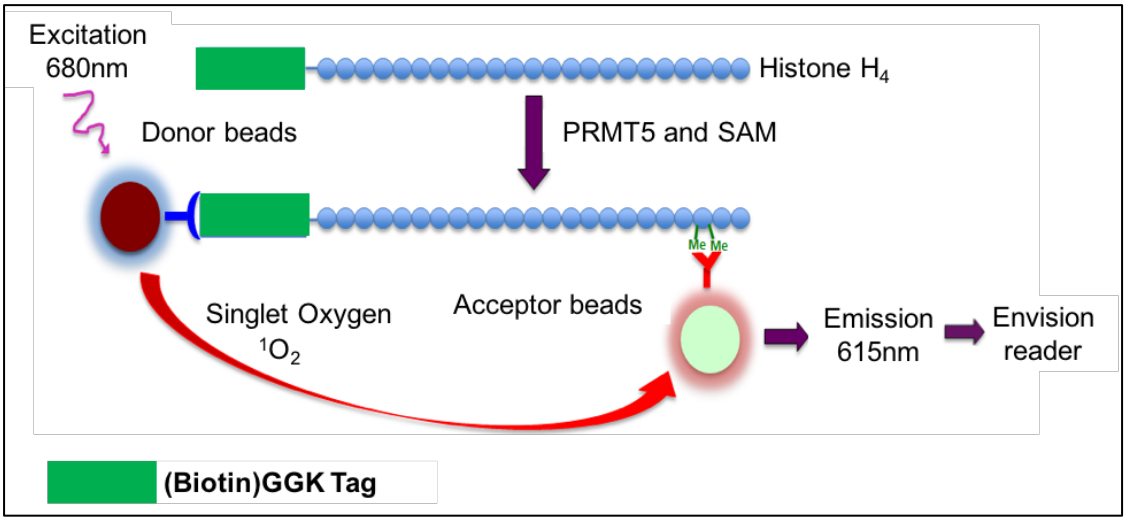

Figure 16. Schematic Illustration of the AlphaLISA Technique
Biotinylated histone H4 is incubated with PRMT5 and methyl donor SAM. PRMT5 symmetrically dimethylated H4 on its arginine 3, a product that is recognized by Acceptor beads. Following the binding of Donor beads, the chemiluminescent signal is emitted and detected by the EnVision® Reader. The intensity of the Alpha signal is proportional to the PRMT5 activity.

4.2 Results

4.2.1 Development and Optimization of PRMT5-Specific AlphaLISA HTS Assay

The first step in developing an HTS for PRMT5 inhibitors was to design an assay that could accurately measure PRMT5 methyltransferase activity and was adaptable to a large-scale screening platform, such that reduction in enzyme activity in presence of inhibitors could be quantified. For this purpose, we utilized the AlphaLISA assay as per the principle described in **Figure 16**.

AlphaLISA protocol requires several critical components, including substrate H4R3, the methyl donor SAM, PRMT5 enzyme as well as Acceptor and Donor beads (**Table 1**). We purified PRMT5 enzyme using co-immunoprecipitation experiments with Flag beads from 293-PRMT5-Flag cells. 293-PRMT5-Flag cells have overexpressed Flag-tagged PRMT5 (**Figure 17**) and allow for efficient purification of PRMT5. The manufacturer-recommended dilutions for the Acceptor as well as the Donor beads helped us to obtain the desired signal. The major optimization was necessary for the unmethylated H4R3 substrate (unmeH4R3) and SAM concentrations to be used in the experiment. First, we optimized the substrate concentration by running the AlphaLISA assay with 10-100nM final concentration of the unmeH4R3 substrate in the reaction well. We observed that with increasing concentrations of substrate, there was a predictable increase in the AlphaLISA signal (**Figure 18A**). Since using the lower concentrations provided a robust signal in the pilot experiment, we decided to use 30nM of unmeH4R3 as our final condition.

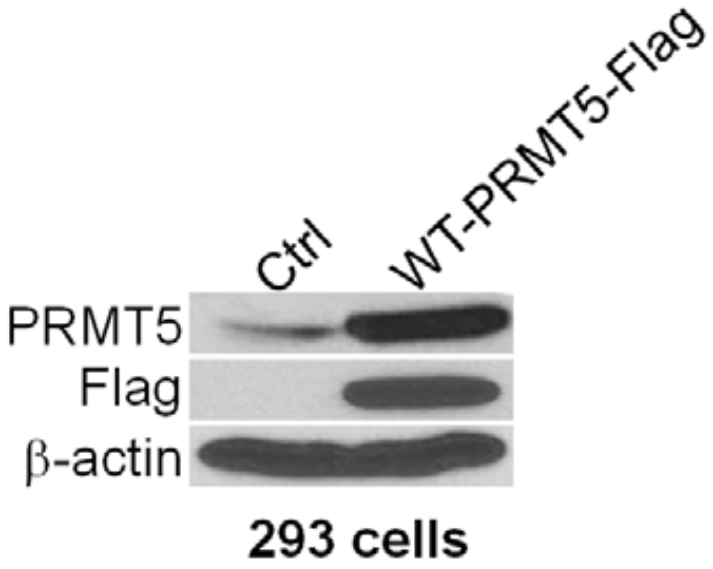

Figure 17. PRMT5 was Overexpressed in the 293-WT-PRMT5-Flag Cells
Western blot, showing that Flag-tagged WT-PRMT5 was overexpressed in the 293-WT-PRMT5-Flag cells as compared to the control 293 line. The 293-WT-PRMT5-Flag cell line was used to purify PRMT5 enzyme for the AlphaLISA assay, using co-immunoprecipitation with anti-Flag beads.

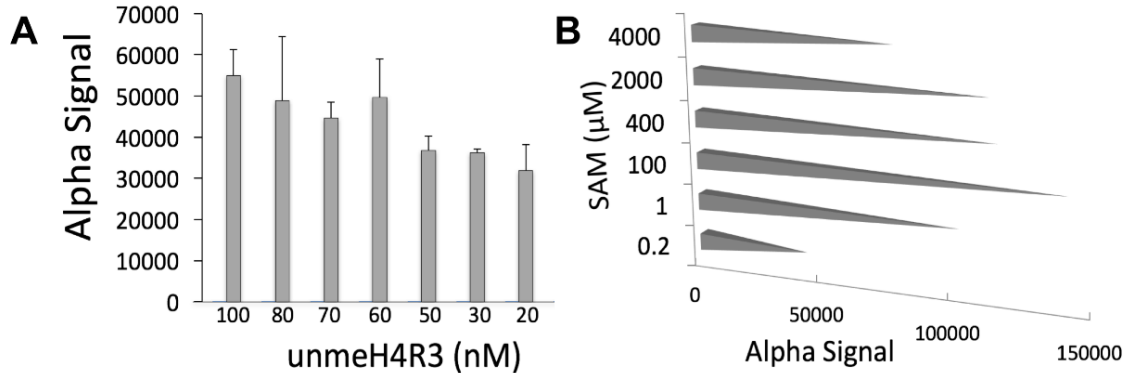

Figure 18. Optimization of the AlphaLISA Protocol
A. Alpha signal graph, showing that the Alpha signal increased with increased substrate (unmeH4R3) concentrations (10-100nM). **B.** Alpha signal graph, showing that increased concentrations of the methyl donor SAM (0.2-4000mM) led to a bell-shaped distribution of Alpha signal strength. We observed an increase in the Alpha signal, with a peak at 100mM of SAM, followed by a subsequent decrease with further increased SAM concentrations.

Next, with the aim to maximize the AlphaLISA signal, we determined if a specific concentration of the methyl donor SAM worked best in this assay. We tested a wide range of SAM concentrations (0.2μM to 2000μM) while keeping all the other components same, including the substrate concentration at 30nM as described above. We observed a steady increase in AlphaLISA signal, with a peak at 100μM SAM, that decreased at higher concentrations (**Figure 18B**). Thus, we decided to choose a final concentration of 100μM SAM in our HTS assay. These assays also allowed us to adjust and test volumes and concentrations that were permissible for the robotic approach, thus helping us to automate the addition of these reagents in the actual HTS.

4.2.2 Conduction of the Z' Experiment to Test the Sensitivity of the PRMT5-specific AlphaLISA HTS Technology

After successfully determining the important parameters for assay development, we executed the Z' test to check the robustness of the assay. Calculation of the Z' factor allows for evaluation and validation of HTS assays (Zhang *et al.*, 1999), as it allows to assess the range of signal generated in the assay as well as accounts for *variation* associated with the signal measurements. We used a 384-well white opaque plate to run the Z' test. Briefly, half of the plate was used as "maximum signal" wells (with the PRMT5 enzyme added) and the other half was used as "background wells" (with *no* PRMT5 enzyme, only assay buffer added) (**Figure 19A**). We used a 20μl reaction volume as described in **Table 1**. The graph for Z' factor determination is illustrated in **Figure 19B**. An

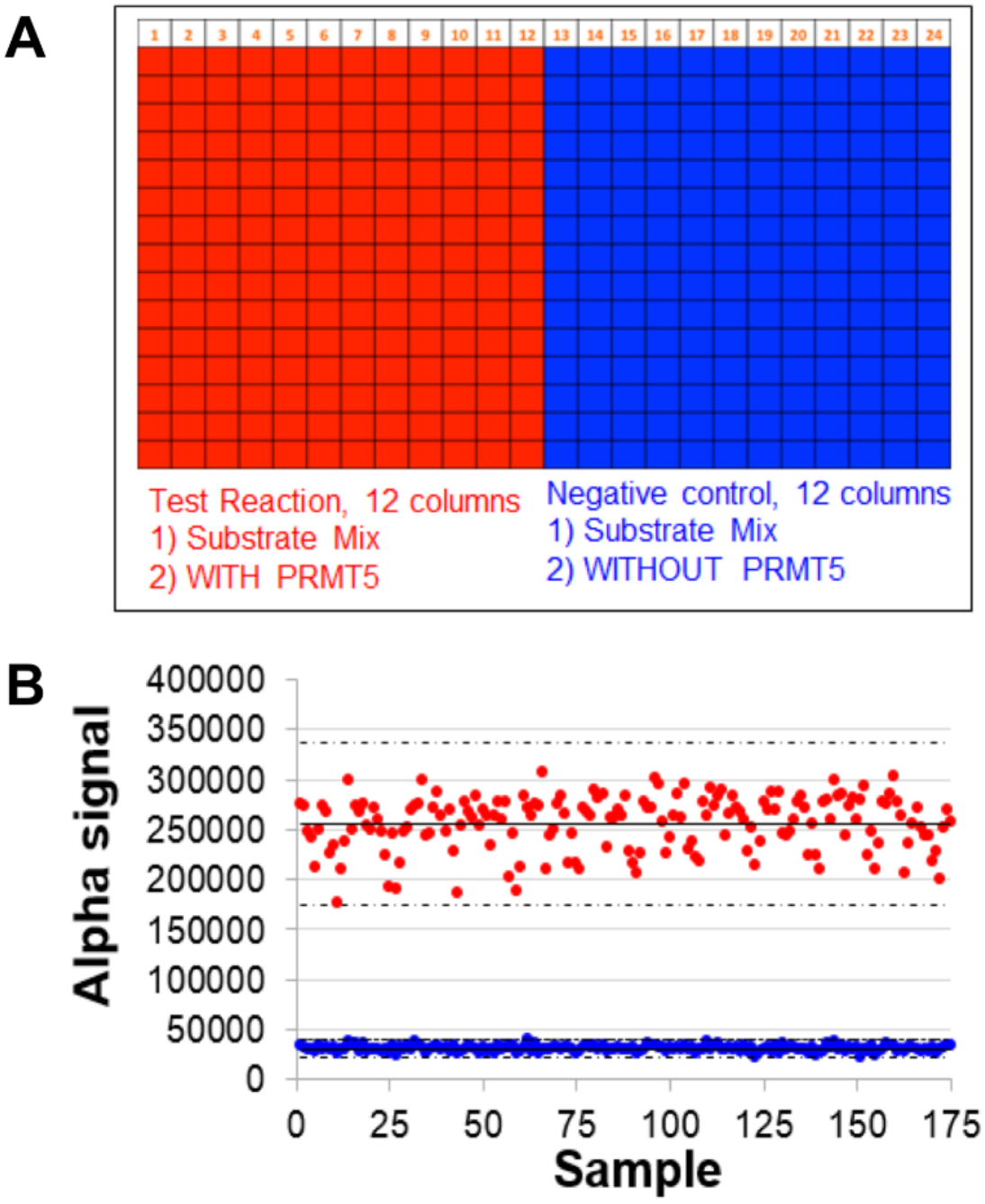

Figure 19. Z' Assay Design
A. Plate design to calculate the Z' ratio. **B.** Z'-plot of AlphaLISA assay, showing that Alpha signal with PRMT5 (red dots) is significantly higher than those without PRMT5 (blue dots). The mean values are represented with solid horizontal lines in the center of each sample group. Z' value for our experiment was 0.6.

assay with a Z' value > 0.5 is widely considered to be sensitive enough for a successful HTS. The Z' factor was calculated to be 0.6 and a signal/background ratio of ~7. This test confirmed that our adapted PRMT5-specific AlphaLISA HTS technique was sensitive, robust, and successful. Once the assay was proven HTS-compatible, the next step was to scale it up to run a HTS screen using large-scale small compound libraries.

4.2.3 Using PRMT5-Specific AlphaLISA HTS to Identify a Novel Small-Molecule Inhibitor of PRMT5: PR5-LL-CM01

Using PRMT5-specific AlphaLISA HTS technique, we successfully screened a library with 10,000 small molecules purchased from ChemDiv Inc. A representative 384-well plate in the HTS (**Figure 20**) shows a potential hit highlighted in red, with a significant decrease observed in the AlphaLISA signal, as compared to that with no inhibitor.

Several top hits were identified and confirmed using both AlphaLISA and MTT assay in PDAC and CRC cells. Among these, the leading compound was PR5-LL-CM01. PR5-LL-CM01 consists of a pyrozolo-pyrimidine core and three peripheral A, B and C groups (**Figure 21**).

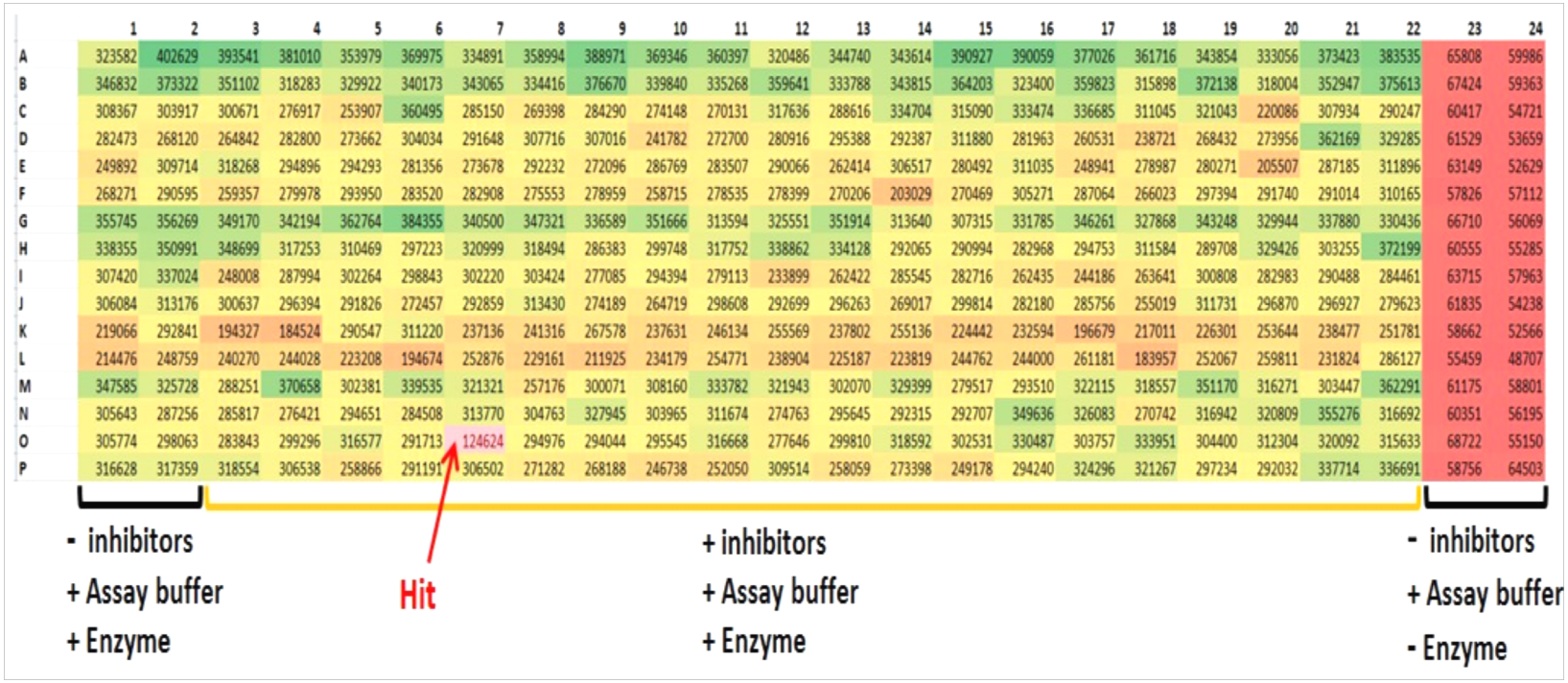

Figure 20. Representation of a 384-well Plate used in the HTS
The plate was designed such that wells in rows 1-2 represent the positive control (no inhibitor, with enzyme), rows 3-22 represent test compounds (inhibitor and enzyme present) and negative controls (no inhibitor, no enzyme) are in rows 23-24. A potential hit with decreased AlphaLISA signal is indicated with a red arrow.

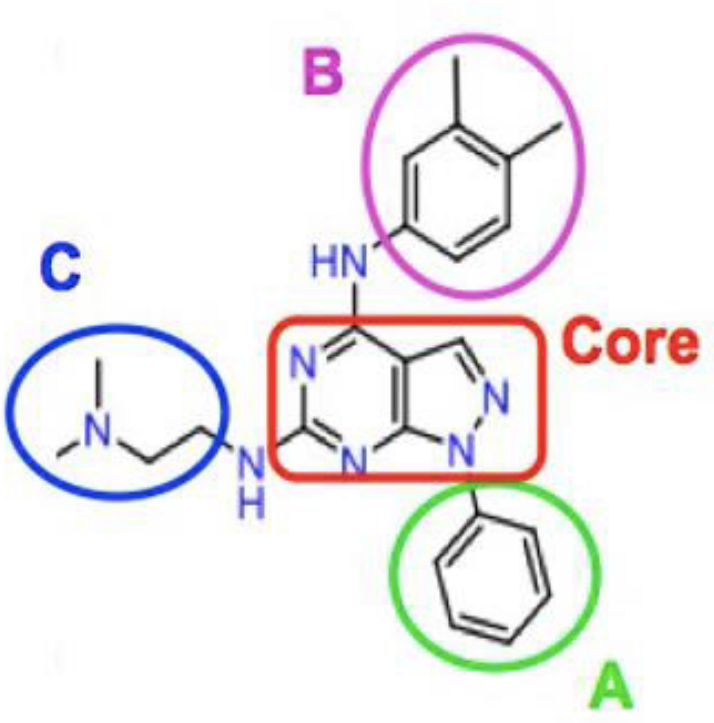

Figure 21. Structure of PR5-LL-CM01
The core structure of a pyrozolo-pyrimidine group is highlighted in a red box and three surrounding groups A, B and C, respectively with colored circles in the structure of PR5-LL-CM01. This structure is part of the patent filed under International Patent Appl. PCT/US2017/058572.

4.2.4 Confirmation of PRMT5 Inhibition Effect of PR5-LL-CM01 by AlphaLISA Technique

In order to confirm the effect of the inhibitor on PRMT5, we used the AlphaLISA approach with increasing concentrations of PR5-LL-CM01 to determine its effect on PRTM5 methyltransferase activity. We would expect a concentration-dependent decrease in PRMT5 activity with increasing concentrations of PR5-LLCM01 if it was specific for inhibiting PRMT5 methyltransferase activity. We saw the expected concentration dependent effect with PR5-LL-CM01 and confirmed that the IC_{50} of PR5-LL-CM01 was 7.5μM by the AlphaLISA approach (**Figure 22**). Here, we have not excluded if the inhibitor just inhibits the Ab binding or the biotin:streptavidin reaction to show decrease in Alpha signal that we observe. With the fact that the binding affinity of biotin-avidin and the Ab-methyl group reaction is quite high, the inhibitor interfering with those reactions is highly unlikely. More specific controls can be included in the future.

4.2.5 MTT Assay to Determine IC_{50} in PDAC and CRC Cells

In order to determine the efficacy of PR5-LL-CM01, we used both PDAC and CRC cells as the *in vitro* models. These are the same set of cancer cell lines used in **Chapter 3** to check for PRMT5 expression (**Figure 9**). Both PDAC and CRC cells were treated with increasing concentrations of PR5-LL-CM01 and quantified for cell viability with the MTT assay. We showed that PR5-LL-CM01 had a range of IC_{50} at 2-4μM in PDAC cells (PANC1, MiaPaCa2 and AsPC1) (**Figures 23A and C**), and a range of IC_{50} at 10-11μM in CRC cells (HT29,

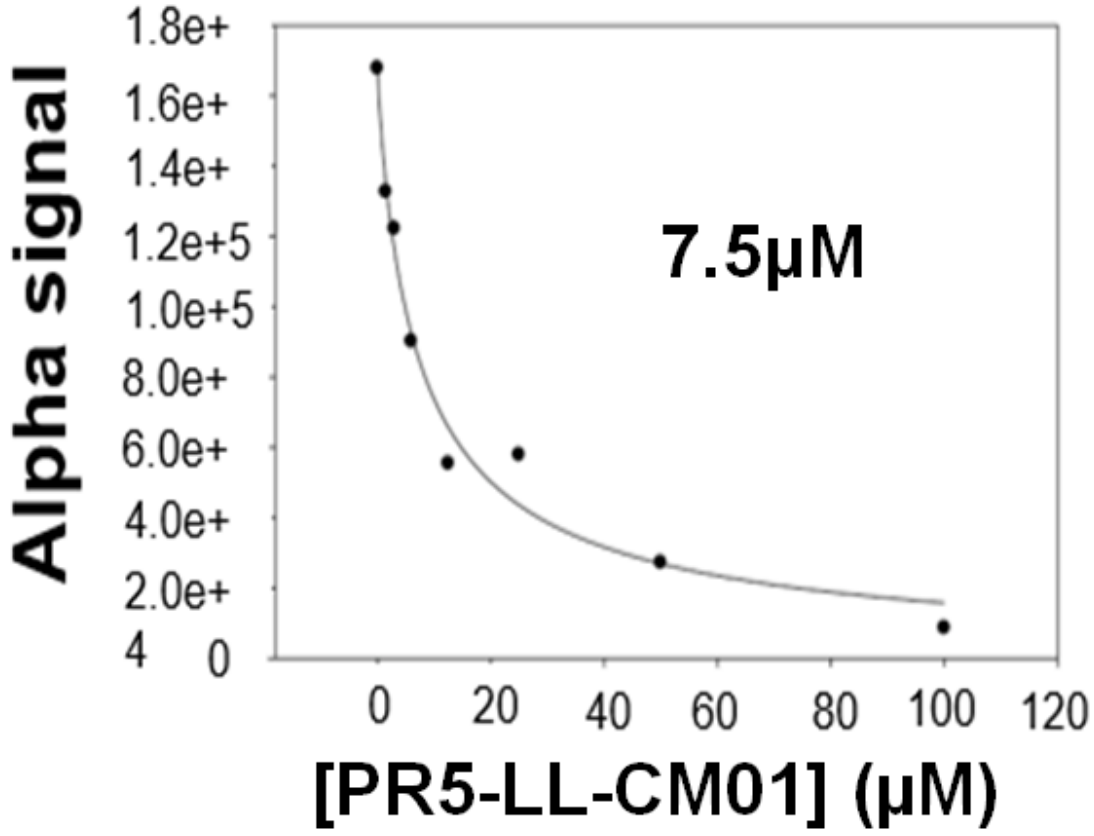

Figure 22. PR5-LL-CM01 shows a Concentration-Dependent Decrease in Methyltransferase Activity.
Using AlphaLISA, increasing concentrations of PR5-LL-CM01 showed a relative decrease in Alpha signal, indicative of decrease in methyltransferase activity of PrMT5. The IC_{50} was ~7.5µM.

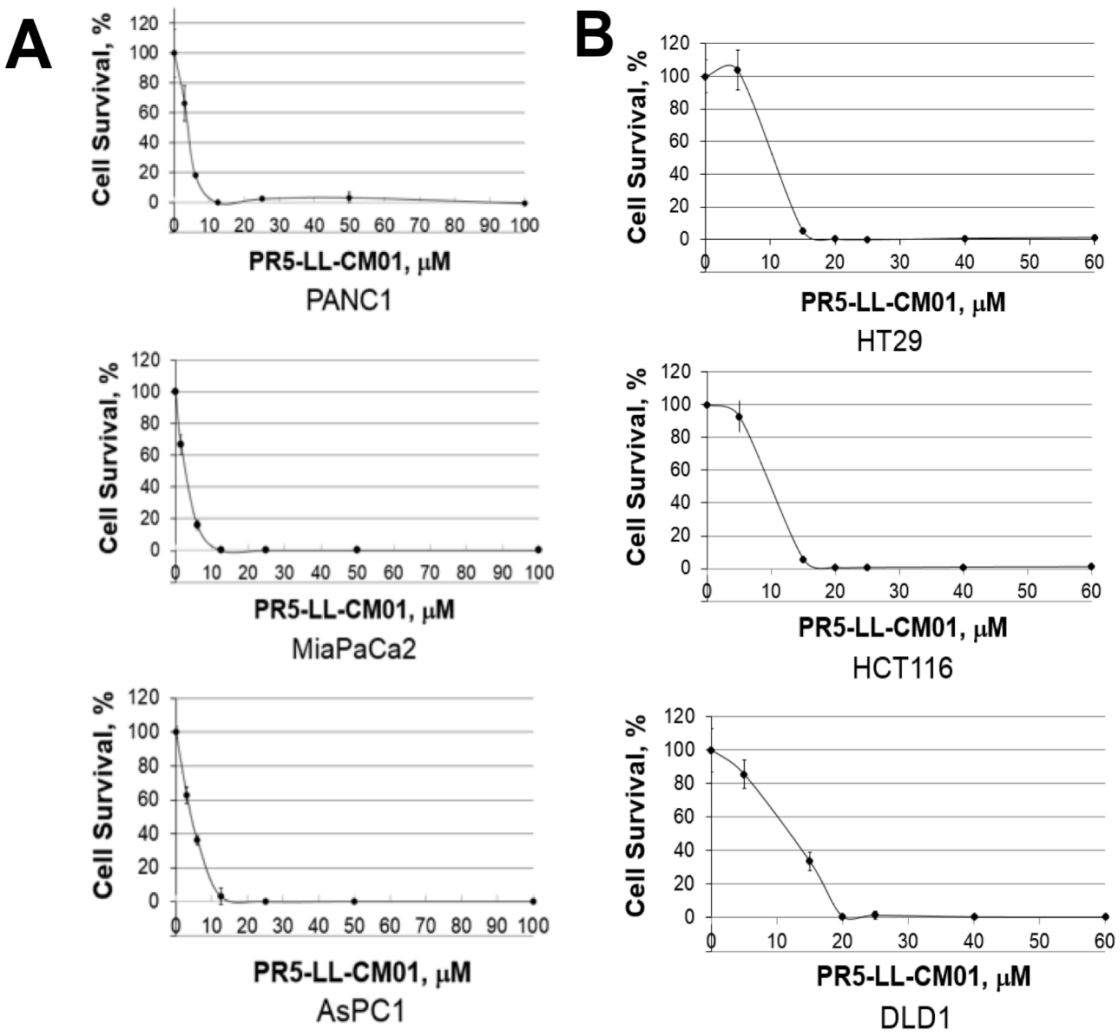

C

Cancer Type	Cell line	IC50, μM
PDAC	PANC1	4
	MiaPaCa2	2
	AsPC1	4
CRC	HT29	10
	HCT116	10
	DLD1	11

Figure 23. PR5-LL-CM01 is a Potent Inhibitor of PRMT5 in PDAC and CRC Cells

A. MTT assay in PDAC cells (PANC1, MiaPaCa2 and AsPC1), showing that cell viability decreased significantly in presence of increasing concentrations of PR5-LL-CM01. **B.** MTT assay in CRC cells (HT29, HCT116, and DLD1), showing dramatic decrease of cell viability in presence of increased concentrations of PR5-LL-CM01. **C.** Table, summarizing the IC_{50} values for PR5-LL-CM01 in PDAC and CRC cells, respectively.

HCT116 and DLD1) (**Figures 23B and C**). Overall, the IC_{50} of PR5-LL-CM01 was in the low μM range for both sets of cell lines.

Recently, Chan-Penebre *et al.* identified a PRMT5 inhibitor, EPZ015666 and showed its high efficacy in inhibiting PRMT5 in mantle cell lymphoma disease models. We wanted to understand whether EPZ015666 would be effective in PDAC and CRC. Since this compound is commercially available, we tested it in our PDAC and CRC cell lines. Our data suggested that EPZ015666 was much less effective as compared to PR5-LL-CM01, with a range of IC_{50} at 50-95μM for PDAC cells, and a range of IC_{50} at 180-195μM for CRC cells (**Figure 24**). Therefore, our data suggested that PR5-LL-CM01 is a more potent PRMT5 inhibitor than EPZ015666 in PDAC and CRC cells.

4.2.6 PR5-LL-CM01 Inhibits Anchorage-Independent Growth of PDAC and CRC Cells

Next, we used the anchorage-independent assay described previously to check if treatment with PR5-LL-CM01 affected colony formation of either PDAC or CRC cells. We observed that treatment with PR5-LL-CM01 at increasing concentrations strongly inhibited colony forming ability in both PANC1 and HT29 cells (**Figure 25**). This indicates that PR5-LL-CM01 successfully impeded the colony forming ability in PDAC and CRC cells.

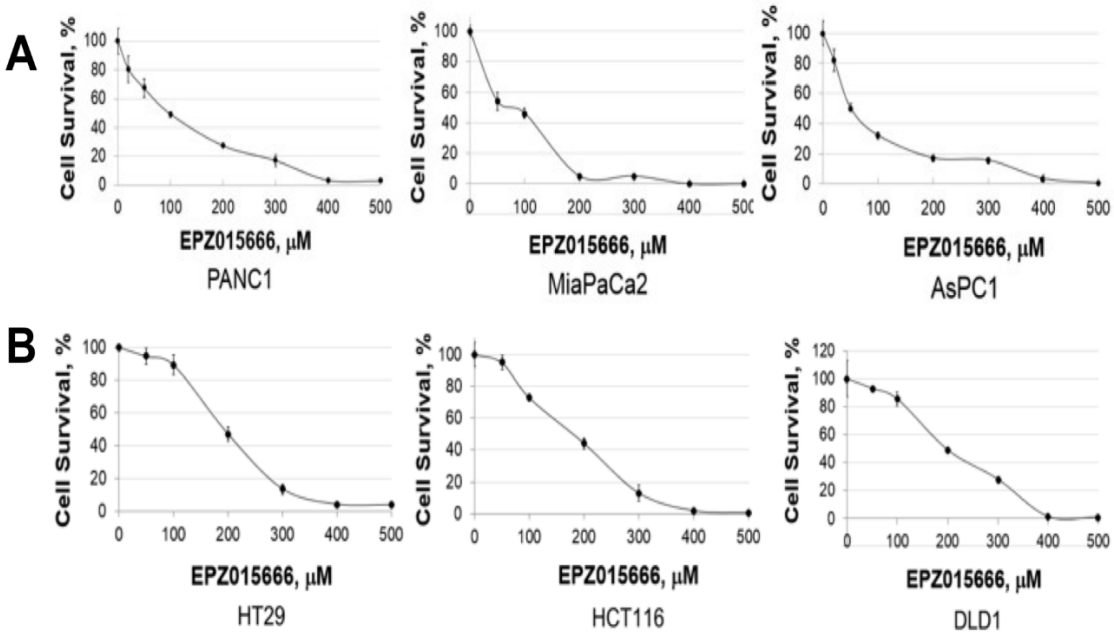

C

Cancer Type	Cell line	IC50, μM
PDAC	PANC1	95
	MiaPaCa2	62
	AsPC1	50
CRC	HT29	190
	HCT116	180
	DLD1	195

Figure 24. Effect of EPZ015666 on PDAC and CRC Lines
A. MTT assay, showing that in PDAC cells (PANC1, MiaPaCa2 and AsPC1) EPZ015666 decreased cell viability, however had a lower efficacy to decrease cell viability than that of PR5-LL-CM01. **B.** MTT assay, showing that in CRC cells (HT29, HCT116, and DLD1), EPZ015666 decreased cell viability, but had lower efficacy to decrease cell viability than that of PR5-LL-CM01. The data represent the means ± S.D. for three independent experiments. *P < 0.05 *vs.* Ctrl group. **C.** Table summarizing the IC_{50} values for EPZ015666 in PDAC and CRC cell lines.

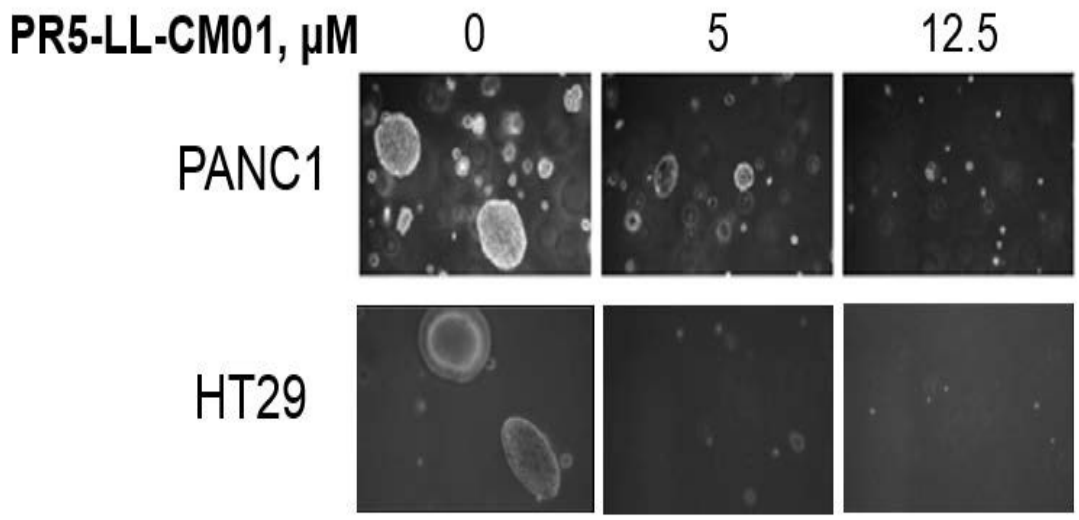

Figure 25. Effect of PR5-LL-CM01 on Anchorage-Independent Growth of PDAC and CRC Lines
Anchorage-independent assay, showing that with increasing concentrations of PR5-LL-CM01, there was a significant decrease in the anchorage-independent growth ability in both PANC1 as well as HT29 cells.

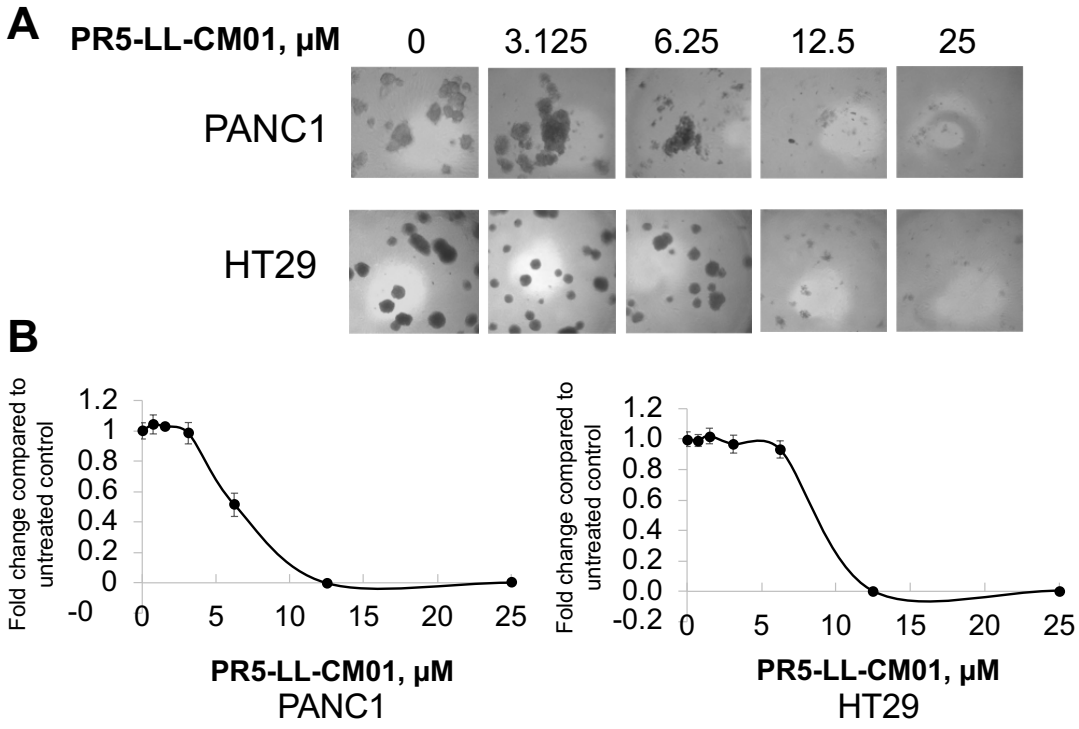

Figure 26. Effect of PR5-LL-CM01 3D Colony Formation of PDAC and CRC Lines

3D colony formation assay, showing that with increasing concentrations of PR5-LL-CM01, there was a significant decrease in the 3D colony formation ability in both PANC1 as well as HT29 cells. **A.** Representative pictures in 4X magnification. **B.** Quantification for the fold change in 3D colony formation, upon treatment with increasing concentrations of PR5-LL-CM01, as compared to the untreated control.

4.2.7 PR5-LL-CM01 Inhibits 3D Culture Growth of PDAC and CRC Cells

In light of recent work suggesting 3D spheroidal cell culture may closely mimic the *in vivo* tumor microenvironment such as having a hypoxic core, decreased spheroid- spheroid contact and greater survival (Fennema *et al.*, 2014; Heylman *et al.*, 2014), we determined the efficacy of PR5-LL-CM01 against 3D spheroids of PDAC and CRC cells. As shown in **Figure 26**, with increasing concentrations of PR5-LL-CM01, we observed a dosage-dependent decrease in the ability of both PANC1 and HT29 cells to form 3D spheroids in culture, highlighting the tumor-inhibiting potential of PR5-LL-CM01 *in vitro*.

4.2.8 PR5-LL-CM01 Inhibits NF-κB Symmetric Dimethylation and Downstream Activation

Previously we found that PRMT5 activated NF-κB through methylation of its p65 subunit (Wei *et al.*, 2013). Therefore, we would expect that treatment with a specific PRMT5 inhibitor, PR5-LL-CM01 would reduce NF-κB methylation and subsequent activation. Accordingly, we first tested the effect of PR5-LL-CM01 on the symmetric dimethylation status of p65, the active subunit of NF-κB. 293 cells engineered to overexpress Flag-p65 were treated with 20μM PR5-LL-CM01 for 24h. Flag-p65 was pulled down with anti-Flag-M2 beads and further analyzed with Western blot by probing with anti-dimethylated arginine antibody (**Figure 27**). We show that, compared to the untreated control cells, treatment with PR5-LL-CM01 significantly inhibited PRMT5-mediated p65 methylation. This result

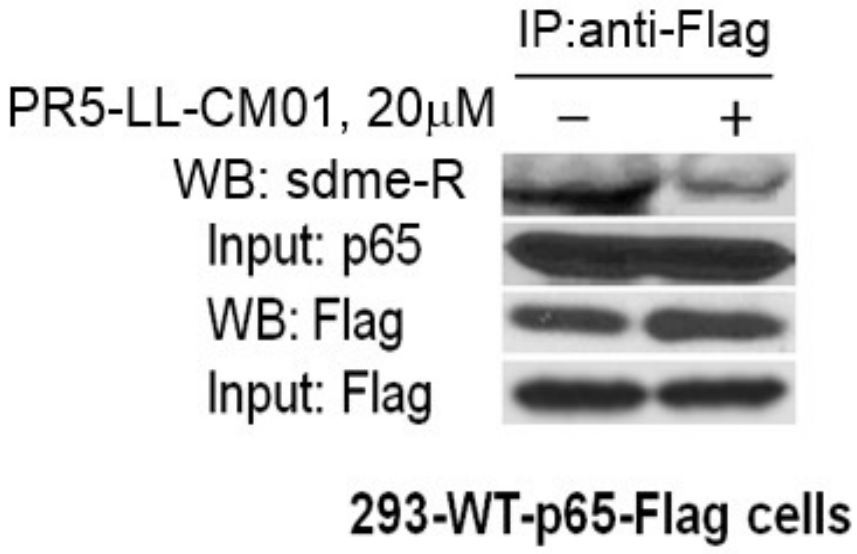

Figure 27. PR5-LL-CM01 Inhibits NF-κB Symmetric Dimethylation Status
Co-IP-Western blot, showing that treatment with 20μM PR5-LL-CM01 inhibited p65 methylation, a PRMT5 substrate, in 293-WT-p65-Flag cells. Flag beads were used to pull down WT-p65-Flag and samples were probed with anti-symmetric dimethyl arginine motif (sdme-RG) antibody.

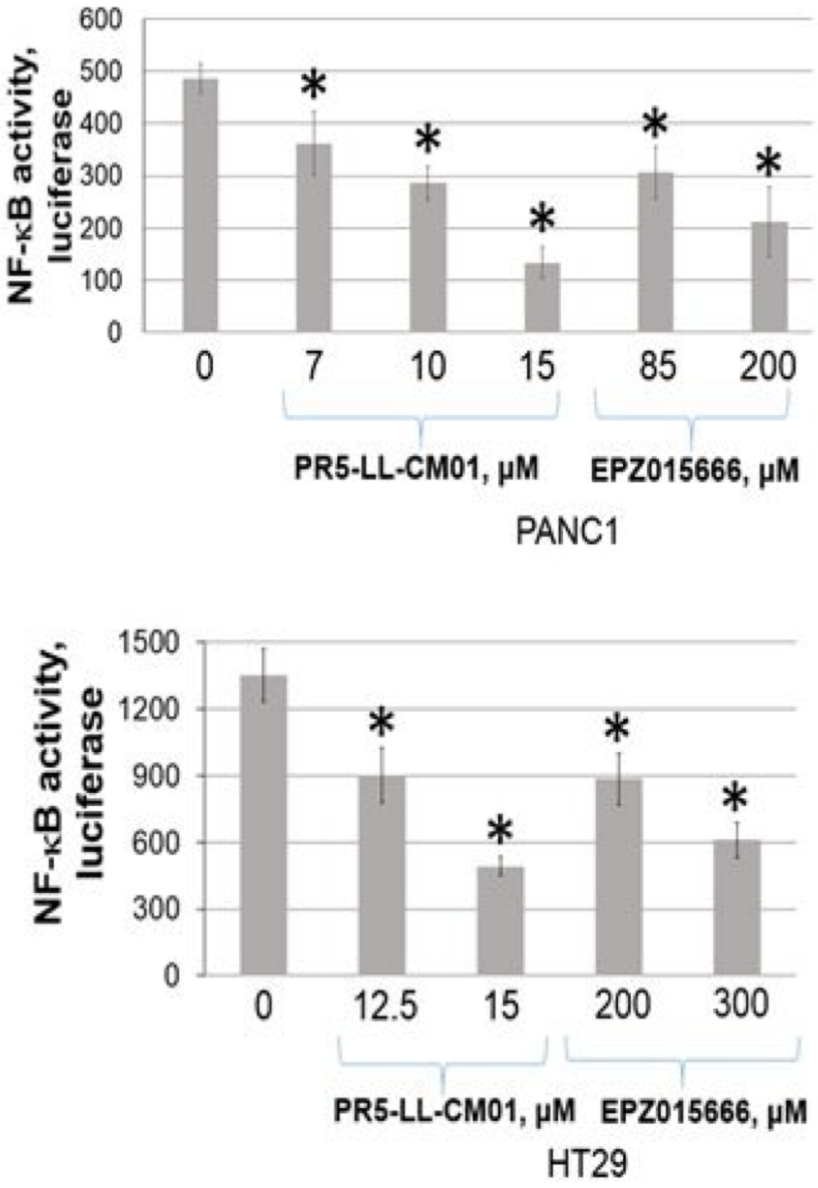

Figure 28. PR5-LL-CM01 Inhibits NF-κB Activity in PDAC and CRC Cells
Luciferase assay, showing a decrease in NF-κB activation with increasing concentrations of PR5-LL-CM01 in PANC1 (upper panel) and HT29 cells (lower panel). A much higher concentration of EPZ015666 is needed in order to reach similar level of NF-κB inhibition as that of PR5-LL-CM01. The data represent the mean ± S.D. for three independent experiments. *P < 0.05 *vs.* Vehicle group (0μM).

confirmed that PR5-LL-CM01 inhibited PRMT5-specific methyltransferase activity *in vitro*.

In order to further examine if PR5-LL-CM01-mediated inhibition of PRMT5 affected subsequent activation of NF-κB, we conducted a luciferase assay as described previously. As shown in **Figure 28**, treatment with increasing concentrations of PR5-LL-CM01 resulted in a corresponding decrease in NF-κB activation in PANC1 and HT29 cells. Alongside PR5-LL-CM01, we also tested how efficacious EPZ015666 was in reducing NF-κB activation (**Figure 28**). These data demonstrate that PR5-LL-CM01 was significantly more potent in decreasing NF-kB in PDAC and CRC cells than the commercially available PRMT5 inhibitor, EPZ015666.

We further tested if a decrease in NF-κB activation observed above resulted in a corresponding decrease in the induction of NF-κB target genes that are critical in promoting the hallmarks of cancer. We observed that treatment with PR5-LL-CM01 led to a significant decrease in both NF-κB target genes, IL8 and TNFα (**Figure 29**), indicating that PR5-LL-CM01 significantly decreased PRMT5-mediated NF-κB-dependent gene activation. Overall, we observed that PR5-LL-CM01 had significant efficacy in inhibiting NF-κB methylation, its subsequent activation and its downstream gene expression in PDAC and CRC cells.

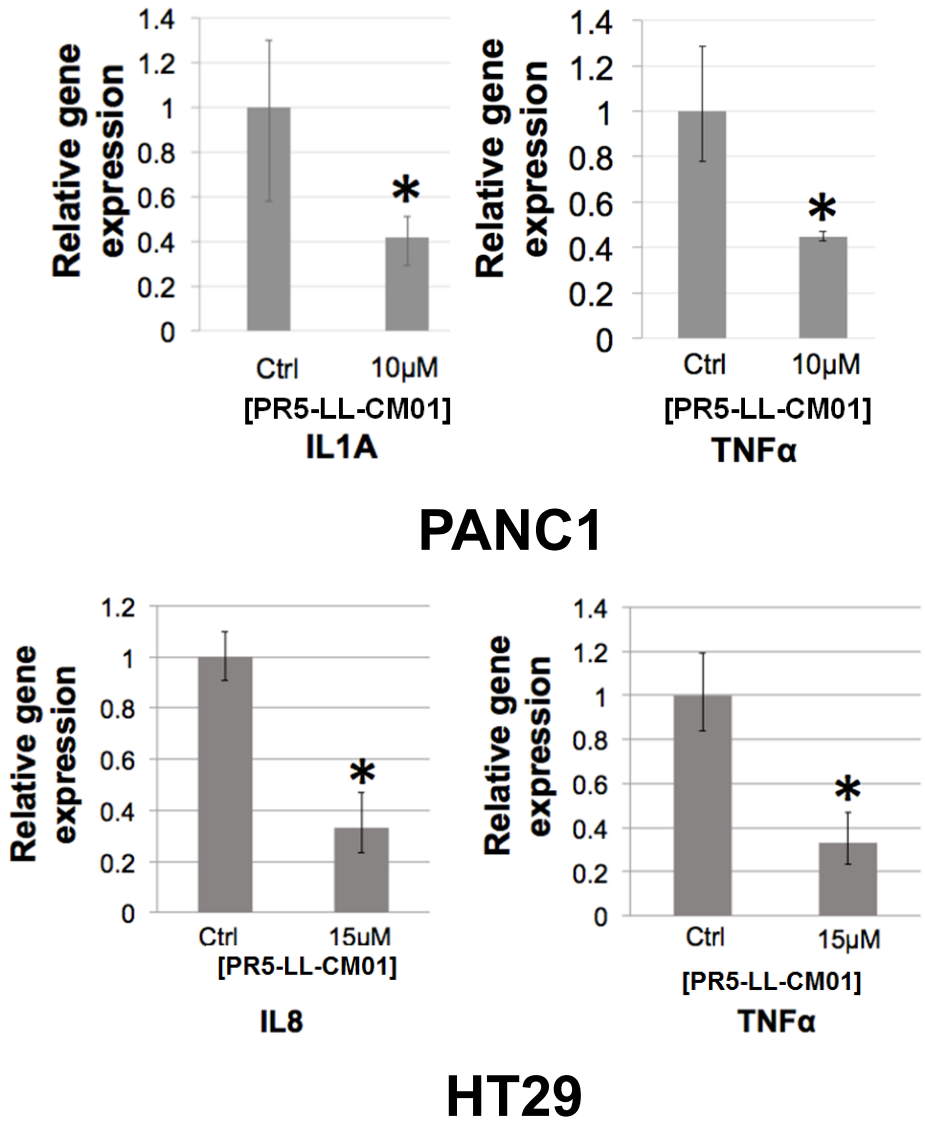

Figure 29. PR5-LL-CM01 Inhibits the Expression of NF-κB Target Genes in PDAC and CRC Cells

qPCR analysis, showing that treatment with PR5-LL-CM01 dramatically decreased TNFα and IL8 expression, in both PANC1 and HT29 cells. The data represent the means ± SD for three independent experiments. *P < 0.05 *vs.* "0μM" group.

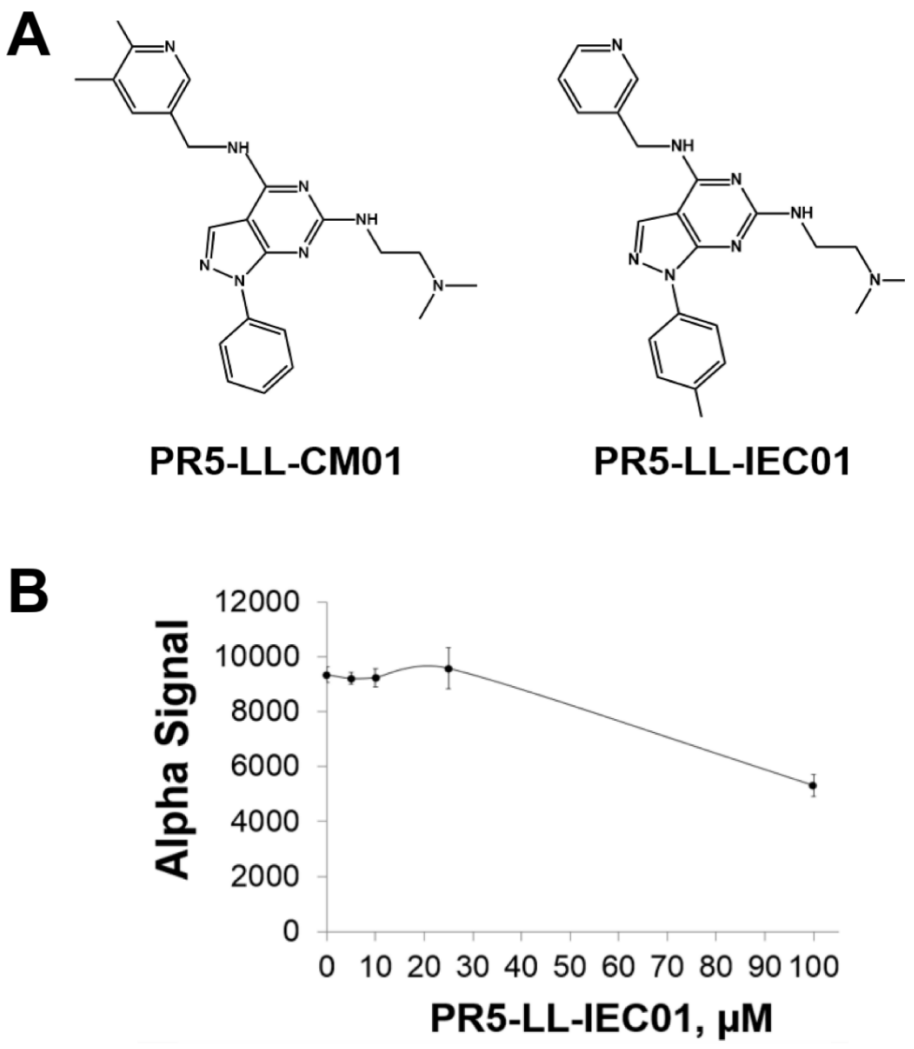

Figure 30. PR5-LL-IEC01, a Structural Analog of PR5-LL-CM01
A. Structure of PR5-LL-IEC01, in side-by-side comparison to the lead compound, PR5-LL-CM01. **B**. Calculation of IC_{50} of PR5-LL-IEC01 using AlphaLISA, with IC_{50} calculated to be ~118μM, several fold higher than the lead compound PR5-LL-CM01.

4.2.9 Selectivity of PRMT5 Inhibition Effect of PR5-LL-CM01

In order to check the specificity of PR5-LL-CM01 to PRMT5, we generated PR5-LL-IEC01, a structural analog of PR5-LL-CM01 (**Figure 30A**). Multiple analogs, including PR5-LL-IEC01 were generated for the SAR analysis that has been described later in **Section 4.2.17**. We tested all of them versus the parental compound. PR5-LL-IEC01. This particular analog, PR5-LL-IEC01 was chosen to be used as a representative compound here based on the fact that this analog had amongst the very least difference in its structure from the parental compound as demonstrated in **Figure 30** and thus was chosen for the purpose of this study. The IC_{50} of PR5-LL-IEC01 was calculated to be 118μM by AlphaLISA (**Figure 30B**), about 16-fold higher than that of PR5-LL-CM01 (**Figure 22**), affirming that the inhibition of PRMT5 methyltransferase activity observed by AlphaLISA assay was specific to small-molecule inhibitor PR5-LL-CM01.

Furthermore, we examined the inhibition by PR5-LL-CM01 against other PRMT family members using the HotSpot radioisotope-based platform (Reaction Biology Corp) (Horiuchi *et al.*, 2013), as described in **Section 2.1.18**. This assay allows for detection of the levels of SAM being turned over in the reaction by loss of its methyl group, thereby enabling quantification of the respective enzyme activity. As shown in **Figure 31**, these PRMTs showed zero effect, or at least a 10-fold higher IC_{50} than that of PRMT5, indicating the high selectivity of PR5-LL-CM01 for PRMT5 over its other family members.

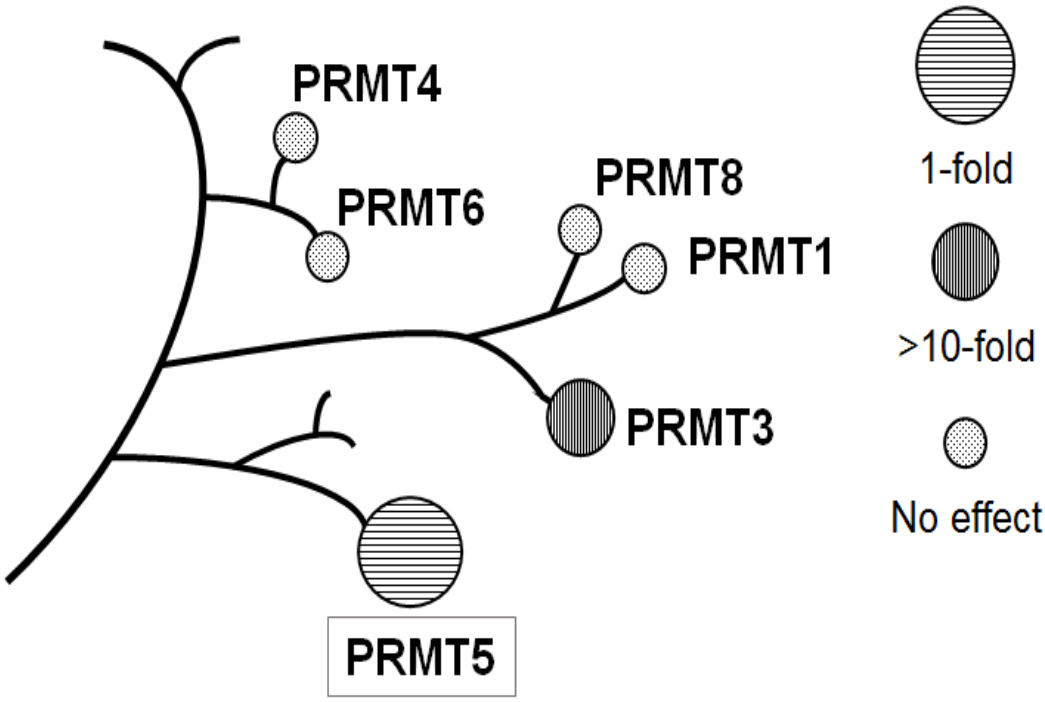

Figure 31. Selectivity of Inhibition by PR5-LL-CM01 against the Enzymatic Activity of Protein Arginine Methyltransferase Family Members
The specificity of inhibition was analyzed using the HotSpot radioisotope-based platform (Reaction Biology Corp). PR5-LL-CM01 showed high specificity to PRMT5, while showed either zero effect or at least a 10-fold higher IC_{50} to other PRMT family members than that of PRMT5. 1-fold means no difference as it is compared to PRMT5.

Table 3. Percent survival in normal control cells at the IC_{50} of cancer cells

Cancer	Cancer Cells	IC_{50}, μM	% survival in control cells (treated with IC_{50} of respective cancer cell line)
PDAC Normal control: HPNE	PANC1	4	80%
	MiaPaCa2	2	90%
	AsPC1	4	80%
CRC normal control: FHC	HT29	10	80%
	HCT116	10	80%
	DLD1	11	80%

A

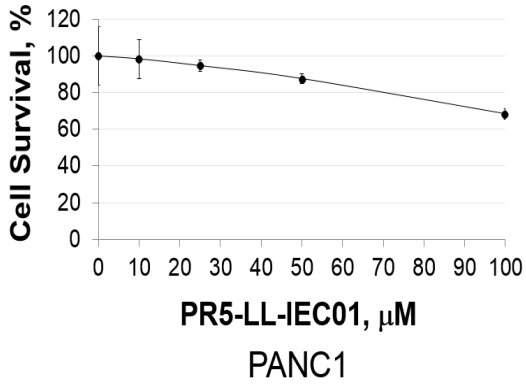

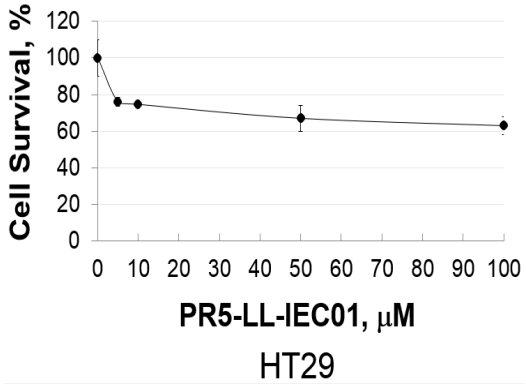

B

Cell Lines	PR5-LL-CM01 IC_{50}, µM	PR5-LL-IEC01 IC_{50}, µM
PANC1	4	161
HT29	10	138

Figure 32. Effect of PR5-LL-IEC01 on Cell Viability of PDAC and CRC Lines

A. MTT assay in PDAC (PANC1) and CRC (HT29), showing a high IC_{50} for PR5-LL-IEC01 in both the cell lines. **B.** Table, summarizing the IC_{50} values for PR5-LL-IEC01 in PANC1 and HT29 cells, respectively.

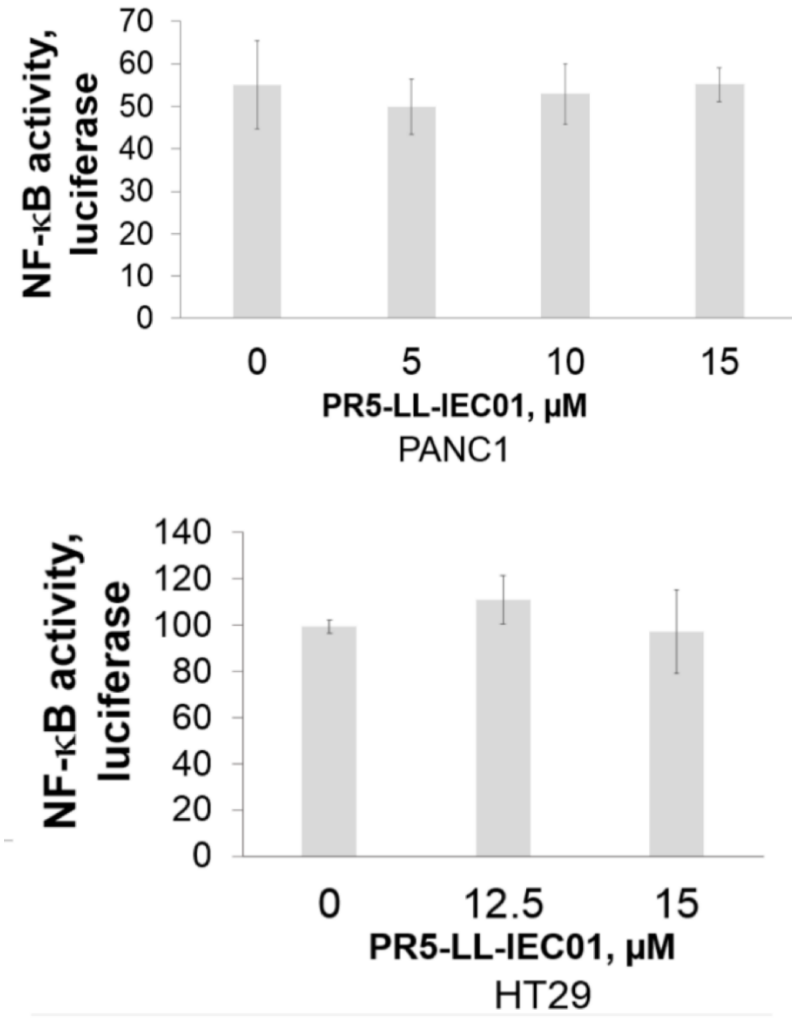

Figure 33. Treatment with PR5-LL-IEC01 had No Effect on NF-κB Activation in PDAC and CRC Cells

NF-κB luciferase assay, showing that upon treatment with increasing concentrations of structural analog PR5-LL-IEC01, there was no change in NF-κB activation in PANC1 and HT29 cells.

Additionally, as compared to cancer cell lines, the respective normal control cells had a much higher survival at the IC_{50} observed in their cancer cell line counterparts (**Table 2**). HPNE and FHC are the normal pancreatic and colon control cell lines respectively, that were used in the present study. This suggested that PR5- LL-CM01 had was more efficacious in specifically inhibiting Additionally, as compared to cancer cell lines, the respective normal control cells had a much higher survival at the IC_{50} observed in their cancer cell line counterparts (**Table 2**). HPNE and FHC are the normal pancreatic and colon control cell lines respectively, that were used in the present study. This cancer cells compared to normal cells from the same tissue of origin. In addition, we determined the IC_{50} of the inactive structural analog PR5-LL-IEC01 in PANC1 and HT29 cells using the MTT assay. Not surprisingly, the potency of PRC-LL-IEC01 was considerably less with an IC50 >14-40 fold compared to PR5-LL-CM01 (**Figure 32**) in the same cell lines. Moreover, when we checked for NF-κB activation upon treatment with inactive analog, PR5-LL-IEC01 had no significant effect on the NF-κB activation in both PDAC and CRC cells, indicating the specificity of PR5-LL-CM01 to decrease NF-κB activation in these cell lines (**Figure 33**). Overall, these data support the specificity of PRMT5 inhibition effect observed upon treatment with PR5-LL-CM01.

4.2.10 Structural Prediction of PR5-LL-CM01 Docked to PRMT5

With all the studies described so far, it is clear that PR5-LL-CM01 is specific for PRMT5 and is efficacious in reducing the cancer phenotype in PDAC and CRC cells. In order to delve deeper into the possible interactions between PR5-LL-CM01 and PRMT5, we employed a structural modeling approach using the existing information of PRMT5 crystal structure (Antonysamy *et al.*, 2012). This work was in collaboration with Dr. Ozlem Demir at the University of California, San Diego under the guidance of Dr. Rommie Amaro. In addition to PR5-LL-CM01, we also included EPZ015666 in the analysis to determine if there were any similarities between the two inhibitors in their respective interactions with PRMT5. As illustrated in **Figure 34**, PR5-LL-CM01 was docked in the presence (SAM-bound) or absence of SAM (Apo-PRMT5). Under SAM-bound condition (**Figure 34, upper left panel**), the binding sites for PR5-LL-CM01 and EPZ015666 on PRMT5 overlap to a great extent, indicating that these two inhibitors probably interact with PRMT5 through largely similar group of binding sites. However, in the Apo-PRMT5 condition, though the binding sites of EPZ015666 remain the same as those in SAM-bound condition, the binding position of PR5-LL-CM01 shifted dramatically from its original binding position in the SAM-bound condition to the new position (pink dotted line, **Figure 34 upper right panel**), which is similar as the SAM binding position in the SAM-bound condition (**Figure 34, upper left panel**). This interesting phenomenon suggested that PR5-LL-CM01 could interfere with the residues involved in SAM binding to PRMT5 in SAM-bound PRMT5, but might also block the binding of

SAM to Apo-PRMT5 by occupying the similar binding site for SAM. In contrast, EPZ015666 binding stayed the same in both SAM-bound or Apo-PRMT5 conditions, thus binding to PRMT5 in a completely independent manner from SAM, which is consistent with previously published data (Chan-Penebre *et al.*, 2016). In addition, we showed that both binding events under SAM-bound or Apo-SAM conditions are energetically beneficial, with the Apo-PRMT5 (-7.911 kcal/mol) being slightly more favorable than the SAM-bound condition (-6.949 kcal/mol) (**Figure 34, lower panel**).

A ligand binding affinity map (**Figure 35A**) further depicts the PRMT5 residues that interact with PR5-LL-CM01 in the SAM-bound condition. Importantly, PR5-LL-CM01 forms a hydrogen bond with the E444 residue in the PRMT5 active pocket. This residue is essential for the methyltransferase activity of PRMT5. There is also another critical interaction observed with F327, which is a residue that is important for determining the symmetric dimethylation activity of PRMT5 vs. other PRMTs, which display asymmetric dimethylation or monomethylation. Both these interactions hint at yet another layer of mechanistic insight regarding how PR5-LL-CM01 may inhibit PRMT5 activity.

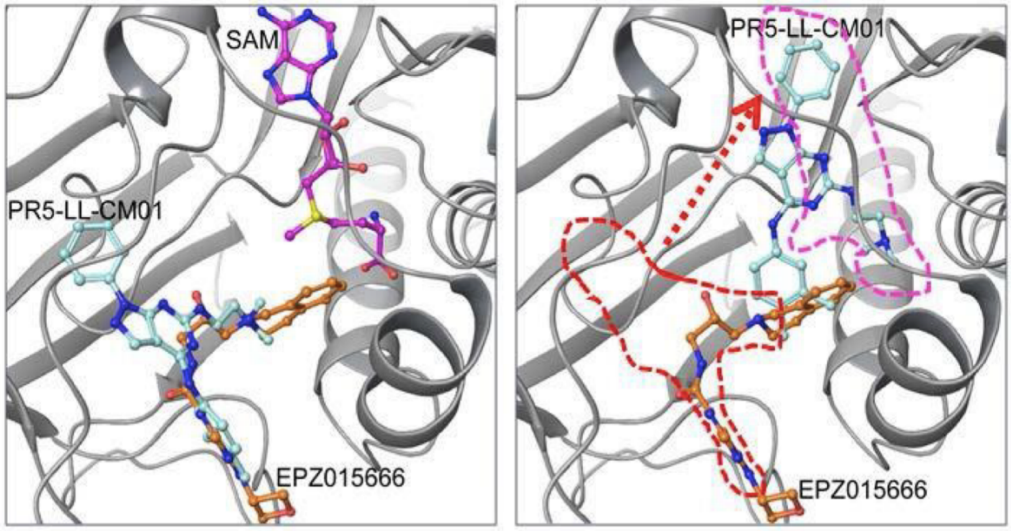

Docking State of PRMT5	PR5-LL-CM01 Docking Score/ Binding affinity (kcal/mol)
SAM-bound PRMT5	-6.949
Apo-PRMT5	-7.911

Figure 34. In Silico Prediction of PR5-LL-CM01 and EPZ015666 respectively Binding to PRMT5

Upper left panel, In SAM (purple color)-bound condition, the binding sites for PR5-LL-CM01 (turquoise color) and EPZ015666 (orange color) on PRMT5 overlap to a great extent, suggesting that these two compounds inhibit PRMT5 through largely similar group of binding sites. *Upper right panel*, in Apo-PRMT5 condition, the binding of EPZ015666 remains the same as that in the *left panel*, however, PR5-LL-CM01 has shifted dramatically from its *left panel's* position (red dotted line) to the new position (pink dotted line), which is same as SAM's position in the *left panel*. *Lower panel,* Table, listing the binding affinities of PR5-LL-CM01-PRMT5 interactions in SAM bound and Apo-PRMT5 conditions. PR5-LL-CM01 showed favorable binding energies under both conditions, with Apo-PRMT5 condition having a slightly stronger binding affinity (-7.911 kcal/mol).

Since under the SAM-bound condition, PR5-LL-CM01 and EPZ015666 bind to PRMT5 in a largely overlapped region (**Figure 34**), we looked at these residues in much more detail in **Figure 35B**. The sites that can solely interact with PRMT5 by PR5-LL-CM01 are denoted in red, solely by EPZ015666 in blue, or by both in green. Most of the residues are present in the Rossman fold, followed by several residues in the β-barrel, and some residues in the linker domain of the PRMT5 structure (**Figure 6**). Since the methyltransferase domain is comprised within the Rossman and β-barrel domains, these evidences further support that PR5-LL-CM01 binds to residues in the catalytic domain of PRMT5. We show that in addition to a few commonly shared binding sites with EPZ015666, PR5-LL-CM01 largely exhibits its quite unique binding sites to PRMT5 (**Figure 35B**), possibly contributing to the different efficacies we observed in the previous figures. Overall, the structural analysis gives us a valuable insight into various binding interactions that could be occurring between PR5-LL-CM01 and PRMT5 and present a plethora of opportunities for further studies to verify these predicted interactions.

4.2.11 Attempts to Determine Direct Binding Between PR5-LL-CM01 and PRMT5

4.2.11A *Using Sepharose Bead-based Conjugation Method to Study Binding Interaction of PR5-LL-CM01 with PRMT5*

In order to provide evidence of a direct binding interaction between PR5-LL-CM01 and PRMT5, we decided to use CNBr-activated Sepharose beads to conjugate with the inhibitor and then incubated with cell lysate that contains the

target, PRMT5 to allow for the binding between the two. The beads were then pulled down, unconjugated from the inhibitor and its potential target PRMT5 that binds to the inhibitor could be detected using Western blotting with PRMT5-specific primary antibody.

We tried combinations of different tube sizes and milk concentrations for blocking the beads in order to reduce background due to non-specific binding to the beads. The 10% milk/15ml Falcon tube worked best to reduce the non-specific background binding of PRTM5, in the absence of inhibitor conjugated to the beads **(Figure 36A**). When we used this condition for the experiment with PR5-LL-CM01, we did not observe any bands in the test sample (**Figure 36B**). One possibility for this result could be that the compounds did not bind to the beads well. One caveat to the usage of these specific beads is that they bind to compounds that contain primary amines in the structure, as per the manufacturer's recommendations. However, PR5-LL-CM01 does not have primary amines, only a secondary amine in its structure. These beads have been shown in the past to conjugate with compounds containing secondary amines (Zhang *et al.*, 2016), hence we decided to attempt it with our compound as well but did not have success. Looking at the docked structure in **Figure 34**, the reason for non-conjugation could be due to the fact the imino group of PR5-LL-CM01 is within its binding pocket with PRMT5 and thus could be shielded from the Sepharose beads. Another reason for absence of conjugation could be that the

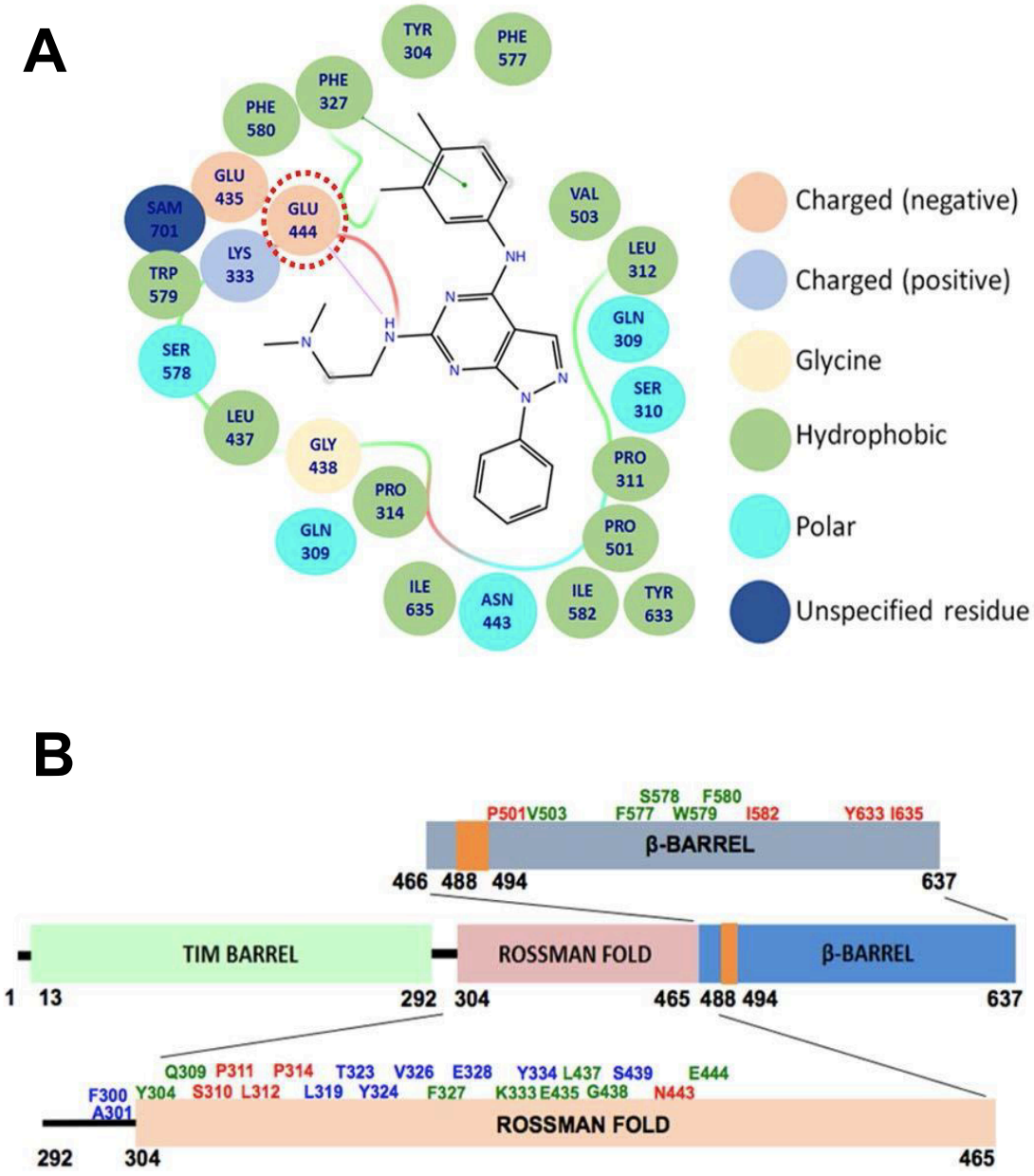

Figure 35. Postulation of PRMT5 Residues Interacting with PR5-LL-CM01
A. Ligand affinity map in the SAM-bound condition, depicting the PRMT5 residues interacted with PR5-LL-CM01. Different bonds or charges are symbolized on the right side of the figure. Key site, E444, is circled in red dotted line. **B**. Binding residue distribution diagram, illustrating the PRMT5 residues that potentially bind to PR5-LL-CM01 alone (red font), EPZ015666 alone (blue font), or both (green font).

concentration of drug we used might be too low. We decided that since the beads were not manufactured to interact with secondary amines and could lead to extensive troubleshooting and low chance of success, it would be wiser to look at other means to achieve this goal.

4.2.11B *Using Isothermal Calorimetry (ITC) Method to Study Binding Interaction of PR5-LL-CM01 with PRMT5*

As an alternative to the Sepharose beads approach, we decided to use the ITC method to test the binding interaction of PR5-LL-CM01 with PRMT5. ITC measures the heat change that occurs when molecules interact in solution (Holdgate 2001). A major advantage of this assay over the Sepharose beads approach was the lack of labelling/conjugation that was required to conduct the study. However, as we began designing experiments for optimizing the assay for our purpose, we quickly realized a major disadvantage of this assay was the large quantities of enzyme needed for each troubleshooting and/or optimization step. Every time, 1-1.2mg of Flag-tagged PRMT5 was purified from mammalian cell lines, which made the method extremely labor intensive, time-consuming and expensive. A representative ITC curve is depicted in **Figure 37,** when PR5-LL-CM01 was added stepwise to the purified PRMT5 enzyme solution in the ITC instrument. This curve suggested that there could be slight turnover of the compound by the enzyme, as observed by the step-wise decrease in the curve. This trend could be because PR5-LL-CM01 bound to PRMT5 in the SAM binding site in the absence of SAM in this reaction, as predicted in **Figure 34**. However, the ITC method is extremely sensitive to errors and this could also be a false

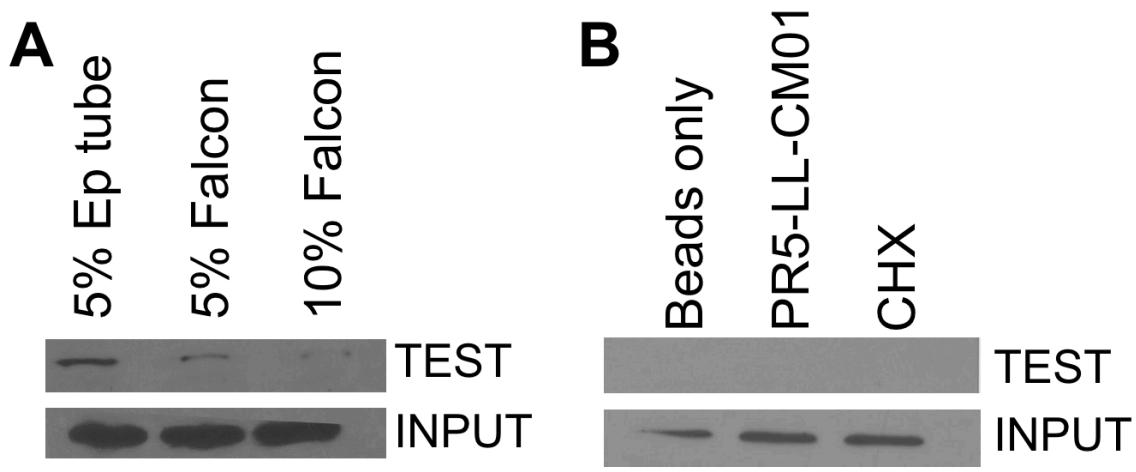

Figure 36. Sepharose Bead-based Conjugation Method to Study Binding Interaction of PR5-LL-CM01 with PRMT5

A. Western blot with conditions to optimize blocking (Eppendorf tube and 15ml Falcon tube; 5% and 10% milk) for reducing background caused due to non-specific binding of components in the cell lysate to the Sepharose beads. In this experiment, the beads are not conjugated to the inhibitor, so one would expect no PRMT5 binding to the beads. 10% milk/15ml Falcon tube worked best in reducing the non-specific PRMT5 background band the most, upon probing for PRMT5 expression. **B**. Conjugation of beads with PR5-LL-CM01, followed by incubation with cell lysate and pulldown to detect PRMT5 did not show much success as no bands were observed when probed for PRMT5 expression. Cycloheximide (CHX) was used as a non-specific protein that does not bind to the Sepharose beads

result due to heat changes that occur on account of buffer mismatch. Since massive troubleshooting was anticipated to verify these results and the purification of enzyme was not proving to be feasible, we decided to think about alternative approaches to this method as described in **Chapter 6**.

4.2.11C *Using Cellular Thermal Shift Assay (CETSA) Method to Study Binding Interaction of PR5-LL-CM01 with PRMT5*

In order to test the binding interaction of PR5-LL-CM01 with PRMT5 in PANC1 and HT29 cells, we used the CETSA approach. Unlike Sepharose beads and ITC, CETSA allows for assessment of the drug-target engagement in cells (Almqvist *et al.*, 2016). The basic principle of this study involves thermal shifts that occur on account of compound binding to the target in cell lysates (Martinez-Molina *et al.*, 2013). Binding quantification was done using Western blotting with a specific antibody that can identify the target. We used the highly specific anti-PRMT5 antibody described in the Methods section for our purpose. Upon treatment with PR5-LL-CM01 for both PANC1 and HT29 cells, we observed an apparent shift in the melting curve of PRMT5 between the treated *vs*. untreated condition in both PANC1 and HT29 cells (**Figure 38**). However, variability between the two groups was high and therefore no statistically significant difference could be detected.

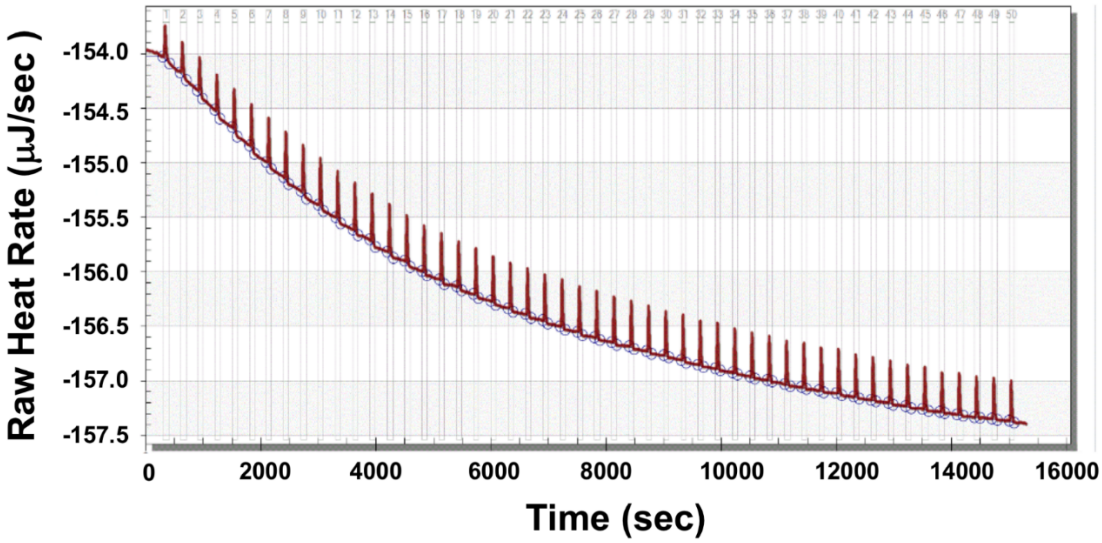

Figure 37. Isothermal Calorimetry (ITC) Approach to Assess Binding Interaction of PR5-LL-CM01 with PRMT5

ITC curve showing the heat changes in solution in μJ/sec, when PR5-LL-CM01 was mixed with PRMT5 over time. The step-wise decrease in the curve suggests that there could be slight turnover of the compound by PRMT5, if PR5-LL-CM01 could be binding to PRMT5 in the SAM binding site in the absence of SAM, as predicted in **Figure 34**.

Moving forward, I have proposed specific experiments in **Chapter 6** that will help in better understanding of possible direct interactions between PR5-LL-CM01 and PRTM5 *in vitro*.

4.2.12 Dose Finding/Chronic Toxicity Study of PR5-LL-CM01 in NSG mice

An important aspect of PR5-LL-CM01 efficacy that was untested so far was its potential in *in vivo* cancer models. Xenograft models of cancer have been well established as a means for early phase drug development to test efficacy in higher model organisms beyond mammalian cell lines cultured in a petri dish (Jung 2014). Hence, the next logical step was to test PR5-LL-CM01 in the *in vivo* models of PDAC and CRC. However, since this compound has never been injected in animal models before, it was imperative to do a preliminary study to determine dosages that would be appropriate for testing without being toxic to the animal. We decided to use mice originally developed at The Jackson Laboratory and bred in-house at the IVT for our purpose. NSG mice strain is extremely immunodeficient strain and they lack mature T cells, B cells, and natural killer (NK) cells (Ishikawa *et al.*, 2005; Shultz *et al.*, 2005). These immunodeficiencies allow engraftment of a wide range of human cells and enable sophisticated modeling of diverse areas of human biology and disease. This experiment was conducted in collaboration with the IVT core. Two dosages of PR5-LL-CM01, 20mg/kg and 50mg/kg, were injected 3X/week in the first week and single injection daily (SID) for the second week. Toxicity in terms of changes in body weight as well as physical observations in gait and posture were checked

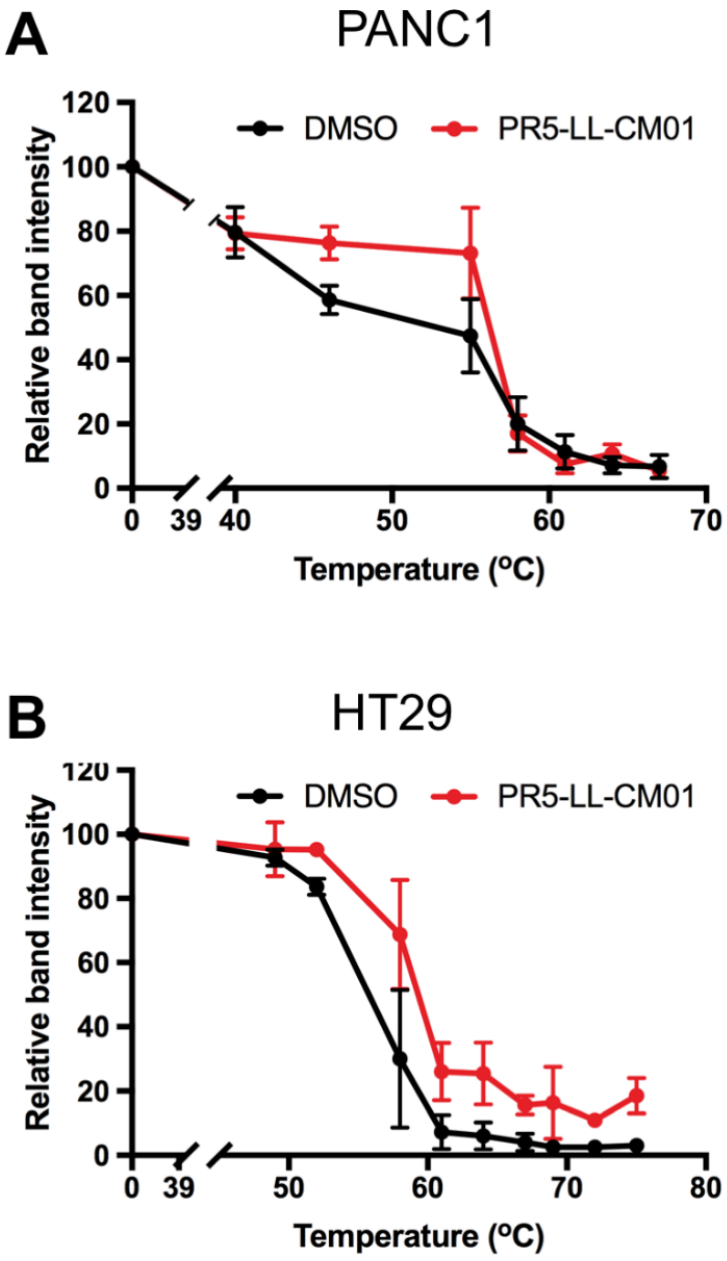

Figure 38. Cellular Thermal Shift Assay to Assess Binding Interaction of PR5-LL-CM01 with PRMT5

Western blot to test the shift in melting curve for PRMT5, in the presence and absence of PR5-LL-CM01 treatment for **A**. PANC1 and **B**. HT29 cells respectively. A slight shift was observed for both cell lines upon compound treatment, however, the difference is not statistically significant.

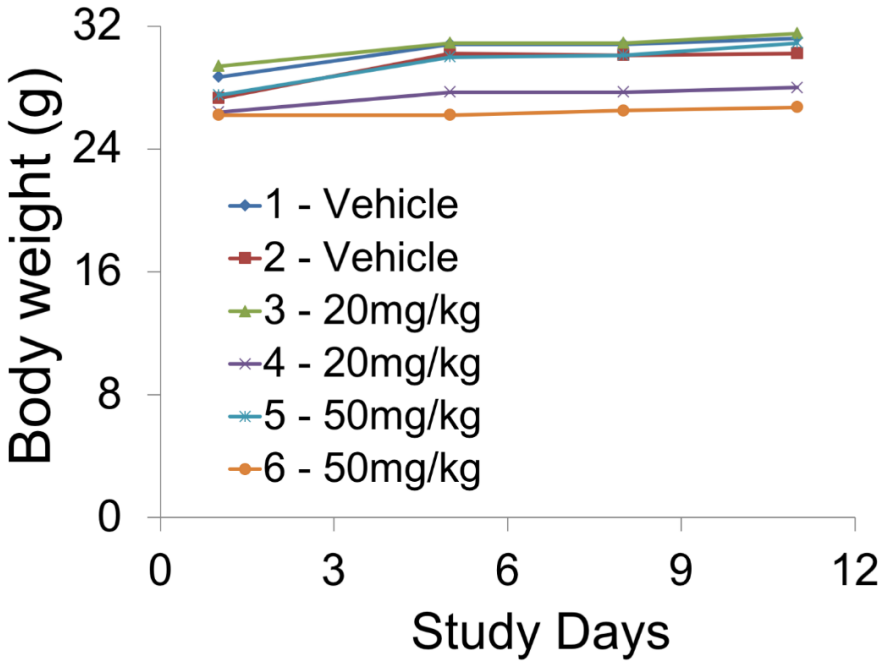

OBSERVATIONS
Week One 3X/week started
10/26/15 - All mice appear normal ~20 min post dose
10/28/15 - All mice appear normal ~15 min post dose
10/30/15 - All mice appear normal ~15 min post dose
Week Two SID started
11/2/15 Had to sonicate 50mg/kg for ~30 seconds
11/2/15 - All mice appear normal ~15 min post dose
11/3/15 - All mice appear normal ~15 min post dose
11/4/15 - All mice appear normal ~10 min post dose
11/5/15 - All mice appear normal ~10 min post dose
11/6/15 - All mice appear normal ~10 min post dose

Figure 39. Toxicity Study of PR5-LL-CM01 in NSG mice
No changes in (Left panel) body weight and (Right panel) gait and posture were observed upon treatment of Vehicle Control, 20mg/kg and 50mg/kg over the course of the toxicity study.

over the course of compound injection and no changes were observed in any of these parameters (**Figure 39**), thus informing that these dosages were not toxic to the mouse and this range could be used in further studies. However, it is important to consider that these mice do not mimic the human situation, which has a normal immune function and these toxicity studies will be replicated in normal mice in the future.

4.2.13 Pharmacokinetic Study of PR5-LL-CM01

In order to determine drug concentrations of PR5-LL-CM01 in pharmacological models, we first needed to characterize the pharmacokinetic (PK) properties of the compounds in mice. PK parameters allow us to get an idea of the absorption, distribution, metabolism and excretion properties of a compound in a chosen model system. In this case, we used NSG mice as our *in vivo* mouse model. Before conducting the *in vivo* study, we collaborated with Dr. David Jones at IU CPAC to develop a method for detection of PR5-LL-CM01 using LC-MS. The details of method development shared by Dr. Jones are listed in **Appendix C**. Next, PK parameters of PR5-LL-CM01 were determined in NSG mice following a single I.P. dose administration of 20mg/kg followed by blood collection using facial saphenous vein at 1, 2, 4, 8, and 24 h. The plasma samples were then sent to the CPAC for detection of the PR5-LL-CM01 using the method developed previously. As observed in **Figure 40**, we observed a time-dependent decrease in the plasma concentrations of PR5-LL-CM01, with an

almost entire elimination at 24 h post injection. The PK parameters are shown in **Table 3**. The half-life of the drug was calculated to be ~3.3 h.

Furthermore, we collected tissue samples at 4 h and 24 h time points for pancreas and colon (sites for PDAC and CRC, respectively), to determine the amount of drug delivered to the target tissues. Interestingly, we could detect the presence of significant quantities of PR5-LL-CM01 at 4 h post injection in the pancreas and colon respectively, indicating that PR5-LL-CM01 was successfully delivered to the target tissues. Our data also suggested a complete clearance at 24 h post injection (**Figure 41**). Further studies are needed with more time points to get a more elaborate idea of the tissue PK dynamics. Some potential experiments have been addressed in **Chapter 6**.

4.2.14 Tumor Growth Pilot for PANC1 and HT29 using Subcutaneous Injection

Before beginning tumor efficacy studies, it was important to determine the proper implant conditions for PDAC and CRC cells to be used for the same. In order to achieve this goal, we injected three different cell numbers of PANC1 cells s.c. in NSG mice: $5X10^6$, $8X10^6$ and $10X10^6$ cells per mouse. We then checked for growth kinetics over a period of time by measuring tumor volume at regular intervals (**Figure 42A**). $2000mm^3$ is the cutoff for tumor size for sacrifice as per the ethical regulations under the approved protocol. As shown in **Figure 42A** here, $10X10^6$ cells managed to reach the peak tumor volume of $2000mm^3$ at around 4 weeks after implant. Hence, we decided to use a cell number of $10X10^6$

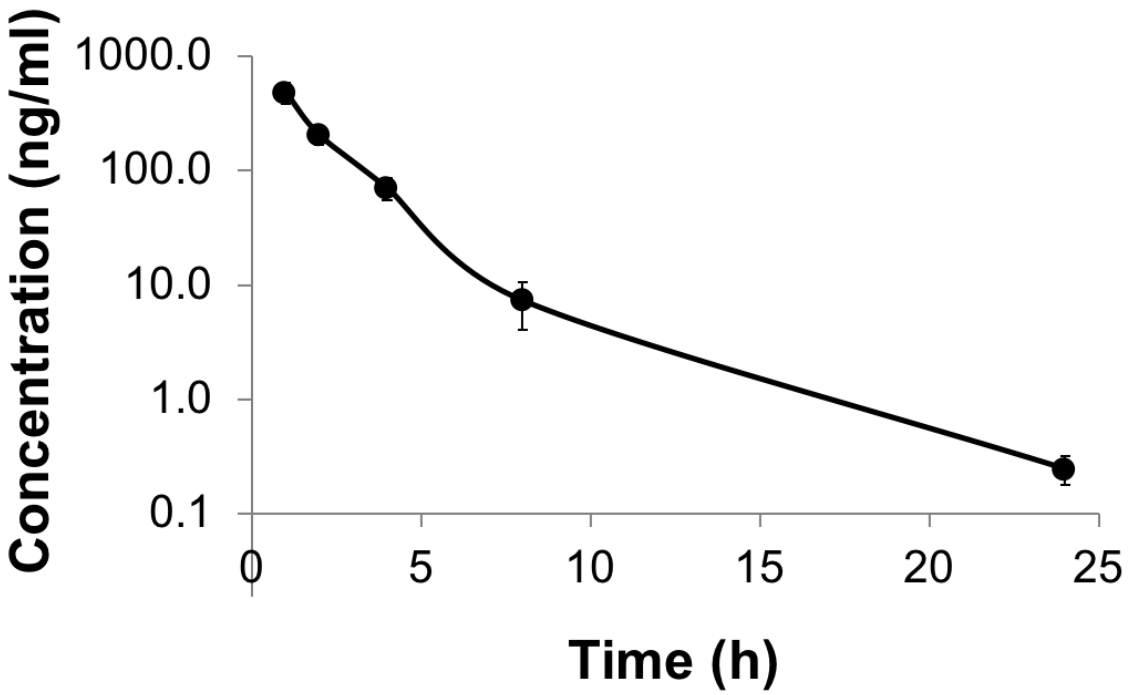

Figure 40. Plasma Pharmacokinetic Graph for PR5-LL-CM01
Graph showing the presence of PR5-LL-CM01 in plasma in a time course of 1,2,4,8,24h. With peak concentration at 1 h after 20mg/kg PR5-LL-CM01injection, it is almost completely cleared out after 24 h. The half-life was calculated to be ~3.3 h.

Table 4. PK parameters of PR5-LL-CM01

Dosage	20mg/kg
Route of Administration	i.p.
C_{max}	489ng/ml (1.2μM)
t_{max}	1h
$AUC_{0-\infty}$	1087ng*mL^{-1}*h
$t_{½}$	3.3h
Cl/F	0.46L/h
Vd_{ss}/F	1.11 L

Abbreviations:
C_{max}: maximum concentration
t_{max}: time of maximum concentration
$AUC_{0-\infty}$: area under the plasma concentration-time curve from 0-infinity
$t_{1/2}$: half-life
Cl/F: clearance/availability
Vd_{ss}/F: apparent volume of distribution

Comments:
Model: NCA-xls, non-compartmental using PK add ins
All PK parameters were derived from average data.
Assumed mouse weight was 25g.
Half-life was estimated using 2 points.

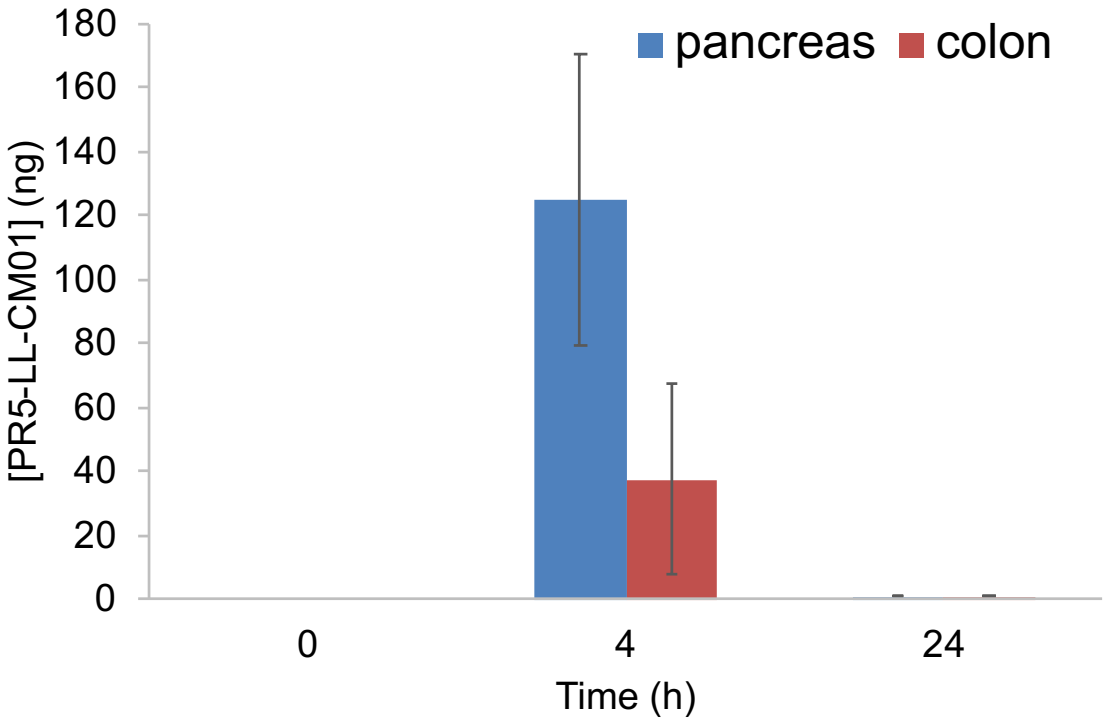

Figure 41. Tissue Pharmacokinetic Graph for PR5-LL-CM01
Graph showing the presence of PR5-LL-CM01 in pancreas and colon tissue in a time course of 0, 4, and 24h. We observe PR5-LL-CM01 in both the pancreas and colon of the mice, and it is completely cleared at 24h. This indicates that PR5-LL-CM01 does reach the sites of where PDAC and CRC originate respectively.

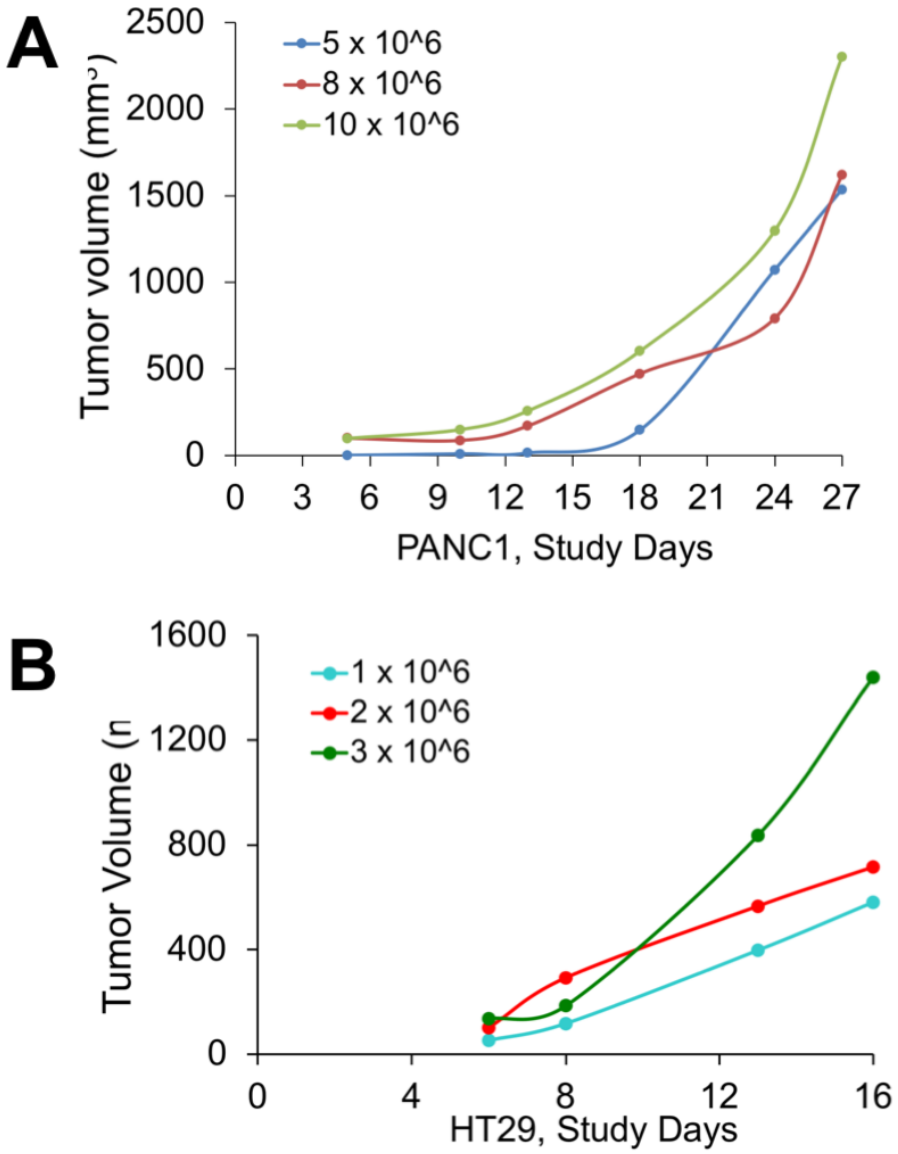

Figure 42. Tumor Growth Pilot Study for PANC1 and HT29 Using Subcutaneous Injection

Graph depicting tumor growth over time for **A.** PANC1 and **B.** HT29 cells when they were subcutaneously implanted respectively in NSG mice.

PANC1 cells per mouse for tumor implant. A similar tumor kinetic study was done for HT29 cells in NSG mice by injecting $1X10^6$, $2X10^6$ and $3X10^6$ cells s.c., in collaboration with IVT. As observed in **Figure 42B**, $3X10^6$ cells reached the $2000mm^3$ mark at the earliest *i.e.* ~2 weeks and was the number we finalized for future implants using HT29 cells.

4.2.15 Anti-tumor Efficacy Study for PR-LL-CM01 in a Subcutaneous Xenograft Model of PDAC and CRC

Once we optimized the dosage and implant conditions, the next logical step was to conduct a tumor efficacy study *in vivo.* Either PANC1 or HT29 cells were subcutaneously xenografted into NSG mice and then treated with PR5-LL-CM01 three times per week at 20mg/kg till the day the mice were sacrificed. Both body weight and tumor size were monitored during this process. As shown in **Figure 43A**, injection of PR5-LL-CM01 did not visibly affect the mice body weight. However, it led to significant tumor inhibition in both PANC1 and HT29 (**Figure 43B**) xenografted mice, demonstrating the strong anti-tumor efficacy of PR5-LL-CM01 in both PDAC and CRC.

4.2.16 Anti-tumor Efficacy Study for PR-LL-CM01 in an Orthotopic Xenograft Model of PDAC and CRC

Orthotopic xenograft models involve introducing tumors directly into the organ of origin for the respective cancers. A main advantage of this model over s.c. type is the ability to have similar tumor microenvironments as the original

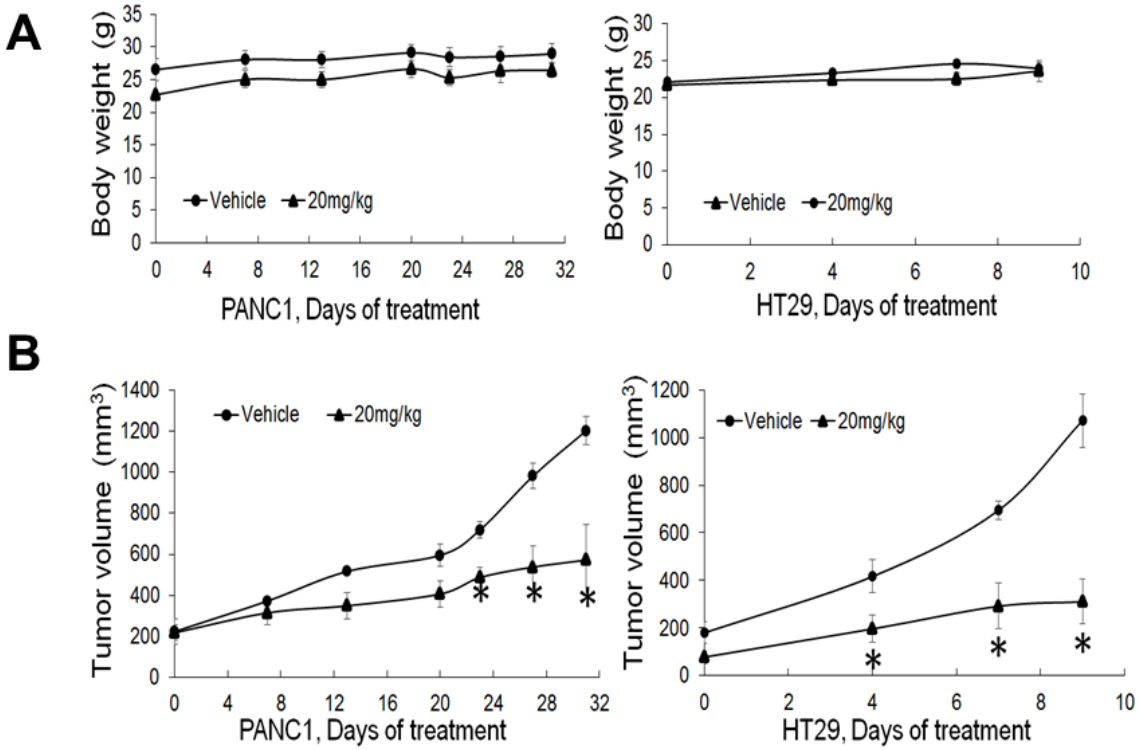

Figure 43. PR5-LL-CM01 displayed significant anti-tumor effect *in vivo*. **A.** No significant changes in body weight were observed over the course of treatment in either PANC1 or HT29 model after treatment with 20mg/kg of PR5-LL-CM01. (*$P < 0.05$, $n = 4$). **B.** Tumor efficacy study for PANC1 or HT29 cells which were subcutaneously implanted in NSG mice. Inhibition of tumor growth was observed upon treatment with 20mg/kg of PR5-LL-CM01 intraperitoneally for 3X/week, as compared to the vehicle control. (*$P < 0.05$, $n = 4$).

tumor and thus are considered to more closely resemble the human condition. Moreover, orthotopic mouse models develop metastasis which is rarely seen in the s.c. model (Qiu and Su, 2012). To this end, we collaborated with IVT to do orthotopic implants in NSG mice with PANC1 cells that contain a fusion protein with cDNA for the luciferase gene (Shannon *et al.*, 2015). After the tumors were allowed to grow for 10 days, SID treatment with 20mg/kg PR5-LL-CM01 was initiated in these mice. Tumor sizes were measured using BLI imaging upon injection of a luciferase substrate as described in the Methods section. We observed a significant decrease in tumor size as per the emission measurements (**Figure 44**), with treatment with PR5-LL-CM01, as compared to the Vehicle control. These results are quite promising as they emphasize the tumor efficacy of PR5-LL-CM01 in a more advanced model system beyond the heterotopic s.c. model. Further studies with an orthotopic model for CRC will be conducted to understand the efficacy of PR5-LL-CM01 in this cancer.

4.2.17 Generation of PR5-LL-CM01 Derivatives

In our studies so far, PR5-LL-CM01 has displayed remarkable efficacy in inhibiting cancer progression. However, as we continue to do more in-depth studies, there are possibilities that we might run into efficacy issues. Alternatively, it would be prudent to develop a series of derivatives with comparable or ideally even higher efficacy than the parental control. In this regard, we collaborated with Dr. Lan Chen and Dr. Lifan Zeng from the IU Chemical Genomics Core, an expert chemist who used structure activity

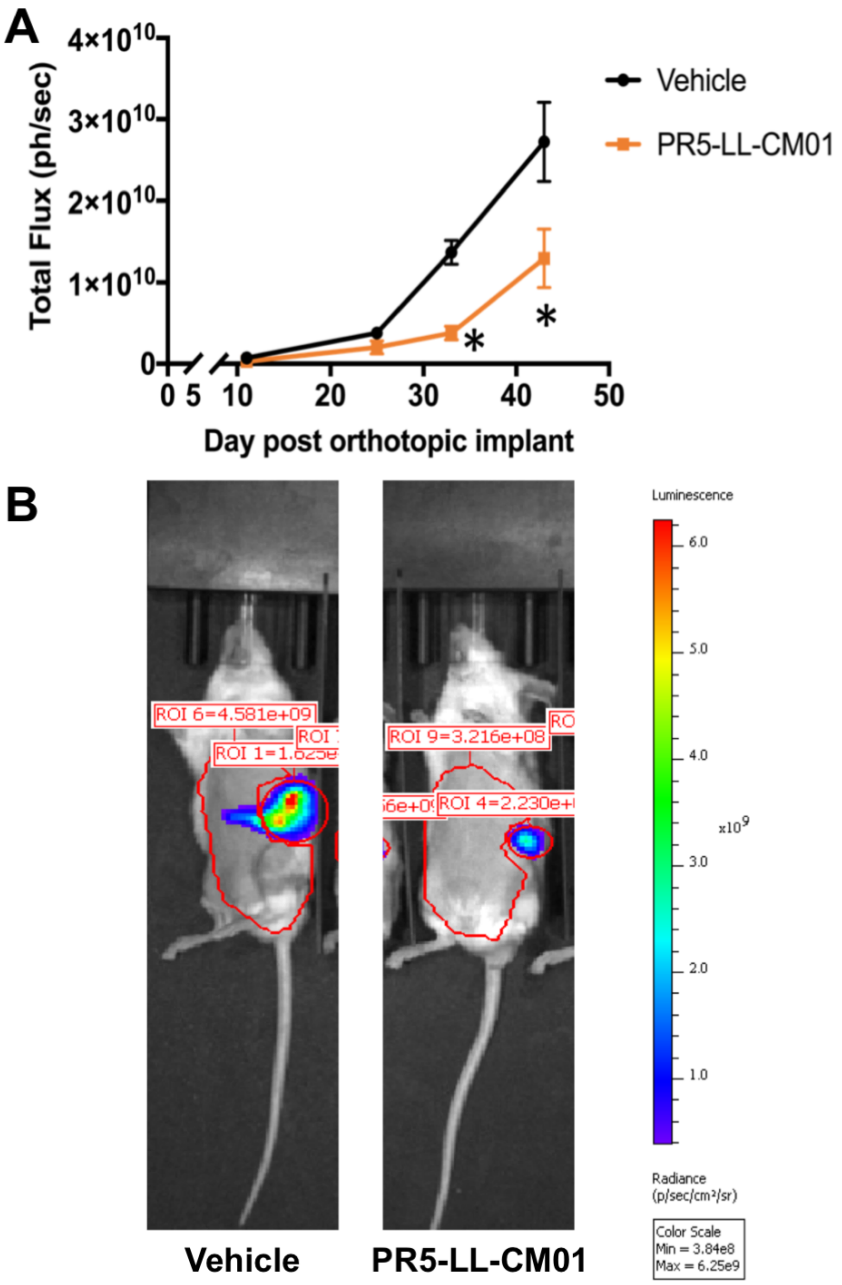

Figure 44. PR5-LL-CM01 Displayed Significant Anti-Tumor Effect In An Orthotopic Model of PDAC

A. Tumor efficacy study in an orthotopically implanted model of PANC1 cells demonstrated that tumor growth was inhibited upon intraperitoneal treatment daily with 20mg/kg of PR5-LL-CM01, as compared to the Vehicle control. Tumor load was measured using bioluminescent imaging and is represented as Total Flux**.** (*P<0.05, n=3-4) **B.** Representative BLI images showing the relative signal intensities for orthotopic implants in both groups.

relationship (SAR) analysis to synthesize several derivatives of PR5-LL-CM01. This involved maintaining the core structure from **Figure 21**, while making slight alterations to the surrounding chemical groups. In this way, Dr. Zeng designed and synthesized 20 derivatives of PR5-LL-CM01. Experimental procedures for derivative synthesis are expounded upon in **Appendix B**. Using MTT assays described previously, we tested the efficacy of these derivatives as compared to the parental compound in both PANC1 and HT29 cell lines. The IC_{50} values for this set of derivatives are summarized in **Table 5**. Only one derivative, PPA-1 showed promise with comparable IC_{50} values in PANC1 and about ~5-fold lower IC_{50} value in HT29 cells. We decided to test this compound further in parallel with PR5-LL-CM01 in an *in vivo* model of PDAC and CRC as described in **Section 4.2.18**.

Furthermore, in collaboration with Dr. Olaf Wiest at University of Notre Dame, we used computer docking analysis to screen ChemDiv libraries with same core group as PR5-LL-CM01. 41 SAM-binding and 40 substrate binding pocket compounds were predicted from these libraries, out of which majority were screened out as they were already part of the ChemDiv library used for the first AlphaLISA HTS described earlier. We further focused on 16 unique compounds that were identified. Similar to the chemically synthesized derivatives, we used MTT assays to compare the efficacies of these structurally analogous compound as compared to Control. As described in **Table 6**, none of the 16 derivatives were as efficacious as the parental compound PR5-LL-CM01

Table 5. MTT IC_{50} values for chemically synthesized PR5-LL-CM01 derivatives by IU Chemical Genomics Core

	Name	IC_{50} (μM) PANC1	IC_{50} (μM) HT29
PR5-LL-CM01 (PARENT)		**5**	**10**
1	STL	35	76
2	PM-1-2	100	Did not reach
3	**PPA-1**	**4**	**2**
4	PTF-1	46	46
5	PAM-1	38	27.5
6	BBL	42	did not reach
7	BAM-1	22	34
8	BPM-1	16	8
9	BTF-1	12	10
10	BAP-1	15	69
11	Pamhp-2-5	did not reach	did not reach
12	Pamhp-1	100	40
13	Pamhp-6pm	79	40
14	Pamhp-8tf	51	37
15	Pamhp-3	did not reach	62
16	Pamhp-5-5	did not reach	94
17	Pamhp-9	13	41
18	Pamhp-4-3	did not reach	did not reach
19	Pamhp-7	13	50
20	Pamhp-10	5	4

Table 6. MTT IC_{50} values for compounds from ChemDiv libraries with similar core structure as PR5-LL-CM01

		Name	PANC1 (μM)		HT-29 (μM)	
			IC_{50}	PR5-LL-CM01	IC_{50}	PR5-LL-CM01
SET 1	1	G932-0007	50	7.5	70	10
	2	G932-0009	18		78	
	3	G932-0014	6		>100	
	4	G932-0018	30		>100	
	5	G932-0173	15		>100	
SET 2	6	G932-0313	10	7	11	10
	7	G932-0323	35		>100	
	8	G932-0810	3		18	
	9	K402-0890	12		*see graph	
	10	K405-2810	34		42	
SET 3	11	K405-3118	74	5	>100	9
	12	K402-0886	8		35	
	13	K405-2750	3		25	
	14	K402-2754	20		31	
	15	G932-3035	12		15.5	
	16	K402-1019	>100	6	>100	10

or the promising derivative PPA-1 collectively for PDAC and CRC cell lines. Finally, moving forward, we would focus on PPA-1, while also continue the SAR analysis to better understand the active parts of the compound structure and check if manipulations in these can significantly improve the efficacy of the parental compound.

4.2.18 Anti-tumor Efficacy Study for PR5-LL-CM01 Derivative PPA-1 in a Subcutaneous Xenograft Model of PDAC and CRC

Next, we wanted to test the *in vivo* tumor efficacy of our most promising inhibitor from our *in vitro* studies, PPA-1 in comparison to PR5-LL-CM01 *in vivo*. What we observed was that the activity of PPA-1 was comparable to PR5-LL-CM01 in decreasing tumor size in NSG mice for both PDAC and CRC cells (**Figure 45A and B; upper panels**). Additionally, there was no visible effect on the mice body weight between the compound or Vehicle-treated groups (**Figure 45A and B; lower panels**). Based on these observations, PPA-1 seemed to be much more effective *in vitro* and comparable to the parental compound *in vivo*. We will continue to further look for even more derivatives which shows several folds difference in efficacy as compared to the parental compound *in vitro* and *vivo*.

4.3 Concluding Remarks

Collectively, the above experiments demonstrated that we have successfully developed a PRMT5-specific AlphaLISA HTS technique by which we discovered a novel PRMT5 inhibitor, PR5-LL-CM01. Furthermore, we

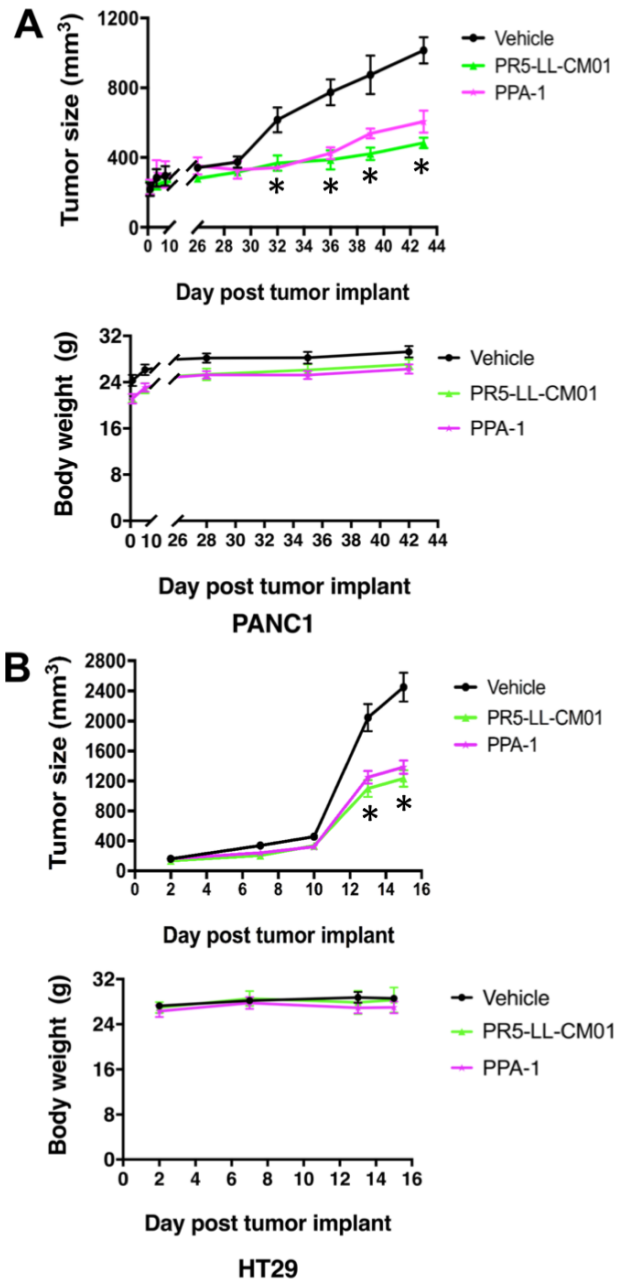

Figure 45. PPA-1 Displayed Significant Anti-Tumor Effect *In Vivo*
Tumor efficacy study for **A.** PANC1 and **B.** HT29 cells which were subcutaneously implanted in NSG mice. Inhibition of tumor growth was observed upon intraperitoneal treatment for 3X/week with 20mg/kg of PR5-LL-CM01 as well as its derivative PPA-1 respectively, as compared to the Vehicle control (Upper panels). No significant changes in body weight were observed over the course of treatment in either PANC1 or HT29 model after treatment with 20mg/kg of PPA-1 or PR5-LL-CM01 (Lower panels). (*P<0.05, n=4).

showed that PR5-LL-CM01 and its promising derivative PPA-1 were able to reduce tumor formation in both *in vitro* and *in vivo* models of PDAC and CRC. Additionally, we also presented evidence for specificity of PR5-LL-CM01 for its target, PRMT5 and the subsequent effect of PRMT5 inhibition on our substrate of interest, NF-κB. Our studies highlight the significant therapeutic potential of PRMT5 in PDAC and CRC. These findings lay a solid foundation for further studies with PR5-LL-CM01 and its derivatives. These efforts may eventually lead to clinical trials in the near future. In the next chapter, we elaborate on efforts to explore even more inhibitors of PRMT5 by running a second round of HTS using compound libraries containing natural compounds and bioactives, distinct from the first round described here containing small molecule compounds.

CHAPTER 5. ADDITIONAL INHIBITORS OF PRMT5 FROM HIGH THROUGHPUT SCREEN #2

5.1 Background and Rationale

In order to take a drug candidate from bench to clinic, there are several early phase efficacy studies in the lab that need to be performed using *in vitro* and *in vivo* models (similar to the ones detailed in **Chapter 4**). This is followed by a lengthy and arduous process of testing the safety, toxicity and efficacy in human patients before the drug can make it to the clinic, besides the time and financial resources involved. Also, the chances of failure remain high, with 1 in 10,000 compounds making it from the bench to bedside.

In the previous chapter, we discovered a novel inhibitor of PRMT5, namely PR5-LL-CM01 that was effective in *in vitro* and *in vivo* models. PR5-LL-CM01 was identified using an HTS screen on chemically synthesized compound libraries. The current chapter details the attempt of a second HTS with a separate set of libraries that contained natural, semi-natural products and known bioactives. The goal was to check if we find even more promising inhibitors of PRMT5 with better efficacy, specificity or both, as compared to the currently available options. This also demonstrates the power of our optimized AlphaLISA protocol to identify compounds that can inhibit the activity of the target of interest, in this case PRMT5. We identified two top hits in the second screen, P1608K04 and P1618J22 which showed efficacy and specificity in PDAC and CRC cells. However, they were not as efficacious as PR5-LL-CM01 in inhibiting PRMT5 and the subsequent NF-κB

activation, as higher concentrations of these compounds were needed with respect to PR5-LL-CM01 to observe similar effects. However, these compounds could prove to be useful for future in other cancers in which PRMT5 is overexpressed, depending if their efficacy is affected by other factors that are unique to the respective tumor microenvironment. However, detailed studies would need to be done to test this possibility. Furthermore, derivatives with better activity than parental compounds and PR5-LL-CM01 could be generated. Overall, the AlphaLISA method is an effective methodology to identify promising drug candidates for specific targets in early phase drug discovery.

5.2 Results

5.2.1 High Throughput Screen Design: Z' Experiment and Quenching

The second round of HTS was designed using the same exact protocol as illustrated in **Table 1** and described in detail in **Chapter 4**. However, there was an extra step we added in order to eliminate any "false hits" which is discussed here. However, as a first step right before running an HTS, it is always advisable to run a Z' experiment to make sure the assay is robust enough to be used for large-scale screening on a repeated basis. We had run a Z' test before our first HTS as described in **Chapter 4.2.2**. Prior to running the second HTS here, we reran the Z' experiment mainly because we prepared a different batch of enzyme prep and used a different batch of beads. The Z' factor was calculated to be 0.7 (**Figure 46**). A Z' factor >0.5 is considered to be robust enough to be used for HTS and thus we proceeded with the second HTS round of screening.

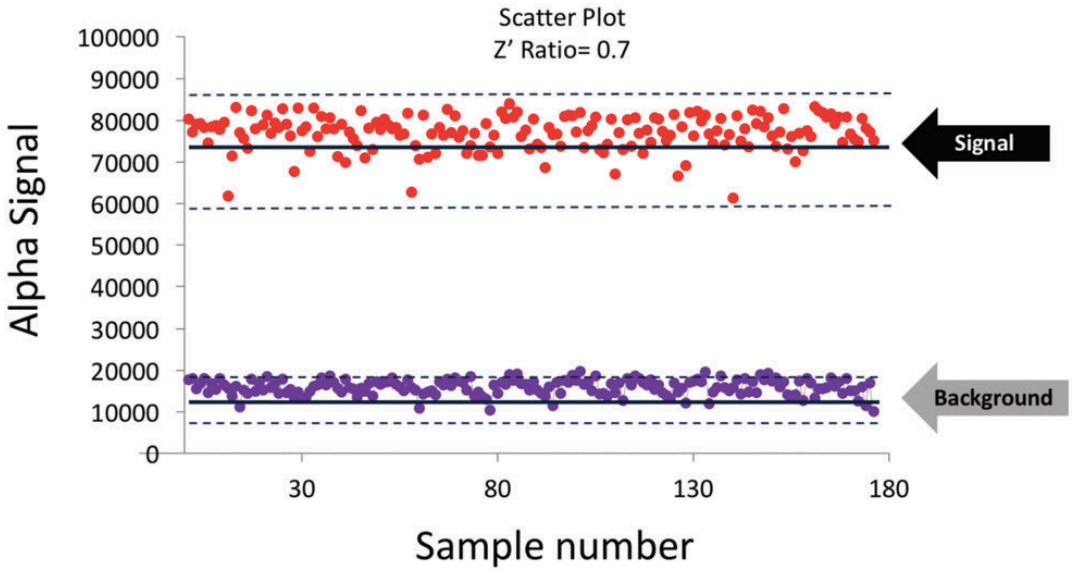

Figure 46. Determination of Z' Factor for PRMT5-specific AlphaLISA Assay

Scatter plot, representing the data points for the 384-well plate, with the red points indicating the ‘‘maximum signal’’ wells and the purple points representing the ‘‘background’’ wells. The solid lines at the center represent the average values and the dotted lines at the top and bottom represent +/- 3 X SD (standard deviation) values for the respective groups. The S/B (signal *vs.* background) ratio was calculated to be 8.3 and the Z' factor was determined to be 0.7.

324 compounds displayed apparent capacity to inhibit PRMT5 methyltransferase activity. These hits were ranked based on their percent inhibition values. However, unlike the library used in the first screen, several of the compounds used in the second screen were colored in nature and thus could autoluminesce. This could lead to the false hits due to interference with the AlphaLISA assay itself rather than inhibiting the enzymatic reaction, resulting in quenching of the Alpha signal. Thus, in order to obtain a more accurate list of positive hits, it was imperative to rule out these “Alpha signal quenchers”. One way to eliminate them was to screen those compounds in a control assay, in which only histone H4 pre-methylated at arginine 3 (Biotin-H4R3me2) was used without adding the PRMT5 enzyme. Under this experimental condition, the Biotin-H4R3me2 peptide will bring the Donor beads and Acceptor beads in close proximity to produce the Alpha signal. In this case, if any compound reduced the Alpha signal, it would be a quencher instead of a real inhibitor. This is because this reduction in signal is unrelated to PRMT5 activity which itself is absent from this reaction.

Figure 47 illustrates the experimental design and plate layout for this filtering experiment among 320 top hits from the HTS screening to eliminate any Alpha signal quenchers. The first and last two columns did not contain compounds, but the first two columns had the pre-methylated peptide substrate which resulted in a high signal; the last two columns did not have me-H4R3 substrate and provided the readings for the background signal. Every well of the

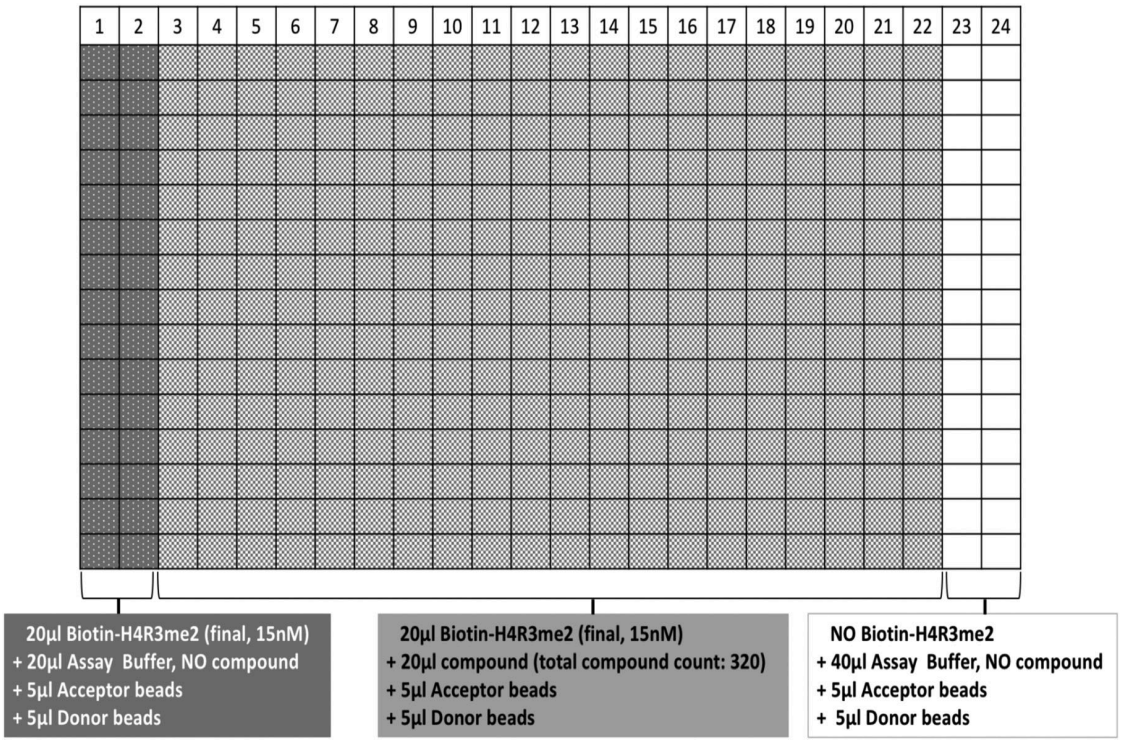

Figure 47. Plate Design for Quenching Experiment to Identify False Positive Hits from AlphaLISA screen

The first two columns (white dots; grey background) do not contain any compound and act as positive controls, signifying ‘‘maximum signal’’. Columns 1-22 had a Biotin-H4R3me2 substrate (dimethylated Biotin-H4R3) added at a final concentration of 15 nM in each well. The last two columns do not have the Biotin-H4R3me2, and act as the ‘‘negative control’’. Acceptor and donor beads were added to each well. No PRMT5 enzyme was included in this experiment. Compounds that exhibited quenching of the Alpha signal were ‘‘false hits’’ and not true PRMT5 inhibitors, and thus were removed from further testing.

plate had both the Acceptor and Donor beads. We identified 64 potential hits that were not false positives and repeated the AlphaLISA to reconfirm their inhibition activity. Several top hits were identified after this rigorous screening process with a cut-off value of over 60% inhibition and were further tested using AlphaLISA assays. The two most promising hits, P1608K04 and P1618J22 were identified as described in the next section. To summarize, we used a systematic screening approach to identify two top hits from a large pool of candidates, as illustrated in **Figure 48A**.

5.2.2 Identification of Top Hits P1608K04 and P1618J22

We conducted preliminary testing on the initial hits using the AlphaLISA assay to check for corresponding effect on PRMT5 methyltransferase activity. Through this testing, P1608K04 and P1618J22 (**Figure 48B**) showed the most promise. In a confirmation experiment, we observed that increased concentrations of both P1608K04 and P1618J22 led to a concurrent decrease in AlphaLISA signal with low IC_{50} values of ~1.5μM and 16.5μM, respectively (**Figure 49A** and **B).** Thus, we employed a stepwise protocol for screening ~10,000 compounds using an AlphaLISA-based approach and identified two promising hits that are specific for reducing the PRMT5 methyltransferase activity.

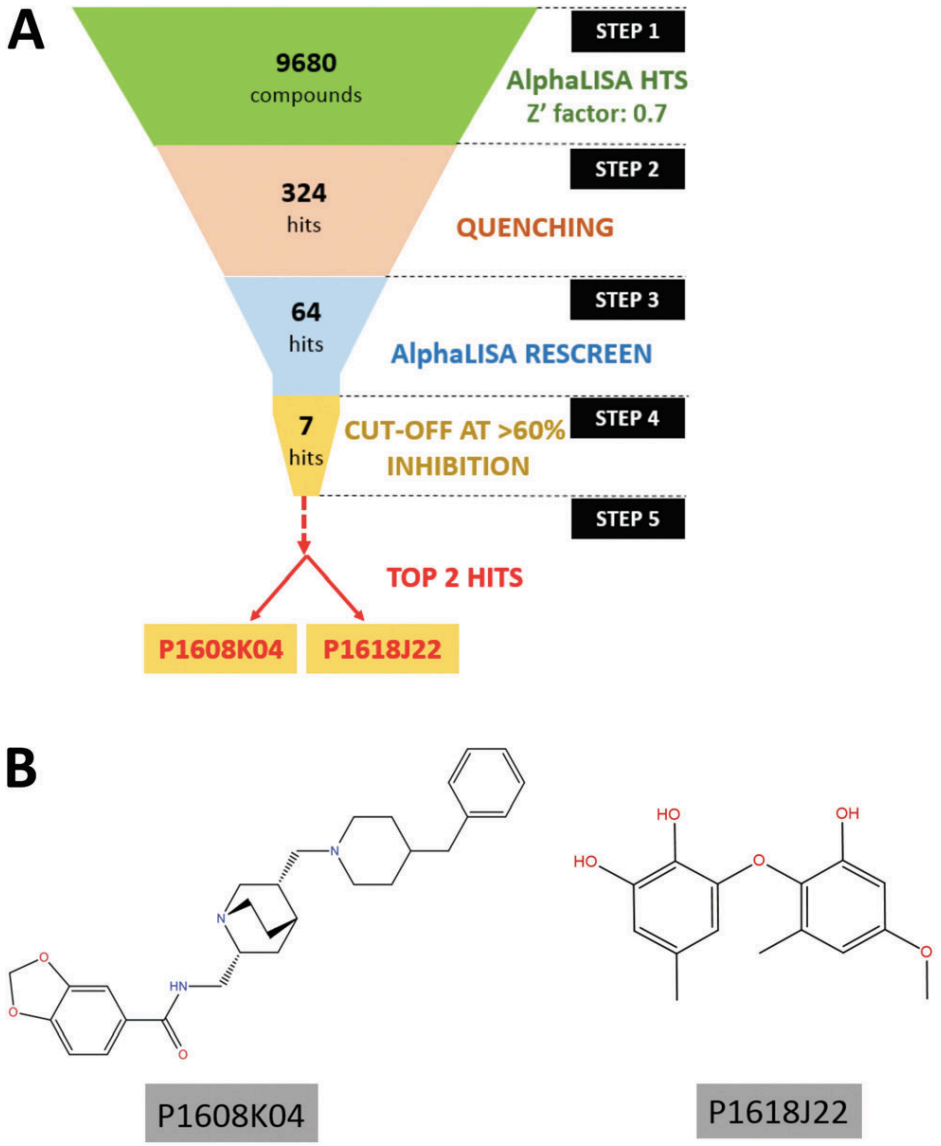

Figure 48. Identification of Top Hits P1608K04 and P1618J22
A. Workflow for the stepwise procedure that eventually led to the shortlisting of two top PRMT5 inhibitors, P1608K04 and P1618J22, among ~10,000 compounds from small compound libraries. Each step represents the experimental approach and the number of compounds to start with.
B. Structures of the 2 top hits: P1608K04 (left panel) and P1618J22 (right panel).

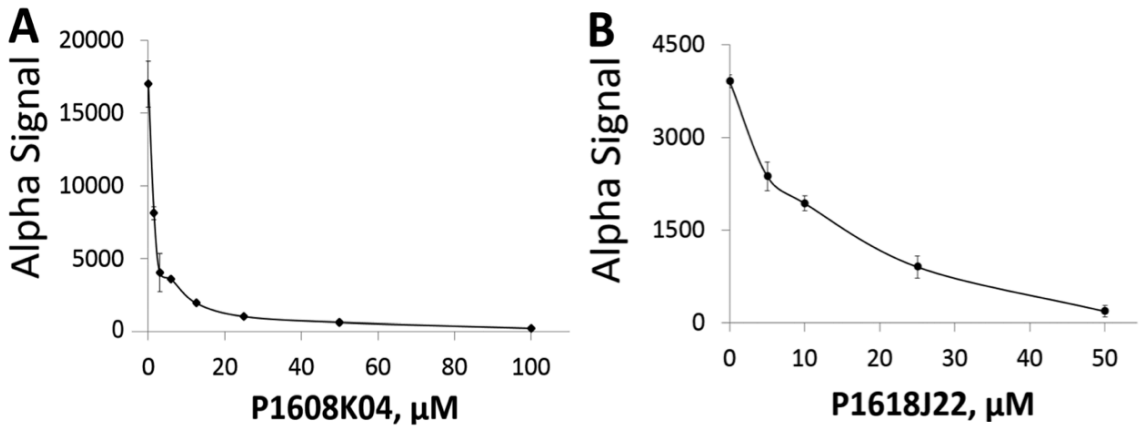

Figure 49. Determination of IC_{50} using the AlphaLISA Assay
A. Calculation of the IC_{50} of P1608K04 using AlphaLISA, showing a concentration-dependent decrease in the Alpha signal. The IC50 was ~1.5µM. **B**. The IC_{50} of P1618J22 was calculated to be 16.5µM, using the same protocol as (A). The data represent the means $\pm$ SD for three independent experiments.

5.2.3 P1608K04 and P1618J22 are Potent PRMT5 Inhibitors *In Vitro*

In order to test the effectiveness of these promising PRMT5 inhibitors in the context of PDAC and CRC, we used the MTT assay with increasing concentrations of P1608K04 and P1618J22 in PDAC and CRC cell lines. Both P1608K04 (**Figures 50A** and **C**) and P1618J22 (**Figures 50B** and **C**) showed great efficacy in decreasing the cell viability in PDAC (PANC1, MiaPaCa2, and AsPC1) and CRC cells (HT29, HCT116, and DLD1). Importantly, both compounds were much more potent (have lower IC_{50}) than the commercial PRMT5 inhibitor EPZ015666 in PDAC and CRC cells (**Figure 24**). Therefore, our data suggested that P1608K04 and P1618J22 are powerful PRMT5 inhibitors in PDAC and CRC cells. Furthermore, the inhibitors identified using our PRMT5-specific AlphaLISA assay could be used as tools to further study PRMT5-driven mechanisms in these cancers.

5.2.4 P1608K04 and P1618J22 Inhibited PRMT5-mediated NF-κB Methylation and Downstream Activation

To test the specificity of PRMT5 inhibitors, we examined their effect on p65 methylation and subsequent activation in both PANC1 and HT29 cells. The first thing we tested was the effect of compound treatment directly on the methylation of p65. In order to detect methylation specifically at the R30 site by PRMT5, we generated a site-specific antibody in collaboration with Genscript Inc. Western analysis with this site-specific antibody against dimethylated R30

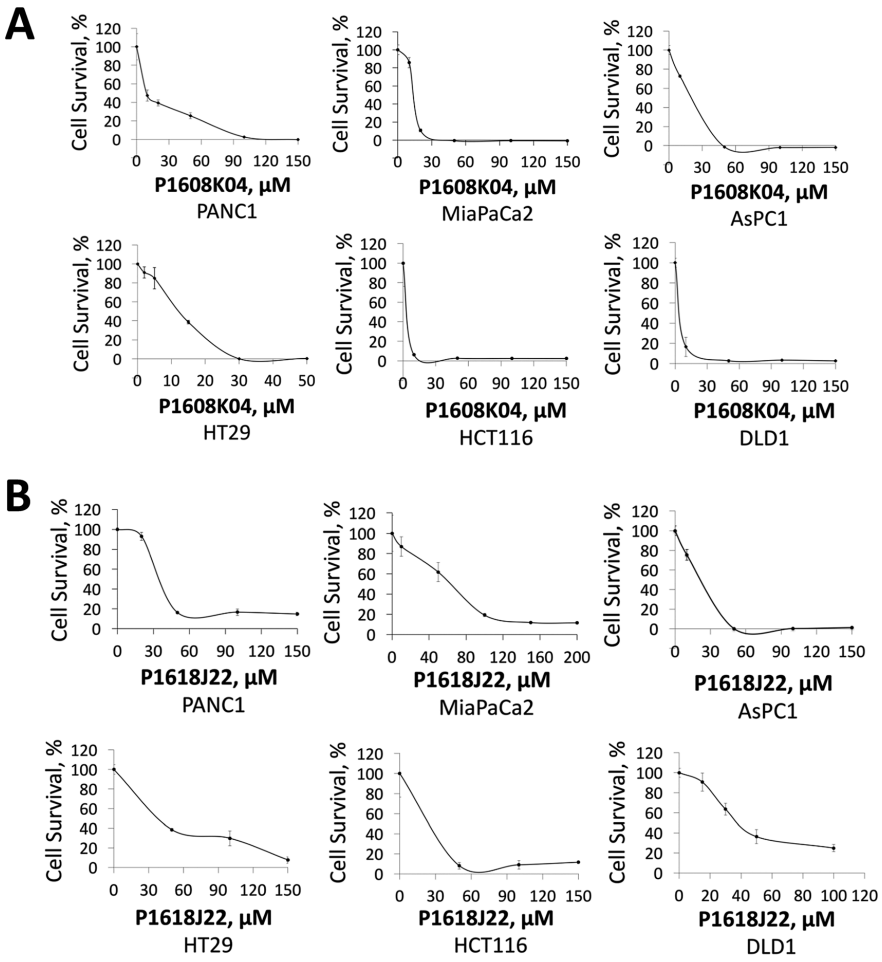

C

		P1608K04 IC_{50}, μM	P1618J22 IC_{50}, μM
PDAC	PANC1	8.5	34
	MiaPaCa2	14	50
	AsPC1	20	21
CRC	HT29	12	37
	HCT116	3	25
	DLD1	3.5	38

Figure 50. P1608K04 and P1618J22 are Potent Inhibitors for Viability in PDAC and CRC Cells

A. MTT assay with the treatment of P1608K04 in both PDAC (PANC1, MiaPaCa2, and AsPC1) and CRC cells (HT29, HCT116, and DLD1), showing that cell viability dramatically decreased in the presence of increasing concentrations of P1608K04. **B**. MTT assay with the treatment of P1618J22 in both PDAC and CRC. The data represent the means ± SD for three independent experiments. **C**. Table summarizing the IC_{50} values for P1608K04 and P1618J22 in PDAC and CRC cells, respectively.

residue of p65 showed decreased R30 methylation on p65 after the treatment of P1608K04 or P1618J22 (**Figures 51A and B**), confirming that these inhibitors specifically attenuated PRMT5-mediated NF-κB methylation in these cells.

We had shown earlier that increased methylation resulted in increased NF-κB activation (Wei *et al.*, 2013). In this regard, we used the NF-κB luciferase assay to determine the effect of compound treatment on PRMT5-mediated NF-κB activation in PDAC and CRC cells. We confirmed that treatment of P1608K04 and P1618J22 for 48 h at the indicated concentrations significantly decreased NF-κB activity in both PANC1 (**Figure 52A**) and HT29 (**Figure 52B**), respectively. It is important to note that it requires a much higher concentration of the commercial PRMT5 inhibitor EPZ015666 (~50-95μM in PANC1 and 190μM in HT29 cells) to observe a similar effect, demonstrating that both P1608K04 and P1618J22 are more effective than EPZ015666 in decreasing PRMT5-mediated NF-κB activation in PDAC and CRC cells (**Figure 28**).

Since NF-κB R30 methylation leads to its activation, we wondered whether P1608K04 and P1618J22 may inhibit NF-κB activation and its target gene expression. In addition to the above evidence, since PRMT5-mediated NF-κB activation leads to the induction of well-known cancer-promoting NF-κB target genes, such as interleukin 8 (IL8) and tumor necrosis α (TNFα) in PDAC and CRC cells, we conducted qPCR to determine the effect of P1608K04 and P1618J22 on the expression of these two genes. As shown in **Figure 53**,

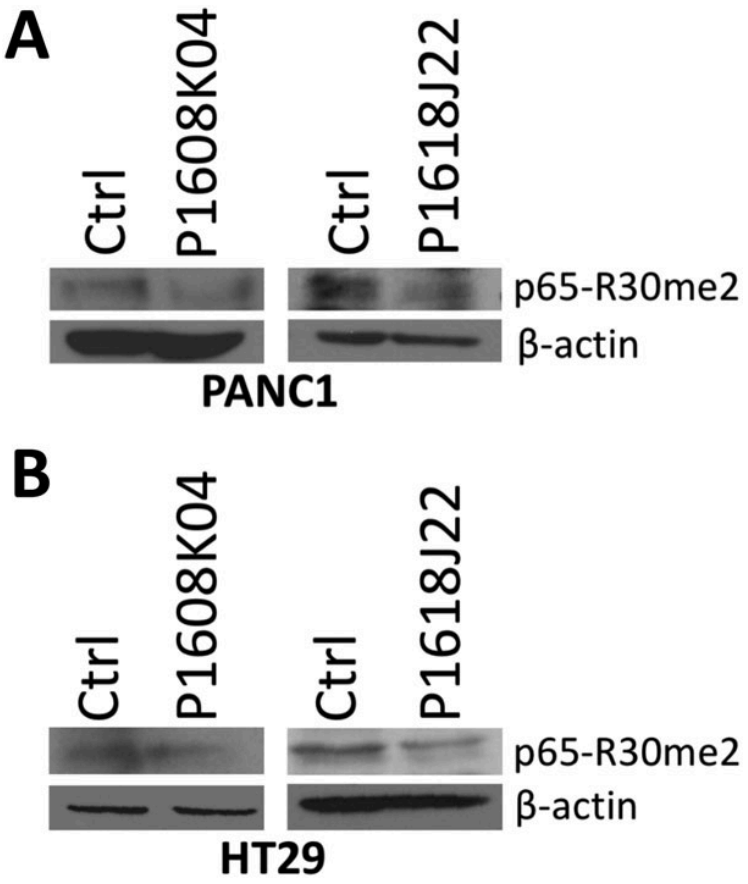

Figure 51. P1608K04 and P1618J22 Decreased Methylation at R30 on the p65 Subunit of NF-κB

Western blot analysis showing **A.** PANC1 and **B**. HT29 cells were treated with P1608K04 (left panels) or P1618J22 (right panels) at their IC_{50} values, respectively. Samples were probed with specific anti-p65-R30me2 antibody. Decreased p65-R30me2 levels were observed in the compound treated groups as compared with the control (Ctrl) groups that are without compound treatment. β-actin was used as a loading control.

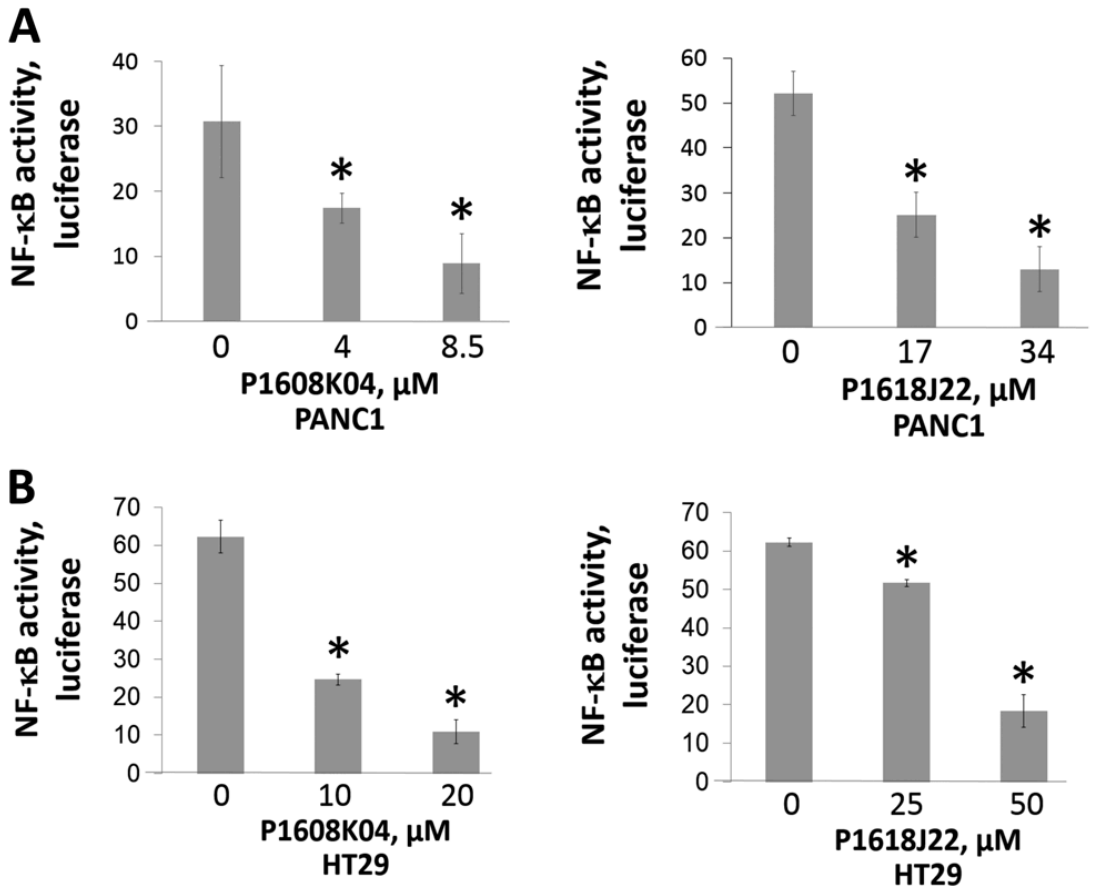

Figure 52. P1608K04 and P1618J22 Inhibited NF-κB Activation and its Target Gene Expression in PDAC and CRC Cells

NF-κB luciferase assay in **A.** PANC1 and **B**. HT29 cells, indicating that treatment with increasing concentrations of P1608K04 or P1618J22 respectively for 48h led to a corresponding decrease in NF-κB activation. The data represent the means ± SD for three independent experiments. *P<0.05 *vs.* 0μM (Vehicle Ctrl).

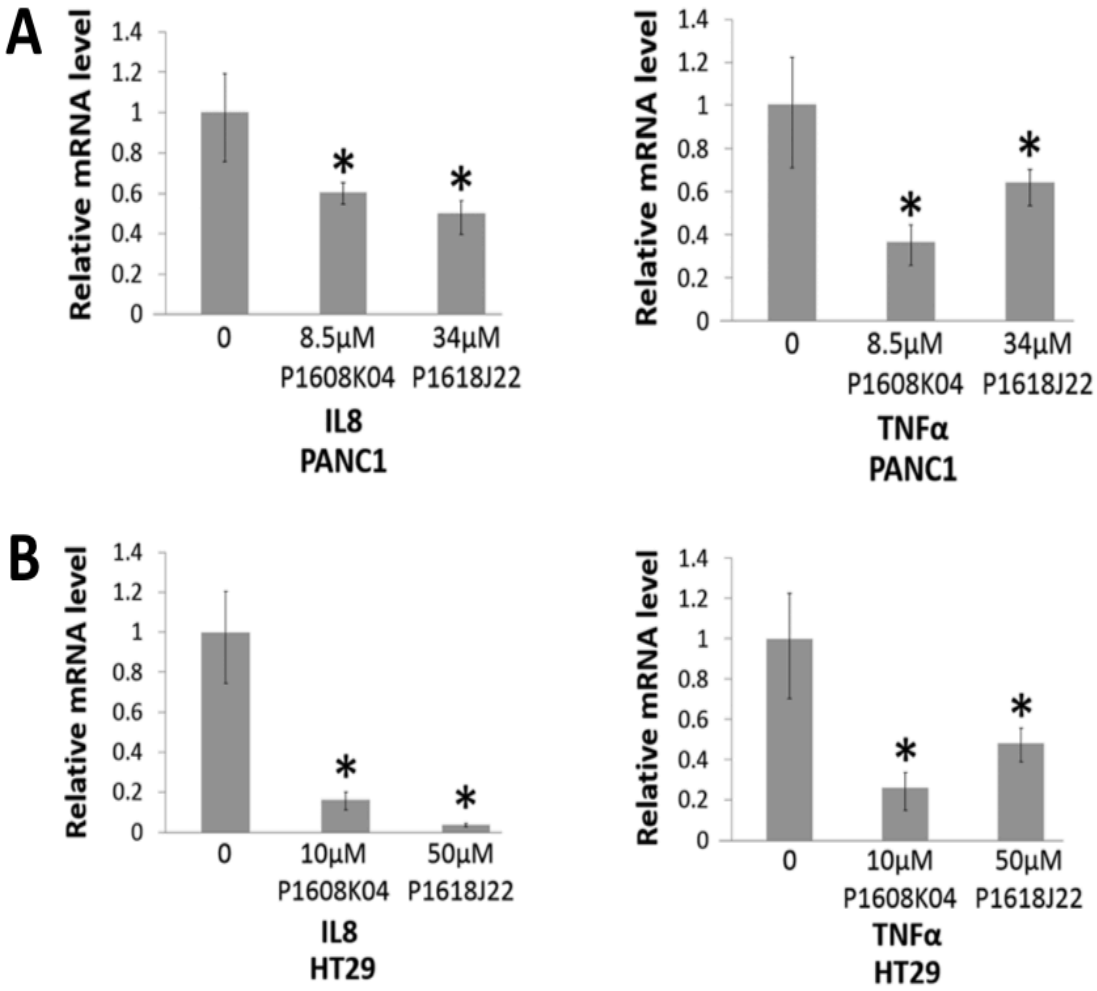

Figure 53. P1608K04 and P1618J22 Inhibited NF-κB Target Gene Expression in PDAC and CRC Cells

qPCR analysis, showing that the expression of the typical NF-kB target genes, IL8 and TNFα, was decreased after the treatment with P1608K04 or P1618J22 respectively in **A**. PANC1 and **B**. HT29 cells. The data represent the means $\pm$ SD for three independent experiments. *P<0.05 *vs.* 0μM.

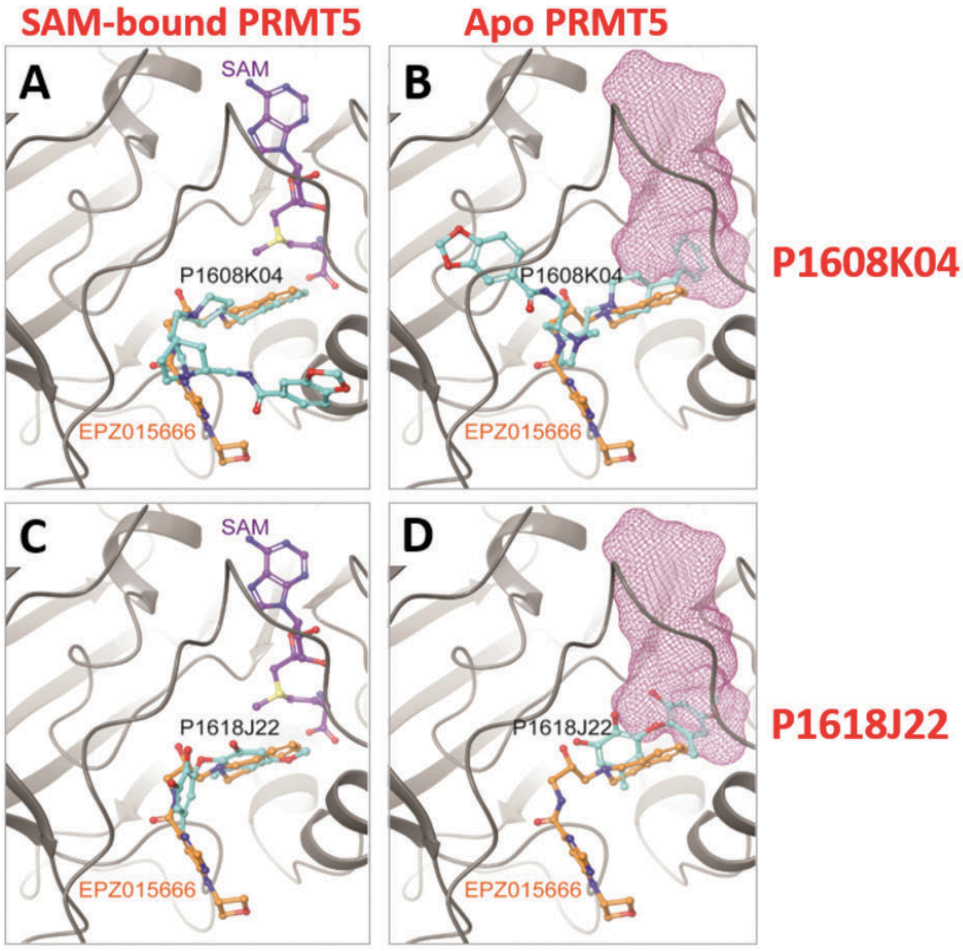

E Docking Scores

	SAM-bound	Apo
P1608K04	-5.627	-6.488
P1618J22	-6.302	-6.555

Figure 54. In Silico Prediction of P1608K04 and P1618J22 Binding to PRMT5

A-D. Binding poses predicted for P1608K04 and P1618J22. (**A and C**), in the presence or **B and D**. in the absence of SAM, respectively. PRMT5 is shown in gray ribbons, while all ligands are shown in balls and sticks and colored with respect to atom type (O atoms in red, N atoms in blue, S atoms in yellow. C atoms are colored in purple, orange, and cyan in SAM, EPZ015666, and the P1608K04 or P1618J22, respectively.) In panels **B and D**, the position of SAM is depicted with a purple wireframe surface to indicate if the docked ligand overlaps. **E**. Docking scores for the docking poses depicted in **A-D**.

treatment of PANC1 (**Figure 53A**) or HT29 (**Figure 53B**) cells with these two compounds led to significantly decreased expression of both IL8 and TNFα. Collectively, the above evidence affirmed that P1608K04 and P1618J22 are PRMT5 specific inhibitors that function through inhibiting PRMT5-mediated NF-κB methylation, activation, and its downstream target gene expression.

5.2.5 Predicted Structural Binding of P1608K04 and P1618J22 to PRMT5

To better understand the potential binding mechanism of P1608K04 and P1618J22 to PRMT5, we used a directed computer-based docking approach of these inhibitors to the PRMT5 crystal structure. This approach was similar to the one used to study PR5-LL-CM01 binding to PRMT5 and was conducted in collaboration with Dr. Ozlem Demir at the University of California, San Diego under the guidance of Dr. Rommie Amaro. Comparing the crystal structure of commercial PRMT5 inhibitor EPZ015666 with the predicted binding poses of the two inhibitors we identified, we explored how our inhibitors bound in conjunction. We also included EPZ015666 in the analysis to check if there is any overlap in residues that interact with our compounds vs. EPZ015666. As illustrated in **Figures 54A** and **B**, the most energetically favorable interaction for P1608K04 has been depicted in the presence (SAM-bound PRMT5) and absence (Apo-PRMT5) of the methyl donor SAM, respectively. As shown in **Figures 54A**, P1608K04 binds to a similar location to that of EPZ015666 in the presence of SAM. Interestingly, in the absence of SAM (**Figure 54B**), P1608K04 partially occupies the SAM binding site, thereby potentially blocks the SAM-PRMT5

interaction. Blocking SAM binding could be a potential avenue through which PRMT5 methyltransferase activity is affected. Based on the docking scores listed in **Figure 54E**, P1608K04 is more likely to bind in the absence of SAM.

In the case of P1618J22, we observed a similar binding pose to that of EPZ015666 which barely overlaps with the SAM binding site in the presence of SAM. On the other hand, we observed a preferential binding to the SAM binding site in the absence of SAM (**Figures 54C** and **D**). However, for P1618J22, binding affinities are very close in the presence or absence of SAM, thus it is impossible to predict which pose the ligand would prefer solely based on structural docking studies.

Next, we wanted to find residues on PRMT5 that closely interact with the respective compounds. The ligand affinity maps in **Figure 55** illustrate the PRMT5 residues that can potentially interact with P1608K04 (Left panels) or P1618J22 (Right panels), in the presence (upper panels) or absence (lower panels) of SAM, respectively. Key residues unique to the PRMT5 protein are involved in these compound interactions as well. Notably these include the E444 residue that is part of the catalytic cleft of PRMT5 and a F327 residue critical for PRMT5 product specificity. The interactions also differ from EPZ015666, possibly leading to the different efficacy between P1618J22 and P1608K04, with the latter showing slightly higher predicted binding affinity (Prabhu *et al.*, 2017). In future, it

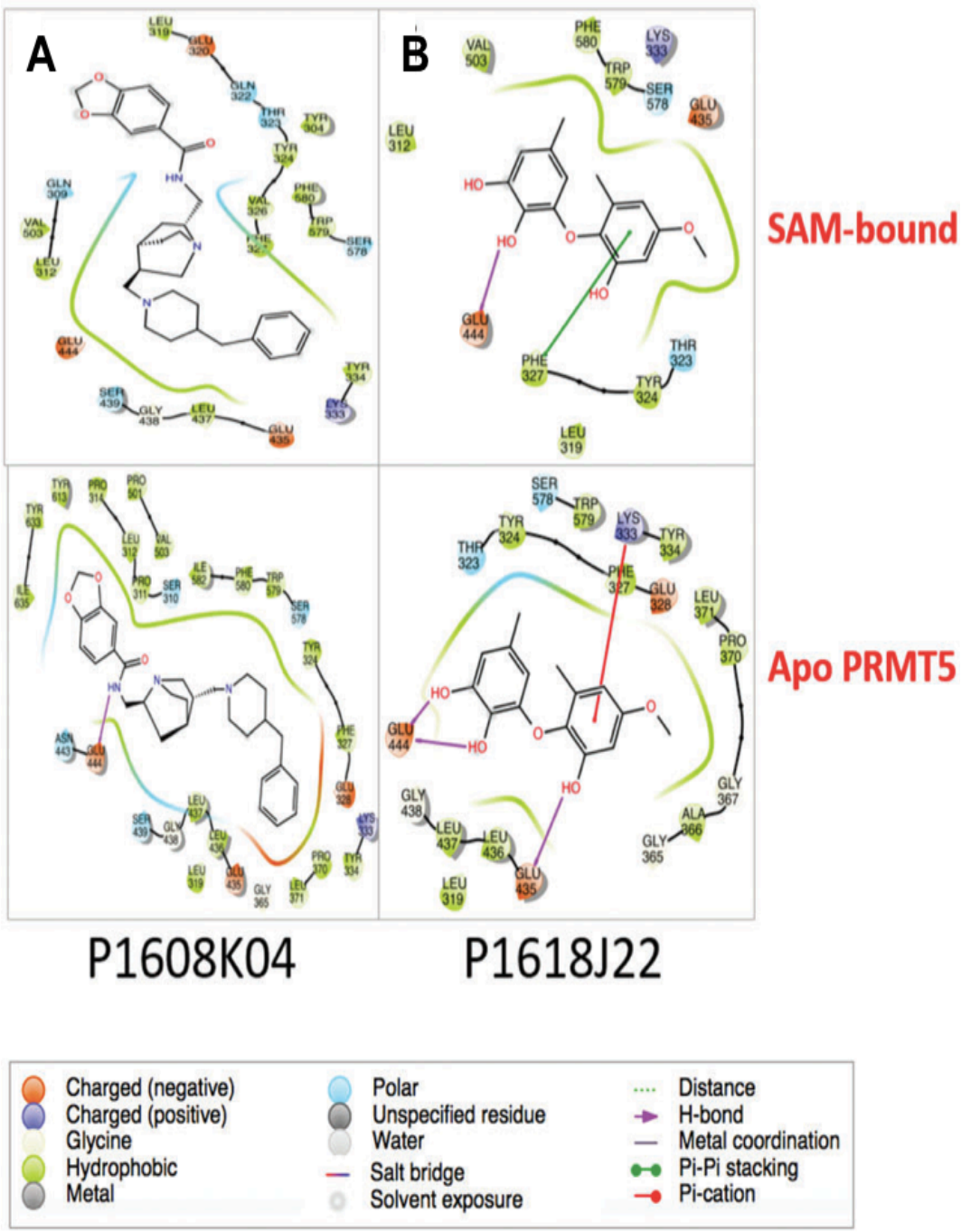

Figure 55. Ligand Affinity Maps for P1608K04 and P1618J22 Binding to PRMT5

Ligand affinity maps depicting the residues of PRMT5 that interact with **A**. P1608K04 or **B**. P1618J22 in the docking poses in Figures **48A-D**.

will be interesting to explore how important these residues (**Figures 55A** and **B**) are in the binding mechanism of these inhibitors to PRMT5.

5.3 Concluding Remarks

Collectively, our data support that inhibitors of PRMT5 such as P1608K04 and P1618J22, like PR5-LL-CM01 inhibit PRMT5-mediated NF-κB activation and its downstream target gene expression in PDAC and CRC. As a whole, PR5-LL-CM01 was the superior PRMT5 inhibitor in terms of efficacy and was the one we focused on for majority of the studies presented in this thesis and in the future. However, this study also emphasizes the power of AlphaLISA technique and the ability to harness it to identify novel inhibitors of a desired epigenetic target, in this case PRMT5. Going forward, AlphaLISA can be adapted for the target of choice to perform a successful HTS and identify robust inhibitors for the respective targets that could serve as tools in research and/or in the clinic.

CHAPTER 6: DISCUSSION

6.1 Summary of Findings and Discussion

As summarized in **Figure 56**, based on the data from **Chapters 3-5**, we hypothesize that PRMT5 is a tumor promoting factor in PDAC and CRC. Novel inhibitors of PRMT5, such as PR5-LL-CM01, P1608K04, and P1618J22, may inhibit the PRMT5-mediated NF-κB activity, therefore decrease its target gene expression, alleviate cancer related characteristics, and impede cancer progression. Detailed summaries and discussion will be elaborated below.

6.1.1 Current Therapeutic Limitations and Challenges in PDAC and CRC Treatment

PDAC and CRC are among the leading causes of cancer-related deaths in the United States. New PDAC and CRC cases were estimated to be 53,670 and 135,430 and deaths in this year were estimated at 43,090 and 50,260 respectively in men and women combined in the US for 2017 (Howlader *et al.*, 2017). This is equivalent to 15% of the total cancer-related deaths in the US and these numbers keep rising every year. Despite important advances in recent years, many patients continue to experience disease recurrence following primary therapy. Both these diseases primarily occur through somatic mutations that can accumulate over time and lead to cancer progression. Furthermore, these cancers are well-known to metastasize to other parts of the body, thereby providing a challenge to clinicians in controlling the disease. There is currently

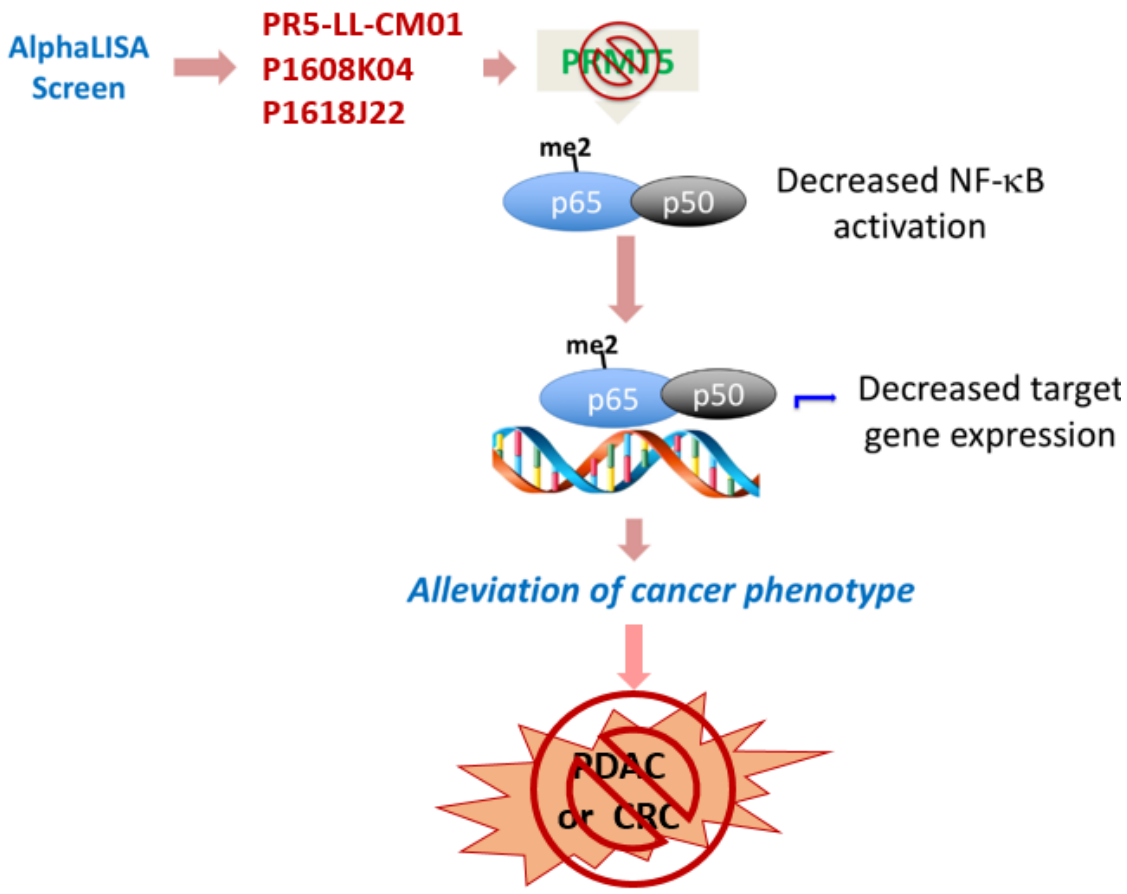

Figure 56. Hypothetical Model
The optimized AlphaLISA screen for PRMT5 inhibitors identified and confirmed the major inhibitor, PR5-LL-CM01 and two other inhibitors, P1608K04 and P1618J22. We demonstrated that this inhibitory effect could partly be via inhibiting PRMT5-mediated NF-κB methylation and subsequent activation, resulting in decreased cancer-associated target gene expression. This process would ultimately lead to the alleviation of cancer phenotype and overall highlights the significance of PRMT5 as a tumor promoter and its therapeutic potential in PDAC and CRC.

“no cure” for a significant number of patients presenting with metastasis upon diagnosis. Finally, an estimated nearly $20 billion were spent on PDAC and CRC care in the United States in 2016, reflecting the urgent medical need for the discovery of newer PDAC and CRC treatment options. In this regard, The *White House Cancer Moonshot* was established in 2016 by then Vice-President Joe Biden, with the aim to double the rate of progress in cancer research and treatment over the next five years.

The treatment for both these cancers is dominated by chemotherapeutic drugs that interfere with DNA synthesis that target rapidly dividing tumor cells. One chemotherapeutic drug may be prescribed on its own or more, depending on the cancer stage as well as inherent health of the patients. Besides not being specific, standard chemotherapy such as the combination of drugs termed as FOLFIRINOX for PDAC and FOLFOX for CRC described before (**Chapter 1**) can have cause a number of side effects. These include fatigue, hair loss, susceptibility to bruising and bleeding, anemia, nausea and vomiting amongst others that take a physical and emotional toll on the patients. Thus, there is a clear unmet need for more targeted therapeutics to treat these diseases.

Specific cellular factors that are significantly upregulated more in cancer cells over normal cells can be indicative of a dependence on these oncogenic factors for sustaining the tumor. Modulation of such factors using targeted inhibitors can prove to be an effective therapeutic measure. A caveat to this

rationale is that some of these factors can be critical in normal cell function and complete inhibition can lead to undesired detrimental effects. Thus, identification of upstream or downstream regulators that can partly affect function of these factors is useful, as modulation of activity via these regulators rather than absolute direct inhibition could result in alleviation of the cancer phenotype while still having negligible effects on normal cells. Of course, these upstream or downstream regulators themselves might be critical in normal cells. In the case of PRMT5, it has been shown to be critical in immune function regulation, embryonic development and regulator of normal adult hematopoiesis (Zheng *et al.*, 2017; Liu *et al.*, 2015; Gkountela *et al.*, 2014). However, PRMT5 is also a critical player in cancer and inhibition of PRMT5 can lead to a decrease in the cancer phenotype as described in this thesis and others, when we demonstrated PRMT5 as a critical activator of a major tumor promoting factor, NF-κB that is constitutively activated in PDAC and CRC. Furthermore, we identified a specific PRMT5 inhibitor, PR5-LL-CM01 with promising therapeutic implications in these deadly cancers. However, in order to prevent deleterious effects caused by non-specific inhibition of PRMT5 in normal cell function, optimal dosing ranges and targeted delivery will need to be considered with future studies.

6.1.2 PRMT5 Promotes PDAC and CRC Progression via NF-κB Activation

PTMs regulate protein function in eukaryotes and have been shown to play important roles in a variety of cancers (Karve and Cheema 2011). Methylation of lysine and arginine is one of the most critical PTMs seen in nature

and are responsible for regulating a variety of signaling pathways in a cell. Changes in expression during disease states such as cancer can have critical implications directly or indirectly via downstream signaling pathways on disease progression. Indeed, in recent times, epigenetic enzymes have emerged as viable drug targets. An understanding of underlying signaling mechanisms implicated in cancer can help to design better drugs against these factors. Our lab recently discovered a novel PTM (arginine methylation) on a known tumor promoter, NF-κB, which in turn led to the activation of NF-κB (Wei *et al.*, 2013). The epigenetic enzyme PRMT5 was identified for being responsible for this modification. Activation of NF-κB has been shown to aggressively promote PDAC and CRC phenotype as well as contribute to chemotherapeutic resistance in the past (Hai *et al.*, 2016, Hassanzadeh 2011). Thus, identification of pathways/factors that can influence this activation could help limit it. Based on this exciting discovery, we hypothesized that PRMT5-mediated NF-κB activation could be important for promotion of PDAC and CRC phenotype, with the ultimate intent to develop PRMT5 as a therapeutic target for these deadly cancers by inhibiting its activity.

In this study, we showed that PRMT5 expression was significantly upregulated in PDAC and CRC, as observed in cancer cell lines as well as tumor tissue from patients. Furthermore, increased expression of PRMT5 in cancer cells led to enhanced cancer-promoting characteristics, including cell proliferation, anchorage-independent growth and cell migration, clearly

highlighting the role of PRMT5 as a tumor promoting function in PDAC and CRC. Furthermore, to determine its effect on to NF-κB activity, we conducted luciferase assays with a consensus binding sequence for NF-κB located upstream of the luciferase reporter gene and showed that PRMT5 indeed promoted NF-κB activation in PDAC and CRC. Furthermore, NF-κB is a transcription factor and can translocate to the nucleus upon activation to promote expression of several genes that are critical for cancer phenotype. qPCR analysis showed that PRMT5-mediated NF-κB activation promoted the expression of its well-known downstream target genes, indicative of the critical role of PRMT5 in NF-κB activation in PDAC and CRC. Overall, these studies emphasize the significance of PRMT5-mediated NF-κB activation for cancer promotion in PDAC and CRC.

While its relationship to NF-κB is significant, it is necessary to consider that PRMT5-mediated signaling in a cell can be complicated. PRMT5 and NF-κB can both have different signaling mechanisms they could target besides each other. We acknowledge that the PRMT5-NF-κB axis studied here represents one aspect of the signaling spectrum that could be occurring in the tumor microenvironment. Recent studies have highlighted the dependence on PRMT5 due to disruption of metabolic activities in cancers and inhibition of PRMT5 led to detrimental effects in the tumor cells (Mavrakis *et al.*, 2016). PRMT5-mediated methylation of substrates beyond NF-κB, such as p53, EFGR, E2F-1 and histones have also been predicted to have an oncogenic role (Hsu *et al.*, 2011, Yuan *et al.*, 2012, Jansson *et al.*, 2008). However, these studies have been done

in a variety of different cancers and the observed results can be very context-dependent and specific to the cell or tissue type being studied. Understanding the signaling pathway that leads to the specific subtypes would allow to explore possible crosstalk between various PRMT5-driven signaling pathways that contribute to cancer promotion in these subtypes. It will also allow us to tease out any possible interactions between other signaling mechanisms and PRMT5-driven axis that collectively contribute to NF-κB activation and opens up a gateway for exciting research in the future.

Hence, even though many mechanisms underlying the role of PRMT5 in cancer are still unclear, the insights provided by this study are highly valuable in understanding the workings of PRMT5. They could perhaps also be applied to other cancers beyond PDAC and CRC. Both NF-κB and PRMT5 are upregulated in various types of cancers, including but not limited to pancreas, colon, breast, prostate, and lung cancers, as well as lymphoma and melanoma (Jiang and Newsham, 2006; Gu *et al.*, 2012; Cho *et al.*, 2012; Zhang *et al.*, 2014; Wang *et al.*, 2008). Due to the commonality of high levels of PRMT5, our current findings with regards to PDAC and CRC could have broader impacts on the understanding of cancer progression as a whole.

6.1.3 PR5-LL-CM01 is a Potent PRMT5 Inhibitor and Shows Anti-Tumor Efficacy in Disease Models of PDAC and CRC

NF-κB is a critical transcription factor that is hyperactivated in various cancers (Wei *et al.*, 2013). Since it also plays a crucial role in normal cellular functioning, direct targeting of NF-κB has not proven to be a successful therapeutic approach, as previous attempts for complete inhibition has resulted in severe cell death even in normal cells (Martin *et al.*, 2016). These obstacles highlight the importance of identifying pathway-specific inhibition of NF-κB activity in cancer treatment. Thus, upstream modulators of NF-κB activity could be targeted, such as inhibitors directed towards the degradation machinery of inhibitor IκBα that sequesters NF-κB in the cytoplasm (**Figure 3**) or inhibitors of the mTOR pathway that can activate NF-κB through a series of downstream signaling events (Dan *et al.*, 2008). All these different pathways could modulate different aspects of the disease etiology and a better understanding of the signaling mechanisms can help in determining the best multi-pathway therapeutic strategies. In this regard, the discovery of PRMT5-mediated activation of NF-κB and its targeted inhibition in PDAC and CRC is of great importance and significance. Furthermore, the successful development and application of the PRMT5-specific AlphaLISA HTS technique in this study constitutes another layer of unique contribution to the drug discovery field. Using this sensitive approach, we successfully identified PR5-LL-CM01 as our leading hit and confirmed that it is a highly potent and specific PRMT5 inhibitor (**Figure 21**). Using a closely related structural analog, PR5-LL-IEC01, we demonstrated the selectivity of the

effect shown by PR5-LL-CM01 (**Figures 30, 32-33**). When we first began developing the assay to screen for PRMT5 inhibitors, there were no known PRMT5 inhibitors in existence. Since then, Epizyme Inc. developed EPZ015666 as the first-ever selective PRMT5 inhibitor that is commercially available (Chan-Penebre *et al.*, 2016). They reported that EPZ015666 was very effective in inhibiting mantle cell lymphoma. Since we were curious how EPZ015666 would work in a direct comparison to PR5-LL-CM01, we decided to test its efficacy in our PDAC and CRC models. We showed that PR5-LL-CM01 was ~10-15 fold more effective than EPZ015666 in PDAC and CRC models, making PR5-LL-CM01 the first PRMT5 inhibitor to be highly effective in the treatment of solid tumors (**Figures 23-24**). We speculate that PR5-LL-CM01 could be more effective than EPZ015666 in the treatment of other solid cancers with hyper PRMT5 expression and would be exciting to test this possibility in the future.

Additionally, using Western blotting we showed that there was a decrease in p65 methylation *in vitro* upon PR5-LL-CM01 treatment, demonstrating that the effect of this inhibitor observed in cells could be via decrease in PRMT5-mediated NF-κB methylation and subsequent activation (**Figure 27**). We also conducted a screen to check for the specificity of inhibition of arginine methyltransferase family members activity via PR5-LL-CM01 and demonstrated that it was highly selective for PRMT5 over other PRMTs (**Figure 31**). More importantly, we also tested the toxicity and efficacy of PR5-LL-CM01 in animal models of PDAC and CRC. We observed no obvious toxicity up to 50mg/kg of

PR5-LL-CM01 in the mice (**Figure 39**). Treatment with 3X/week demonstrated a significant decrease in tumor size in both PDAC and CRC models, showing great promise to be tested further for clinical efficacy (**Figure 43**). In addition, we generated derivatives to check if we could increase the efficacy of the parental compound and found that PPA-1 was the most promising derivative so far (**Table 4, Figure 45**). Further efforts to understand PPA-1's efficacy and generate even more derivatives have been described in **Section 6.3.**

Moreover, we used structural modeling experiments to understand the possible mechanisms through which that PR5-LL-CM01 could interact with PRMT5. We also looked into comparing these interactions with those of EPZ015666 and found that both these inhibitors interact with PRMT5 through quite different mechanisms (**Figure 34**). Particularly, PR5-LL-CM01 interacts with E444 on PRMT5, a critical residue for the catalytic activity of PRMT5 (Antonysamy *et al.*, 2012). F327 is another residue implicated in contributing to the specific symmetric dimethylation activity of PRMT5. Interestingly, we observed that all the residues participating in the binding interactions between PR5-LL-CM01 and PRMT5 span over the Rossman fold and β-barrel domains of PRMT5, which have been previously shown to comprise the catalytic methyltransferase domain of PRMT5 and the region where SAM and its substrates bind. On the other hand, EPZ015666 binds to PRMT5 independent from SAM binding sites (**Figure 35**). These quite different PRMT5 binding

mechanisms could shed light on why PR5-LL-CM01 is more selective than EPZ015666 in killing PDAC and CRC cells, but need to be further tested.

All these studies have highlighted the potential of PRMT5 as viable target and PR5-LL-CM01. Further experiments to explore the efficacy and mechanism of action of PR5-LL-CM01 in PDAC and CRC are elaborated on in **Section 6.3**.

6.1.4 Development of AlphaLISA as a Powerful Tool to Identify Potent Inhibitors

Epigenetic modifications play an important role in normal cellular function and development in nearly every aspect of biology, making it one of the most important fields in scientific research. Dysregulation of epigenetic modifications leads to serious disruptions of regular functioning in humans and is the underlying cause of promoting a wide range of disorders including cancers. A plethora of studies have linked overexpression of epigenetic enzymes with promotion and metastasis of varied cancers. Thus, a great deal of interest has been generated in the field to exploit these epigenetic enzymes as potential therapeutic targets. To date, successful attempts at developing inhibitors for epigenetic targets have been made, with the histone deacetylases (HDAC) family being the most prominent example. Vorinostat and romidepsin are HDAC inhibitors that are already FDA approved for blood cancers, and many others are currently under clinical trials (Yu *et al.*, 2015). Unfortunately, the clinical success of HDAC inhibitors in solid tumors has been very limited. Thus, it is imperative to

explore other critical epigenetic enzyme families like PRMTs by developing HTS screens and identifying potential inhibitors of clinical significance.

Various assays for HTS that have been used in recent times were considered to screen for PRMT family member inhibitors. Among the current available technologies, AlphaLISA proved to be an excellent choice for this purpose for various reasons. For instance, in the case of radiometric assays, the cost and danger associated with its usage and the generation of radioactive waste are a huge deterrent. Enzyme-based assays like ELISA have been quite popular for screening in the past. However, with these assays, the scaling-up approach can prove to be quite expensive and cumbersome. As the HTS field grows, there is a dire need to develop economical and scalable approaches to screen for active compounds against potential targets. AlphaLISA is a viable option because it provides a straightforward protocol for assay development, and its robustness, sensitivity, cost-effectiveness, and ease of use makes it an attractive screening tool. We conducted extensive troubleshooting and adapted all the loading volumes and concentrations to be compatible with a *robotic* system. A big limitation of the non-robotic approach is the cumbersome and expensive nature of the study, with addition of 10,000 compounds and reagents involved as part of the screening protocol. The ease of automation provided by our technique will help to drive high scale screening studies. Additionally, the robotic system allowed for higher accuracy with its state-of-the-art pipetting system as well as cost efficiency as it enables use of very low volumes of

reagents. If using the appropriate biotinylated substrate, methyl donor, epigenetic-tag specific Acceptor beads, and Streptavidin-coated Donor beads, this assay can be customized for other epigenetic targets as well.

We employed a multi-step approach to identify top hits from small compound libraries with PRMT5 as our target. PR5-LL-CM01 was identified from the first screen and has already been discussed in the previous section. We conducted a 2nd HTS with compound libraries containing natural products and bioactives to identify even more inhibitors of PRMT5. Before running the second HTS, we tested its robustness using the reliable Z' test, which was determined to be 0.7 (**Figure 46**). Upon completion of the screen of libraries containing natural products and biologically active compounds, we then sorted through the top hits. Our results indicated that P1608K04 and P1618J22 are the most effective PRMT5 inhibitors from our 2nd screen. Both compounds demonstrated considerable efficacy in concentration-dependent AlphaLISA assays (**Figure 49**), and in MTT assays in PDAC and CRC cells (**Figure 50**), respectively. We also confirmed the significant inhibitory effect of P1608K04 and P1618J22 on PRMT5-mediated NF-κB methylation, activation, and its downstream target gene expression (**Figures 51-53**). Overall, our findings support the activity of these inhibitors against PRMT5.

To understand how P1608K04 and P1618J22 may bind to PRMT5, we delved deeper into the mechanism of the inhibitor-enzyme interaction using

structural docking analyses, similar to PR5-LL-CM01. As shown in **Figures 54A and B**, we identified specific residues in the binding interaction between these two compounds and PRMT5. This analysis suggested that both inhibitors can potentially inhibit PRMT5 through certain similar but also varied mechanisms. For instance, both seem to bind to residues that intersect with the SAM binding site in the Apo states, suggesting that one possible way these inhibitors work is by interfering with SAM binding to its consensus site on PRMT5 structure. Ligand affinity map analysis (**Figures 55A**) suggests that both P1608K04 and P1618J22 interact with two key residues (E444 and F327) that are unique to the PRMT5 structure, also alluding to their specificity. As mentioned previously, both these residues play a crucial role in the PRMT5 methyltransferase activity (Schapira 2014). Both P1608K04 and P168J22 could contribute to PRMT5 inhibition via the interaction with these two key residues. This binding poses of P1608K04 and P168J22 are also different from that of EPZ015666, suggesting that there is a distinction between our compounds and EPZ015666, and could possibly contribute to the different efficacies in inhibiting PRMT5 (**Figures 54A-D**). In the future, mutating some of these residues can help us locate critical sites on PRMT5 for the inhibitor-enzyme interactions and elucidate the mechanism of action of P1608K04 and P1618J22 for PRMT5 inhibition. Furthermore, several unique residues to each type of interaction such as E444 and F327 in the ligand affinity maps (**Figures 55A and B**) can be further pursued and analyzed in detail. Additionally, it would be of great interest to employ SAR analyses to design derivatives of the top hits. This would assist in maximizing the efficacy of these

compounds by reducing the therapeutic dosages needed to obtain significant anti-tumor efficacy. From a broader perspective, epigenetic enzymes are proving to be increasingly critical in a wide variety of diseases, and the approach described here can accelerate the development of important tools required for this purpose.

In summary, we have identified the significant role of PRMT5 as a promoter of the various hallmarks of cancer in PDAC and CRC, as well as highlighted its potential to be exploited as an important therapeutic target (**Figure 56**). Overall, the discovery of PR5-LL-CM01 may lead to promising new PDAC and CRC therapies and will help to better understand the workings behind PDAC and CRC. In the long run, we will move toward clinical trials with the few best-characterized PR5-LL-CM01 derivatives with the ultimate goal of improving PDAC and CRC patient survivorship and treatment.

6.2 Key Points for Consideration

In this study, we highlighted a novel mechanism by which PRMT5 overexpression could contribute to its tumor-promoting activity by affecting cell proliferation, migration, and anchorage independent growth of cancer cells, possibly via mediating NF-κB activation and could be therapeutically targeted by using PRMT5- selective inhibitors. We did not encounter any major obstacles while performing the work described in this thesis. However, I would like to describe some potential limitations associated with the experiments and the

results presented here. We generated stable overexpression and knockdown cell lines for PRMT5 expression in PANC1 and HT29 cells. We used a common vector control for both these cell lines but did not include scramble controls specifically for the shPRMT5 cell line for the phenotypic assays discussed in **Chapter 3**. The reason was because we cloned the PRMT5 gene into a lentiviral vector. It is a similar lentiviral vector as the shRNAs constructs. So predictably, the cells derived from the control vector and the shScramble construct shall be very similar. However, later on, I still generated shscramble cell lines and compared PRMT5 expression to vector control cell lines used in our experiment and confirmed the comparable PRMT5 expression between the two different control cell lines (**Figure 57**). Thus, we would anticipate no differences in the phenotype if we would have included the shscramble control in our studies from the vector control. In the future, the shscramble control will be included alongside any experiments that include the shPRMT5 cell line as an appropriate control though both control vectors are similar lentiviral vectors with same puromycin selection marker.

Furthermore, the AlphaLISA assay is a powerful tool to screen for small molecule inhibitors of the desired target. Indeed, we were able to successfully identify potent inhibitors of PRMT5 activity using this technique. One limitation of this technique is the specific Acceptor beads that contain the antibody tag specific to the modification of interest. PerkinElmer manufactures these Acceptor

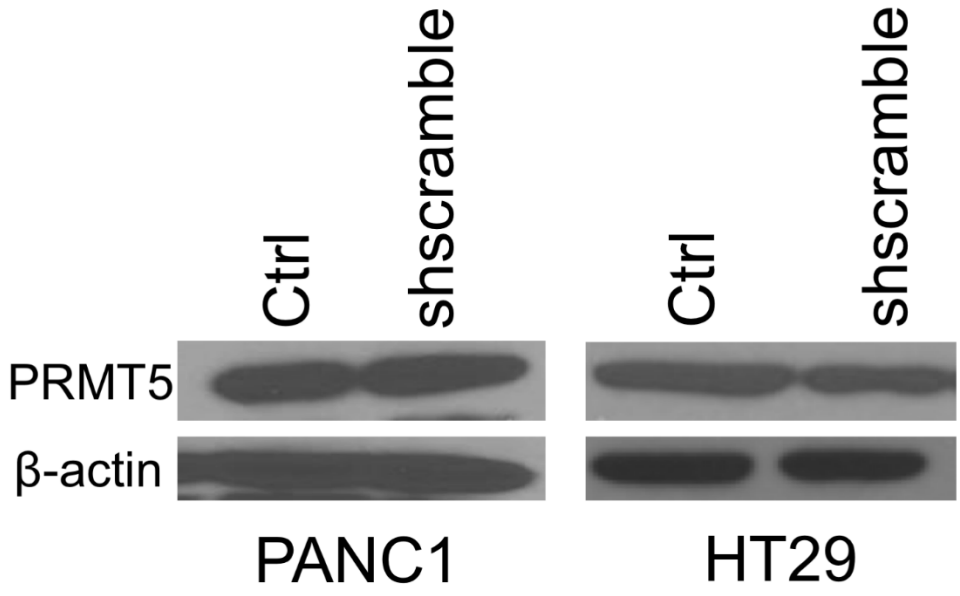

Figure 57. Comparison of PRMT5 Expression in Shscramble versus Ctrl Cell Lines

Western blot, confirming comparable PRMT5 overexpression in shscramble cell lines as compared to the plv-vector control (Ctrl) cell line in (left) PANC1 and (right) HT29 cells. β-actin was used as a loading control.

beads and have a wide repository of beads available that can detect almost all acetylation and arginine-based histone modifications. However, beyond these substrates, their catalog is limited. Thus, if one is interested to use the AlphaLISA assay with substrates not in the repository, it might be difficult to obtain the reagents required for the assay. An alternative is to work with PerkinElmer to design customized Acceptor beads that work with one's time and budget constraints.

Lastly, in this study, we used NSG mice, a widely used immunodeficient strain available as they lack mature T cells, B cells, and NK cells. Immunodeficient models reduce the chances of host rejection when human cell lines are implanted for growing tumors. These models have been widely applied in cancer research for mechanistic studies, early phase drug discovery, etc. but also have certain shortcomings (Lei *et al.*, 2016). Since these mice do not have a functioning immune system, they do not replicate the human microenvironment where the immune system plays a key role in tumor dynamics. Additionally, mice and humans could have different isoforms of the same protein that may react to the drugs differently. Thus, there can be chances of the treatment regimen not being successful when tested in humans. To overcome this hurdle, immunocompetent models such as chemically induced, or genetically engineered models can be used in our studies before we move into the clinical trial phase, as these provide more accurate representation of the immune microenvironment compared to immunocompromised mice.

6.3 Future Directions

The exciting work presented in this study highlights the critical role of PRMT5 in promoting the various hallmarks of cancer as well as NF-κB activation (**Chapter 3**) and presents a promising case for the potential of PRMT5 as a therapeutic target in PDAC and CRC (**Chapters 4 and 5**). It also opens up a plethora of exciting opportunities for future studies in this field.

Building upon this exciting work, our immediate future plan would be to generate more efficacious derivatives of PR5-LL-CM01 with the ultimate goal of moving this discovery to clinical applications. We will do a more in-depth SAR analysis to identify compounds that can be even more efficacious than the parental compound. In terms of how PR5-LL-CM01 inhibits PRMT5, one line of research to pursue would be to further verify the *in silico* model with purified PRMT5 crystal for the structure analysis. Specific residues that are potentially involved in the compound target interaction can be mutated to test if it would affect the binding kinetics. This will help to understand the exact interactions between the compound and target. In addition, structural docking analysis could be carried out for its promising derivative PPA-1, to compare what are the similarities and differences between the parental compound and PPA-1. This in-depth analysis can also better inform in future derivative design that we undertake.

Furthermore, in order to establish the selectivity of PR5-LL-CM01 are at least partly via reducing NF-κB activation, we can probe the mouse tissue from tumor efficacy studies to test the hypothesis that PR5-LL-CM01 treatment would lead to a decrease in p65 methylation in the PDAC and CRC tissue, as PR5-LL-CM01 would inhibit PRMT5-mediated activation of NF-κB. qPCR analyses can also be conducted on this tissue to check if decrease in activation of NF-κB also leads to a decrease in downstream NF-κB target gene expression in the tissue. In addition, we used the Sepharose beads approach as described in **Chapter 4** to test binding of PR5-LL-CM01 directly to PRMT5. This proved to be unsuccessful as the beads did not conjugate with our inhibitor. This perhaps was because PR5-LL-CM01 does not have the required primary amine crucial for conjugation step. Furthermore, we also attempted to use CETSA assays (as described in **Chapter 4**) involving Western blotting for this purpose, but only to limited success as the variation in quantification for the different blots was quite high. Though the result had promising trend, it did not have statistically significant difference. As for *in vitro* binding studies, we attempted the ITC (described in **Chapter 4**) experiment to determine binding. Briefly, this method allows us to measure thermodynamic parameters upon binding of PR5-LL-CM01 and PRMT5 in solution. However, this approach was proved to be unfeasible for our purpose. This is mainly because very high concentrations of enzyme of protein are required for the experiment. In the future, we are planning to work with Dr. Lan Chen (currently at Purdue Chemical Genomics Facility) to fluorescently label PRMT5 using the Monolith NT™ Protein Labeling Kit. Furthermore, we plan to

use microscale thermophoresis approach which is capable of analyzing interactions of proteins/small molecules in pure form or in biological samples such as cell lysates (Wienken *et al.*, 2010). Thermophoresis is related to the directed motion of molecules that is directed by temperature gradients. Briefly, the assay principle is that binding interaction of a fluorescently labeled protein with its partner leads to changes in distribution of infrared laser light. These changes can be measured over time until the reaction reaches equilibrium and can be quantified to get an idea of the binding parameters. A major advantage of this method is that it can be used to conduct both binding studies using protein in pure form as well as present in cell lysates. Overall, this approach could help in demonstrating the direct binding interaction between PR5-LL-CM01 and PRMT5 in the future.

Furthermore, cancer is a heterogeneous disease and a single targeted therapeutic agent could be overly optimistic. Combination studies have shown limited success in the clinic. In the same way, PR5-LL-CM01 could be combined with current chemotherapeutic drugs (for instance, the FOLFIRINOX or FOLFOX regimen mentioned in the Introduction section which is most widely used regimen) for PDAC and CRC to test if this would be an effective way as compared to the therapeutic drugs alone in reducing the disease phenotype. Additionally, thorough safety studies will need to be conducted using larger samples sizes of mice as well as incorporating the female mice in the studies as well, in order to determine the optimal dosing regimen for Phase 1 trials. Going

forward, such studies would provide a more realistic approach if this compound makes it way from the bench to the bedside.

Along with establishing a better understanding of the mechanism of action of PR5-LL-CM01 and its link to NF-κB as a substrate for PRMT5, it is also important to consider that PRMT5 has other substrates besides NF-κB. It would be interesting to check if the inhibitory properties of PR5-LL-CM01 extend beyond PRMT5 and NF-κB and if they have anti-tumor implications. Some PRMT5 substrates are important in the context of cancer, including p53 and EGFR and changes in symmetric dimethylation levels at these sites in the presence of PR5-LL-CM01 can be detected. However, it is important to keep in mind that these site-specific modifications could be specific to the tissue/cell type they were discovered in and not significant in the models described in this study. If shown to be important in the context of PDAC and/or CRC, more detailed studies can be conducted in the future to check if multi-substrate targeting works in concert with reducing the tumor.

Lastly, the therapeutic role of PRMT5 can be extended beyond PDAC and CRC to other cancers. NF-κB is constitutively activated in a variety of cancers and PRMT5 is overexpressed in different cancers as well. It would be of particular interest to test the efficacy of PRMT5 inhibition in slowing down cancer progression. The ultimate goal is to translate the findings from the bench and

bring to the bench side to directly benefit as many patients as possible in the future.

APPENDICES

Appendix A. Permissions

Below is the information pertaining to permission from journals to use my first-author published manuscripts in my thesis:

1. Oncotarget:

Lakshmi Prabhu <prabhul@iu.edu>

Copyright query

Editorial Office <editorialoffice@oncotarget.com> Tue, Feb 13, 2018 at 3:51 AM
To: Lakshmi Prabhu <prabhul@umail.iu.edu>

You may use the paper as needed, as long as Oncotarget is cited as the source, in accordance with the license we use for all our papers: http://creativecommons.org/licenses/by/3.0/

On Thu, Feb 8, 2018 at 2:37 PM, Lakshmi Prabhu <prabhul@umail.iu.edu> wrote:

> Heelo,
>
> I published a first author paper last year in Oncotarget, and am currently writing my thesis. I planned to use the published text from this paper as part of my thesis. Can you please help me understand what would be the copyright permissions I would need to get from you and how would you like them to be included in the thesis? Students in the past have included permissions in the appendix section of the manuscript/mentioned it at the beginning of respective chapters.
>
> Thanks very much for your time,
>
> Lakshmi
>
> --
> **Lakshmi Prabhu**
> LinkedIn | Email
> PhD Candidate, Pharmacology
> Indiana University School of Medicine
> [redacted]

--

2. Molecular Biosystems:

Lakshmi Prabhu <prabhul@iu.edu>

Copyright query

MolOmics (Shared) <MolOmics@rsc.org> Mon, Feb 12, 2018 at 1:08 PM
To: Lakshmi Prabhu <prabhul@umail.iu.edu>

Dear Mr Prabhu,

Permission is granted to reproduce your article in your thesis as long as it is fully acknowledged and includes a link back to the article on our website. Please ensure that all authors are aware that it is being included.

If you have any further questions, please let me know.

With thanks,

Molecular Omics Editorial Office

Royal Society of Chemistry, Thomas Graham House Science Park, Milton Road, Cambridge CB4 0WF

From: Lakshmi Prabhu [mailto:prabhul@umail.iu.edu]
Sent: 08 February 2018 20:35
To: MolOmics (Shared) <MolOmics@rsc.org>
Subject: Copyright query

Hi Susan,

I recently published a first author paper in the last issue of Molecular Biosystems, and am currently writing my thesis. I planned to use the published text from this paper as part of my thesis. Can you please help me understand what would be the copyright permissions I would need to get from you and how would you like them to be included in the thesis? Students in the past have included permissions in the appendix section of the manuscript/mentioned it at the beginning of respective chapters.

Thanks very much for your time,

Lakshmi

--

Lakshmi Prabhu

LinkedIn | Email

PhD Candidate, Pharmacology
Indiana University School of Medicine
[redacted]

Appendix B. List of qPCR Primers

Gene Name	Primer	Lab Record	Primer Sequence Used
GAPDH	1	F326	CCATCACCATCTTCCAGGAGCG
	2	R468	AGAGATGATGACCCTTTTGGC
IL8	3	F139	TCCTGATTTCTGCAGCTCTGT
	4	R245	AAATTTGGGGTGGAAAGGTT
IL1α	5	F218	TGGCCCAGGCAGTCAGA
	6	R286	GGTTTGCTACAACATGGGCTACA
TNFα	7	F412	GACGCCCTCAATCAAAGTATAATTC
	8	R500	TCAAATTTCACTGCTTCATCCAGAT

Appendix C. Synthesis Rationale for 1st Set of Derivatives

Synthesis of derivatives was conducted by Dr. Lifan Zeng from the IU Chemical Genomics Core as described by him below.

1. Synthesis of PM-1

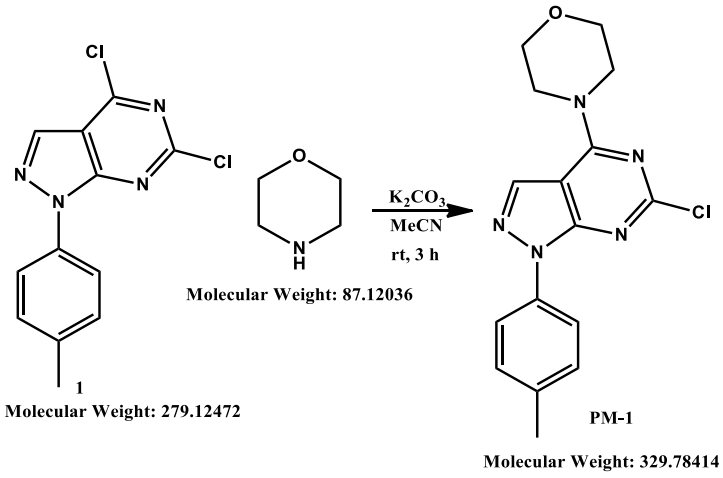

The mixture of the compound 1 (55.8mg, 0.2mmol), morpholine (17.42mg, 18.9mg, 0.2mmol), and K_2CO_3 (55.2mg, 0.4mmol) in MeCN (9 mL) was stirred at 30^oC for 16h, The reaction was monitored by TLC, after completion of the reaction, the reaction mixture was filtered and concentrated in vacuum to obtain crude product. The crude product was purified through silica gel column chromatography using DCM and DCM/EtOAc（20/1-5/1） to afford compound PM-1 as an off-white solid (65 mg, Yield 42%). ^1H NMR (400 MHz, $CDCl_3$) δ 8.04 (s, 1H), 7.92 (d, *J*=8.5, 2H), 7.30 (d, *J*=8.3, 2H), 4.01 – 3.96 (m, 4H), 3.88 – 3.85 (m, 4H), 2.40 (s, 3H).

2. Synthesis of PPA-1

Not included as part of a pending patent application.

3. Synthesis of PTF-1

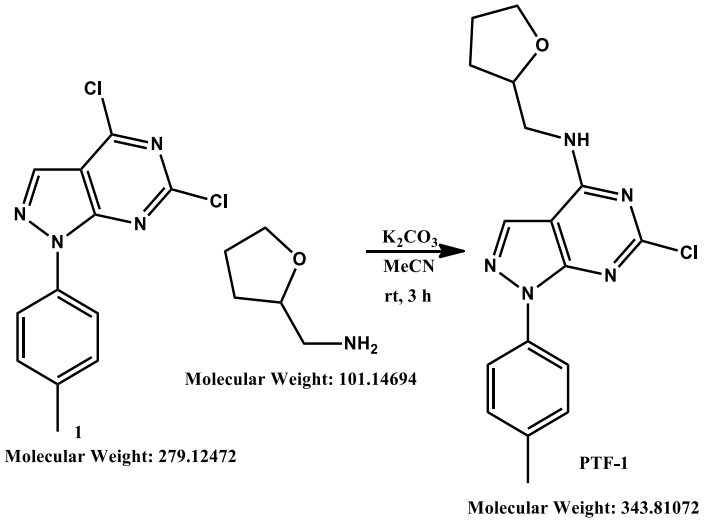

The mixture of the compound 1 (111.6mg, 0.4mmol) and K_2CO_3(110.4 mg, 0.8 mmol) in MeCN (16mL). To the reaction mixture was added tetrahydrofurfurylamine (43.2 mg, 50.8mg, 0.4mmol) and then stirred at 30^oC for 16 h, The reaction was monitored by TLC, after completion of the reaction, the reaction mixture was filtered and concentrated in vacuum to obtain crude product. The crude product was purified through silica gel column chromatography using DCM and DCM/EtOAc (4/1-2/1) to afford compound PTF-1 as an off-white solid (70 mg, Yield 45%).

4. Synthesis of PAM-1

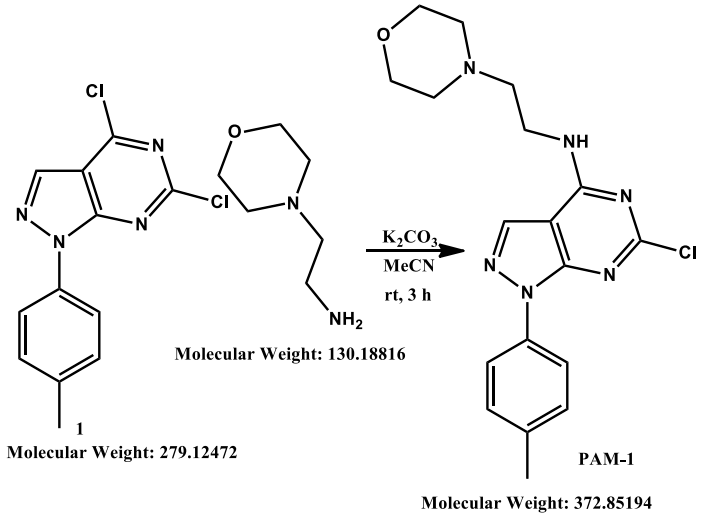

To the mixture of the compound 1 (111.6 mg, 0.4 mmol) and K_2CO_3(110.4 mg, 0.8 mmol) in MeCN(16 mL) was added 4-(2-Aminoethyl)morpholine (52 mg,54.3 mg, 0.4 mmol) and then stirred at 30 ^oC for 16 h, The reaction was monitored by TLC, after completion of the reaction, the reaction mixture was filtered and concentrated in vacuo to obtain crude. The crude product was purified through silica gel column chromatography using DCM and DCM/EtOAc（1/1） to afford compound PAM-1 as an off-white solid (65 mg, Yield 40%).

5. Synthesis of BAM-1

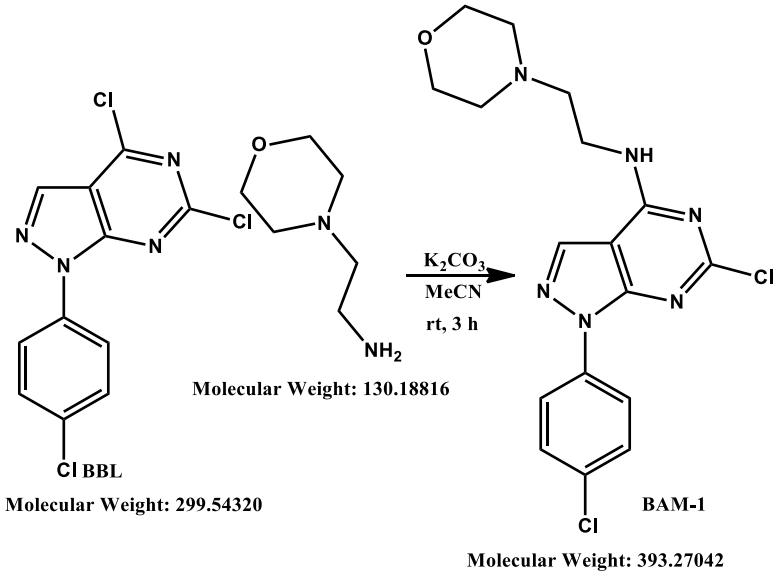

To the mixture of compound BBL (120.0 mg, 0.4 mmol) and K_2CO_3(110.4 mg, 0.8 mmol) in MeCN(16 mL) was added 4-(2-Aminoethyl)morpholine (52 mg, 55.3 mg, 0.4 mmol) and then stirred at 30 °C for 16 h, The reaction was monitored by TLC （DCM/MeOH=12/1）, after completion of the reaction, the reaction mixture was filtered and concentrated in vacuo to obtain crude. The crude product was purified through silica gel column chromatography using EtOAc and EtOAc/MeOH（100/1） to afford compound BAM-1 as an off-white solid (46 mg, Yield 26.7%).

7. Synthesis of BPM-1

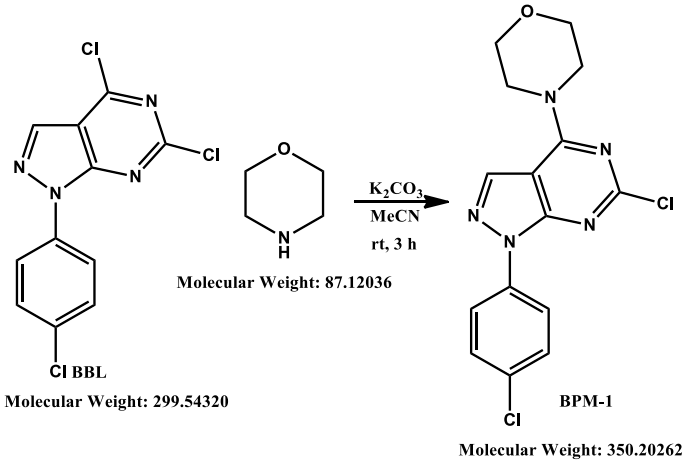

To the mixture of the compound BBL (120 mg, 0.4 mmol), morpholine (34.84 mg, 37.4 mg, 0.4 mmol), and K_2CO_3(110.4 mg, 0.8 mmol, 111.3 mg) in MeCN(15 mL) was stirred at 30 ^oC for 16 h, The reaction was monitored by TLC, after completion of the reaction, the reaction mixture was filtered and concentrated in vacuo to obtain crude. The crude product was purified through silica gel column chromatography using DCM/Hexane (1/1) and DCM to afford compound BPM-1 as an off-white solid (52 mg, Yield 32.9%).

8. Synthesis of BTF-1

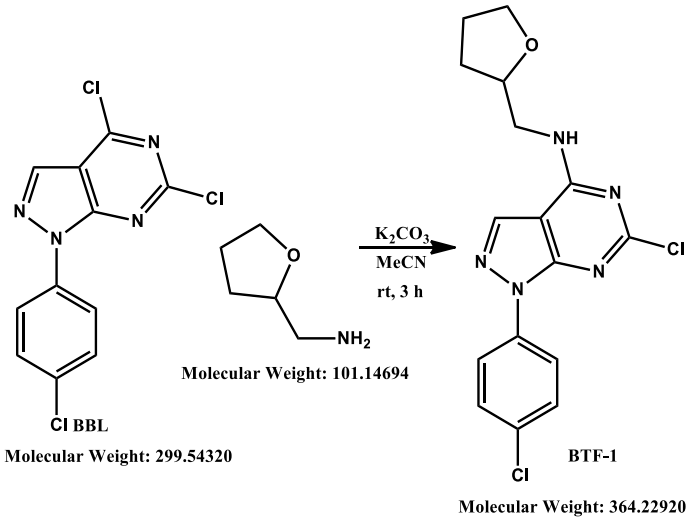

To the mixture of the compound BBL (120.6 mg, 0.4 mmol) and K_2CO_3 (110.4 mg, 0.8 mmol, 115 mg) in MeCN(16 mL) was added tetrahydrofurfurylamine (43.2 mg, 49.1 mg, 0.4 mmol) and then stirred at 30 °C for 16 h, The reaction was monitored by TLC (DCM/EtOAc=4/1), after completion of the reaction, the reaction mixture was filtered and concentrated in vacuum to obtain crude product. The crude product was purified through silica gel column chromatography using DCM and DCM/EtOAc（4/1） to afford compound BTF-1 as an off-white solid (48 mg, Yield 29.4%).

10. Synthesis of BAP-1

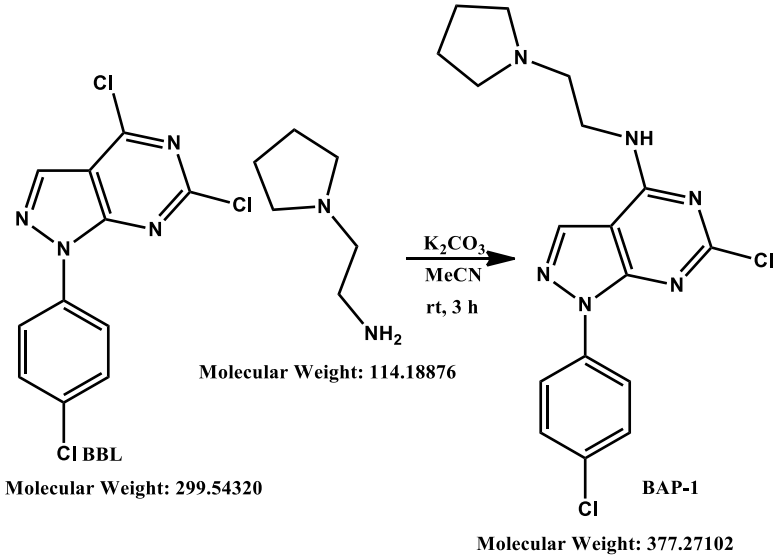

The mixture of the compound BBL (120.6 mg, 0.4 mmol, 122 mg) and K_2CO_3 (110.4 mg, 0.8 mmol, 116.4 mg) in MeCN(16 mL). To the reaction mixture was added 1-(2-Aminoethyl)pyrrolidine (45.6 mg, 50 mg, 0.4 mmol) and then stirred at 30 °C for 16 h, The reaction was monitored by TLC（DCM/MeOH=8/1）, after completion of the reaction, the reaction mixture was filtered and concentrated in vacuo to obtain crude. The crude product was purified through silica gel column chromatography using EtOAc and EtOAc / MeOH（20/1-10/1） to afford compound BAP-1 as an off-white solid (46 mg, Yield 27.8%). ^{1}H NMR (400 MHz, $CDCl_3$) δ = 8.48 (s, 1H), 8.12 (d, *J*=8.9, 2H), 7.46 (d, *J*=8.9, 2H), 4.02 (s, 2H), 3.30 (s, 6H), 2.59 (s, 1H), 2.17 (s, 4H).

11. Synthesis of PAMHP-2-5

Not included as the synthesis involves PPA-1 which is confidential as part of pending patent application.

12. Synthesis of PAMPH-1

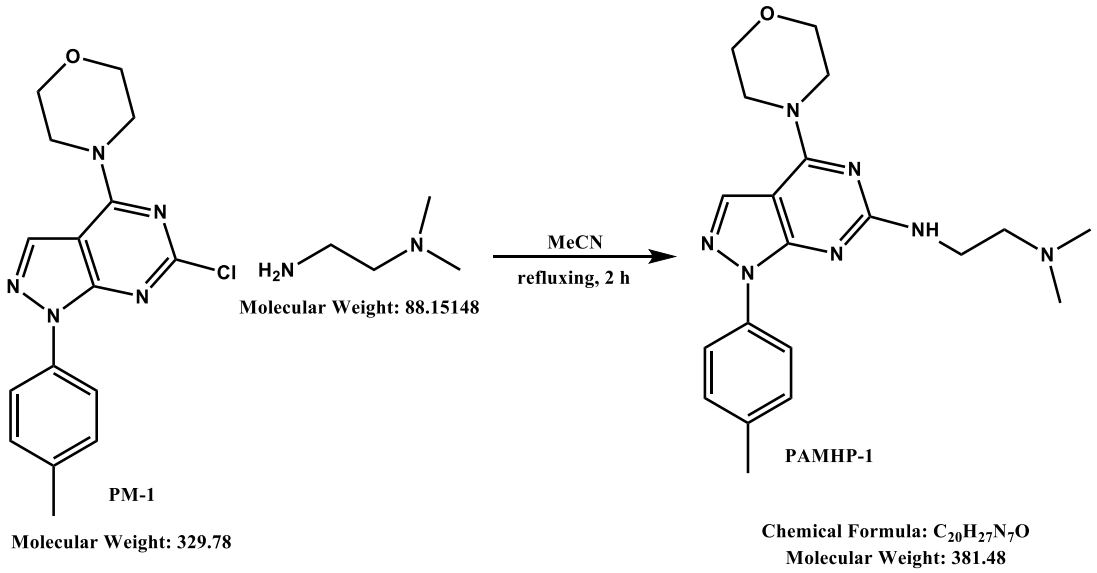

N^1,N^1-dimethyl-N^2-(4-morpholino-1-(p-tolyl)-1H-pyrazolo[3,4-d]pyrimidin-6-yl)ethane-1,2-diamine. The mixture of the compound PM-1 (30.1 mg, 0.1 mmol) and triethylamine (0.5 mL) in N,N-Dimethylethylenediamine (3 mL) was stirred at 30 °C for 3 h, and then warmed to 120 °C and stirred for 16 h. The reaction was monitored by TLC (DCM/Hexane/triethylamine =6/3/0.5), after completion of the reaction, the reaction mixture was filtered and concentrated in vacuum to obtain crude product, which was purified through silica gel column chromatography using (DCM/ Hexane/triethylamine =6/6/0.5) to afford compound PAMPH-1(6.2

mg) as an off-white solid. ^{1}H NMR (400 MHz, $CDCl_3$) δ = 8.06 (d, *J*=7.6, 2H), 7.88 (s, 1H), 7.25 (s, 2H), 3.93 – 3.88 (m, 4H), 3.86 – 3.82 (m, 4H), 3.68 – 3.52 (m, 4H), 2.39 (s, 3H), 2.30 (s, 6H). ESI-MS: $(M + H)^+$ calculated for $C_{20}H_{27}N_7O$, 381.47; found,382.23.

13. Synthesis of PAMHP-6PM

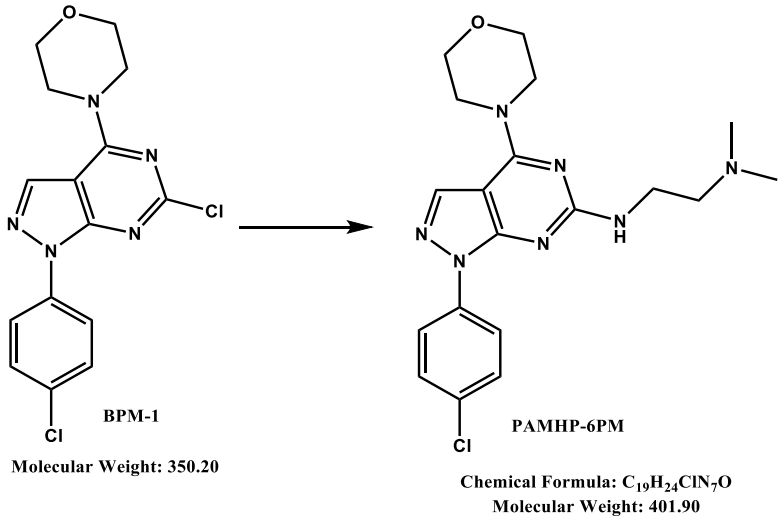

N^1-(1-(4-chlorophenyl)-4-morpholino-1H-pyrazolo[3,4-d]pyrimidin-6-yl)-N^2,N^2-dimethylethane-1,2-diamine. The mixture of the compound BPM-1 (35 mg, 0.1 mmol)and triethylamine (0.5 mL) in N,N-Dimethylethylenediamine (3 mL) was stirred at 30 °C for 3 h, and then warmed to 120 °C and stirred for 16 h. The reaction was monitored by TLC (DCM/Hexane /triethylamine =6/3/0.5), after completion of the reaction, the reaction mixture was filtered and concentrated in vacuum to obtain crude product, which was purified through silica gel column chromatography using (DCM/ Hexane/triethylamine =6/6/0.5) and (DCM/ Hexane/triethylamine =6/3/0.5) to afford compound PAMHP-6PM (10.0 mg) as

an off-white solid. ^{1}H NMR (400 MHz, $CDCl_3$) δ = 8.23 (d, *J*=8.6, 2H), 7.89 (s, 1H), 7.42 (d, *J*=9.0, 2H), 3.93 – 3.87 (m, 4H), 3.86 – 3.82 (m, 4H), 3.69 – 3.62 (m, 4H), 2.34 (s, 6H). ESI-MS: $(M + H)^+$ calculated for $C_{19}H_{24}ClN_7O$, 401.89; found,402.18.

14. Synthesis of PAMHP-8TF

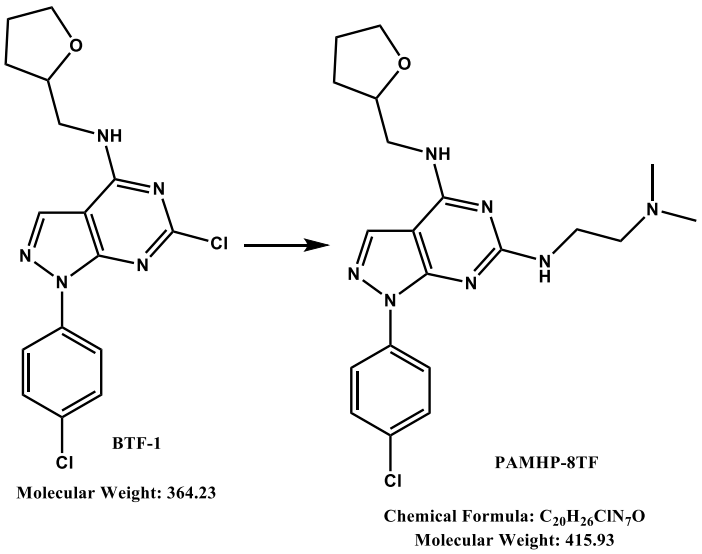

The mixture of the compound BTF-1 (36.4 mg, 0.1 mmol) and triethylamine (0.5 mL) in N,N-Dimethylethylenediamine (3 mL) was stirred at 30 °C for 3 h, and then warmed to 120 °C and stirred for 16 h. The reaction was monitored by TLC (DCM/Hexane /triethylamine =6/3/0.5), after completion of the reaction, the reaction mixture was filtered and concentrated in vacuum to obtain crude product, which was purified through silica gel column chromatography using (DCM/ Hexane/triethylamine =6/3/0.5) to afford compound PAMHP-8TF (12.7 mg) as an off-white solid. ^{1}H NMR (400 MHz, $CDCl_3$) δ = 8.24 (d, *J*=8.7, 2H),

7.84 (s, 1H), 7.41 (d, *J*=9.0, 2H), 4.13 (d, *J*=7.2, 1H), 4.00 – 3.86 (m, 2H), 3.81 (d, *J*=8.2, 1H), 3.67 – 3.54 (m, 4H), 2.64 (t, *J*=6.1, 2H), 2.36 (s, 6H), 1.97 (s, 4H).ESI-MS: $(M + H)^+$ calculated for $C_{20}H_{26}ClN_7O$, 415.92; found,416.2.

15. Synthesis of PAMHP-3

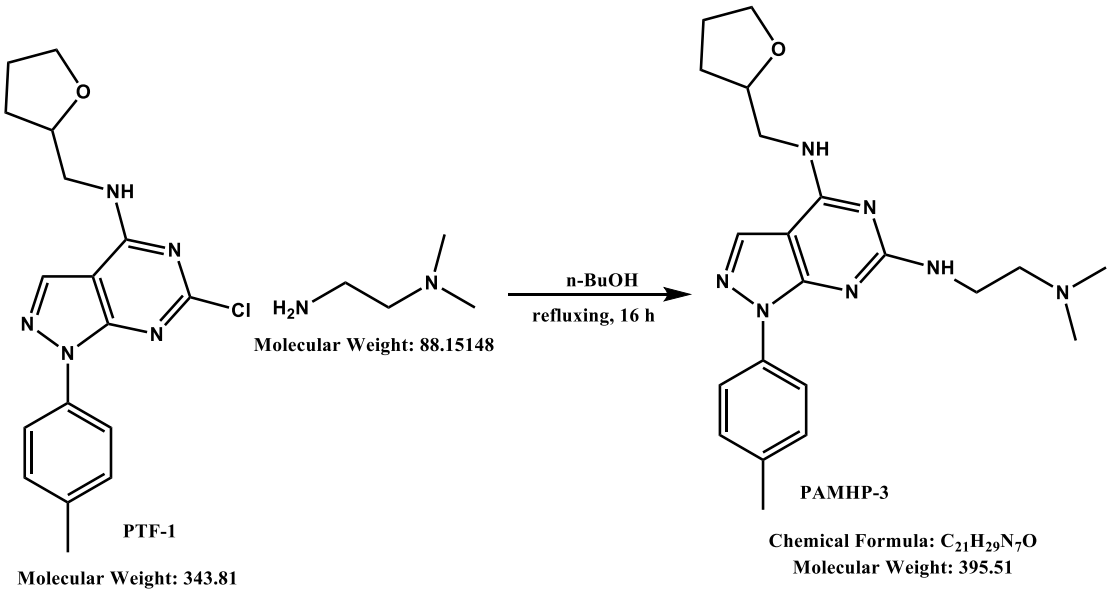

N^6-(2-(dimethylamino)ethyl)-N^4-((tetrahydrofuran-2-yl)methyl)-1-(p-tolyl)-1H-pyrazolo[3,4-d]pyrimidine-4,6-diamine. The mixture of compound PTF-1 (34.1 mg, 0.1 mmol), N,N-Dimethylethylenediamine (0.2 mL), and K_2CO_3(100 mg, 0.8 mmol) in n-BuOH (12 mL) was stirred at 30 °C for 3 h, and then warmed to 130 °C and stirred for 16 h. The reaction was monitored by TLC (EtOAc/DCM/MeOH=3/6/1), after completion of the reaction, the reaction mixture was filtered and concentrated in vacuo to obtain crude product, which was purified through silica gel column chromatography using DCM and DCM/EtOAc（

1/1），and then preparative HPLC with gradient started at 20% MeCN in water, increase to 40% MeCN at 8 min and ended at 100% water after 11 min with 0.1% of TFA to afford compound PAMHP-3 (6.4 mg) as an off-white solid. ^{1}H NMR (400 MHz, $CDCl_3$) δ 9.40 (s, 1H), 8.10 (s, 1H), 7.77 (d, *J* = 8.0 Hz, 2H), 7.29 (d, *J* = 8.1 Hz, 2H), 4.28-4.21 (m, 1H), 3.97-3.87 (m, 3H), 3.84-3.68 (m, 3H), 3.30 (s, 2H), 2.83 (s, 6H), 2.41 (s, 3H), 2.18-2.12 (m, 1H), 2.05-1.97 (m, 2H), 1.80-1.71 (m, 1H). ESI-MS: $(M + H)^+$ calculated for $C_{21}H_{29}N_7O$, 395.50; found,396.3. Purity: 98.4% (254nm).

16. Synthesis of PAMPH-5-5

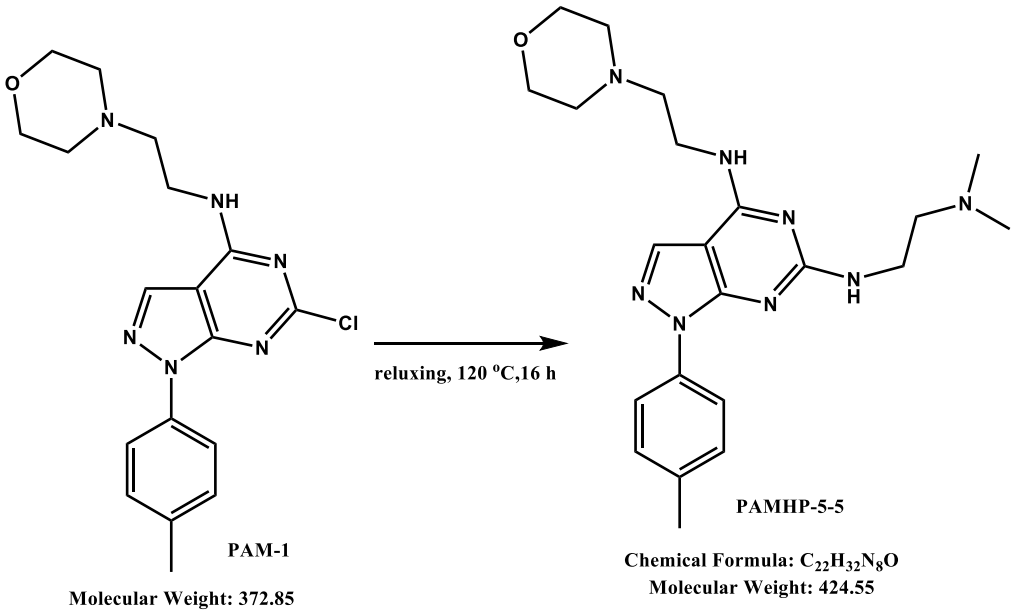

N^6-(2-(dimethylamino)ethyl)-N^4-(2-morpholinoethyl)-1-(p-tolyl)-1H-pyrazolo[3,4-d]pyrimidine-4,6-diamine. The mixture of the compound PAM-1 (75 mg, 0.2 mmol) and triethylamine (0.5 mL) in N, N-Dimethylethylenediamine

(3 mL) was stirred at 30 °C for 3 h, and then warmed to 120 °C and stirred for 16 h. The reaction was monitored by TLC (DCM/ triethylamine =8/0.5), after completion of the reaction, the reaction mixture was filtered and concentrated in vacuum to obtain crude product, which was purified through silica gel column chromatography using DCM/ triethylamine (8/0.5), and then the preparative HPLC gradient started at 20% MeCN in water, increase to 40% MeCN at 8 min and ended at 100% water after 11 min with 0.1% of TFA to afford compound PAMPH-5-5 (6.9 mg) as an off-white solid.^{1}H NMR (400 MHz, CD_3OD) δ 7.98 (s, 1H), 7.79 (d, *J* = 8.4 Hz, 2H), 7.35 (d, *J* = 8.3 Hz, 2H), 3.96 (d, *J* = 5.8 Hz, 6H), 3.78 (t, *J* = 5.4 Hz, 2H), 3.48 (t, *J* = 5.7 Hz, 4H), 3.39 – 3.32 (m, 4H), 2.81 (s, 6H), 2.41 (s, 3H). ESI-MS: $(M + H)^+$ calculated for $C_{22}H_{32}N_8O$, 424.54; found,425.3. Purity: >98% (HPLC).

17. Synthetic of PAMHP-9

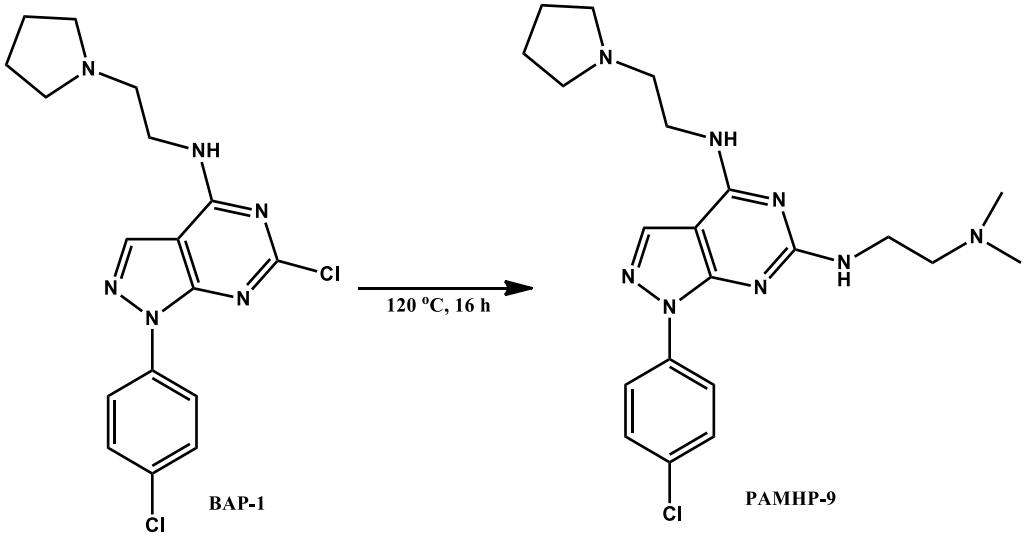

1-(4-chlorophenyl)-N^6-(2-(dimethylamino)ethyl)-N^4-(2-(pyrrolidin-1-yl)ethyl)-1H-pyrazolo[3,4-d]pyrimidine-4,6-diamine. The mixture of the compound BAP-1 (37.7 mg, 0.1 mmol) and triethylamine (0.5 mL) in N,N-Dimethylethylenediamine (3 mL) was stirred at 120 °C for 16 h. The reaction was monitored by TLC (DCM/ triethylamine =20/1), after completion of the reaction, the reaction mixture was filtered and concentrated in vacuum to obtain crude. The crude product was purified through silica gel column chromatography using DCM / petroleum ether/trimethylamine (100/10/5), DCM/triethylamine (20/1) and DCM / MeOH / triethylamine (200/15/109), and then the preparative HPLC gradient started at 20% MeCN in water, increase to 40% MeCN at 8 min and ended at 100% water after 11 min with 0.1% of TFA to afford compound PAMHP-9 (6.6 mg) as an off-white solid. ^{1}H NMR (400 MHz, CD_3OD) δ 8.10 (d, *J* = 8.9 Hz, 2H), 8.01 (s, 1H), 7.50 (d, *J* = 8.9 Hz, 2H), 3.92 (t, *J* = 5.6 Hz, 2H), 3.84 (t, *J* = 5.8 Hz, 4H), 3.51 (t, *J* = 5.7 Hz, 2H), 3.42 (t, *J* = 5.8 Hz, 2H), 3.17 (s, 2H), 2.90 (s, 6H), 2.16 (s, 2H), 2.05 (s, 2H). ESI-MS: $(M + H)^+$ calculated for C21H29ClN8, 428.96; found,429.2. Purity: >98% (HPLC).

18. Synthetic of PAMHP-4

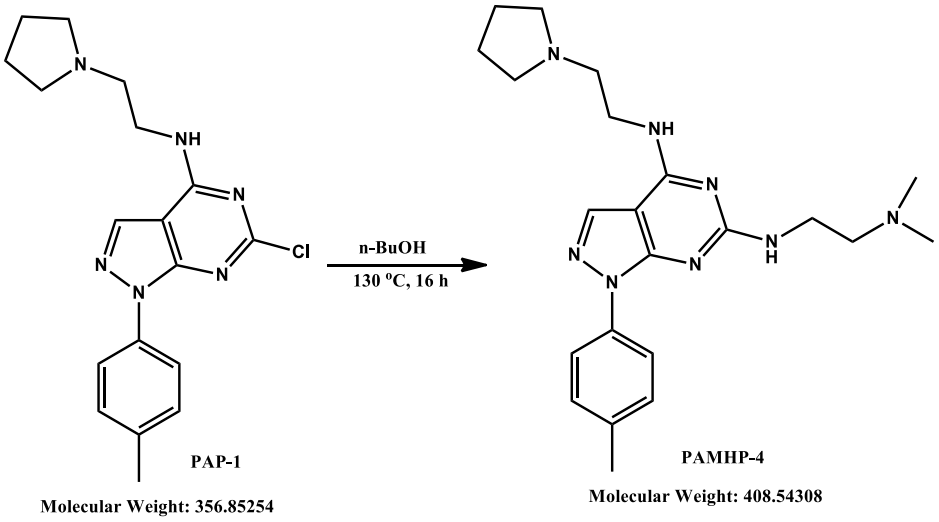

The mixture of the compound PAP-1 (~55.1 mg, 56.8 mg, 0.15 mmol), N,N-Dimethylethylenediamine (0.15 mL), and K_2CO_3(75 mg, 0.6 mmol, 79.8 mg) in n-BuOH (15 mL) was stirred at 30 °C for 3 h, and then warmed to 130 °C and stirred for 16 h. The reaction was monitored by TLC (EtOAc/DCM/MeOH=3/6/1), **No reaction.**

19. Synthesis of PAMHP-7

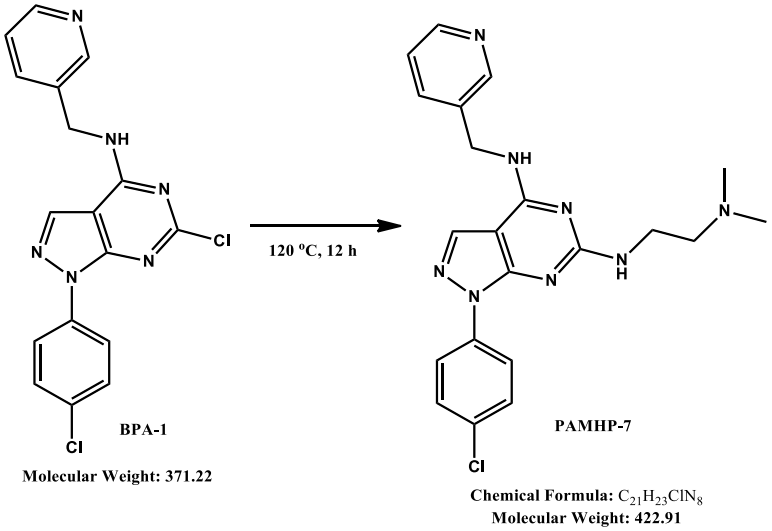

The mixture of the compound BPA-1 (37.1 mg, 0.1 mmol) and triethylamine (0.5 mL) in N,N-Dimethylethylenediamine (3 mL) was stirred at 120 °C for 16 h. The reaction was monitored by TLC (DCM/MeOH/triethylamine =10/1/0.5), after completion of the reaction, the reaction mixture was filtered and concentrated in vacuum to obtain crude product, which was purified through silica gel column chromatography using DCM and (DCM/MeOH/triethylamine =10/1/0.5) to afford compound PAMHP-7 (10 mg) as an off-white solid. Yield 10.5 mg, 32%. ^{1}H NMR (400 MHz, CD_3OD) δ 8.87 (s, 1H), 8.72 (s, 1H), 8.51 (s, 1H), 8.14 (d, *J* = 9.0 Hz, 2H), 8.07 (s, 1H), 7.93 (s, 1H), 7.52 (d, *J* = 8.9 Hz, 2H), 4.93 (s, 2H), 3.80 (t, *J* = 5.8 Hz, 2H), 3.38 (t, *J* = 6.5 Hz, 2H), 3.20 (s, 1H), 2.89 (s, 6H). ESI-MS: $(M + H)^+$ calculated for $C_{21}H_{23}ClN_8$, 422.91; found,423.2.

20. Synthesis of PAMPH-10

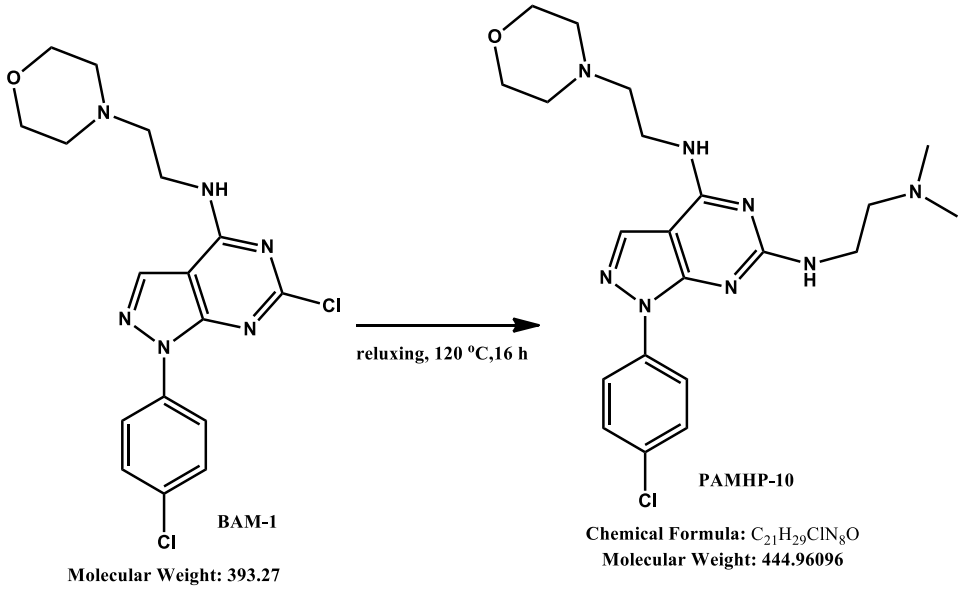

The mixture of the compound BAM-1 (39.3 mg, 0.1 mmol) and triethylamine (0.5 mL) in N,N-Dimethylethylenediamine (3 mL) was stirred at 30 °C for 3 h, and then warmed to 120 °C and stirred for 16 h. The reaction was monitored by TLC DCM /triethylamine (8/0.5), after completion of the reaction, the reaction mixture was filtered and concentrated in vacuum to obtain crude product, which was purified through silica gel column chromatography using DCM /triethylamine (8/0.5) to afford compound PAMHP-10 as an off-white solid. Yield 25 mg, 57%. ^{1}H NMR (400 MHz, CD_3OD) δ 8.87 (s, 1H), 8.72 (s, 1H), 8.51 (s, 1H), 8.14 (d, *J* = 9.0 Hz, 2H), 8.07 (s, 1H), 7.93 (s, 1H), 7.52 (d, *J* = 8.9 Hz, 2H), 4.93 (s, 2H), 3.80 (t, *J* = 5.8 Hz, 2H), 3.38 (t, *J* = 6.5 Hz, 2H), 3.20 (s, 1H), 2.89 (s, 6H). ESI-MS: $(M + H)^+$ calculated for C21H29ClN8O, 444.96; found,445.2.

Appendix D. Conditions Optimized for Detection of PR5-LL-CM01 using LC-MS

This work was conducted by Dr. David Jones and colleagues at the IU Clinical Pharmacology Analytical Core.

HPLC conditions

Column: Agilent Zorbax 300SB-C8 150 x 4.6 mm 5 micron

Mobile Phase: acetonitrile: 0.1% formic acid

A: 20:80; v/v

B: 80:20; v/v

Flow: 600µL/min

Time (min.)	%A	%B
0	100	0
2	0	100
7	0	100
7.1	100	0
10	100	0

Mass spectrometry conditions

Positive mode

Compound	Q1	Q3	Time (msec)	DP	EP	CE	CXP
PR5-LL-CM01	402.1	357.3	100	50	10	30	15
Acetaminophen (IS)	152.0	109.3	100	80	12	20	10

Temperature: 600

Curtain Gas: 15

Source Gas 1: 50

Resolution: Unit for Q1 and Q3

CAD: medium

IS: 3000

Source Gas 2: 50

REFERENCES

Agarwal A, Das K, Lerner N, Sathe S, Cicek M, Casey G, and Sizemore N. The AKT/IκB kinase pathway promotes angiogenic/metastatic gene expression in colorectal cancer by activating nuclear factor-κB and β-catenin. Oncogene. 2005; 24: 1021-31. doi: 10.1038/sj.onc.1208296.

Ahmed D, Eide PW, Eilertsen IA, Danielsen SA, Eknæs M, Hektoen M, Lind GE, Lothe RA. Epigenetic and genetic features of 24 colon cancer cell lines. Oncogenesis. 2013; 2: e71. doi: 10.1038/oncsis.2013.25.

Almqvist H, Axelsson H, Jafari R, Dan C, Mateus A, Haraldsson M, Larsson A, Martinez Molina D, Artursson P, Lundbäck T, Nordlund P. CETSA screening identifies known and novel thymidylate synthase inhibitors and slow intracellular activation of 5-fluorouracil. Nat Commun. 2016; 7:11040. doi: 10.1038/ncomms11040.

Antonysamy S, Bonday Z, Campbell RM, Doyle B, Druzina Z, Gheyi T, Han B, Jungheim LN, Qian Y, Rauch C, Russell M, Sauder JM, Wasserman SR, *et al*. Crystal structure of the human PRMT5:MEP50 complex. Proc Natl Acad Sci USA. 2012; 109: 17960-5. doi: 10.1073/pnas.1209814109.

Arora S, Bhardwaj A, Singh S, Srivastava SK, McClellan S, Nirodi CS, Piazza GA, Grizzle WE, Owen LB, and Singh AP. An undesired effect of chemotherapy:

gemcitabine promotes pancreatic cancer cell invasiveness through reactive oxygen species-dependent, nuclear factor κB- and hypoxia-inducible factor 1α-mediated up-regulation of CXCR4. J Biol Chem. 2013; 288: 21197-207. doi: 10.1074/jbc.M113.484576.

Bandyopadhyay S, Harris DP, Adams GN, Lause GE, McHugh A, Tillmaand EG, Money A, Willard B, Fox PL, Dicorleto PE. HOXA9 methylation by PRMT5 is essential for endothelial cell expression of leukocyte adhesion molecules. Mol Cell Biol. 2012; 32:1202-13. doi: 10.1128/ MCB.05977-11.

Beltran-Alvarez P, Espejo A, Schmauder R, Beltran C, Mrowka R, Linke T, Batlle M, Pérez-Villa F, Pérez GJ, Scornik FS, Benndorf K, Pagans S, Zimmer T, Brugada R. Protein arginine methyl transferases-3 and -5 increase cell surface expression of cardiac sodium channel. FEBS Lett. 2013; 587: 3159-65. doi: 10.1016/j.febslet.2013.07.043.

Błogowski W, Deskur A, Budkowska M, Sałata D, Madej-Michniewicz A, Dąbkowski K, Dołęgowska B, Starzyńska T. Selected cytokines in patients with pancreatic cancer: A preliminary report. PLoS One. 2014; 9: e97613. doi: 10.1371/journal.pone.0097613.

Boffa LC, Karn J, Vidali G, Allfrey VG. Distribution of NG, NG,-dimethylarginine in nuclear protein fractions. Biochem Biophys Res Commun. 1977; 74: 969-76. doi:

Borowicz S, Van Scoyk M, Avasarala S, Karuppusamy Rathinam MK, Tauler J, Bikkavilli RK, Winn RA. The Soft Agar Colony Formation Assay. Journal of Visualized Experiments: JoVE. 2014: 51998. doi: 10.3791/51998.

Brahms H, Meheus L, de Brabandere V, Fischer U, Luhrmann R. Symmetrical dimethylation of arginine residues in spliceosomal Sm protein B/B0 and the Sm-like protein LSm4, and their interaction with the SMN protein. RNA. 2001; 7: 1531-42. doi: 10.1017.S135583820101442X.

Branscombe TL, Frankel A, Lee JH, Cook JR, Yang Z, Pestka S, Clarke S. Prmt5 (Janus kinase-binding protein 1) catalyzes the formation of symmetric dimethylarginine residues in proteins. J Biol Chem. 2001; 276, 32971-76. doi: 0.1074/jbc.M105412200.

Butler JS, Zurita-Lopez CI, Clarke SG, Bedford MT, Dent SY. Protein-arginine methyltransferase 1 (PRMT1) methylates Ash2L, a shared component of mammalian histone H3K4 methyltransferase complexes. J Biol Chem. 2011; 286: 12234-44. doi: 10.1074/jbc.M110.202416.

Chabot GG. Clinical pharmacokinetics of irinotecan. Clin Pharmacokinet. 1997; 33: 245-59. doi: 10.2165/00003088-199733040-00001.

Chan-Penebre E, Kuplast KG, Majer CR, Boriack-Sjodin PA, Wigle TJ, Johnston LD, Rioux N, Munchhof MJ, Jin L, Jacques SL, West KA, Lingaraj T, Stickland K, *et al*. A selective inhibitor of PRMT5 with *in vivo* and *in vitro* potency in MCL models. Nat Chem Biol. 2015; 11: 432-7. doi: 10.1038/nchembio.

Chen H, Lorton B, Gupta V, Shechter D. A TGFβ-PRMT5-MEP50 axis regulates cancer cell invasion through histone H3 and H4 arginine methylation coupled transcriptional activation and repression. Oncogene. 2017; 36: 373-86. doi: 10.1038/onc.2016.205.

Cheng D, Cote J, Shaaban S, Bedford MT. The arginine methyltransferase CARM1 regulates the coupling of transcription and mRNA processing. Mol Cell. 2007; 25: 71-83. doi: 10.1016/j.molcel.2006.11.019.

Cheng X, Collins RE, Zhang X. Structural and sequence motifs of protein (histone) methylation enzymes. Annu Rev Biophys Biomol Struct. 2005; 34: 267-94. doi: 10.1146/annurev.biophys.34.040204.144452.

Cho EC, Zheng S, Munro S, Liu G, Carr SM, Moehlenbrink J, Lu YC, Stimson L, Khan O, Konietzny R, McGouran J, Coutts AS, Kessler B, *et al.* Arginine methylation controls growth regulation by E2F-1. EMBO J. 2012; 31: 1785-97. doi: 10.1038/emboj.2012.

Clarke TL, Sanchez-Bailon MP, Chiang K, Reynolds JJ, Herrero-Ruiz J, Bandeiras TM, Matias PM, Maslen SL, Skehel JM, Stewart GS, Davies CC. PRMT5-Dependent Methylation of the TIP60 Coactivator RUVBL1 Is a Key Regulator of Homologous Recombination. Mol Cell. 2017; 65: 900-16. doi: 10.1016/j.molcel.2017.01.019.

Conroy T, Desseigne F, Ychou M, Bouche O, Guimbaud R, Becouarn Y, Adenis A, Raoul JL, Gourgou-Bourgade S, de la Fouchardiere C, Bennouna J, Bachet JB, Khemissa- Akouz F, *et al.* FOLFIRINOX versus gemcitabine for metastatic pancreatic cancer. N Engl J Med. 2011; 364: 1817-25. doi: 10.1056/NEJMoa1011923.

Corrie P, Qian W, Basu B, Jodrell DI, Falk S, Iwuji C, Wasan H, Palmer DH, Scott-Brown M, Wadsley J, Arif SS, Babaoglan AB, Dalchau KM, *et al.* A randomized phase II trial comparing different schedules of nab-paclitaxel (nabP) combined with gemcitabine (GEM) as first line treatment for metastatic pancreatic adenocarcinoma (PDAC). Journal of Clinical Oncology. 2017; 35: 342-42. doi: 10.1200/JCO.2017.35.4_suppl.342.

Dan HC, Cooper MJ, Cogswell PC, Duncan JA, Ting JP, Baldwin AS. Akt-dependent regulation of NF-{kappa}B is controlled by mTOR and Raptor in association with IKK. Genes Dev. 2008; 22: 1490-500. doi: 10.1101/gad.1662308.

Daniluk J, Liu Y, Deng D, Chu J, Huang H, Gaiser, S, Cruz-Monserrate Z, Wang H, Ji B, and Logsdon CD. An NF-κB pathway-mediated positive feedback loop amplifies Ras activity to pathological levels in mice. J Clin Invest. 2012; 122: 1519-28. doi: 10.1172/JCI59743.

Deer EL, González-Hernández J, Coursen JD, Shea JE, Ngatia J, Scaife CL, Firpo MA, Mulvihill SJ. Phenotype and genotype of pancreatic cancer cell lines. Pancreas. 2010; 39: 425-35. doi: 10.1097/MPA.0b013e3181c15963.

De Sousa Cavalcante L, Monteiro G. Gemcitabine: metabolism and molecular mechanisms of action, sensitivity and chemoresistance in pancreatic cancer. Eur J Pharmacol. 2014; 741: 8-16. doi: 10.1016/j.ejphar.2014.07.041.

De Vita F, Ventriglia J, Febbraro A, Laterza MM, Fabozzi A, Savastano B, Petrillo A, Diana A, Giordano G, Troiani T, Conzo G, Galizia G, Ciardiello F, Orditura M. NAB-paclitaxel and gemcitabine in metastatic pancreatic ductal adenocarcinoma (PDAC): from clinical trials to clinical practice. BMC Cancer. 2016; 16: 709. doi: 10.1186/s12885-016-2671-9.

Dhar S, Vemulapalli V, Patananan AN, Huang GL, Di Lorenzo A, Richard S, Comb MJ, Guo A, Clarke SG, Bedford MT. Loss of the major Type I arginine methyltransferase PRMT1 causes substrate scavenging by other PRMTs. Sci Rep. 2013; 3: 1311. doi: 10.1038/srep01311.

Dong Y, Song C, Wang Y, Lei Z, Xu F, Guan H, Chen A, Li F. Inhibition of PRMT5 suppresses osteoclast differentiation and partially protects against ovariectomy-induced bone loss through downregulation of CXCL10 and RSAD2. Cell Signal. 2017; 34: 55-65. doi: 10.1016/j.cellsig.2017.03.004.

Eckschlager T, Plch J, Stiborova M, Hrabeta J. Histone deacetylase inhibitors as anticancer drugs. Int J Mol Sci. 2017; 18: 1414. doi: 10.3390/ijms18071414.

Fennema E, Rivron N, Rouwkema J, van Blitterswijk C, de Boer J. Spheroid culture as a tool for creating 3D complex tissues. Trends Biotechnol. 2013; 31: 108-15. doi: 10.1016/j.tibtech.2012.12.003.

Ferlay J, Soerjomataram I, Dikshit R, Eser S, Mathers C, Rebelo M, Parkin DM, Forman D, and Bray F. Cancer incidence and mortality worldwide: Sources, methods and major patterns in GLOBOCAN 2012. Int J Cancer. 2015; 136: E359-86. doi: 10.1002/ijc.29210.

Friesner RA, Banks JL, Murphy RB, Halgren TA, Klicic JJ, Mainz DT, Repasky MP, Knoll EH, Shelley M, Perry JK, Shaw DE, Francis P, and Shenkin PS. Glide: A New Approach for Rapid, Accurate Docking and Scoring. 1. Method and Assessment of Docking Accuracy. J Med Chem. 2004; 47: 1739-49. doi: 10.1021/jm0306430.

Fujioka S, Sclabas GM, Schmidt C, Frederick WA, Dong QG, Abbruzzese JL, Evans DB, Baker C, and Chiao PJ. Function of nuclear factor κB in pancreatic cancer metastasis. Clin Cancer Res. 2003; 9: 346-54. doi:

Ghosh S, May MJ, Kopp EB. NFκB and Rel proteins: evolutionarily conserved mediators of immune responses. Annu Rev Immunol. 1988; 16: 225-60. doi: 10.1146/annurev.immunol.16.1.225.

Gilmore TD. Introduction to NF-κB: players, pathways, perspectives. Oncogene. 2006; 25: 6680-4. doi: 10.1038/sj.onc.1209954.

Girardot M, Hirasawa R, Kacem S, Fritsch L, Pontis J, Kota SK, Filipponi D, Fabbrizio E, Sardet C, Lohmann F, Kadam S, Ait- Si-Ali S, Feil R. PRMT5-mediated histone H4 arginine-3 symmetrical dimethylation marks chromatin at G+C-rich regions of the mouse genome. Nucleic Acids Res. 2014; 42: 235-48. doi: 10.1093/nar/gkt884.

Gkountela S, Li Z, Chin CJ, Lee SA, Clark AT. PRMT5 is required for human embryonic stem cell proliferation but not pluripotency. Stem Cell Rev. 2014; 10: 230-9. doi: 10.1007/s12015-013-9490-z.

Gu Z, Gao S, Zhang F, Wang Z, Ma W, Davis RE, and Wang Z. Protein arginine methyltransferase 5 is essential for growth of lung cancer cells. Biochem J. 2012; 446: 235-41. doi: 10.1042/BJ20120768.

Guderian G, Peter C, Wiesner J, Sickmann A, Schulze-Osthoff K, Fischer U, Grimmler M. RioK1, a new interactor of protein arginine methyltransferase 5 (PRMT5), competes with pICln for binding and modulates PRMT5 complex composition and substrate specificity. J Biol Chem. 2011; 286: 1976-86. doi: 10.1074/jbc.M110.148486.

Gullà A, Hideshima T, Bianchi G, Fulciniti M, Kemal Samur M, Qi J, Tai YT, Harada T, Morelli E, Amodio N, Carrasco R, Tagliaferri P, Munshi NC, Tassone P, Anderson KC. Protein arginine methyltransferase 5 has prognostic relevance and is a druggable target in multiple myeloma. Leukemia. 2018; 32: 996-1002. doi: 10.1038/leu.2017.334.

Guo Z, Zheng L, Xu H, Dai H, Zhou M, Pascua MR, Chen QM, Shen B. Methylation of FEN1 suppresses nearby phos- phorylation and facilitates PCNA binding. Nat Chem Biol. 2010; 6: 766-73. doi:10.1038/nchembio.422.

Hai Ping P, Feng Bo T, Li L, Nan Hui Y, Hong Z. IL-1β/NF-kb signaling promotes colorectal cancer cell growth through miR-181a/PTEN axis. Arch Biochem Biophys. 2016; 604: 20-6. doi: 10.1016/j.abb.2016.06.001.

Halgren TA, Murphy RB, Friesner, RA, Beard HS, Frye LL, Pollard WT, and Banks JL. Glide: a new approach for rapid, accurate docking and scoring. 2. Enrichment factors in database screening. J.Med Chem. 2004; 47: 1750-9. doi: 10.1021/jm030644s.

Hanahan D, Weinberg RA. Hallmarks of cancer: the next generation. Cell. 2011; 144: 646-74. doi: 10.1016/j.cell.2011.02.013.

Harris DP, Bandyopadhyay S, Maxwell TJ, Willard B, DiCorleto PE. Tumor necrosis factor (TNF)-alpha induction of CXCL10 in endothelial cells requires protein arginine methyltransferase 5 (PRMT5)-mediated nuclear factor (NF)-kappaB p65 methylation. J Biol Chem. 2014; 28: 15328-39. doi: 10.1074/jbc.M114.547349.

Harris DP, Chandrasekharan UM, Bandyopadhyay S, Willard B, DiCorleto PE. PRMT5-mediated methylation of NF-κB p65 at Arg174 is required for endothelial CXCL11 gene induction in response to TNF-α and IFN-γ costimulation. PLoS One. 2016; 11: e0148905. doi: 10.1371/journal.pone.0148905.

Hassanzadeh P. Colorectal cancer and NF-κB signaling pathway. Gastroenterol Hepatol Bed Bench. 2011; 4(3): 127-132. doi:

Hawk ET, Levin B. Colorectal cancer prevention. J Clin Oncol. 2005; 23: 378-91. doi: 10.1200/JCO.2005.08.097.

Heylman C, Sobrino A, Shirure VS, Hughes CC, George SC. A strategy for integrating essential three-dimensional microphysiological systems of human organs for realistic anticancer drug screening. Exp Biol Med. 2014; 239: 1240-54. doi: 10.1177/1535370214525295.

Hezel AF, Kimmelman AC, Stanger BZ, Bardeesy N, Depinho RA. Genetics and biology of pancreatic ductal adenocarcinoma. Genes Dev. 2006; 20: 1218-49. doi: 10.1101/gad.1415606.

Hidalgo M. Pancreatic cancer. N Engl J Med. 2010; 362: 1605-17. doi: 10.1056/NEJMra0901557.

Hingorani SR, Petricoin EF, Maitra A, Rajapakse V, King C, Jacobetz MA, Ross S, Conrads TP, Veenstra TD, Hitt BA, Kawaguchi Y, Johann D, Liotta LA, Crawford HC, Putt ME, Jacks T, Wright CV, Hruban RH, Lowy AM, Tuveson DA. Preinvasive and invasive ductal pancreatic cancer and its early detection in the mouse. Cancer Cell. 2003; 4: 437-50. doi: 10.1016/S1535-6108(03)00309-X.

Holdgate GA. Making cool drugs hot: isothermal titration calorimetry as a tool to study binding energetics. Biotechniques. 2001; 31: 164-6, 168, 170 passim. doi:

Horii A, Nakatsuru S, Miyoshi Y, Ichii S, Nagase H, Ando H, Yanagisawa A, Tsuchiya E, Kato Y, Nakamura Y. Frequent somatic mutations of the APC gene in human pancreatic cancer. Cancer Res. 1992; 52: 6696-98. doi:

Horiuchi K, Eason M, Ferry J, Planck J, Walsh C, Smith R, Howitz KT, and Ma H. Assay development for histone methyltransferases. Assay Drug Dev Technol. 2013; 11: 227–36. doi: 10.1089/adt.2012.480.

Howlader N, Noone AM, Krapcho M, Miller D, Bishop K, Kosary CL, Yu M, Ruhl J, Tatalovich Z, Mariotto A, Lewis DR, Chen HS, Feuer EJ, Cronin KA (eds). SEER Cancer Statistics Review, 1975-2014, National Cancer Institute. Bethesda, MD, https://seer.cancer.gov/csr/1975_2014/, based on November 2016 SEER data submission, posted to the SEER web site, April 2017.

Hsu JM, Chen CT, Chou CK, Kuo HP, Li LY, Lin CY, Lee HJ, Wang YN, Liu M, Liao HW, Shi B, Lai CC, Bedford MT, Tsai CH, Hung MC. Crosstalk between Arg 1175 methylation and Tyr 1173 phosphorylation negatively modulates EGFR-mediated ERK activation. Nat Cell Biol. 2011; 13: 174-81. doi: 10.1038/ncb2158.

Ishikawa F, Yasukawa M, Lyons B, Yoshida S, Miyamoto T, Yoshimoto G, Watanabe T, Akashi K, Shultz LD, Harada M. Development of functional human blood and immune systems in NOD/SCID/IL2 receptor {gamma} chain(null) mice. Blood. 2005; 106: 1565-73. doi: 10.1182/blood-2005-02-0516.

Jansson M, Durant ST, Cho EC, Sheahan S, Edelmann M, Kessler B, La Thangue NB. Arginine methylation regulates the p53 response. Nat Cell Biol. 2008;10: 1431-9. doi: 10.1038/ncb1802.

Jiang W and Newsham IF. The tumor suppressor DAL-1/4.1B and protein methylation cooperate in inducing apoptosis in MCF-7 breast cancer cells. Mol Cancer. 2006; 5: 4. doi: 10.1186/1476-4598-5-4.

Jiang H, Zhu Y, Zhou Z, Xu J, Jin S, Xu K, Zhang H, Sun Q, Wang J, Xu J. PRMT5 promotes cell proliferation by inhibiting BTG2 expression via the ERK signaling pathway in hepatocellular carcinoma. Cancer Med. 2018; 7:869-82.

Jin Y, Zhou J, Xu F, Jin B, Cui L, Wang Y, Du X, Li J, Li P, Ren R, Pan J. Targeting methyltransferase PRMT5 eliminates leukemia stem cells in chronic myelogenous leukemia. J Clin Invest. 2016; 126:3961-80. doi: 10.1172/JCI85239.

Jing P, Zhao N, Ye M, Zhang Y, Zhang Z, Sun J, Wang Z, Zhang J, Gu Z. Protein arginine methyltransferase 5 promotes lung cancer metastasis via the epigenetic regulation of miR-99 family/FGFR3 signaling. Cancer Lett. 2018; 427: 38-48. doi: 10.1016/j.canlet.2018.04.019.

Jung J. Human Tumor Xenograft Models for Preclinical Assessment of Anticancer Drug Development. Toxicol Res. 2014; 30: 1-5. doi: 10.5487/TR.2014.30.1.001.

Karve TM, Cheema AK. Small changes huge impact: the role of protein posttranslational modifications in cellular homeostasis and disease. J Amino Acids. 2011; 2011: 207691. doi: 10.4061/2011/207691.

Kern SE. Molecular genetic alterations in ductal pancreatic adenocarcinomas. Med Clin North Am. 2000; 84: 691-95. doi: 10.1016/S0025-7125(05)70251-0.

Kim MS, Pinto SM, Getnet D, Nirujogi RS, Manda SS, Chaerkady R, Madugundu AK, Kelkar DS, Isserlin R, Jain S, Thomas JK, Muthusamy B, Leal-Rojas P, *et al.* A draft map of the human proteome. Nature. 2014; 509: 575-81. doi: 10.1038/nature13302.

Kwak YT, Guo J, Prajapati S, Park KJ, Surabhi RM, Miller B, Gehrig P, Gaynor RB. Methylation of SPT5 regulates its interaction with RNA polymerase II and transcriptional elongation properties. Mol Cell. 2003; 11: 1055-66; doi: org/10.1016/S1097-2765(03)00101-1.

Lakatos PL, Lakatos L. Risk for colorectal cancer in ulcerative colitis: Changes, causes and management strategies. World J Gastroenterol. 2008; 14: 3937-47. doi: 10.3748/wjg.14.3937.

Lind DS, Hochwald SN, and Malaty J. Nuclear factor-κB is upregulated in colorectal cancer. Surgery. 2001; 130: 363-9. doi: 10.1067/msy.2001.116672.

Ling J, Kang Y, Zhao R, Xia Q, Lee DF, Chang Z, Li J, Peng B, Fleming JB, Wang H, Liu J, Lemischka IR, Hung MC, Chiao PJ. KrasG12D-induced IKK2/β/ NF-κB activation by IL-1α and p62 feedforward loops is required for development of pancreatic ductal adenocarcinoma. Cancer Cell. 2012; 21: 105-20. doi: 10.1016/j.ccr.2011.12.006.

Liou GY, Döppler H, Necela B, Krishna M, Crawford HC, Raimondo M, and Storz P. Macrophage-secreted cytokines drive pancreatic acinar-to-ductal metaplasia through NF-κB and MMPs. J Cell Biol. 2013; 202: 563–77. doi: 10.1083/jcb.201301001.

Liu CD, Cheng CP, Fang JS, Chen LC, Zhao B, Kieff E, Peng CW. Modulation of Epstein–Barr virus nuclear antigen 2-dependent transcription by protein arginine methyltransferase 5. Biochem Biophys Res Commun. 2013; 430: 1097-102. doi: 10.1016/j.bbrc.2012.12.032

Liu F, Cheng G, Hamard PJ, Greenblatt S, Wang L, Man N, Perna F, Xu H, Tadi M, Luciani L, Nimer SD. Arginine methyltransferase PRMT5 is essential for sustaining normal adult hematopoiesis. J Clin Invest. 2015; 125: 3532-44. doi: 10.1172/JCI81749.

Lee J, Bedford MT. PABP1 identified as an arginine methyltransferase substrate using high-density protein arrays. EMBO Rep. 2002; 3: 268-73. doi: 10.1093/embo-reports/kvf052.

Lei ZG, Ren XH, Wang SS, Liang XH, Tang YL. Immunocompromised and immunocompetent mouse models for head and neck squamous cell carcinoma. Onco Targets Ther. 2016; 9: 545-55. doi: 10.2147/OTT.S95633.

Lu T, Jackson MW, Wang B, Yang M, Chance MR, Miyagi M, Gudkov AV, Stark GR. Regulation of NF-kappaB by NSD1/FBXL11-dependent reversible lysine methylation of p65. Proc Natl Acad Sci U S A. 2010; 107: 46-51. doi: 10.1073/pnas.0912493107.

Lu T, Prabhu L. Small molecule protein arginine methyltransferase 5 (PRMT5) Inhibitors and methods of treatment. International Patent Appl. PCT/US2017/058572, filed October 26, 2017.

Mager LF, Wasmer M, Rau TT, Krebs P. Cytokine-induced modulation of colorectal cancer. Front Oncol. 2016; 6: 96. doi: 10.3389/fonc.2016.00096.

Maniati E, Bossard M, Cook N, Candido JB, Emami-Shahri N, Nedospasov SA, Balkwill FR, Tuveson DA, Hagemann T. Crosstalk between the canonical NF-κB and Notch signaling pathways inhibits Pparγ expression and promotes PC progression in mice. J Clin Invest. 2011; 121: 4685-99. doi: 10.1172/JCI45797.

Martin M, Hartley A, Lu T. Colorectal Cancer Therapeutics: Present and the Future. In: Cancer Therapeutics. Hyderabad, India: Avid Science. 2018; 2-32. ISBN: 978-93-86337-78-8.

Martin G, Ostareck-Lederer A, Chari A, Neuenkirchen N, Dettwiler S, Blank D, Rüegsegger U, Fischer U, Keller W. Arginine methylation in subunits of mammalian pre-mRNA cleavage factor I. RNA. 2010; 16: 1646-59. doi: 1261/rna.2164210.

Martin M, Wei H, Lu T. Targeting tumor microenvironment in cancer therapeutics. Oncotarget. 2016; 7: 52575-83. doi: 10.18632/oncotarget.9824.

Martinez Molina D, Jafari R, Ignatushchenko M, Seki T, Larsson EA, Dan C, Sreekumar L, Cao Y, Nordlund P. Monitoring drug target engagement in cells

and tissues using the cellular thermal shift assay. Science. 2013; 341 :84-7. doi: 10.1126/science.1233606.

Meister G, Bühler D, Pillai R, Lottspeich F, Fischer U. A multiprotein complex mediates the ATP-dependent assembly of spliceosomal U snRNPs. Nat Cell Biol. 2001; 3: 945-9. doi: 10.1038/ncb1101-945.

Migliori V, Müller J, Phalke S, Low D, Bezzi M, Mok WC, Sahu SK, Gunaratne J, Capasso P, Bassi C, *et al.* Symmetric dimethylation of H3R2 is a newly identified histone mark that supports euchromatin maintenance. Nat Struct Mol Biol 2012; 19: 136-44. doi: 10.1038/nsmb.2209.

Mundade R, Imperiale TF, Prabhu L, Loehrer PJ, Lu T. Genetic pathways, diagnosis and treatment in sporadic colon cancer. Oncoscience. 2014; 1: 400-6. doi: 10.18632/oncoscience.59.

Pal S, Baiocchi RA, Byrd JC, Grever MR, Jacob ST, Sif S. Low levels of miR-92b/96 induce PRMT5 translation and H3R8/H4R3 methylation in mantle cell lymphoma. EMBO J. 2007; 26: 3558-69. doi: 10.1038/sj.emboj.7601794.

Pal S, Vishwanath SN, Erdjument-Bromage H, Tempst P, Sif S. Human SWI/SNF-associated PRMT5 methylates histone H3 arginine 8 and negatively

regulates expression of ST7 and NM23 tumor suppressor genes. Mol Cell Biol. 2004; 24: 9630-45. doi: 10.1128/MCB.24.21.9630-9645.2004.

Prabhu L, Wei H, Chen L, Demir O, Sandusky G, Sun E, Wang J, Mo J, Zeng L, Fishel M, Safa A, Amaro A, Korc M, Zhang Z-Y, Lu T. Adapting AlphaLISA high throughput screen to discover a novel small-molecule inhibitor targeting protein arginine methyltransferase 5 in pancreatic and colorectal cancers. Oncotarget. 2017; 8: 39963-77. doi: 10.18632/oncotarget.18102.

Prabhu L, Chen L, Wei H, Demir O, Safa A, Zeng L, Amaro R, O'Neill B, Zhang Z-Y, Lu T. Development of AlphaLISA high throughput technique to screen for small molecule inhibitors targeting protein arginine methyltransferases. Mol BioSyst. 2017; 13: 2509-20. doi: 10.1039/C7MB00391A.

Prabhu L, Mundade R, Korc M, Loehrer PJ, Lu T. Critical role of NF-κB in pancreatic cancer. Oncotarget. 2014; 5: 10969-75. doi: 10.18632/oncotarget.2624.

Powers MA, Fay MM, Factor RE, Welm AL, Ullman KS. Protein arginine methyltransferase 5 accelerates tumor growth by arginine methylation of the tumor suppressor programmed cell death 4. Cancer Res. 2011; 71: 5579-87. doi: 10.1158/0008-5472.CAN-11-0458.

Ren J, Wang Y, Liang Y, Zhang Y, Bao S, Xu Z. Methylation of ribosomal protein S10 by protein-arginine methyltransferase 5 regulates ribosome biogenesis. J Biol Chem. 2010; 285: 12695-705. doi: 10.1074/jbc.M110.103911.

Qiu T, Zhou L, Zhu W, Wang T, Wang J, Shu Y, Liu P. Effects of treatment with histone deacetylase inhibitors in solid tumors: a review based on 30 clinical trials. Future Oncol. 2013; 9: 255-69. doi: 10.2217/fon.12.173.

Qiu W, Su G. Development of orthotopic pancreatic tumor mouse models. Methods Mol Biol. 2013; 980: 215-223. doi: 10.1007/978-1-62703-287-2_11.

Quinn AM, Allali-Hassani A, Vedadi M, Simeonov A. A chemiluminescence-based method for identification of histone lysine methyltransferase inhibitors. Mol Biosyst. 2010; 6: 782-8. doi: 10.1039/b921912a.

Raymond E, Faivre S, Woynarowski JM, Chaney SG. Oxaliplatin: mechanism of action and antineoplastic activity. Semin Oncol. 1998; 25: 4-12. doi:

Richon VM, Johnston D, Sneeringer CJ, Jin L, Majer CR, Elliston K, Jerva LF, Scott MP, Copeland RA. Chemogenetic analysis of human protein methyltransferases. Chem Biol Drug Des. 2011; 78: 199-210. doi: 10.1111/j.1747-0285.2011.01135.x.

Rustum YM. Biochemical rationale for the 5-fluorouracil leucovorin combination and update of clinical experience. J Chemother. 1990; 1: 5-11. doi:

Sakamoto K, Maeda S, Hikiba Y, Nakagawa H, Hayakawa Y, Shibata W, Yanai A, Ogura K, Omata M. Constitutive NF-kappaB activation in colorectal carcinoma plays a key role in angiogenesis, promoting tumor growth. Clin Cancer Res. 2009; 15: 2248-58. doi: 10.1158/1078-0432.CCR-08-1383.

Sastry GM, Adzhigirey M, Day T, Annabhimoju R, and Sherman W. Protein and ligand preparation: Parameters, protocols, and influence on virtual screening enrichments. J Comput Aid Mol Des. 2013; 27: 221-34. doi: 10.1007/s10822-013-9644-8.

Schapira M, Ferreira de Freitas R. Structural biology and chemistry of protein arginine methyltransferases. MedChem-Comm. 2014; 19; 5: 1779-88. doi: 10.1039/C4MD00269E.

Simard JR, Plant M, Emkey R, Yu V. Development and implementation of a high-throughput AlphaLISA assay for identifying inhibitors of EZH2 methyltransferase. Assay Drug Dev Technol. 2013; 11: 152-62. doi: 10.1089/adt.2012.481.

Shannon HE, Fishel ML, Xie J, Gu D, McCarthy BP, Riley AA, Sinn AL, Silver JM, Peterman K, Kelley MR, Hanenberg H, Korc M, Pollok KE, Territo PR.

Longitudinal bioluminescence imaging of primary versus abdominal metastatic tumor growth in orthotopic pancreatic tumor models in NSG mice. Pancreas. 2015; 44: 64-75. doi: 10.1097/MPA.0000000000000238.

Shaw LM. Tumor cell invasion assays. Methods Mol Biol. 2005; 294: 97-105. doi:

Shire K, Kapoor P, Jiang K, Hing MN, Sivachandran N, Nguyen T, Frappier L. Regulation of the EBNA1 Epstein–Barr virus protein by serine phosphorylation and arginine methylation. J Virol. 2006; 80: 5261-72. doi: 10.1128/ JVI.02682-05.

Shultz LD, Lyons BL, Burzenski LM, Gott B, Chen X, Chaleff S, Kotb M, Gillies SD, King M, Mangada J, Greiner DL, Handgretinger R. Human lymphoid and myeloid cell development in NOD/LtSz-scid IL2R gamma null mice engrafted with mobilized human hemopoietic stem cells. J Immunol. 2005; 174: 6477-89.

Siegel R, Naishadham D, Jemal A. Cancer statistics, 2013. CA Cancer J Clin I. 2013; 63: 11-30. doi: 10.3322/caac.21166.

Slattery JL. Diet, lifestyle, and colon cancer. Semin Gastrointest Dis. 2000; 11: 1142-46. doi:

Slingerland M, Guchelaar HJ, Gelderblom H. Histone deacetylase inhibitors: an overview of the clinical studies in solid tumors. Anticancer Drugs. 2014; 25: 140-9. doi: 10.1097/CAD.0000000000000040.

Sun L, Wang M, Lv Z, Yang N, Liu Y, Bao S, Gong W, Xu RM. Structural insights into protein arginine symmetric dimethylation by PRMT5. Proc Natl Acad Sci USA. 2011; 108: 20538-43. doi: 10.1073/pnas.1106946108.

Tamiya H, Kim H, Klymenko O, Kim H, Feng Y, Zhang T, Han JY, Murao A, Snipas SJ, Jilaveanu L, Brown K, Kluger H, Zhang H, Iwai K, Ronai ZA SHARPIN-mediated regulation of protein arginine methyltransferase 5 controls melanoma growth. J Clin Invest. 2018; 128: 517-30. doi: 10.1172/JCI95410.

Tee WW, Pardo M, Theunissen TW, Yu L, Choudhary JS, Hajkova P, Surani MA. Prmt5 is essential for early mouse development and acts in the cytoplasm to maintain ES cell pluripotency. Genes Dev. 2010; 24: 2772-7. doi: 10.1101/gad.606110.

Tsai WW, Niessen S, Goebel N, Yates JR 3rd, Guccione E, Montminy M. PRMT5 modulates the metabolic response to fasting signals. Proc Natl Acad Sci USA. 2013; 110: 8870-5. doi: 10.1073/pnas.1304602110.

Wang L, Pal S, Sif S. Protein arginine methyltransferase 5 suppresses the transcription of the RB family of tumor suppressors in leukemia and lymphoma cells. Mol Cell Biol. 2008; 28: 6262-77. doi: 10.1128/MCB.00923-08.

Wang W, Abbruzzese JL, Evans DB, Larry L, Cleary KR, Chiao PJ. The nuclear factor-κB RelA transcription factor is constitutively activated in human pancreatic adenocarcinoma cells. Clin Cancer Res. 1999; 5: 119-27. doi:

Wei H, Wang B, Miyagi M, She Y, Gopalan B, Huang DB Ghosh G, Stark GR, Lu T. PRMT5 dimethylates R30 of the p65 subunit to activate NF-κB. Proc Natl Acad Sci USA. 2013; 110: 13516-21. doi: 10.1073/pnas.1311784110.

Wei H, Mundade R, Lange KC, Lu T. Protein arginine methylation of non-histone proteins and its role in diseases. Cell Cycle. 2013; 13: 32-41. doi: 10.4161/cc.27353.

Wei TY, Juan CC, Hisa JY, Su LJ, Lee YC, Chou HY, Chen JM, Wu YC, Chiu SC, Hsu CP, Liu KL, Yu CT. Protein arginine methyltransferase 5 is a potential oncoprotein that upregulates G1 cyclins/cyclin-dependent kinases and the phosphoinositide 3-kinase/AKT signaling cascade. Cancer Sci. 2012; 103: 1640-50. doi: 10.1111/j.1349-7006.2012.02367.x.

Wienken CJ, Baaske P, Rothbauer U, Braun D, Duhr S. Protein-binding assays in biological liquids using microscale thermophoresis. Nat Commun. 2010; 1:100. doi: 10.1038/ncomms1093.

Wilczek C, Chitta R, Woo E, Shabanowitz J, Chait BT, Hunt DF, Shechter D. Protein arginine methyltransferase Prmt5–Mep50 methylates histones H2A and H4 and the histone chaperone nucleoplasmin in Xenopus laevis eggs. J Biol Chem. 2011; 286: 42221-31. doi: 10.1074/jbc.M111.303677.

Yang M, Sun J, Sun X, Shen Q, Gao Z, Yang C. Caenorhabditis elegans protein arginine methyltransferase PRMT-5 negatively regulates DNA damage induced apoptosis. PLoS Genet. 2009; 5: e1000514. doi: 10.1371/journal.pgen.1000514.

Yang Y, Hadjikyriacou A, Xia Z, Gayatri S, Kim D, Zurita-Lopez C, Kelly R, Guo A, Li W, Clarke SG, Bedford MT. PRMT9 is a Type II methyltransferase that methylates the splicing factor SAP145. Nat Commun. 2015; 6: 6428. doi: 10.1038/ncomms7428.

Ye N, Zhou J. KRAS – An evolving cancer target. Austin J Cancer Clin Res. 2014; 1: 1004. doi:

Yu HG, Zhong X, Yang YN, Luo HS, Yu JP, Meier JJ, Schrader H, Bastian A, Schmidt WE, and Schmitz F. Increased expression of nuclear factor κB/RelA is correlated with tumor angiogenesis in human colorectal cancer. Int J Colorectal Dis. 2004; 19: 18-22. doi: 10.1007/s00384-003-0494-z.

Yu XR, Tang Y, Wang WJ, Ji S, Ma S, Zhong L, Zhang CH, Yang J, Wu XA, Fu ZY, Li LL, Yang SY. Discovery and structure-activity analysis of 4-((5-nitropyrimidin-4-yl)amino)benzimidamide derivatives as novel protein arginine methyltransferase 1 (PRMT1) inhibitors. Bioorg Med Chem Lett. 2015; 25: 5449-53. doi: 10.1016/j.bmcl.2015.06.095.

Yuan C-C, Matthews Adam GW, Jin Y, Chen Chang F, Chapman Brad A, Ohsumi Toshiro K, Glass Karen C, Kutateladze Tatiana G, Borowsky Mark L, Struhl K, Oettinger Marjorie A. Histone H3R2 symmetric dimethylation and histone H3K4 trimethylation are tightly correlated in eukaryotic genomes. Cell Reports. 2012; 1:83-90. doi: 10.1016/j.celrep.2011.12.008.

Yue M, Li Q, Zhang Y, Zhao Y, Zhang Z, Bao S. Histone H4R3 methylation catalyzed by SKB1/PRMT5 is required for maintaining shoot apical meristem. PLoS ONE. 2013; 8: e83258. doi: 10.1371/journal.pone.0083258.

Zhang B, Dong S, Li Z, Lu L, Zhang S, Chen X, Cen X, Wu Y. Targeting protein arginine methyltransferase 5 inhibits human hepatocellular carcinoma growth via

the downregulation of beta-catenin. J Transl Med. 2015; 13:349. doi: 10.1186/s12967-015-0721-8.

Zhang HT, Zhang D, Zha ZG, and Hu CD. Transcriptional activation of PRMT5 by NF-Y is required for cell growth and negatively regulated by the PKC/c-Fos signaling in prostate cancer cells. Biochim Biophys Acta. 2014; 11: 1330-40. doi: 10.1016/j.bbagrm.2014.09.015.

Zhang JH, Chung TDY, and Oldenburg KR. A simple statistical parameter for use in evaluation and validation of high throughput screening assays. J Biomolecular Screening. 1999; 4: 67–73.

Zhao DY, Gish G, Braunschweig U, Li Y, Ni Z, Schmitges FW, Zhong G, Liu K, Li W, Moffat J, Vedadi M, Min J, Pawson TJ, Blencowe BJ, Greenblatt JF. SMN and symmetric arginine dimethylation of RNA polymerase II C-terminal domain control termination. Nature. 2016; 529: 48-53. doi: 10.1038/nature16469.

Zheng Y, Huang L, Ge W, Yang M, Ma Y, Xie G, Wang W, Bian B, Li L, Nie H, Shen L. Protein arginine methyltransferase 5 inhibition upregulates Foxp3$_+$ regulatory T Cells frequency and function during the ulcerative colitis. Front Immunol. 2017; 23: 8:596. doi: 10.3389/fimmu.2017.00596.

Zobel-Thropp P, Gary JD, Clarke S. delta-N-methylarginine is a novel posttranslational modification of arginine residues in yeast proteins. J Biol Chem. 1998; 273: 29283-6. doi:

CURRICULUM VITAE

Lakshmi Milind Prabhu

EDUCATION

2013-2018 Doctor of Philosophy in Pharmacology
Indiana University
Indianapolis, IN
Mentor: Tao Lu, Ph.D.

2010-2013 M.S. Cell and Molecular Biology
San Diego State University
San Diego, CA
Mentor: Sanford Bernstein, Ph.D.

2009-2010 Postgraduate Diploma in Clinical Analysis
Sophia College
Mumbai, India

2006-2009 B.S. Biotechnology
Mithibai College, University of Mumbai
Mumbai, India

PROFESSIONAL EXPERIENCE

10/2017-11/2017 **Student Participant**
Eli Lilly & Company
Lilly Student Industry Xperience (SiX) Program

2013-present **Graduate Research Assistant**
Indiana University School of Medicine, Indianapolis, IN
Department of Pharmacology and Toxicology

2011-2013 **Teaching Assistant**
San Diego State University, San Diego, CA
Department of Biology

2010 **Biology Tutor**
San Diego State University, San Diego, CA
Office of Equal Opportunity

PATENT

Lu T, Prabhu L. “Small Molecule Protein Arginine Methyltransferase 5 (PRMT5) Inhibitors and Methods of Treatment”, International Patent Appl. PCT/US2017/058572, filed October 26, 2017.

PEER-REVIEWED PUBLICATIONS

***co-first author**

Research Articles

1. **Prabhu L**, Chen L, Wei H, Demir O, Safa A, Zeng L, Amaro R, O'Neill B, Zhang Z-Y, Lu T. Development of AlphaLISA high throughput technique to screen for small molecule inhibitors targeting protein arginine methyltransferases. Molecular Biosystems. 2017; 13: 2509-20. doi: 10.1039/C7MB00391A.
   ****Article chosen for cover image***

2. **Prabhu L**, Wei H, Chen L, Demir O, Sandusky G, Sun E, Wang J, Mo J, Zeng L, Fishel M, Safa A, Amaro A, Korc M, Zhang Z-Y, Lu T. Adapting AlphaLISA high throughput screen to discover a novel small-molecule inhibitor targeting protein arginine methyltransferase 5 in pancreatic and colorectal cancers. Oncotarget. 2017; 8: 39963-77. doi: 10.18632/oncotarget.18102.
   ****Article chosen for cover image***

3. Martin, M, Hua L, Wang B, Wei H, **Prabhu L**, Hartley A, Jiang G, Liu Y, Lu T. Novel serine 176 phosphorylation of YBX1 activates NF-κB in colon cancer. Journal of Biological Chemistry. 2017; 292: 3433-44. doi: 10.1074/jbc.M116.740258.

4. **Prabhu L***, Mundade R*****, Wang B, Wei H, Hartley A, McElyea K, Temm C, Sandusky G, Liu Y, Lu T. Critical role of phosphorylation of serine 165 of YBX1 on the activation of NF-κB in colon cancer. Oncotarget. 2015; 6: 29396-412. doi: 10.18632/oncotarget.5120.

5. Wang B, Wei H, **Prabhu L**, Zhao W, Martin M, Hartley A, Lu T. Role of novel serine 316 phosphorylation of the p65 subunit of NF-κB in differential gene regulation. Journal of Biological Chemistry. 2015; 290: 20336-47. doi:10.1074/jbc.M115.639849.

Review Articles

1. **Prabhu L**, Hartley A, Martin M, Warsame F, Sun E, Lu T. Role of post-translational modification of the Y box binding protein 1 in human cancers. Genes & Diseases. 2015; 2: 240-6. doi: 10.1016/j.gendis.2015.05.001.

2. **Prabhu L**, Mundade R, Korc M, Loehrer P, Lu T. Critical role of NF-κB in pancreatic cancer. Oncotarget. 2014; 5: 10969-75. doi: 10.18632/oncotarget.2624.

3. Mundade R, Ozer H, Wei H, **Prabhu L**, Lu T. Role of ChIP-seq in the discovery of transcription factor binding sites, differential gene regulation

mechanism, epigenetic marks and beyond. Cell Cycle. 2014; 13: 2847-52. doi: 10.4161/15384101.2014.949201.

4. Mundade R, Imperiale T, **Prabhu L**, Loehrer P, Lu T. Genetic pathways, prevention, and treatment of sporadic colorectal cancer. Oncoscience. 2014; 1: 400-6. doi: 10.18632/oncoscience.59.

Book Chapters

1. Wei H, **Prabhu, L**, Hartley A, Martin M, Sun E, Jiang G, Liu Y, Lu T. Methylation of NF-κB and its role in gene regulation. Gene expression and regulation in mammalian cells-transcription from general aspects, Dr. Fumiaki Uchiumi (Ed.). InTech. 2018; ISBN 978-953-51-3856-3.

2. Hartley A, Wei H, **Prabhu L**, Martin M, Lu T. NF-κB: Its role in colorectal cancer. Transcriptional factors: their role in gastrointestinal malignancies, Nagaraju G, Bramhachari P (Eds.). Springer Publishing. 2017; ISBN: 978-981-10-6727-3.

Thesis

Prabhu L. Effect of mutations in DUNC-45 on its activity as a myosin chaperone, using Drosophila as a model. [San Diego, Calif.]: San Diego State University 2013. Thesis.

PRESENTATIONS

Oral Presentations

Prabhu L. Protein arginine methyltransferase 5 as a therapeutic target in gastrointestinal cancers. October 2017. Biochemistry Research Day, Indianapolis, IN.

Prabhu L. The role of PRMT5 as a tumor promoter and a therapeutic target in pancreatic & colon cancer. March 2017. Department of Pharmacology Student Seminar Series, Indianapolis, IN.

Prabhu L. Epigenetic enzyme PRMT5, a new frontier for anti-cancer drug discovery. March 2016. Department of Pharmacology Student Seminar Series, Indianapolis, IN.

Poster Presentations

Prabhu L, *et al.* and Lu T. Protein arginine methyltransferase 5 as a tumor promoter and therapeutic target in gastrointestinal cancers. April 2018, American Association of Cancer Research Annual Meeting, Chicago, IL.

Prabhu L, *et al.* and Lu T. Protein arginine methyltransferase 5 as a therapeutic target in gastrointestinal cancers. October 2017, Biochemistry Research Day, Indianapolis, IN.

Prabhu L, *et al.* and Lu T. Investigating the role of epigenetic enzyme protein arginine methyltransferase 5 as a tumor promoter as well as a therapeutic target in gastrointestinal cancers. July 2017, Gordon Research Conference, Holderness, NH.

Prabhu L, *et al.* and Lu T. Investigating the role of epigenetic enzyme protein arginine methyltransferase 5 as a tumor promoter as well as a therapeutic target in gastrointestinal cancers. April 2017, IU Simon Cancer Center Annual Cancer Research Day, Indianapolis, IN**.**

Prabhu L, *et al.* and Lu T. Phosphorylation of serine 165 on YBX1 mediates NF-κB activation in colon cancer. April 2016, IU Simon Cancer Center Annual Cancer Research Day, Indianapolis, IN.

Prabhu L, *et al.* and Lu T. Critical role of phosphorylation of serine 165 of YBX1 on the activation of NF-κB in colon cancer. October 2015, Indiana University School of Medicine Poster Showcase, Indianapolis, IN.

Prabhu L, *et al.* and Lu T. Critical role of phosphorylation of serine 165 of YBX1 on the activation of NF-κB in colon cancer. June 2015, 28th Annual Great Lakes Chapter ASPET Regional Meeting, Chicago, IL.

Prabhu L, *et al.* and Lu T. Critical role of phosphorylation of serine 165 of YBX1 on the activation of NF-κB in colon cancer. April 2015, Indiana University Student Research Day, Indianapolis, IN.

Prabhu L, Huxford T, Bernstein S. Importance of conserved region of DUNC-45 in its chaperone function using Drosophila as a model. March 2012, Student Research Symposium, San Diego State University, San Diego, CA.

HONORS/AWARDS

Fall 2018	K.K. Chen Fellowship in Pharmacology and Toxicology
Fall 2018	Erica Daniel Kepner Award for Scientific Achievement Honorable Mention
Spring 2018	IUPUI Dr. Charles R. Bantz Award for Excellence
Spring 2018	Elite 50 Award, Indiana University-Purdue University (IUPUI)
Spring 2018	IUPUI Travel Fellowship
Spring 2018	IUSM Graduate Student Travel Award
Fall 2017	Erica Daniel Kepner Award for Scientific Achievement Honorable Mention
Fall 2017	Graduate Student Volunteer of the Year Honorable Mention

Spring 2017	Paradise Travel Award
Spring 2017	Best Poster in Basic Science Student Category Honorable Mention, Cancer Research Day 2017
Spring 2017	IUSM Graduate Student Travel Award
Fall 2016	Graduate-Professional Education Grant
Fall 2016	Nominated by Indiana University School of Medicine as applicant for NIH/NCI Predoctoral to Postdoctoral Transition Award (F99/K00)
Spring 2016	Nominated by Indiana University School of Medicine as applicant for HHMI International Student Research Fellowship
Fall 2015	Paradise Travel Award
Fall 2012	Mabel Myers Memorial Scholarship
Spring 2010	Tatachem Golden Jubilee Foundation Scholarship for graduate studies abroad
Spring 2010	R.D. Sethna Scholarship for graduate studies abroad

TEACHING & MENTORING

Jun-Aug 2016	Mentor of high-school students Indiana University School of Medicine, Indianapolis IN
Feb-Apr 2015	Mentor of pre-med student Indiana University School of Medicine, Indianapolis IN
Aug '11-May '13	Teaching Assistant, Bio203L (Principles of Cell and Molecular Biology Lab) Department of Biology, San Diego State University, CA
Jan-May 2011	Teaching Assistant, Bio100L (General Biology Lab for Non-Majors) Department of Biology, San Diego State University, CA
Sep-Dec 2010	Biology Tutor Office of Educational Opportunity Programs & Ethnic Affairs San Diego State University, CA

SERVICE

2017-2018	President and Treasurer Scientific Toasters at IUSM Toastmasters International
2016-2017	Graduate Student President

	Department of Pharmacology and Toxicology Indiana University School of Medicine
2016-2017	Vice President-Education Scientific Toasters at IUSM Toastmasters International
2016-2017	Admissions Committee Student Representative Indiana University School of Medicine Biomedical Gateway program Indiana University School of Medicine
2016-2017	Member of Graduate Division Travel Grant Review Committee Indiana University School of Medicine Biomedical Gateway program Indiana University School of Medicine
August 2016	Volunteer, IUPUI 2016 Regatta Indiana University-Purdue University (IUPUI)
February 2016	Organized and Hosted Toaster Talks Ted talks for prospective graduate students Indiana University School of Medicine Biomedical Gateway program Indiana University School of Medicine
October 2015	Central Indiana Science Outreach (CINSO), event volunteer
2014-current	International Graduate Student Welcome Volunteer Office of International Affairs Indiana University-Purdue University (IUPUI)
2013-current	Student Ambassador for Graduate Student Campus Recruitment Visits Indiana University School of Medicine Biomedical Gateway program Indiana University School of Medicine
2012-2013	Volunteer at Association of Women in Sciences San Diego Chapter